Polymersomes mediated intracellular delivery of antibodies: implication in anticancer therapy.

Luca Chierico

University College London

Faculty of Mathematical and Physical Sciences

Department of Chemistry

Thesis submitted to the University College London for the Degree of Doctor of Philosophy

2015

DECLARATION

I, Luca Chierico confirm that the work presented in this thesis is my own. Where information has been derived from other sources, I confirm that this has been indicated in the thesis.

Luca Chierico

Department of Chemistry
University College London
London, UK
November 2014

To Silvia

"Creativity does not mean free improvisation without method"

Bruno Munari

List of Publications and Presentations

PUBLICATIONS:

Surface interactions between polymeric assemblies and proteins.

Chierico L, Martijn Cohen, and Battaglia G.
(JACS, in preparation - 2014).

Anomalous Ki-67 degradation pathway in cancer cells.

Chierico L, Rizzello L, Guan L, Joseph A, Lewis A, and Battaglia G.
(eLife, Submitted - 2014).

Novel aspects of encapsulation and delivery using polymersomes.

Messager L, Gaitzsch J, Chierico L, and Battaglia G.
Current Opinion in Pharmacology 2014;18(0): 104-11.

Live cell imaging of cytoskeleton interactions and membrane topology.

Chierico L, Joseph A, Lewis A, and Battaglia G.
Sci. Rep. 2014;4.

pH-sensitive tubular polymersomes: formation and applications in cellular delivery.

Robertson JD, Yealland G, Avila-Olias M, Chierico L, Bandmann O, Renshaw SA, and Battaglia G.
ACS Nano 2014.

Fully synthetic polymer vesicles for intracellular delivery of antibodies in live cells.

Canton I, Massignani M, Patikarnmonthon N, Chierico L, Robertson J, Renshaw SA, Warren NJ, Madsen JP, Armes SP, Lewis AL, and Battaglia G.
FASEB J 2013;27(1): 98-108.

Encapsulation of biomacromolecules within polymersomes by electroporation.

Wang L*, Chierico L*, Little D*, Patikarnmonthon N*, Yang Z, Azzouz M, Madsen J, Armes SP, and Battaglia G.
Angew Chem Int Ed Engl 2012;51(44): 11122-5.
*WL, CL, LD, PN contributed equally.

PRESENTATIONS:

Exploring the molecular bases of cytoskeleton-cell membrane interactions, by live imaging approach.

Chierico L, Joseph A, Lewis A, and Battaglia G. 248th ACS National Meeting, San Francisco, CA (2014).

Oral presentation.

Exploring the molecular bases of cytoskeleton-cell membrane interactions, by means of real time, live imaging approach.

Chierico L, Joseph A, Lewis A, and Battaglia G. IOP The Physics of Soft and Biological Matter, Cambridge, UK (2014).

Oral presentation.

PMPC-PDPA polymersomes: multi-cargo delivery in live cells.

Chierico L, Lewis A, Canton I, and Battaglia G.

ASME 2nd Global Congress on NanoEngineering for Medicine and Biology, Boston, MA (2013).

Oral presentation.

PMPC-PDPA polymersomes: new tools for live cell imaging.

Chierico L, and Battaglia G.

IOP Physics meets Biology, Oxford, UK (2012).

Poster presentation.

PMPC-PDPA polymersomes: new tools for live cell imaging.

Chierico L, and Battaglia G.

9th International Symposium on Polymer Therapeutics: From Laboratory to Clinical Practice, Valencia ES (2012).

Poster presentation.

Acknowledgements

First of all I would like to acknowledge my supervisor, Professor Giuseppe Battaglia that gave me the opportunity to carry out my PhD under his guidance and that over the years always founded the time to give me suggestions and encouragements to proceed with my research.

I would also like to thanks BTG / Biocompatibles for sponsoring my studentship.

Another special thanks is for all the people that helped me in the lab during my experiments and for the finalisation of this thesis giving me useful suggestions and corrections.

For this reason I would like to thanks Dr. Loris Rizzello, Dr. Adrian S. Joseph, Guy Yealland, Dr. Priya Viswanathan, Dr. Daniel Little and Dr. Irene Canton.

I would like to extend my acknowledgements to all the other current and past members of the Battaglia research group that in a way or another helped me over the years and made me have fun time during the working and pubs hours.

For this reason thanks to Dr. Denis Cecchin, Gavin Fullstone, Russell Pearson, Dr. Carla Pegoraro, Dr. Nisa Patikarnmonthon, James Robertson, Guan Lijuan, Dr. Linge Wang, Dr. Xiaohe Tian, Dr. Milagros Avila Olias, Kamonchanok Ngamkam, Dr. Jens Gaitzsch, Dr. Alessandro Poma, Dr. Lea Messager, Dr. Lorena Ruiz Perez, Claudia Contini, Monika Magon, Sophie Nyberg and Dr. Jeppe Peter Madsen.

A very special thanks goes to all my friends here in UK and to the ones that are in Italy which have always found the way to support me despite the distance.

Thanks to my family, my mum, my dad and my brother for their help and encouragements during this adventure oversea.

Finally, the biggest thanks goes to Silvia.

Thank you for your love, patience, perseverance and courage.

Abstract

Cancer is one of the leading causes of death in the developed world. Nevertheless, many pharmaceutical products available in the clinic lack of tissue specificity, and often have severe side effects. Nowadays, advances in molecular biology and biotechnology have allowed the development of biological therapeutic approaches aimed to give a step forward on cancer treatment. Biotherapy involves the use of biomolecules such as antibodies that have the potential to increase the specificity of anticancer treatments, thus limiting the side effects. Unfortunately, the effectiveness of such biomolecules is hindered by their pharmacokinetics, and their translation into patient care is heavily restricted by low solubility in water, instability / degradation *in vivo* and low efficiency. Besides that, such biomolecules require appropriate delivery strategies to penetrate cellular barriers, thus being able to interfere with pathways that can be involved in cancer development.

This research project aims to bridge the lack of technology regarding the development of an effective and biocompatible delivery system. The pH sensitive PMPC-PDPA ((poly(2-(methacryloyloxy)ethyl phosphorylcholine) - poly(2-(diisopropylamino)ethyl methacrylate)) polymersome was employed as candidate for the intracellular delivery of functional therapeutic antibodies in live cells. The PMPC-PDPA diblock copolymer combines the ability to release the loaded cargo upon acidification within the endosomes with an overall biocompatibility.

First, the antifouling proprieties of polymersomes were investigated, and then compared to micelles. Subsequently, electroporation was exploited as reliable technique to effectively encapsulate antibodies within polymersomes. The delivery of antibodies in live cells was assessed using anti γ-tubulin antibody as a model system.

Finally, Ki-67 was explored as a possible target for anticancer therapy. Interestingly, relevant differences in the biological functions of this marker were revealed between cancerous and non-cancerous cells. Furthermore, antibodies against Ki-67 were delivered in live cells, and their activity was tested to explore the potential of Ki-67 as a target for anticancer therapy.

Contents

List of Abbreviations

'A375	Human melanoma cells'
'ARF6	ADP-ribosylation factor 6'
'ATCC	American type culture collection'
'ATF6	Activating transcription factor 6'
'ATP	Adenosine triphosphate'
'ATRP	Atom transfer radical polymerisation'
'AuNP-IgG	Gold labeled immunoglobulin G'
'B cells	B-Lymphocytes'
'BAX	Bcl-2-like protein 4'
'BCA	Bicinchoninic acid assay'
'bEnd3	Murine brain endothelial cells'
'BSA	Bovine Serum Albumin'
'Bak	Bcl-2 antagonist'
'Bcl-2	B-cell lymphoma 2'
'BiP	Molecular chaperone binding immunoglobulin protein'
'CAC	Critical aggregate concentration'
'CDC42	Cell division cycle 42'
'CDKIs	Cyclin-dependent kinase inhibitors'
'CDNA	Complementary DNA'
'CE-SDS	Capillary-electrophoresis-sodium dodecyl sulfate'
'CLSM	Confocal Laser Scanning Microscopy Analysis'
'CME	Clathrin-mediated endocytosis'
'COPII	Cytoplasmic coat protein complex II'
'CTLs	T lymphocytes'
'Cdks	Cyclin dependent kinases'
'DLS	Dynamic light scattering'
'DMEM	Dulbecco Modified Eagle Medium'
'DMSO	Dimethyl sulfoxide '
'DOPE	Dioleoyl phosphatidylethanolamine'
'DPA	2-(diisopropylamino)ethyl methacrylate'
'ECM	Extracellular matrix'

'EDTA	Ethylenediaminetetraacetic acid'
'ELISA	Enzymatic Linked Immunosorbent Assay'
'EPR	Enhanced permeability and retention'
'ER	Endoplasmic reticulum'
'ERAD	ER-associated protein degradation'
'ERK 1/2	Extracellular-signal-regulated kinases 1/2'
'FBS	Fetal bovine serum'
'FC	Fluorescence cytometry'
'Fc domain	Fragment crystallisable IgG domain'
'FDA	Food and Drug Administration'
'FHA	Forkhead associated domain'
'FRET	Förster resonance energy transfer'
'FaDu	Human pharyngeal squamous carcinoma cells'
'GAPDH	Glyceraldehyde 3-phosphate dehydrogenase'
'GIT	Gastrointestinal tract'
'GnRH	Gonadotropin releasing hormone'
'HDF	Human Dermal Fibroblasts'
'HEMA	Poly(2-hydroxyethyl methacrylate)'
'HER2	Human epidermal growth factor receptor-2'
'HRP	Horseradish peroxidase'
'HUVECs	Human umbilical vein endothelial cells'
'HeLa	Human adenocarcinoma cells'
'Hklp2	Kinesin-like protein'
'IL-8	Interleukin 8'
'ITC	Isothermal Titration Calorimetry'
'Ig-CAMs	Immunoglobulin cell adhesion molecules'
'IgG	Immunoglobulin G'
'Ire1	Inositol-requiring enzyme 1'
'LSGS	Low Serum Growth Supplement '
'MAb	Monoclonal antibodies'
'MDA-MB-231	Breast cancer cells'
'MDSCs	Myeloid-derived suppressor cells'
'MEM	Eagle Minimum Essential Medium'
'MEWO	Human skin melanoma cells'
'MPS	Mononuclear phagocyte system'

'mRNA	Messenger RNA'
'MTT	3-(4,5-Dimethyl-2-thiazolyl)-2,5-diphenyl-2H-tetrazolium bromide'
'MVB	Multivesicular bodies'
'MW	Molecular weight'
'NHS	National Health Service'
'NIFK	Nucleolar protein interacting factor'
'NIH-3T3	Murine embryonic fibroblasts'
'NK	Natural killer'
'NTera2	Human embryonal carcinoma stem cells'
'p53	Tumor protein p53'
'PAP	Prostatic acid phosphatase antigen'
'PBD	Polybutadiene'
'PBS	Phosphate buffered saline'
'PCR	Polymerase chain reaction'
'PDB	Protein Data Bank'
'PDMA	Poly(2-dimethylamino)ethyl methacrilate'
'PDMS	Poly(dimethylsiloxane)'
'PDPA	Poly(2-(diisopropylamino)ethyl methacrylate)'
'PEG	Polyethylene glycol'
'PEI	Polyethyleneimine'
'PEO	Poly(oligo(ethylene glycol) methacrylate)'
'PERK	Protein kinase RNA-like ER kinase'
'PHPMA	Poly(2-hydroxypropyl methacrylate)'
'PI	Propidium iodide'
'PLGA	Poly(lactic-co-glycolic acid)'
'PMOXA	Poly(2-methyloxazoline)'
'PMPC	Poly(2-methacryloyloxyethyl phosphorylcholine)'
'PS	Polystyrene'
'PTDs	Presenting transduction domain sequence'
'PVA	Polyvinyl alcohol'
'PVP	Polyvinylpyrrolidone'
'RES	Reticuloendothelial system'
'RGD	Arginyl-glycyl-aspartic acid peptide'
'RIPA	Radio-immunoprecipitation buffer'

'ROS	Reactive oxygen species'
'RP-HPLC	Reversed phase high pressure liquid chromatography'
'RPMI	Roswell Park Memorial Institute Medium'
'RT-PCR	Reverse transcription polymerase chain reaction'
'RT-qPCR	Reverse transcription quantitative PCR'
'RT112	Urinary bladder transitional carcinoma cells'
'Rb	Retinoblastoma protein'
'rpm	Rounds per minutes'
'SASAs	Solvent Accessible Surface Areas'
'SAXS	Small-Angle X-ray Scattering'
'SEC	Size Exclusion Chromatography'
'SKOV3	Ovarian carcinoma cells'
'SLS	Static light scattering'
'SR-B1	Scavenger receptor class B member 1'
'ShRNA	Short hairpin RNA'
'T cells	T-Lymphocytes'
'TEM	Transmission Electron Microscopy'
'TFA	Trifluoroacetic acid'
'TFA-DODAPL	Trifluoroacetylated lipopolyamine'
'TGF-β	Transforming growth factor beta'
'TGN	Trans Golgi network'
'TRIM21	Tripartite motif-containing 21'
'TSP-1	Thrombospondin 1'
'Tregs	Regulatory T cells'
'UPR	Unfolded protein response'
'UV-Vis	Ultraviolet-Visible'
'VEGF-A	Vascular endothelial growth factor-A'
'VEGFR-1-3	VEGF receptors 1,3'
'VH	Immunoglobulin G heavy chain variable domains'
'VL	Immunoglobulin G light chain variable domains'

List of Figures and Tables

Project Impact

Cancer is one of the leading causes of death in the developed world. According to the American Cancer Society, only in U.S.A, more than 580,000 people died from this disease in 2013, while the latest data in UK have reported more than 159,000 cases (CancerResearchUK, 2014; Siegel et al., 2013) (see Figure 1). In the last few decades, academic researchers as well as pharmaceutical industries have spent considerable resources in cancer research, and yet we do not have a universal cure. As far as UK healthcare, cancer care is one of the largest expenditures for the National Health Service (NHS). Latest economical figures show that between 5-7% of the NHS budget is spent on cancer care in the UK. This is a total of £9.5 billion in 2011 and it is predicted to rise over £15 billion by 2021 (NHS-UK, 2014). Although many pharmaceutical products are already available in the clinic, these are mainly based on traditional 1950-60's chemotherapeutic agents (i.e. alkylating-like agents and DNA intercalators) with little or none tissue specificity and consequently severe side effects (Ruoslahti et al., 2010). Much hope is coming from recent advances in molecular biology and biotechnological sciences, finding specific molecular markers and biochemical singularities in cancer cells (Ruoslahti et al., 2010). Potentially, these new approaches could bring innovative therapies for the treatment of solid tumours. A good example of this is the use of monoclonal antibodies, such as trastuzumab (Herceptin®) (Pegram et al., 2000a). Today, there are 23 therapeutic products in the market based on monoclonal antibodies and other 3 based on antibody fragments.

Their economic impact is calculated to be over 1$ billion per year (Sidhu and Fellouse, 2006). Although antibodies have high potential, their use is heavily restricted to extracellular targets because of their inability to enter the cell cytosol. Antibodies are possibly the closest system to Ehrlich's "magic bullet" (Strebhardt and Ullrich, 2008), this because they have high specificity. However, their clinical implementation is hindered by chemical instability, aggregation and protease sensitivity, with consequent poor pharmacokinetics (Blanco et al., 2011). Here is where nanotechnology can greatly help with the

design of fully synthetic nanocarriers to efficiently deliver biomolecules such as antibodies, in order to enable a new strategy for cancer treatment.

With nanotechnology, there is a real possibility to develop the state-of-the-art in antitumoural therapy; a step closer to patient-tailored strategies and to restrict side effects on existing treatments.

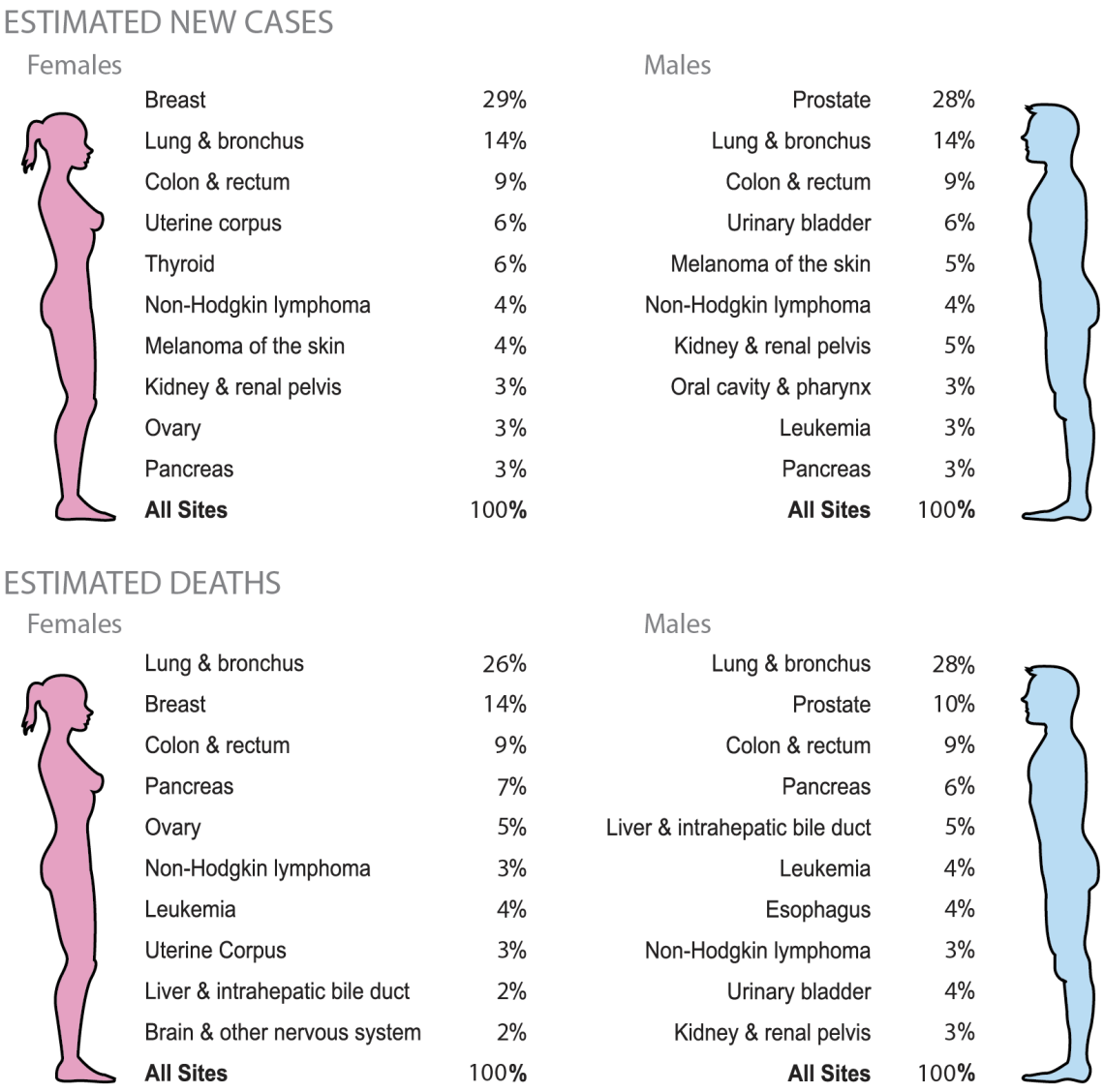

Figure 1. Estimated new cases and deaths by sex in USA, considering the ten most common types of cancer (Siegel et al., 2013).

Chapter 1

Introduction

1.1. CANCER CELL BIOLOGY

Cancer is a cellular disease that is due to an uncontrolled cellular proliferation. This results from the losses of multiple intracellular controls mechanisms that lead to an abnormal cell growth. Naturally, the cell life is characterised by well programmed consecutive phases such as: proliferation, maturation, division and death. Cancerous cells lose the ability to regulate these steps properly and this promotes continuous cycles of growth and cellular division. Moreover, cancer cells lose or alter their phenotypical functions with associated physiological disorders. In addition, their incessant proliferation causes local damage on the surrounding tissues, and finally, cancer cells can also escape their primary site and spread into other organs (i.e. metastasis). Cancer development is not just produced from a single genetic modification. Computational analyses indicate that the minimal number of mutations developed in a cell to induce tumorigenesis is between five to eight (Balmain et al., 1993). These genetic alterations can lead to the development of disease and promote the cancer hallmarks that can be summarised as shown in Figure 1.1.

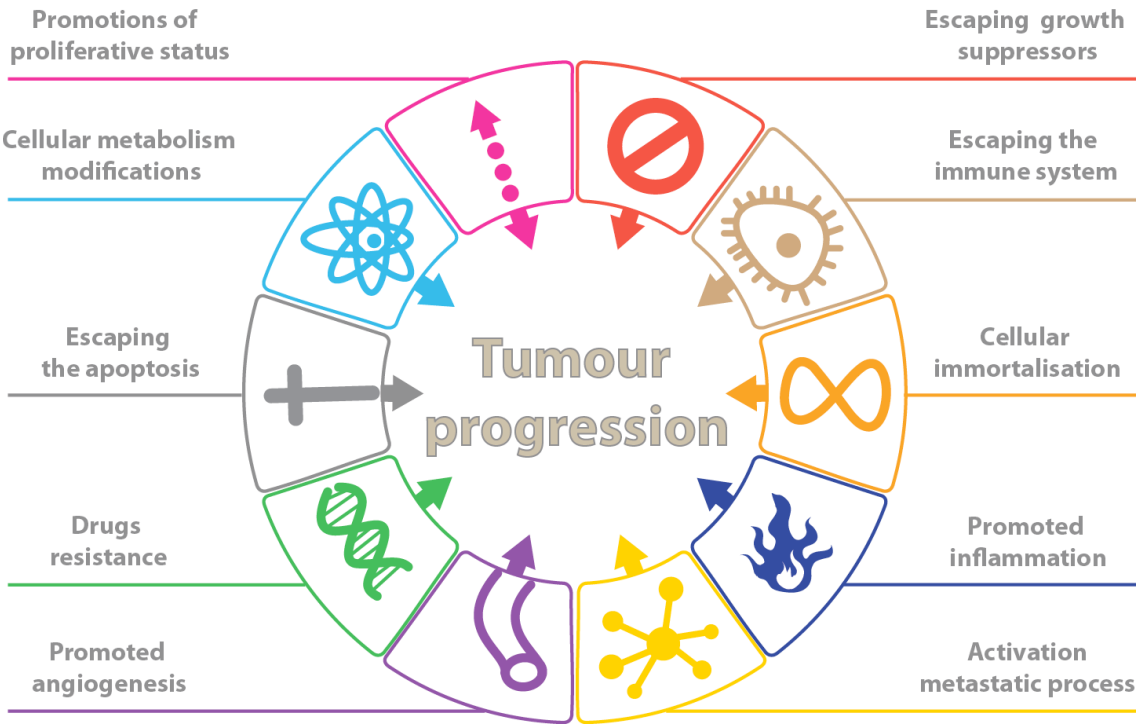

Figure 1.1. Illustration that summarises the ten hallmarks of cancer pathogenesis (Hanahan and Weinberg, 2011).

1.1.1. Escaping from growth suppressors

The cellular division is a process controlled from a complex intracellular machinery, and it is divided in sequential steps that define a unique cycle.
The understanding of the multiple factors involved in such important mechanisms are critical to design anticancer therapies. At the same time, it is very important to recognise that most of the mutations affecting cancerous cells involve the dysregulation of this fundamental biological process, namely the cell cycle (Sherr, 1996). As schematised in Figure 1.2, four different phases characterise the cell cycle, and the passage from one phase to another is regulated by dedicated proteins machineries.
The different cellular cycle steps are reported below with a brief description of their respective function:

G_1	In this phase the cell is preparing its metabolic machinery for the subsequent DNA replication (gap1).
S	At this point, the DNA is first synthesised and then replicated.
G_2	Here, the cell start to prepare all “protein materials” needed for the subsequent mitosis (gap2).
M	Cellular division, mitosis.

Furthermore, as shown in Figure 1.2, the M phase progresses through different sub-phases:

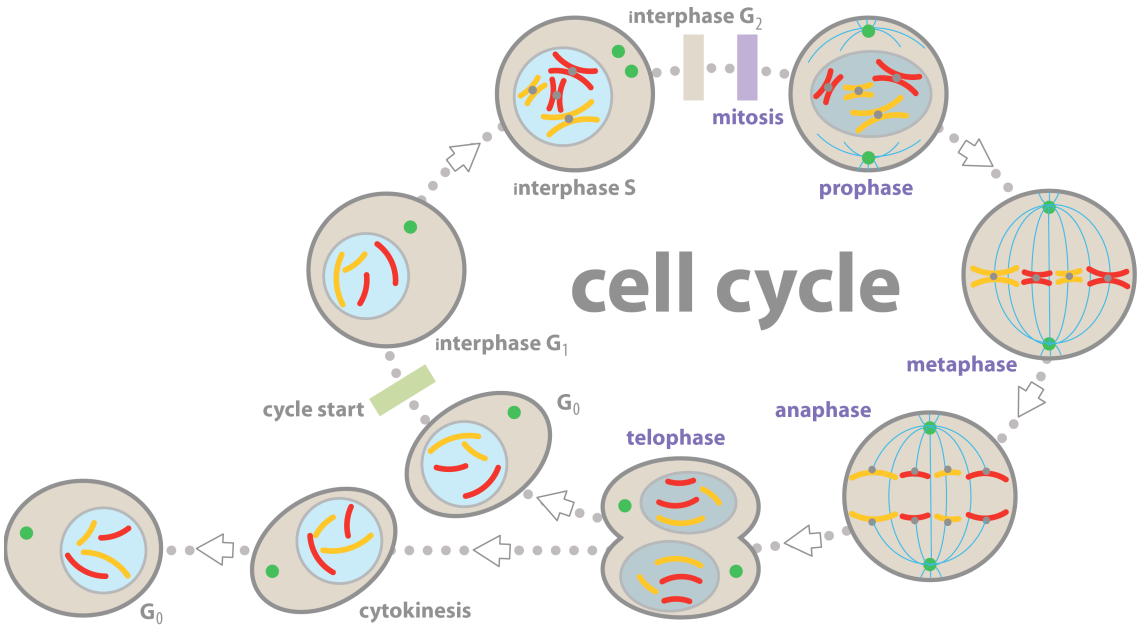

Prophase	Chromosomes assemble with chromatids and centromere. Simultaneous formation of the mitotic spindle.
Metaphase	Mitotic spindle interaction with centromeres present in the relative chromosomes.
Anaphase	Centromeres division and consequent separation of equal chromatids to the opposite pole.
Telophase	Chromatids decondensation and new chromosomes formation.

Figure 1.2. Schematic of the eukaryotic cell cycle. The phases G_1, S and G_2 constitute the interphase (I) while the M phase includes mitosis and cytokinesis. In the table are described the four phases composing the mitosis.

When the cell cycle is concluded after the M phase, the cell remains in a quiescent state called G_0 phase. During this phase, the cell does all the routine actions, aimed to maintain its functionality.

Most of the adult human body cells are non proliferating, and maintain a permanent quiescent state. Out of these, some specific cells have the ability to withdrawn from the G_0 phase and become temporarily proliferating (e.g. glial cells and hepatocytes) as a function of a given stimulus, which are typically nutrients and mitogens (Hall and Watt, 1989; Pardee, 1974; Williams and Stoeber, 2007) .

Finally, there is a minority of permanently proliferating cells, mostly located in confined niches, which feed self renewing tissues (e.g. bone marrow and epithelia) (Potten and Loeffler, 1990) .

The intracellular proteins that have the critical role to control the cell cycle are the cyclins and their corresponding kinases, cyclin dependent kinases (Cdks). The interaction between Cdks and cyclins, as well as other correlated factors, drive the cell cycle across the different phases (Morgan, 1995). Furthermore, the variable expression of cyclins, between different phases of the cycle, directly mediate the Cdk activity, thus working as internal control mechanism. Depending on the cycle phase, different cyclins are engaged for the Cdk regulation. For this reason, the latter can be divided in four different groups: G_1 cyclins, such as the cyclin D that push the cell to the G_1 phase; G_1/S cyclins, such as the cyclin E that induce the cell to enter to the S phase; S cyclins, such as the cyclin A that drive the cell across the S phase; and the M cyclins, such as the cyclin B that control the mitosis (Sherr, 1996; Sherr, 2000).

The importance of cyclins is indeed well known for the above explained role that they have in the cell cycle regulations and progression. Moreover, it also well established that their abnormal gene expression can lead to cancer development (Sherr, 2000; Sutherland and Musgrove, 2004; Tetsu and McCormick, 1999; Yu et al., 2001). The Cdk factors are also subjected to specific regulative pathways. For this propose, there are proteins called Cdk inhibitors (CDKIs), that serve as fundamental negative controllers for the Cdk biological action. In such a way, these proteins act as “brake” of the cell cycle progression by regulating the Cdk activity. Two principal classes of proteins constitute the CDKI family: the INK4 class that acts on the Cdk D and the KIP that inhibits Cdk E and A (Sherr and Roberts, 1999). These proteins represent an important biological element to

prevent abnormal cell cycle progression and thus cellular proliferation. For this reason, genes that encode for CDKIs factors are named tumour suppressor genes (Reed et al., 1996; Solomon and Kaldis, 1998; Talve et al., 1997). Among these, the most studied are the transcription factor p53 and the retinoblastoma protein (Rb). p53 binds DNA to control the expression of several factors involved in the cell cycle. A typical example of p53 function is during DNA damage, where its expression is activated to stop cell proliferation to facilitate DNA repair. If the latter is beyond repair, p53 can than force the cell to undergo controlled death (i.e., apoptosis) (Hickman et al., 2002; Sandal, 2002). While p53 acts as a controller of intracellular abnormalities, ranging from DNA damage to inadequate nutrients and insufficient oxygen level, the Rb factor is implicated in the transduction of extracellular signals within the cell. This protein is in fact able to sense external factors and modulate the cellular machinery in response to growth or inhibitory inputs. Rb is able to control the cellular proliferation and eventually stop the cell cycle entry in the presence of inhibitory conditions (Burkhart and Sage, 2008).

One of the critical landmark of cancer cells is their inability to control the cell cycle together with the presence of non-functioning tumour suppressors genes. This could be the effect of specific mutations that lead to the synthesis of non-functional proteins, leading then to tumour development. For instance, mutations that affect p53 activity result in serious consequences for the cell genetic stability and could rapidly promote a non-controlled cellular proliferation that can lead to a cancerous phenotype (Sherr, 2004). Similarly, mutations that are expressed at the level of Rb gene (chromosome 13) could promote a constitutive Rb active state. In this case, the cell is pushed to an unregulated progression on the S phase with a consequent high risk of malignant phenotype development (Giacinti and Giordano, 2006).

1.1.2. Promotions of a proliferative status

Cancerous cells are characterised from genetic modifications on tumour suppressors genes that allow their escape from cell cycle arrest. Furthermore, by comparing cancerous with normal cells, the former also develop mechanisms aimed to accelerate cellular division and proliferation.

In this context, one well controlled mechanism in normal tissues is the highly regulated extracellular release of proliferative inducing factors. These signals have the specific role to drive the targeted cells into a progressive cell cycle with a consequent increase on their proliferative status.

To this respect, cancerous cells acquire the ability to deregulate these mechanisms, becoming able to proliferate independently.

In normal tissues, the extracellularly released growing molecules bind the cell surface receptors, typically characterised by an intracellular tyrosine kinase domain. The intracellular portions of the receptor mediate several cascade effects, ranging from cellular proliferation to metabolism modifications.

Cancerous cells are able to maintain active this induced proliferation signalling pathway by exploiting several strategies. For example, they can increase the production and release of growing molecules, or force normal cells to do so (Bhowmick et al., 2004; Cheng et al., 2008). Alternatively, they can directly over express these growth factor receptors on their surface (Wang and Hung, 2001). Moreover, the mutation of growth factor receptors, or the mutation of correlated proteins, is associated with the promotion of constitutively active functional state.

To this respect, an example of this category of oncoproteins is represented by the Ras proteins. Ras is an inner-membrane anchored class of proteins, part of the small GTPases family. The intracellular function of this molecule is the translations of signals that could be triggered from different origins. Indeed, Ras proteins exploits their actions by interacting either with trans-membrane proteins such as growth factor receptors, and with intracellular proteins such as the oestrogen receptor-a (Olson and Marais, 2000). The constitutive active state of Ras proteins could be the result of point mutations occurring on its gene. These mutations may then lead to a continuous Ras active state, thus continuously promoting the correlated kinase cascade. This persistent signal transmission at the nuclear level will result in cellular abnormal proliferation and growth (Lowy and Willumsen, 1993).

1.1.3. Escaping the apoptosis

In normal cells, the controlled death, i.e. apoptosis, serves to limit abnormal cellular growth and to maintain the normal physiology of the tissue. It is

established that the programmed cell death is triggered as consequence of external stress that induces the activation of intracellular factors, which then culminate with the cell destruction (Adams and Cory, 2007). Several regulation proteins are involved in this process, and they can be classified into two distinct categories. The first category includes factors that respond to intracellular signals. The second category senses extracellular stimuli.

In both cases, the triggering of one of these two pathways results with the activation of the intracellular proteolytic caspases 8 and 9, and consequently this culminates with the cell death.

The class of proteins called Bcl-2 are among the most important apoptosis effectors. The Bcl-2 members bind, and thus inhibit, the apoptotic triggering factors Bak and Bax. If not inhibited, these two factors induce the mitochondrial membrane destabilisation and consequently the cytochrome c release. The latter, in turn, activates the caspases 8 and 9 (Adams and Cory, 2007).

Different strategies are adopted from the mutated cancerous cells to escape this irreversible mechanism, including mutations that preclude the p53 protein activity (see Section 1.1.1). Furthermore, the same result can be obtained with the over-expression of anti-apoptotic factors, such as the discussed Bcl-2, or by down-expressing the pro-apoptotic Bak/Bax proteins.

1.1.4. Cellular immortalisation

Normal cells have a very defined number of proliferative cycles, finely controlled by an enzyme known as the telomerase. This is a specialised protein that has the role to add repeated hexanucleotidic sequences at the terminus part of the chromosomes, termed as telomeres. The telomeres sequence has the vital function to protect the chromosome extremity, thus preserving the genetic materials. However, the telomerase loses its activity as function of cell ageing and the telomeres sequences are progressively lost as the cell undergoes several division cycles (i.e. senescence). This ultimately leads to expose the chromosomes DNA ends that can fuse to each other causing a decreasing in the cellular viability (Blasco, 2005).

It is observed that cancerous cells develop telomerase able to continuously perform their enzymatic action, thus maintaining over time the ending chromosomal telomeres protecting sequences (Shay and Wright, 2011). This

DNA preserving mechanism is the base for cell immortalisations. Indeed, its emergence allows the cancerous cells to escape from mechanisms such as senescence and apoptosis, entering in an unlimited number of replicative cycles.

1.1.5. Cellular metabolism modifications

The exponential growth that defines a tumour tissue leads to an hypoxic environment (i.e. oxygen depletion). This, in turn, affects the cell metabolism and cancer cells have developed several strategies to cope with such an inhospitable environment. These modified metabolic strategies have the role to promote the fast production of energy, and the synthesis of macromolecules for the continuos cellular proliferation. Normally, cells in aerobic conditions accumulate energy in the form of adenosine triphosphate (ATP) through two subsequent steps: initially, the assimilated glucose is metabolised in pyruvate during the glycolysis process and, subsequently, the latter is converted in CO_2 via the Krebs cycle. These sub-sequential metabolic steps are very profitable from the energetic point of view, but it is necessary to remember the elevate request of oxygen necessary to exploit the Krebs cycle.
Cancerous cells mostly produce ATP through glycolysis process, as it requires lower provision of oxygen (Weinhouse, 1956). Furthermore, there are studies showing that cancerous cells are able to use the glycolytic intermediates for the synthesis of biomolecules such as amino acids (Vander Heiden et al., 2009). Other recent biological investigations proved the existence of two metabolically correlated sub-populations of cells in tumour tissues. These two cellular population are linked by a symbiotic relation. Whilst one cell population bases its energetic production on glycolysis, releasing extracellularly lactate, the other group bases their energy production on the excess of lactate (Feron, 2009; Kennedy and Dewhirst, 2010).

1.1.6. Promoted angiogenesis

All the body tissues need for their maintenance an adequate provision of nutrients. The vasculature network has thus the function to distribute the essential components around the human organism. In normal conditions, the vascular system is essentially evolved during the embryonic development.

Endothelial cells are responsible for the vessels tubular formations (vasculogenesis), and for the spreading of new vasculature ramifications (angiogenesis). After the vessels establishment and maturations, these cells became thus essentially quiescent (Hanahan and Folkman, 1996).

Unlike normal tissues, tumours require an increased supply of nutrients and oxygen to sustain their fast growth. For this reason, cancerous cells are able to promote a *neo*-vasculature formations. The *neo*-formed vessels are however characterised by irregular branching, leakiness and abnormal capillary morphology (Nagy et al., 2010; Nagy and Dvorak, 2012). Cancer cells control angiogenesis via the expression of angiogenic regulators that stimulate and / or inhibit endothelia growth. This feedback mechanism is regulated by the inducer vascular endothelial growth factor-A (VEGF-A), and by the inhibitor thrombospondin-1 (TSP-1), respectively. The binding of VEGF-A to its associated tyrosine kinases receptors (VEGFR-1-3) is at the base of the activations of endothelial cells for the formations of new vessels. Cancerous cells are therefore capable of considerably increasing the secretion in the extracellular environment of this protein, thus stimulating the surrounding vasculature formations (Ferrara, 2009; Mac Gabhann and Popel, 2008). On the other hand, they are also capable of down-regulating the TSP-1 factor, which acts as anti-angiogenic signal, thus reinforcing the VEGF-A function (Kazerounian et al., 2008).

1.1.7. Promoted inflammation

The last decades of studies in cancer research have shown that tumour tissues are interested by the presence of specialised immune cells that promote an inflammatory status. In the past, it was believed that the inflammatory contributions on the neoplastic region was an attempt by the immune system to overcome the developing cancerous cells. Nevertheless, more recent studies proved that the same cancer cell induce immune cells migrations to the tumour site. The inflammatory microenvironment, supported by the cancerous cells, favours the accumulations of growth factors, proliferative signals, angiogenic molecules, and of other biomolecules that increase the tumour development (Grivennikov et al., 2010; Qian and Pollard, 2010).

Furthermore, tumour penetrating immune cells release active molecules such as

reactive oxygen species (ROS) that contribute to the mutagenic process (Grivennikov et al., 2010; Qian and Pollard, 2010).

1.1.8. Escaping the immune system

The complex role that the immune system has on tumour progression was tackled only in the last decades. It is experimentally established that both the adaptive and the innate immune system are involved in tumorigenesis. Indeed, reduced activity of cells such as $CD8^+$ cytotoxic T lymphocytes (CTLs), $CD4^+$ T_h1 helper T cells, and natural killer (NK), are associated with increased tumour development (Teng et al., 2008). Different strategies can be used by cancerous cells to escape the immune detection. One mechanism involves the production of inhibiting factors such as the transforming growth factor beta (TGF-β), that decreases the NK cells functionality (Yang et al., 2010). Another strategy includes the activation of inflammatory cells such as the myeloid-derived suppressor cells (MDSCs) and regulatory T cells (Tregs) that, in turn, produces an immunosuppressive effect (Mougiakakos et al., 2010).

1.1.9. Activation of the metastatic process

The metastasis is a multistep process that allows the cancerous cells to spread around the subjected organism. This diffusive mechanism can be divided in several consecutive steps. Initially, the cancerous cells become able to invade the surrounding space. Afterwards, their permeations into the lymphatic and blood vessels allows them to extravasate into other distal tissues. At this point, the colonisation process is complete and the established neoplastic colonies continue their growth, distributed around the affected organism. Important factors that plays a key role in this tumour development are several classes of cell surface proteins. These proteins have, in normal conditions, the function to anchor the cells to the surrounding elements, such as others cells or the extracellular matrix (ECM). The cadherins, namely immunoglobulin cell adhesion molecules (Ig-CAMs), and the integrins are the principal class of proteins that allow this function (Cavallaro and Dejana, 2011). The role of these proteins in tumour development is strongly related with the loss of cellular adhesion capacity, and consequent metastasis. This is considerably due by

either a down-expression or a defect of these structural proteins that becomes unable to correctly function, thus driving cancerous cell to spread into the neighbours tissues (Cavallaro and Christofori, 2004; Cox et al., 2006).

1.1.10. Drug resistance

The acquired ability of cancerous cells to elude therapeutic anticancer drugs activity is defined as drug resistance. Cancerous cells can make ineffective a drug treatment either by hindering its adsorption or by activating intracellular protective pathways. These include protein factors involved in DNA repair, anti-apoptotic effectors (e.g. cytochrome P450) and ATP-dependent efflux pumps that secrete the drug out of the cell (Holohan et al., 2013).

1.2. BIOLOGICAL BARRIERS

Although the steps forward obtained in recent years into the developing of new approaches in anticancer therapy, these are often restricted from several limitations. Indeed, an important biological aspect that have to be considered for the effectiveness of therapeutic agents, ranging from chemical compounds, biomolecules and polymeric nano-carriers, is represented by their capacity to overcome the biological barriers encountered during and after their administration.

Furthermore, to improve the efficacy of the treatment, it is necessary to optimise properties such as half-life time blood circulation, targeting selectivity, enhanced stability and decreased clearance. The biological barriers define all the mechanisms of preservations that our organism exploits to avoid the internalisation and diffusions of an external factor. The latter, could be represented by a virus, a toxin, a bacteria, but also from an administered drug. Thus, the biological barriers can be summarised as follows:

- Physical barriers.
- Molecular interactions.
- Reticuloendothelial system (RES).

- Vascular wall.
- Cellular barrier.

1.2.1. Physical barriers

Depending on the nature of the drug treatment, different administration routes can be considered. Oral, pulmonary, dermal and intravenous represent some examples of the exploitable ways to administer a therapeutic compound. Nevertheless, they characterise the first biological barrier that has to be overcome. Indeed, each of these routes presents physical limitations that can hinder the effectiveness of the treatment. Between the previously listed ways, the oral administration denotes the higher patient compliance. Also for this reason, drugs formulations such as capsules and tablets are the most diffused in the market (Calleja et al., 2012). Nevertheless, the presence in the gastrointestinal tract (GIT) of adverse conditions such as low pH, degradative enzymes and thick mucus lining the digestive tract, are all aspects that limit the resulting bioavailability (Ensign et al., 2012; Roger et al., 2010).
Looking to another non-invasive route, the drug administration through the pulmonary way has to be considered. The neutral pH conditions present at this level, combined with the high permeability of the alveoli epithelium, represent characteristics that favourite this approach. However, the pulmonary surfaces coated with mucous and the abundant immune system presence on this site, constitute challenging barriers to overcome (Ruge et al., 2013).
Also the transdermal delivery can be exploited as route for drugs administration. However, the skin as a physical barrier constitutes a major limitation for drugs absorption through this way. In fact, the two multilayers tissues, namely epidermis and dermis, which compose this organ are an important challenge to be overtaken. In particular, the epidermic layer, which is principally constituted by keratinocyte, is specialised to prevent the penetrations through this route of external factors including drugs (Alexander et al., 2012).
The last mentioned administration route is the intravenous. This is the most direct way to make a drug accessible into the organism, as it is directly injected in the bloodstream. Nevertheless, also in this case the possible aggregative

process between the exposed active compounds and biomolecules (e.g., proteins present in the circulation) represent the major limitation that affect this administration route (Timerbaev et al., 2006).

1.2.2. Molecular interactions

As mentioned before, upon accessing the circulation, drugs formulations are exposed to their interaction with blood protein components. The establishment of these surface-surface attractive forces generates a phenomena referred as protein adsorption. Polymeric formulations such as drug loaded nano-carriers (which are going to be discussed in detail in the following sections) are also affected by this process. In this case, the proteins surface interaction cause the formation of the so called protein corona (Lynch and Dawson, 2008; Monopoli et al., 2011). The protein adsorption process can thus modify the physical / chemical properties such as external charge and size of the subjected compound. As a consequence of this mechanism, the therapeutic agent can lose its effectiveness and thus became easily recognisable from the reticuloendothelial system (RES). This can culminate with its premature elimination from the blood circulation (Lynch et al., 2009; Owens and Peppas, 2006).

Proteins with different nature can participate at the absorption process. These are generally referred as opsonin, and include proteins such as immunoglobulins, albumin, fibrinogen, apolipoproteins, fibronectin, complement components and many others. Nevertheless, forces with different nature can be implicated to explain the dynamic aspect of the proteins adsorption equilibrium, established within a therapeutic compound.

Thus, externally exposed charges could be indicated as contributing factors, as well as the hydrophilic / hydrophobic balance between the serum components and the introduced therapeutic formulations (Lundqvist et al., 2008; Shannahan et al., 2013).

1.2.3. Reticuloendothelial system

The reticuloendothelial system, also called mononuclear phagocyte system (MPS), represents another physiological barrier that an introduced therapeutic

compound must face, when it reaches the blood circulation. The RES is formed by immune cells such as monocytes and macrophages. These cells are distributed into the reticular connective tissues of organs such as liver, spleen, bone marrows, lungs and lymph nodes. The RES has the role to protect our body from the penetrations and consequent diffusion of external potentially dangerous elements such as toxins, virus and bacteria (Hume, 2006). Furthermore, also drug formulations introduced into the bloodstream are subjected at the RES recognition and consequent elimination. As previously described (see Section 1.2.2), the interactions between the therapeutic agents and opsonins is at the base of the RES activation, leading to the phagocytosis and destruction of the drug (Storm et al., 1995).

1.2.4. Vascular wall

From the blood vessels, the drug formulation has to be able to diffuse to the targeted tissue. To do this, the therapeutic agent has to overcome the vascular endothelium which has the function to control the transport and exchange of nutrients, macromolecules, oxygen and fluids between the bloodstream and the surrounding interstitial space. The vascular endothelium can be divided in three different categories namely continuous, fenestrated and discontinuous, depending on its permeability. The continuous endothelium is present in organs such as skin, muscles, lung, fat, nervous system and several connective tissues (Pappenheimer et al., 1951). At the central nervous system level, the molecular diffusion from the blood vessels to the brain is controlled by the so called blood-brain barrier. This imposes a further selective molecular permeation (Pardridge, 2012). On the other hand, organs such as kidney, intestine, exocrine glands and parts of the central nervous system (e.g. the choroid plexus) are characterised by a fenestrated endothelium that allow a more permissive molecular diffusion to the surrounding tissues (Gentile et al., 2008). The discontinuous endothelium is present on vessels that supply organs such as spleen, bone marrow and liver. For this reason, the latter are naturally subjected to drugs passive diffusion and accumulation (Gentile et al., 2008).

1.2.5. Cellular barriers

The last barrier that a therapeutic agent has to overcome is represented by the cell itself. Indeed, a drugs formulation has to penetrate the cell membrane to be effective. Typically, the cell membrane allows the passage of non-polar small molecules and stops the passage of polar and large ones (including most biological macromolecules). The latter are transported within the cells either via specific molecular transporter (e.g. ion channels) or via the deformation of the cell membrane, in a process called endocytosis. The endocytosis is composed by a set of mechanisms that are fundamental for various activities involved on cell maintenance, including adhesion, migration, nutrient uptake, and signalling. This cellular entry route is the most preferred by cellular parasite including most viruses and several bacteria. The endocytic process generally takes place in three principal subsequent steps that are:

I. interaction between cell membrane and extracellular compound;
II. membrane adaptive modification;
III. activations of specialised intracellular endocytic pathways.

The first step is defined as the binding step. Most of the endocytic mechanisms involve, at this stage, the mediation of specific extracellular receptor-proteins to bind the molecule of interest and to continue within the internalisation process. Most endocytic pathways, with the exception of macro-pinocytosis, involve specific membrane signalling events often activated by the binding.
The second step is the resulting membrane adaptive modification. This stage is promoted by a concatenated cascade of events that allow the recruitment of several proteins working together to produce the necessary cell membrane deformation, invagination and trafficking vesicle genesis.
Finally, when the vesicular cargo is internalised, it is sorted through the appropriate endocytic pathway having the function to sort the material accordingly.
The most important endocytic pathways are summarised below:

A. Clathrin-mediated

Clathrin-mediated endocytosis (CME) is implicated in the internalisation route for several different compounds in eukaryotic cells. Nutrients, synaptic recycled

vesicles, and viruses are internalised through this pathway. CME endocytosis works thanks to the assembly of clathrin triskelion proteins into polygonal structures, with the help of several other correlated factors (adaptor proteins - APs) that produce the vesicular internalisation of the cargo (McMahon and Boucrot, 2011; Pearse, 1976; Schmid, 1997).

B. Caveolae-mediated

Caveolae-mediated endocytosis is the mechanism that involves the membrane anchored caveolins proteins for the formations of the endocytic vesicle. This route is implicated in several cellular mechanisms such as vesicular transport, lipid regulations and cell signalling. Furthermore, caveolae-mediated endocytosis is implicated in various diseases including cancer (Rothberg et al., 1992).

C. RhoA-mediated

RhoA is a protein factor involved in the actin cytoskeleton recruitment and in its dynamics modulation. Since the F-actin network has a critical function in almost all the endocytic mechanisms, consequently RhoA assumes the role of principal actor across almost all of them (Robertson et al., 2009).

D. CDC42-mediated

Cell division cycle 42 (CDC42) belongs to the Ras superfamily of GTP-binding proteins. Its activity is associated with the cytoskeleton recruitment and F-actin polymerisation. Moreover, this factor is also correlated with the modulation of GRAF1. GRAF1 protein is, in turn, involved in the promotion of cell membrane deformations (Klein et al., 2009; Lundmark et al., 2008).

E. ARF6-mediated

ADP-ribosylation factor 6 (ARF6) is a member protein of ARF family, a group of 6 GTPases. ARF6 function is correlated with membrane curvature modelling through its interaction with the phospholipids bilayer and others factors (Donaldson, 2008).

F. Flotillin-mediated

Flotillin is a protein that present a structural conformation that have similarity to both caveolin-1 and clathrin proteins. Despite that, flotillin functions seems to be different and uncorrelated with these two class of proteins. Its role is most likely related to membrane clustering formation and vesicular internalisation process (Glebov et al., 2006; Riento et al., 2009).

G. Macropinocytosis

Macropinocytosis is an endocytic pathways that does not dependent to the initial cargo-receptors interactions. This process exploits the actin cytoskeleton ability to model the plasma membrane in structures like: lamellipodia, circular ruffles and blebs. The macropinocytosis allows the internalisation of a considerable amount of extracellular material into macropinosomes vesicles (Lim and Gleeson, 2011; McNeil, 1984).

H. Phagocytosis

The phagocytosis process is a well used mechanism in specific cells belonging to the immune system such as: neutrophils, monocytes, macrophages, dendritic and mast cells. It is exploited mostly for the internalisation of pathogens, but it is also used for nutrients uptake. Phagocytosis is initiated by specific receptor “sensing” of the extracellular environment and it progresses through the modulation of F-actin network. This in turn promotes the plasma membrane modification and the external element internalisation (Flannagan et al., 2012).

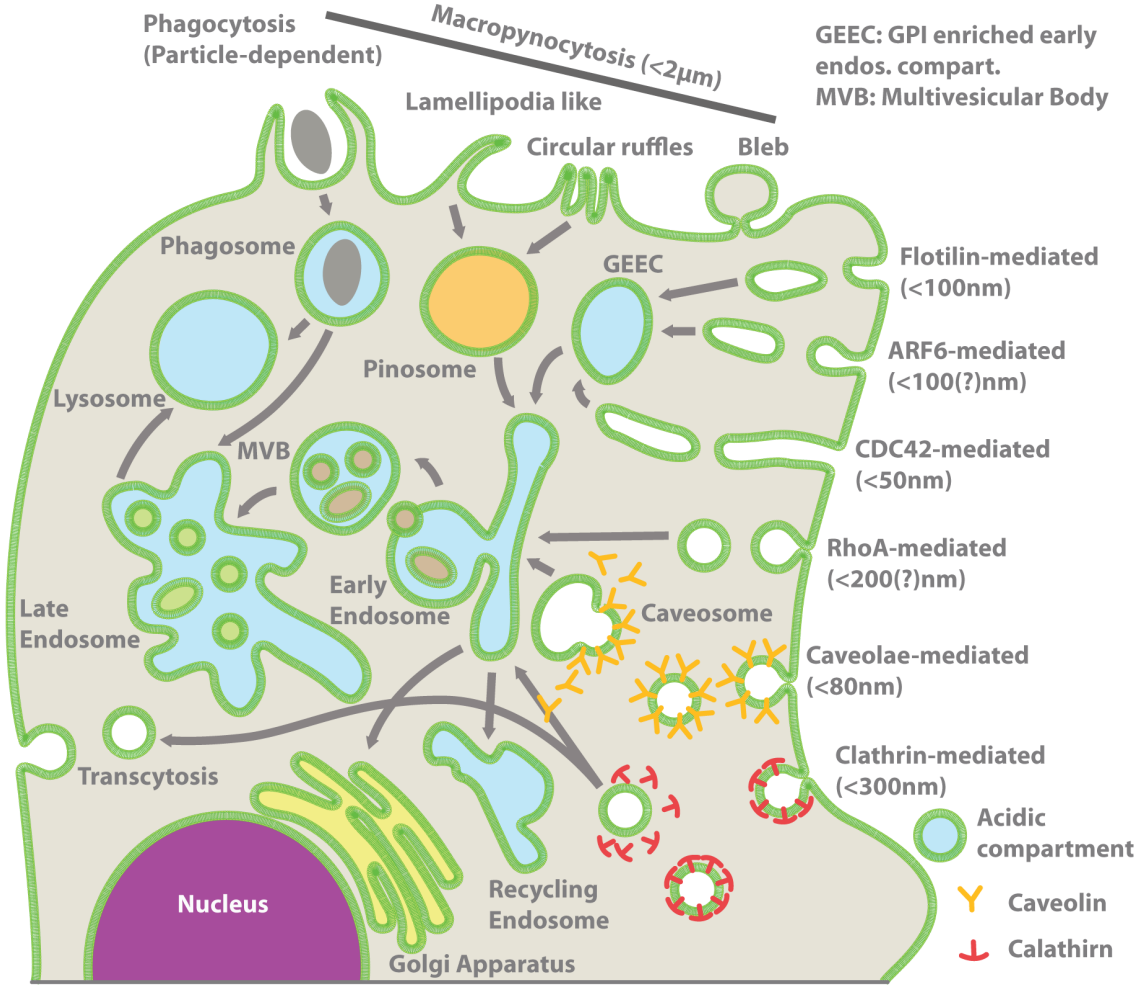

Figure 1.3. Illustration summarising the endocytic pathways that occurs in eukaryotic cells (Canton and Battaglia, 2012).

Generally, the common destination for the internalised cargo during one of the above mentioned uptake processes is the endosomal pathway. During this route, the internalised vesicle follows three consecutive steps. Initially the cargo is accumulated into the so called early endosome where it can be processed into three different destinations: (*i*) delivered back to the cell membrane either via or not recycling endosomes, (*ii*) transported to the trans Golgi network (TGN) via specific modulator known as retromers, or (*iii*) sorted into multivesicular bodies (MVB). From the MVB, the internalised cargo can be included within the late endosomal compartments where is, in turn, vehicled to the lysosome organelle. In this compartment the presence of enzymes called lysosomal hydrolases, induce an acidic pH with an average value between 4 and 5. In these conditions, the internalised cargo is finally degraded and the resulting constituents are sorted to the appropriate cellular site (Canton and Battaglia, 2012).

1.3. STRATEGIES IN ANTICANCER THERAPIES

As herein described, the cancer development and tumour progression is characterised by the acquisition of an abnormal functionality of a population of cells. The latter thus becomes able to highly proliferate and to further modulate the surrounding environment to support this process. Over the years, different approaches were developed aiming to stop this degenerative disease, and the most important strategies besides surgery and radiotherapy can be divided in chemotherapy and biotherapy.

1.3.1. Chemotherapeutic approach

Chemotherapeutic drugs were first used in the 1940's with the discovery of alkylating agents and their effects on mice tumours (DeVita and Chu, 2008; Goodman et al., 1946). Although different in their clinical activity, all alkylating agents such as nitrogen mustards (e.g. cyclophosphamide, mechlorethamine and uramustine), nitrosoureas (e.g. carmustine and lomustine) and alkyl sulfonates (e.g. busulfan) share the same biochemical mechanism. This mechanism of action is therefore based on their cross-linking with DNA, thus causing abnormal base pairing and preventing cellular division.

Besides the alkylating agents and the alkylating-like drugs such as cisplatin, others chemotherapeutic molecules were developed. Thus, depending on their mechanism of action, chemotherapeutic agent can be divided into three principal groups: antimetabolites, anthracyclines and vinca alkaloids / taxanes.

The antimetabolite drugs have chemical structure similarity to natural molecules such as vitamins, amino acids, and precursors of DNA or RNA. Once these agents are incorporated in the cell metabolism, they inhibit the synthesis of DNA or RNA therefore interfering within the cell division process. Examples of molecules that belongs to this class, include methotrexate (Abitrexate®), fluorouracil (Adrucil®), hydroxyurea (Hydrea®), and mercaptopurine (Purinethol®). Others popular antimetabolite chemotherapeutic drugs are thioguanine, cytarabine, cladribine, alimta, gemcitabine, and fludarabine (Grem and Keith, 2005).

The second mentioned group, namely anthracyclines, are able to induce direct chemical damage on DNA and RNA molecules through the production of free

radicals. Furthermore, the latter can cause the malfunction of the DNA and RNA replication process and consequently lead to the production of nonsense nucleic acid sequences (i.e. the new DNA or RNA does not code for anything functional). These chemotherapeutic agents can also inhibit the topoisomerase II enzyme. The topoisomerase exploits its functionality supercoiling the DNA, thus allowing its repair, transcription and replication. Drugs that belongs to this class of chemotherapeutic antibiotics include molecules such as daunorubicin (Cerubidine®), doxorubicin (Adriamycin®), etoposide (VePesid®). Furthermore, epirubicin (Pharmorubicin®) and mitoxantrone (Novantrone®) are others two examples of commonly used anthracycline in anticancer therapy (Minotti et al., 2004).

The last group of therapeutic agents is represented by vinca alkaloids and taxanes. This drugs produce their effect interacting within the mitotic spindle during the M-phase of the cell cycle. They induce either the inhibitions of its formation or the breakdown of it, thus causing the arrest of the cellular division. Examples of mitotic disrupting drugs include: vinblastine (Velban®), vincristine (Oncovin®) and paclitaxel (Taxol®) (Dumontet and Jordan, 2010; Rowinsky, 2003). The mechanism of action of this classes of anticancer drugs is in overall based on the fact that cancerous cells do not respond to normal growth patterns and proliferate much faster than normal cells. Hence, the basic chemotherapeutic approach is to target highly dividing cells without any specificity. Consequently, this leads to the typical side effects associated with cancer chemotherapy. Because the general aim of chemotherapeutic agents is to decrease the growth rate of the highly dividing cancerous cells, side effects are mainly seen in organs and tissues that naturally have a rapid turnover of cells and these include: skin, hair, gastrointestinal and bone marrow.

1.3.2. Negative aspects of chemotherapy

Dosage is a critical problem that affect the current chemotherapy based treatments. Due to the lack of specificity of these agents, chemotherapeutic molecules are linked to severe off-target toxicity, serious reduction in patients life quality and even death. Furthermore, therapies with a decreased dosage, aimed to reduce side effects, could instead lead to an inactive and incomplete treatment via induction of drug resistance. Despite several progress are over the

years achieved to reduce the side effects correlated with these drugs, there are still a number of challenges which need to be addressed:

I. to specifically target to the tumour to reduce toxicity and improve the therapeutic efficacy;

II. to overcome the biological barriers for the delivery of drugs to the location where they need to act (often intracellular targeting);

III. to increase the solubility of hydrophobic chemotherapeutics enabling a lower administered dose;

IV. to improve the drug circulations times avoiding its premature degradation and clearance by the body.

Newer technologies in nanomedicine may be able to tackle these problems and thus change the chemotherapy based treatment of cancer.

1.3.3. Biotherapy

The progressive understanding of biological processes, including cell cancer molecular biology, is promoting nowadays the development of new avenues in cancer treatment. In the last decade, many research efforts were made to develop innovative biological based therapies, designed to be more selective on cancerous cells. This new anticancer approach is defined as biotherapy. The final goal of biotherapy, similarly to the classic chemotherapy, is the cancerous cells eradication from the treated patient. To do so, biotherapy exploits the possible modulations and controls of biological pathways implicated in tumour progression that are over-expressed in cancerous cells. In such a way, the specificity of the biotherapy action aims to reduce the side effects usually occurring in patients treated with unspecific chemotherapeutic drugs (NHS-UK, 2013). The most important biotherapeutic approaches are listed below:

A. Gene therapy

The use of genetic material to kill cancerous targeted cells define the gene cancer therapeutic approach (McCormick, 2001). Various strategies were studied and developed to stop the tumour progression.

The following are some examples:

I. Gene supplementation therapy: with this technology, cancerous cells are supplemented with a wild type gene. The aim is to restore the normal cellular ability to start the apoptotic process in response to severe biological malfunctions. For this reason, p53 was extensively evaluated in this approach since its well know function for the cell cycle and apoptosis regulation (Tazawa et al., 2013).

II. Gene-directed enzyme prodrug therapy: in this case the intracellular delivered gene encodes for an enzyme that provides the conversion of an internalised inefficient drug substrate into an extremely toxic molecule. This approach could thus promote an enhanced selectivity of the therapeutic drug treatment. The genetically modified cancerous cells, expressing the exogenous enzyme, should became in this way vulnerable to the drug actions (Both, 2009).

III. Immunogene-therapy: here the strategy is to induce in cancer cells (through genetic transfection) the expression and external plasma membrane exposition of proteins, that can be easily recognised by the immune system. The obtained enhanced immunogenicity of these genetically modified cancerous cells will promote the migration of immune effectors to the tumour site and consequently its eradications (Lichtor and Glick, 2012).

B. Cytokines

These are proteins produced by the immune system after antigen recognition. These proteins work as signaling factors, triggering the differentiation, activation and chemotaxis of white blood cells. The lymphocytes cytokines production, resulting after the immune cell activation, is followed by a cascade of events that finally promotes the elimination of the uncovered antigen (Khan, 2008). An important example of cytokine approved for the used in cancer therapy is represented from the interferon-α. Interferon-α is commercialised with the name of INTRON®A and its activity is associated with the activation of memory T-Lymphocytes (T cells), natural killer (NK) cells and B-Lymphocytes (B cells) (Pasquali and Mocellin, 2010). The general aim of the cytokines

application in anti-cancer therapy is to enhance the immune system functionality. In such a way it is exploited the ability of the immune system to recognise and subsequently destroy the identified cancerous cells.

C. Cell-based immunotherapy

Cell-based immunotherapy represents an other biotherapeutic approach correlated with the activations of the immune system (Alderton and Bordon, 2012). The consecutive steps characterising the cellular immunotherapy can be summarised as follows:

I. Antigen presentation to the immune system (the antigen has to be an externally exposed protein characterising cancerous cells).

II. Activation and recruitment to the tumour site of effectors cells.

III. Recognition and destruction of abnormal cancerous cells.

Different approaches are adopted in cell-based immunotherapy and they includes protocols aimed to stimulate immune cells such as dendritic cells and T lymphocytes to mediate the cytotoxic action versus cancerous cells.
An example of cell-based immunotherapy treatment approved in the 2010 from the U.S. Food and Drug Administration (FDA) is a therapeutic prostate cancer vaccine, commercialised with the named of PROVENGE®. This vaccine involves the patient dendritic cells activation against the prostatic acid phosphatase (PAP) antigen. PAP is an enzyme which is over-expressed in cancerous prostate cells. For this reason it is used to stimulate the action of effector cells that can synergically act to destroy the abnormal tissues that present this antigen (Plosker, 2011).

D. Antibody

Albeit therapeutic proteins are still in a pioneristic stage, they nowadays have a significant role in several fields of medicine.
Nevertheless, therapeutic biomolecules, such as antibodies, have to reach their site of action to be effective. Although antibodies are of great interest as therapeutics, their pharmacokinetics is very much limited. For this reason, antibodies has to be associated with an appropriated delivery method. This

enables to avoid their degradation promoted for instance by enzymes such as protease, which are abundant in biological fluids.

Monoclonal antibodies (mAb) are currently developed for the treatment of immunological diseases and cancer, with a particularly increasing interest on the latter application (Nelson and Reichert, 2009). An example of this is Herceptin®, a therapeutic mAb against the Human Epidermal Growth Factor Receptor-2 (HER2, also known as Neu, ErbB-2 and CD340 receptor). This protein is implicated in cell survival, adhesion, differentiation and migrations (Pegram et al., 2000b).

Antibodies are produced by immune cells known as B–Lymphocytes (B-cells), and their function is the recognition and neutralisation of foreign-body targets, named antigens. The immunoglobulin G (IgG) is a complex protein composed of four peptide chains. The full IgG antibody has a distinctive Y shape configuration composed of a complex of two identical light chains (Molecular weight (MW) ~25 KDa). These present a constant and a variable domain, and two heavy chains (MW ~50 KDa) that are composed by three constant domains and one variable domain. Disulphide bonds are also presents in the structure with the role to interconnect the light chain to each heavy chain, and to bridge the gap between the two heavy chains (see Figure 1.4).

The IgG structural regions can be moreover defined in respect to their functionality. In this way, the IgG variable region, namely Fab fragment, represents the antigen binding portion of the protein, while the Fc fragment, correspond to the inactive, glycosylated and conserved portion of it. Two constant and two variables domains characterised the IgG-Fab region and each of them belongs respectively to the light and heavy chains of the protein (Putnam et al., 1979). Both light chain variable (VL) and heavy chain variable domains (VH) are formed by three β-strands loops that have the function to recognise the antigen. Furthermore, the variables domains constituting the protein structure (VL and VH) changes between different IgG molecules depending on their antigen specificity (North et al., 2011).

On the other hand, the conserved Fc region has the important role to mediate the antibody interactions with other proteins, such as the complement factors and the Fc receptors. The latter is a class of receptors that belongs to competent immune cells such as natural killer cells (NK), macrophages, neutrophils and

others. Thus, the Fc fragment recognitions mediates the immune response aimed to eliminate the IgG identified antigen (Heyman, 1996).

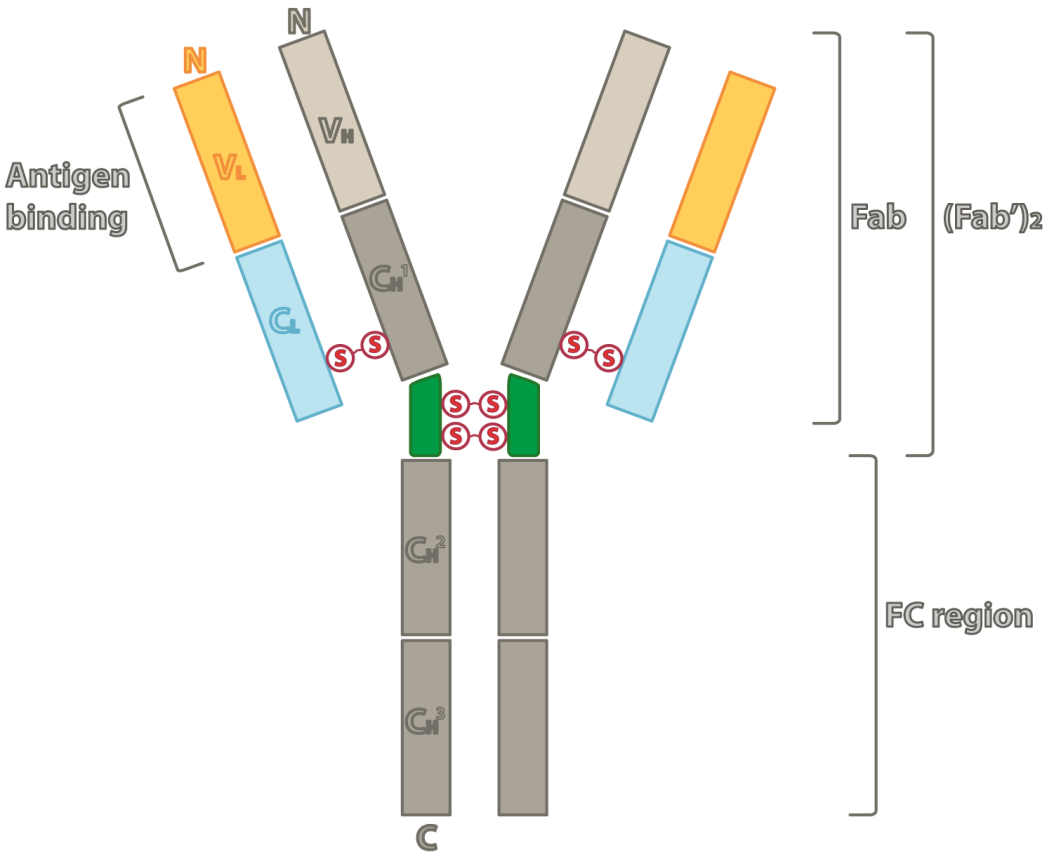

Figure 1.4. IgG structure.

1.4. NANOMEDICINE IN CANCER THERAPY

Nanomedicine in cancer therapy is a rapidly expanding field, which is heavily involved with pharmacokinetics improvement of existing drugs. Indeed, most of the therapeutic drugs applied in anticancer therapy are affected by problems such as poor water solubility and wide range of side effects. Nevertheless, tackling side effects in cancer therapy is not an easy task to achieve.

In this context, nanomedicine applied in cancer therapy has the important role to increase drug accessibility to the tumour site, decreasing the distribution of the latter in healthy tissues, thus reducing the correlated drug side effects.

To achieve this purpose, defined as targeting, two distinct mechanisms can be used, and they are termed as (*i*) passive targeting and (*ii*) active targeting.

The passive targeting exploits the modified structural anatomy of tumour vasculature. Growing tumours require a big supply of nutrients and this is achieved through the extensive promotions of angiogenic process. Nevertheless, the new formed abnormal vessels do not have the typical barrier properties that belongs to normal tissues, and they are characterised by large fenestrations that can reach up to 800 nm. This enables the permeation into the tumour site of large macromolecules that would be otherwise restricted. This process, known as enhanced permeability and retention (EPR) effect, is also characterised by the local impairment of the lymphatic system, with a consequent decreased drainage from the tumour site (Maeda et al., 2000; Matsumura and Maeda, 1986). Thanks to the EPR effect, macromolecules with molecular mass above 40 kDa (value above the renal excretion threshold) can be accumulated into solid tumours. This was reported in experimental studies, where the quantified concentration at the tumour site of such macromolecule resulted 10-30 times superior compared with the systemic blood (Maeda et al., 2009; Maeda et al., 2000). Furthermore, the EPR effect is common in all hypervascular tumours, and hence it become a typical target strategy in nanomedicine (Maeda et al., 2009).

On the other hand, the second targeting mechanism, defined as active targeting, implies the use of nanocarriers presenting properties that enables their direct recognition by cancerous cells. The use of polymeric formulation constituted, for example, by hyaluronic acid, can promote the recognition promoted by CD44 receptors that are over-expressed in cancerous cells (Platt and Szoka,

2008). Furthermore, nanocarriers functionalised with an adequate targeting moieties, such as folic acid or arginyl-glycyl-aspartic acid (RGD) peptide, can be exploited for active targeting. Also in this case, it was established that cancerous cells over-express the folic acid and integrins receptors on their surfaces. This, in turn, promotes the accumulation at the tumour site of vectors presenting these molecules (Moghimi et al., 2001).

1.4.1. Strategies in drug delivery

Many different strategies were developed over the years to enhance the effectiveness of a therapeutic agent. These technologies aim to improve the pharmacological properties such as drug solubility, drug distribution, bioavailability, targeting, and controlled release of the therapeutic agent over time. All these approaches are defined as drug delivery systems. This definition includes a broad range of carriers such as polymer-drug conjugates, dendrimers, polymeric micelles, carbon nanotubes, non-viral vectors for intra-cytoplasmic transport, liposomes, polymersomes and others (LoPresti et al., 2009; Markman et al., 2013).

To describe the drug delivery systems, it is possible to begin from the structurally simplest approach, which is represented by the polymer-drug conjugates. A typical polymer-drug conjugate is constituted by a single polymer chain covalently bounded to a drug. This therefore produces a new chemical entity that has different characteristics compared to the initial free drug, and it is defined as prodrug (Kopeƒçek, 2013). In such a way, the pharmacological properties belonging to the active molecule can be considerably increased.

These chemical modifications, can improve pharmacological aspects of a given drug, such as increased solubility at physiological conditions, escape from the RES, bioavailability, etc.

A more complex drug delivery system is represented by dendrimers. Dendrimers (*dendros* from ancient greek-tree) are tree-like macromolecules formed by the oligomerisation of multifunctional units that can grow to form 1, 2, 3 up to 10 generation of branches with consequent amplification of the single unit valency. The end groups of those branches allows controlled conjugation with the therapeutic agents and / or with targeting moieties. Also in the case of dendrimer conjugates, the final pharmacological aspects of the drug are

improved compared with the free molecule. Nevertheless, the use of dendrimers as drug delivery system is also characterised by downsides. Criticisms arise from the high costs behind their synthesis. Furthermore, several studies associated this delivery system with cells toxicity, including cases of serious haemolytic activity on red blood cells (Chen et al., 2004). All together, these negative factors about the use of dendrimers, hinder their commercialisation as drug delivery platform in cancer therapy.

Polymer-drug conjugates and dendrimers are examples of classes of nanocarriers, whose structural assembly is mediated by covalent bonds. Besides this class of drug delivery systems, another category is represented by inorganic nanocarriers such as carbon nanotubes, quantum dots, gold, silica and magnetic nanoparticles. Gold nanoparticles can be applied for thermal therapy and can be further conjugated with therapeutic molecules (Jain et al., 2012). However, excluding carbon nanotubes, the other nanocarriers belonging to the category of inorganic nanocarriers can only be externally functionalised with the therapeutic compound of interest. For this reason, they presents the limitation to expose on their surface the active agent that can then be subjected at unfavourable physiological conditions and be further recognised by the RES.

Furthermore, there is still some concern in the scientific community about the in vivo toxicity of this class of nanocarriers (Soenen et al., 2011).

In addition to these technologies, a very important class of drug delivery systems is represented by self-assembled nanocarriers. These nanocarriers can be formed by supramolecular forces between their constituents that range from polymer chains to lipids. Indeed, hydrophobicity, aromatic interactions, hydrogen bounds and coulomb forces can be all implicated for the molecular self assembly process that characterised this class of nanocarriers. The main self-assembly drug delivery systems can thus be summarised in liposomes, micelles and polymersomes (Figure 1.5).

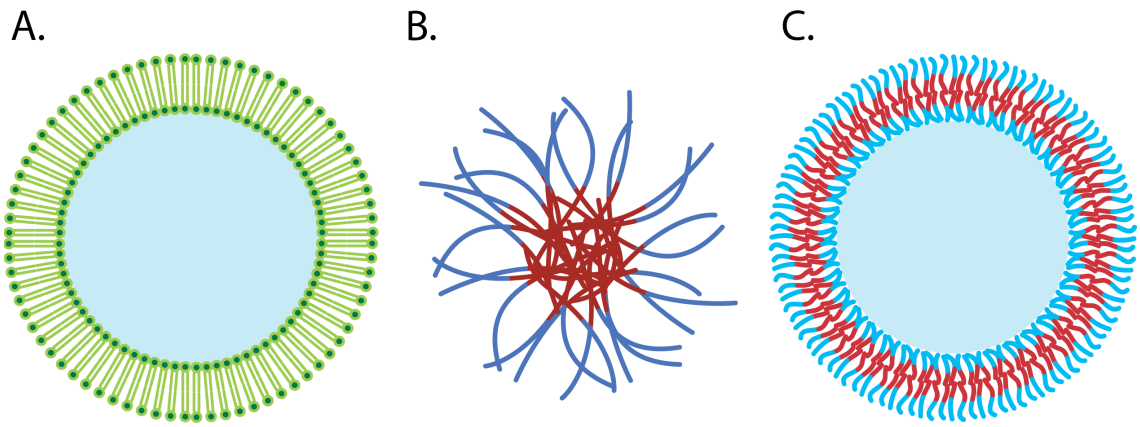

Figure 1.5. Schematic of the main self-assembly delivery systems: (A) liposome; (B) micelle; (C) polymersome.

In the following the main characteristics that belongs to the (A) liposomes and (B) micelles are reported, while the (C) polymersome delivery system will be extensively discussed in the next chapters of this thesis.

A. Liposomes

The liposome is a vesicular nanocarrier with approximately 100 nm in diameter. This nanoconstruct is made by lipids that naturally self-assemble into a bilayer which enclosed the aqueous lumen space. This particular conformation allows the encapsulations of both hydrophilic (into the aqueous core) and hydrophobic / amphiphilic (into the bilayer) molecules. Two different doxorubicin liposome formulations such as Doxil® (pegylated) and Myocet® (non-pegylated) are nowadays commercially available for cancer treatment and several others are undergo clinical trials (Allen and Cullis, 2013).
However, there are still some limitations concerning liposomal preparations. These limitations are mainly due to the liposomes lack of stability and shelf life overtime, and to their eliminations from the blood circulation produced by the RES activity. Furthermore, an adequate liposomal drug release profile is not an easy task to achieve. To this respect, reported experimental data have described liposomal formulations unable to release the cargo at physiological conditions or, vice-versa, they are affected by a too fast release of the drug (Discher et al., 2007; Duncan, 2003; Lasic, 1997).

B. Polymer micelle

The micelle is a spherical nanostructure with a diameter ranging between 10 to 50 nm. This nanocarrier is formed by the self-assembly of amphiphilic block copolymers in aqueous solution. In contrast with liposomes, micelles are characterised by a hydrophobic central core which is surrounded by a hydrophilic corona. Anticancer drugs can be chemically conjugated to the polymer chains that form the micelle or physically trapped inside the hydrophobic core. Several clinical trials are underway for micelle based anticancer therapies (Gong et al., 2012). Furthermore, recently South Korea has approved a paclitaxel loaded micellar formulation made by poly(ethylene glycol)-poly(D,L-lactide) with antineoplastic activity named as Genexol®PM (Lee et al., 2008).
Nevertheless, also in the case of micelle formulations, problems such as inadequate drug release profile can affect the final activity of the delivered drug (Trivedi and Kompella, 2010).

Both liposomes and micelle represent very interesting delivery systems for enhancing the activity of therapeutic drugs. Liposomes are able to entrap both hydrophobic / amphiphilic compounds within their membrane and hydrophilic molecules into their lumen space. Nevertheless, this delivery system is also characterised by negative aspects such as limited loading efficiency, lack of chemical / physical stability overtime, and restricted chemical versatility (Barenholz, 2001).
An alternative to liposome formulations is a drug delivery system made by block copolymers. Block copolymers with amphiphilic properties allows the assembly of nanocarriers that, compared with liposomes, show an enhanced structural stability and chemical versatility (Bermudez et al., 2002; LoPresti et al., 2009). The superior structural stability of bock copolymer assemblies is mainly due to the major length of the amphiphilic copolymers chain, compared with lipids. This favours the so called entanglement effect between polymer molecules constituting the formed nanostructure, hence promoting the stability of polymeric carriers. Furthermore, block copolymer posses also a lower Critical Aggregate Concentration (CAC), which make the derived polymeric assemblies non-ergodic (Won et al., 2003).

The above discussed micellar structures represent an important example of block copolymer based delivery system. The micellar nano-vector is particularly efficient for the encapsulation and subsequent delivery of hydrophobic compounds trapped inside the hydrophobic-micellar core (Werner et al., 2013). However, the impossibility to use this nano-vector for the delivery of hydrophilic therapeutic molecules is an important limitation of this approach. For this reason, the development of polymeric vesicular assemblies, defined as polymersomes, represents a promising progress on drug delivery. Polymersomes combine the multi-cargo properties that belongs to liposomes to the enhanced structural stability and chemical versatility that derives from the constituents block copolymer units.

1.5 POLYMERSOME

The polymersomes are in essence very similar to liposomes. They are membrane enclosed structures made from the self-assembly of amphiphilic block copolymers in aqueous solutions (Discher et al., 1999). However, they have many advantages over liposomal formulations. The synthetic nature of the amphiphilic block copolymers, which make up polymersomes, allows a greater control over their properties (Discher and Eisenberg, 2002), including stability (Photos et al., 2003), reduced or selective permeability of the membrane (Battaglia et al., 2006; Discher et al., 1999), long circulation times in blood (Photos et al., 2003) and response release of cargo according to stimuli (Ben-Haim et al., 2008; Cerritelli et al., 2007; Du et al., 2005; Meng et al., 2005; Rameez et al., 2008).

Polymersome leads the encapsulation of hydrophobic and amphiphilic molecules within their synthetic membrane, and hydrophilic molecules in their central aqueous enclosed space (see Figure 1.6)(Discher et al., 1999; Discher and Eisenberg, 2002; Onaca et al., 2009).

The combination of all the chemical and physical properties, which give flexibility and stability to those particles, makes them good candidates for a vast range of applications, from drug delivery to diagnostic (Discher et al., 2007). Polymersomes are stable vectors for long retention time and protection of hydrophilic cargoes. This because the loading of hydrophilic molecules occurs by encapsulation, rather than a complexation or a conjugation. Ironically, the

same reason that makes them such protective and stable vectors, gives them perhaps their biggest disadvantage. Indeed, often the drugs encapsulations inside these polymeric vesicles is affected by low efficiency (when there is no interaction with the polymers), especially considering hydrophilic molecules (Photos et al., 2003). In many cases this is not an issue, as it is validated that cells uptake polymersomes very rapidly and in big numbers (Massignani et al., 2009). However, the optimisation of protocols for hydrophilic drug loading is very much recommended.

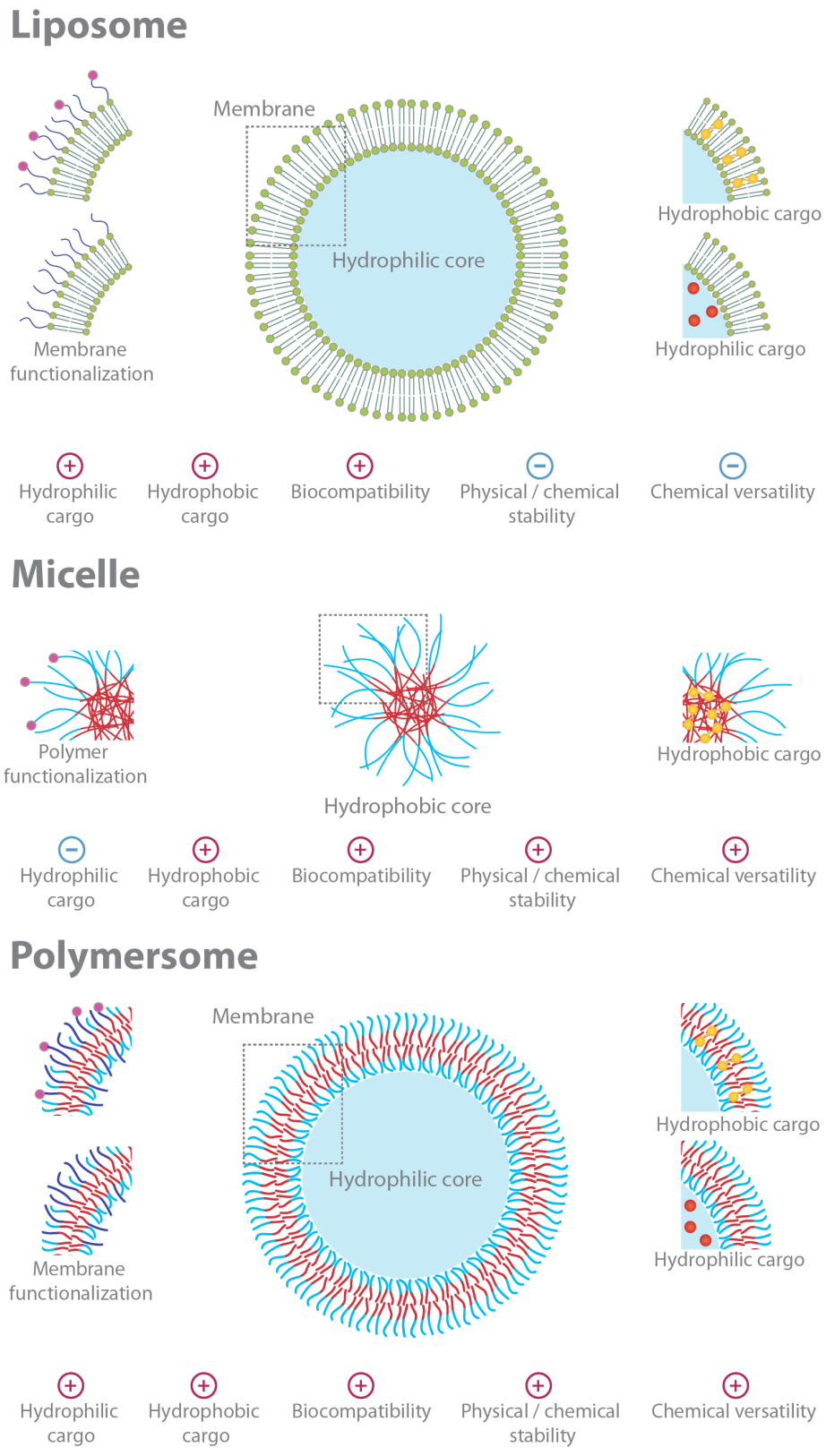

Figure 1.6. Descriptive illustration about the three main self-assemblies delivery systems namely liposome, micelle and polymersome. Both, polymersomes and liposomes are characterised respectively by a synthetic and lipid membrane that encloses a central aqueous space. On the other hand, micelles do not present an internal lumen, instead they are characterised by a hydrophobic core.

The building blocks of polymersomes are the block copolymers. The physical / chemical properties that belongs to the polymersomes unit are discussed below. These properties are fundamental to control and mediate the polymersomes assembly mechanism.

1.5.1 Block copolymers

Block copolymers are macromolecules that are constituted from two or more different polymeric units. Furthermore, depending on the number of distinct polymerised constituents characterising the copolymer, the latter could be defined in different ways. For instance, a polymeric chain of a single polymerised monomer is referred as one block. With this logic, the chemical synthesis of a copolymer of two unequal repeated blocks of monomers will result in a diblock. Thus, a copolymer is defined as triblock when it is constituted from three different blocks of monomers, and a tetrablock when it presents four unequal polymeric blocks. Thus, a diblock copolymer is defined with the following scheme: A_m-b-B_n. Where A and B represent the two distinct polymeric blocks, whilst m and n described the final average degree of polymerisation that belongs to each copolymer constituents. This brief definition of block copolymer can give an idea about the different advantages on the use of the latter as an initial moiety for the assembly of derived vectors.
To this respect, properties such as molecular weight, degradation under specific conditions, conjugations with targeting moieties and many others characteristics can be controlled and modified depending on the final requirements. This enhanced chemical versatility (LoPresti et al., 2009), combined with the high chemical and mechanical stability (Bermudez et al., 2002), favoured the development of block copolymers as new important tools, applicable in several research fields, including drug delivery.

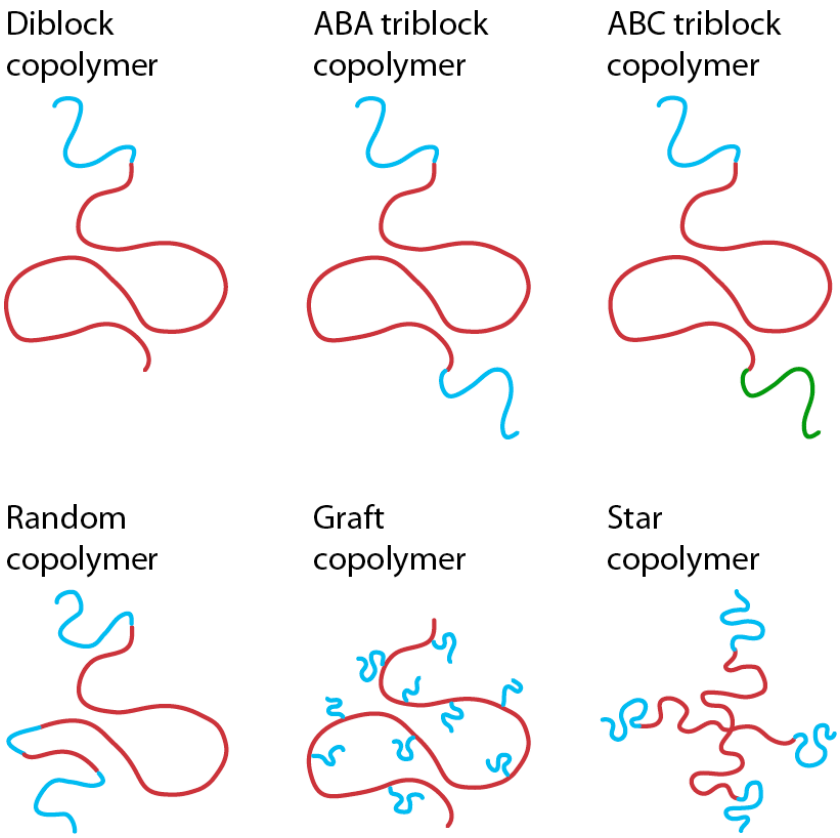

Figure 1.7. Illustration representing different obtainable block copolymer architectures following diverse synthetic approaches.

1.5.2. Self-assembling process of block copolymers

Taking inspiration from nature, the synthesis of block copolymers can be aimed to obtain synthetic molecules that presents physical / chemical properties that mimic biological molecules, such as the phospholipids. The design of such amphiphilic block copolymers will result in artificial macromolecules that have different behaviour depending on the solvent. The solubilisation of the latter in an aqueous solution, for example, could promote a spontaneous self-assembling process that can drive the formations of structures with high complexity. The self-assembling process of dissolved block copolymers directly depend on their concentration on the solution. While the polymer chains are singularly dispersed on the solvent at low concentration, as the concentration value increases and reaches the CAC, the polymer chains becomes close enough to reciprocally interact. This interaction is driven by supramolecular forces, including the hydrophobic effect and hydrogen bonds and, in special cases, aromatic forces and coulombic attractions.

Moreover, properties such as the final shape, the number of aggregates, and the grade of curvature are defined from one important parameter termed as molecular packing factor (*p*).

The *p* value is directly dependent on the molecular properties that characterise the relative copolymer, and it is calculated taking into account three distinct factors: *v*, a_o and *l*. Where *v* is the molecular volume occupied by the hydrophobic part of the polymer chain, a_o is the optimal surface area on the interface between the hydrophilic and hydrophobic portions of it, and *l* corresponds to the length of its hydrophobic part (Nagarajan, 2002; Smart et al., 2008).

The *p* value equation is expressed as follow:

$$p = \frac{v}{a_0 l}$$

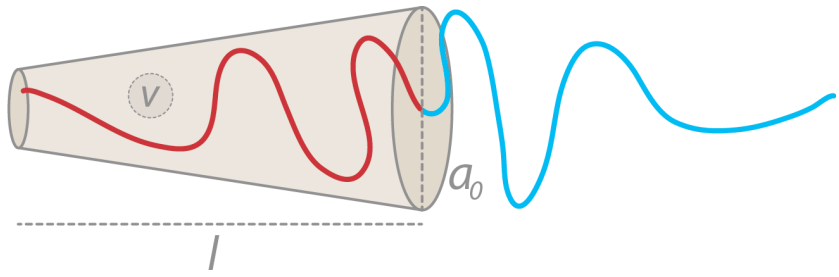

Figure 1.8. Visualisation of the geometrical variables namely (*l*) length and (*V*) volume of the hydrophobic block and (a_0) optimal surface area per molecule that determine the (*p*) packing factor of a single amphiphilic copolymer chain. The hydrophobic block is represented in red while the hydrophilic one in blue.

Considering the *p* value, amphiphilic block copolymers can mostly allows the formations of three different categories of structures: spherical micelles *(p≤1/3)*, cylindrical micelles *(1/3≤p≤1/2)* and membranes *(1/2≤p≤1)* (Figure 1.9)(Bates and Fredrickson, 1990; Fredrickson and Bates, 1996; Matsen and Bates, 1996a; Matsen and Bates, 1996b).

The spherical micelles presents the hydrophobic copolymer part condensed into the core of the structure. *Vice versa*, the hydrophilic block is distributed externally, directly interacting with the aqueous environment.

Cylindrical micelles have high similarity with the spherical shaped. Also in this case, the hydrophobic part is condensed into the core, while the hydrophilic block is distributed externally. Nevertheless, in this case, the higher length

belonging to the hydrophobic block promotes the formation of worms like structures.

Finally, spherical vesicular structures, termed as polymersomes, differ from the others two tridimensional arrangements by the formations of a polymeric membrane that spatially confine an internal aqueous lumen. The size represents an other physical difference between micellar like structures and vesicles. The micelles polymeric arrangement produces, in fact, particles that in aqueous solution have an average in diameter between 10 to 50 nm. On the other hand, at the same solvent conditions, the vesicular particles diameter, ranges from 50 nm up to a micron.

The Figure 1.9 shows schematic representations of these three copolymer based structures.

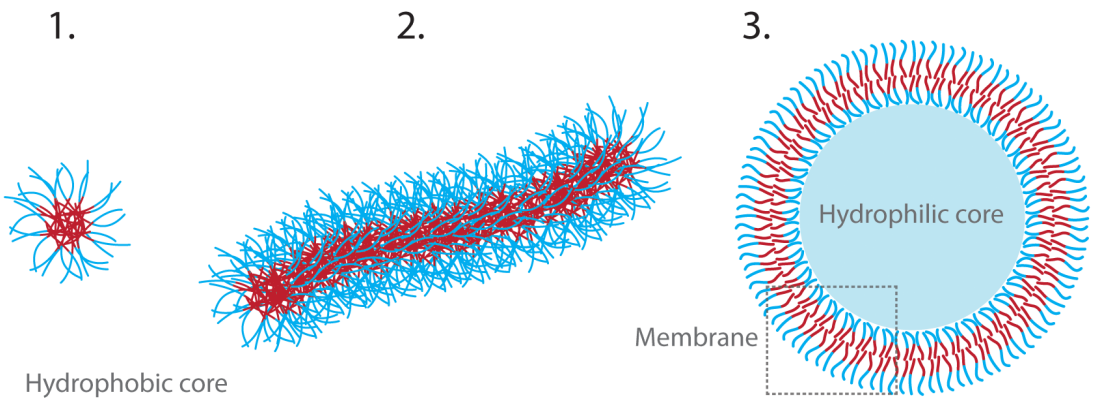

Figure 1.9. Schematic of different self-assembly structures derived from amphiphilic block-copolymer. (1) Spherical micelle, (2) cylindrical micelle, (3) polymersome (Discher et al., 1999).

1.5.3. PMPC-PDPA block copolymer

PMPC-PDPA (Poly(2-methacryloyloxyethyl phosphorylcholine)-co-poly(2-(diisopropylamino)ethyl methacrylate)) block copolymer is a well established polymeric constituent for obtaining pH sensitive polymersomes-like structures. The first block of the copolymer, PMPC, is well known to be highly biocompatible, and characterised by non-fouling proprieties. For this reason, it is approved for many medical uses and it is conventionally applied, in combinations with other polymers, for coating stent implants to avoid thrombus formation, and in contact lens to prevent eye irritation (Lewis, 2000). Furthermore, it is studied as lubricant to mimic the native cartilage extracellular matrix that covers the synovial joints surface (Kyomoto et al., 2014). One of the main advantage of MPC monomers is that they can be polymerised using controlled radical polymerisation, in order to lead to several copolymer combination including: poly(2-dimethylamino)ethyl methacrylate (PDMA) (Yuan et al., 2006), poly(oligo(ethylene glycol) methacrylate) (PEO), poly(2-hydroxypropyl methacrylate) (PHPMA) (Madsen et al., 2009), poly(2-hydroxyethyl methacrylate) (HEMA) (Madsen et al., 2006) and 2-(diisopropylamino)ethyl methacrylate (DPA) (Ma et al., 2003).

The DPA repeated unit, constituting the hydrophobic part of PMPC-PDPA copolymer, has a pH responsive behaviour. The DPA indeed has a pKa of 6.4 at physiological conditions (Bories-Azeau et al., 2004; Pearson et al., 2013).

This gives to the DPA different solubility behaviour depending on the pH of the aqueous. At pH lower than its pKa (pH ~6.4), its tertiary amine group is protonated. Consequently, the PDPA is positively charged and water soluble. When the pH of the solution increases over its molecular pKa (pH ~6.4), it loses the protonations on the amine group and it becomes hydrophobic.

MPC and DPA monomers can be then combined with the aim to obtain pH-responsive copolymers that allow the molecular self assembly, depending on the solvent pH value.

Furthermore, it is also possible to customise the block ratio between PMPC and PDPA to control the type and the size of the structures that the copolymer will form in solution. In this context, it is shown that pH sensitive $PMPC_{30}$-$PDPA_{60}$, produces a pH ~7.2 micellar structures with an average diameter of ~40 nm (Ma et al., 2003). On the other hand, a considerable increase on the DPA degree

of polymerisation drives the formations of vesicular polymeric particles (polymersome) and of other more complex macromolecular assemblies, with size correlated with the final length of the DPA block. Indeed, at room temperature and at neutral pH, copolymers such as: $PMPC_{25}$-$PDPA_{77}$, $PMPC_{25}$-$PDPA_{94}$ and $PMPC_{25}$-$PDPA_{147}$ allows the formations of polymeric structures with respective diameter of: ~100, ~150, ~250 nm (Pearson et al., 2013).

The figure below aims to explain the PMPC-PDPA polymersomes self-assembly process in aqueous solution.

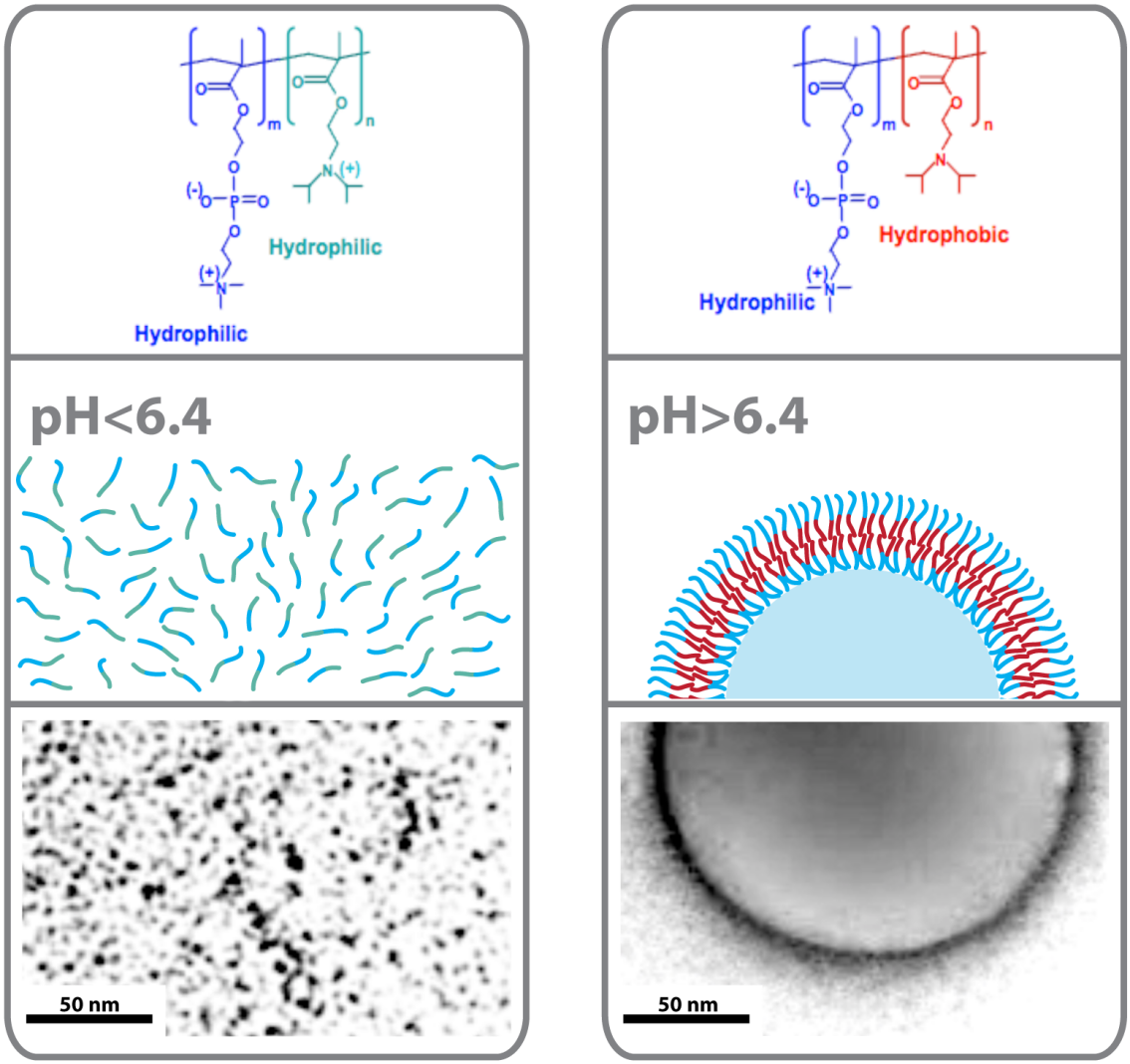

Figure 1.10. Illustration explaining the polymersomes self-assembly process. At acidic pH (lower than 6.4) the PDPA block is water soluble, instead when the pH solution increase over the PDPA molecular pKa (pH ~6.4), the latter loses the protonations on its amine group and it becomes hydrophobic, thus promoting the polymersome assembling.

1.6. POLYMERSOME CARGO ENCAPSULATION

As discussed before, the polymersome-based nanocarrier can be exploited for the encapsulation and subsequent delivery of various cargoes, ranging from hydrophilic to hydrophobic / amphiphilic molecules. In this section, the most common approaches used to efficiently include functional cargoes inside the vector are explained.

1.6.1. Polymersome cargo encapsulation during vesicle formation

The cargo loading can be obtained during the vesicular formation, following two distinct strategies: the top-down or the bottom-up approach.

A. Top-down approach

Top-down approach defines a technique that allows the encapsulation of hydrophilic / hydrophobic-amphiphilic molecules within polymersomes during their formations. This approach includes first the creation of a thin polymeric film on a flat surface. For the encapsulation of hydrophilic molecules in such a way, the new-formed polymer layers are initially placed in an appropriate buffered solution (e.g. water), containing the hydrophilic cargo aimed to be encapsulated. At this stage, it is necessary to rehydrate the polymeric film for producing enough energy to trigger the self-assembly mechanism.
Good examples of some of these methods are ultrasounds, alternating current, and share rate stirring. In such way, the polymeric film progressively detaches from the basal supporting surface. At the same time, it begins to assemble in a range of subsequent phases. These phases are tightly dependent on the final polymer concentration.
High polymer concentrations, for example, push the formations of lamellar like structures, while low polymer concentration induces the vesicles assembly (Battaglia and Ryan, 2006). In any case, with this procedure, the new-formed polymeric structures will include the hydrophilic cargo within the lumen space. This method was largely assessed by Ahmed and collaborators for the efficient encapsulation of doxorubicin-hydrochloride (Ahmed et al., 2006).
The top-down approach can be further used for the encapsulation of hydrophobic / amphiphilic compounds. In this case, hydrophobic therapeutic

molecules such as Paclitaxel, Flutax or phospholipid derivates can be dissolved together with the block copolymer in organic solvent, and then trapped within the polymeric film during its formation. Subsequently, the film rehydration will allows the polymersome assembly, resulting in the inclusion of the previously added drug between the copolymer membrane (Chierico et al., 2014; Lee and Feijen, 2012; Li et al., 2007b).

B. Bottom-up approach

The bottom-up approach is another strategy that consists in a set of techniques that involves the cargo loading together with the vesicular formations.
Nevertheless, despite the top-down approach, both the cargo and the copolymer have to be first solubilised in an appropriated solvent.
This technique is widely used for the encapsulation of complex hydrophilic molecules such proteins and DNA (Canton et al., 2013; Lomas et al., 2007). However, also small hydrophilic and hydrophobic drugs can be loaded within the vesicles in such a way (Ahmed et al., 2006; Yassin et al., 2012). Using this approach for the blocks constituents, the copolymer is initially dissolved in a suitable solvent. Afterward, the initial solvent can be progressively exchanged with a different one. Alternatively, pH and temperature can be also modified to promotes the vesicular formations (Brown et al., 2010; Luo and Eisenberg, 2001; Zhang and Eisenberg, 1995). One example of this process is given by the solvent switch method. This method involves the use of copolymers whose building blocks have different solubility depending on the organic solvent. Thus, the exchange between one organic solvents to another induces different solubility properties on the subject copolymer, finally promoting its vesicular assembly. Since this protocol involves the use of organic solvents, the latter is restricted for the vesicular encapsulation of hydrophobic / lipophilic molecules, which are stable in these conditions (van Dongen et al., 2009). Another method that belongs to the bottom-up approach includes the use pH sensitive copolymers. In this case the self-assembly process is driven by the change of pH of a buffered aqueous solution. The progressive increase of pH, from acidic conditions (pH = ~6.4) to the neutral one (pH = ~7.4), decreases the solubility of the pH sensitive block of the copolymer, thus promoting the formation of amphiphilic polymer chains. In these conditions the copolymer units self

assemble in vesicular structures that include the cargo within their hydrophilic lumen. In this method, the use of buffered aqueous solution makes it suitable for the encapsulation of hydrophilic biomolecules such proteins, which cannot be exposed to organic solvents.

The further development of these two bottom-up techniques (i.e., the solvent exchange and pH switch) allows the evolution of other more complex methodologies. In this context, for example, the elaborations of the basic solvent switch approach has led to obtain the polymersomes formation and cargo encapsulations via the emulsion / centrifugation method. An example of this technique is given by the work of Marguet and colleagues. They proved the possibility to obtain the encapsulations of small drugs, such as doxorubicin, within polymersomes, and subsequently the encapsulations of the latter into giant polymeric vesicles (vesosomes) (Marguet et al., 2012).

Furthermore, concerning the pH switch development, an interesting approach is represented by microfluidic. This technique, like the other bottom-up approaches, combines the simultaneous vesicular formations with the cargo encapsulations. Compared to the standard pH switch formation / encapsulation method, microfluidic allows a higher control in terms of reproducibility of the new-formed polymersomes, and gives the potential of a constant vesicular production over time (Brown et al., 2010; Thiele et al., 2010).

1.6.2. Polymersome cargo encapsulation after vesicle formation

A completely different approach for the payload encapsulations is based on to starting from an opposite way. This means that the cargo can be loaded after polymersomes formations. Techniques that exploit this strategy belongs to the so called post-formation approach. One applied method that works in this direction takes inspiration from nature, and more precisely from the endocytic process.

The “synthetic” endocytic approach is based on the initial interaction between the polymeric vesicle surface and the cargo of interest. Therefore, the established surfaces-surface interaction can culminate with the internalisation of the latter. The endocytic approach is driven by the spontaneous curvature deformations occurring at the interface between the cargo and the polymeric membrane. This membrane deformation process yield the endocytic-like

internalisation of the molecule of interest, which results trapped in a double membrane-polymersome. In literature, Kroeger and colleagues reported the successful application of this system using poly(dimethylsiloxane)-block-poly(2-methyloxazoline) (PDMS-b-PMOXA) polymersomes. In this case, SiO_2 and polystyrene (PS) nanoparticles were used as prove of concept for the mechanism (Jaskiewicz et al., 2012a; Jaskiewicz et al., 2012b).

Besides the endocytic approach, the electroporation (also called electropermeabilisation) is another post-formation procedure applied to achieve the cargo encapsulation after the polymersomes formation. This technology is widely used in molecular biology to introduce molecules dissolved in appropriate media into the cells.

Electroporation generally consists in an externally applied electrical field. When a cell is subjected to an electric shock, it produces at the plasma membrane level a consistent increase of the electrical conductivity, and thus an enhancement on its permeability (Ho and Mittal, 1996b; Neumann et al., 1982). Nowadays, electroporation is used also as a consistent and reproducible way to introduce different cargoes into polymeric vesicles. The method was developed in this directions during this research project (Wang et al., 2012) and it will be further discussed in this thesis (see Chapter 3).

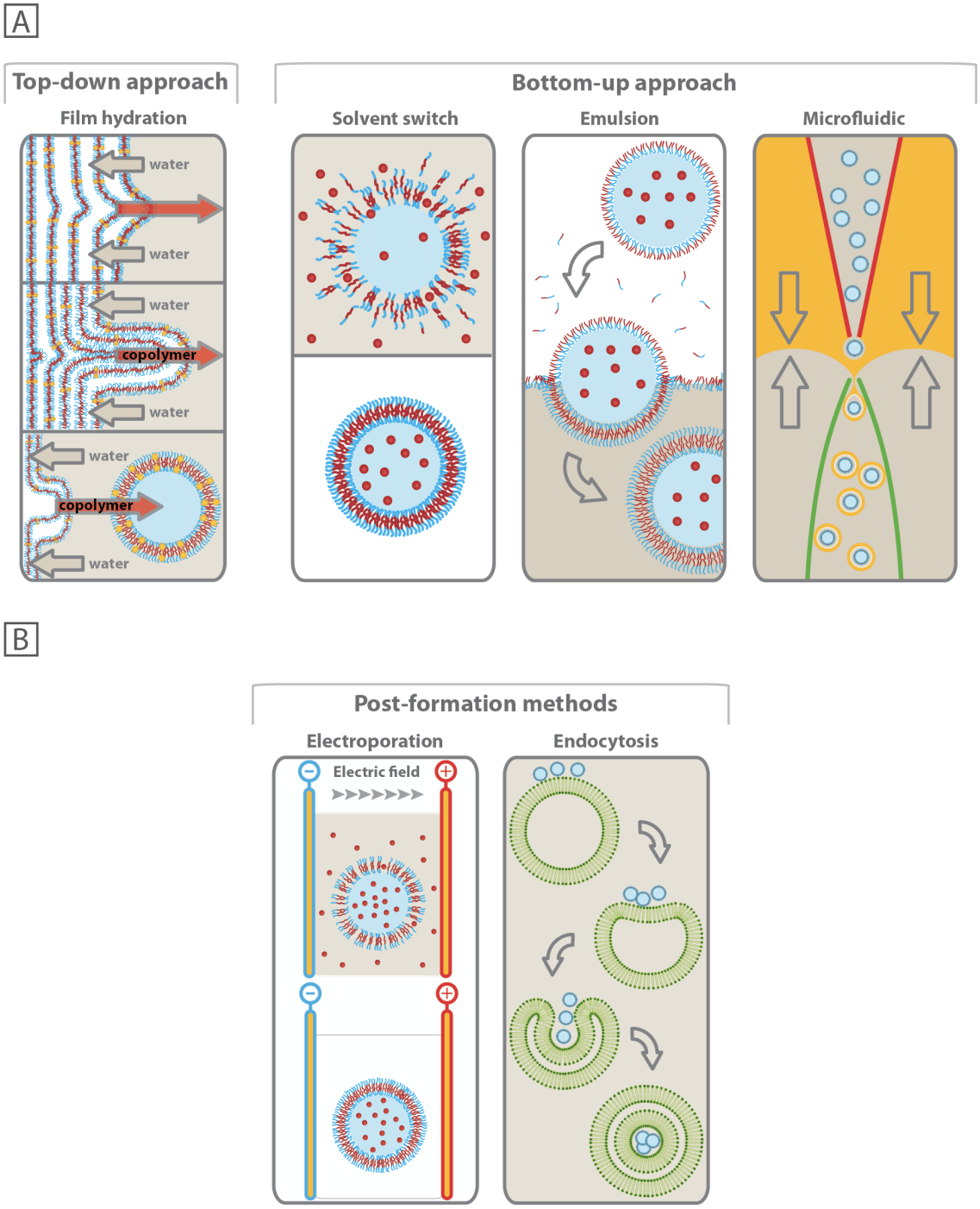

Figure 1.11. The cargo can be loaded within polymersomes during their formation (A) or after that (B). The polymersomes assembly can be obtained starting from the copolymer bulk (e.g. film rehydration; top-down approach) or alternatively starting from a solution containing the free block-copolymer chains (e.g. pH switch; bottom-up approach).

1.7. POLYMERSOME CARGO RELEASE

A critical step for an efficient drug delivery system, beside the achievement of an efficient cargo encapsulation, is represented by the release of the latter on the site of action. The strategies that could be applied for this purpose, with a delivery vector such as polymersome, are typically divided in three distinct release mechanisms. The first one exploits the reverse bottom-up assemble approach, and it is driven, in this case, by the polymersome disassembly under specific chemical conditions. The second approach takes advantage from external physical stimuli, which would force the drug release. The latest herein described mechanism exploits a tuneable release. In this case, the encapsulate drug is released from the synthetic vesicles, with a controlled profile. Therefore, in the tuneable release, the polymersomes gradually increase their membrane permeability. This, in turn, promotes the drug diffusions between intra- and extra-vesicular space.

1.7.1. Polymersomes chemical driven cargo release

One of the most effective and used mechanism to trigger the polymersome cargo release in a specific site (intracellularly for example) is through its disassembly. The polymersome disassembly could be mediated by simply reversing the assembly process. Depending on that, the progressive change of: pH, temperature, CO_2 concentration and eventually the presence of oxidative molecules could lead the copolymer chains dissociation (Lomas et al., 2007; Napoli et al., 2004; Qin et al., 2006; Yan et al., 2013). This dissociation occurs because the chemical / physical properties belonging to the copolymer are modified in these changed conditions. More precisely, the hydrophobic block, composing the latter, switches and becomes hydrophilic. This promotes the elimination of the previous hydrophobic-hydrophobic forces of interactions between different polymer chains, and finally leads to the nano-vector disassembly.

Therefore, in the case of pH sensitive polymersomes, it is shown that the pH switch occurring at the intracellular endosomal compartment (organelle where the polymeric carrier is accumulated after the intracellular uptake) is sufficient to yield the cargo release (Akinc and Battaglia, 2013; Canton and Battaglia,

2012). This intracellular mechanism of release is proper of PDPA based polymersomes, and it will be discussed in details in Section 1.8.
Depending on the chemical nature that constitutes the used block copolymers, polymersomes can exploit other external modifications, such as light or temperature, to achieve the in-situ drug release (Cabane et al., 2010).

1.7.2. Polymersome cargo release under physical stimuli

Beside the chemical driven release approach, other external factors can be use to induce a targeted drug delivery. Physical stimuli, for instance, can be applied to reach this scope. One of these physical factors is defined by the shear forces occurring within the blood vessels. The increase of pressure characterising the capillaries can actually be exploited to produce temporal fenestrations on the subjected polymersomes membrane. This finally leads the outside leakage of internalised drugs (Gaitzsch et al., 2012a; Yassin et al., 2012).
Another release mechanism that responds to physical stimuli works through the vesicular sensing of externally applied UV irradiations. Polymersomes developed to respond to this source of energy possess copolymer chains cross-linked between each other that reinforce their membrane stability. In this case, the UV irradiation, which exposes the delivery site, causes the polymer cross-linking reduction with a consequent increase on the membrane permeability value of the nano-carrier. This would culminate with the cargo release in the external space (Blasco et al., 2013; Cabane et al., 2010; Wang et al., 2014; Yassin et al., 2012).

1.7.3. Polymersome cargo tuneable release

The last way, discussed herein to favour a controlled cargo release, is through a delivery system that combines the characteristics of both the nano-vehicles previously discussed. This means that it would acts by a combination of chemical and physical responses (Chen et al., 2006; Du and Armes, 2005; Yu et al., 2009). Such complex system allows a tuneable drug release that can be controlled over time. The chemically cross-linked membrane of these “swelling” polymersomes are able to react to the changing environment (e.g. pH,

temperature), modifying their membrane permeability in a reversible manner (Yassin et al., 2012).

Polymersomes defined as nanoreactors belongs to this class of delivery system. Nanoreactors are thus vesicles that enclose within their lumen space an enzyme that can be metabolically activated under specific conditions. (Gaitzsch et al., 2012b; Kim et al., 2009). The characteristics belonging to these swelling polymersomes can thus favour the enzyme substrate permeations in certain physiological conditions, thus triggering the metabolic machinery activations. Referring to this typology of vectors, cross-linked synthetic membrane reacting to external stimuli, such as CO_2-controlled acidification, pH, temperature, are exploited to achieve a controlled release. Other reported nanoreactors instead exploit a tunable release, including channels proteins within their membrane. Such transmembrane proteins can thus make the polymersomes lumen space accessible for the cargo diffusion under specific external stimuli (Onaca et al., 2008).

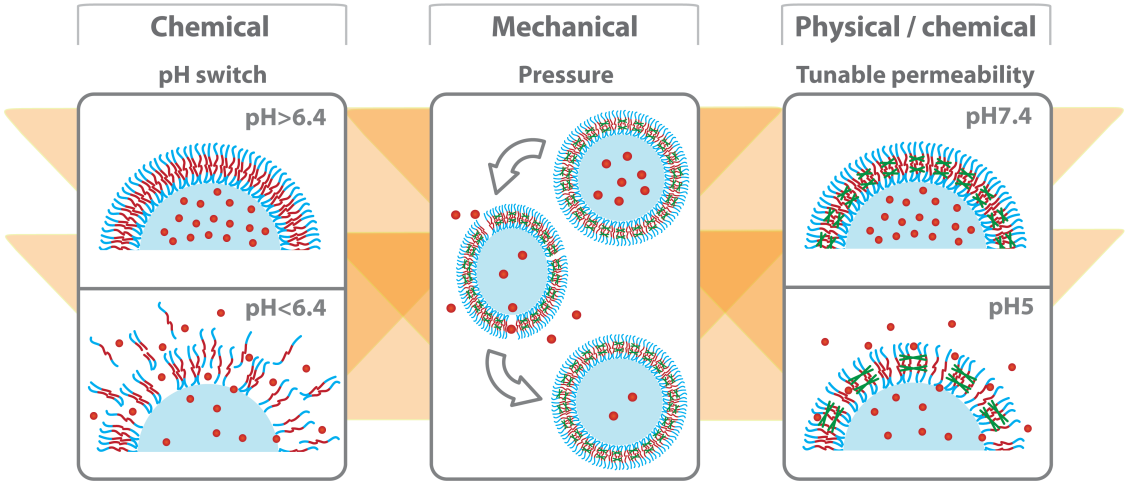

Figure 1.12. The polymersome cargo release can be achieve in different ways and depending on the nanocarrier properties. Chemical release (left), mechanical release (centre) and finally by a combination of chemical and physical responses (right).

1.8. PMPC-PDPA POLYMERSOME CELLULAR UPTAKE AND CARGO RELEASE

A fundamental property characterising an effective drug delivery system is its capacity to be up taken from a targeted cell. Furthermore, after its internalisation, the nano-carrier should allows the escape of the functional cargo intracellularly thus allowing its action.

The biological process that defines the cellular internalisation of extracellular compounds, as previously explained, is called endocytosis (see Section 1.2.5). The endocytosis of synthetic nanocarriers depends from several characteristics that belongs to the latter. The chemical copolymer nature, for example, is one of these important properties that can affect the final vector uptake. In the case of PMPC-PDPA it was recently demonstrated its specific interaction with a precise class of cell membrane receptors. These transmembrane receptors, called scavenger, recognise modified low-density lipoprotein (PrabhuDas et al., 2014).

The phosphorylcholine based chemistry (Poly(2-methacryloyloxyethyl phosphorylcholine)-co-poly(2-(diisopropylamino)ethyl methacrylate), which belongs to the PMPC-PDPA polymersomes, is responsible for the selective interplay of these with the specific scavenger receptor class B member 1 (SR-B1). The recently reported data from Colley et al. correlated the role of this transmembrane protein with the polymersomes interactions within the cells. Moreover, Colley and colleagues correlated the over-expression of SR-B1 in cancerous cells with an enhanced polymersomes uptake (Colley et al., 2014).

Furthermore, not just the copolymer chemistry nature is important to obtain an efficient cellular uptake. Another fundamental parameter that has also to be considered is the final particle size and shape. Several studies already reported that the optimal uptake range size is approximately around 40 nm for polymeric micelles and spherical gold nano-particles (Chithrani et al., 2006; Nakai et al., 2003). The size parameter is critical also for the polymersomes uptake. Recent studies shows that polymersomes uptake is facilitated when these have an average in diameter of 100 nm (Massignani et al., 2009).

Furthermore, is proved that also the nano-vector shape can affect its internalisation within the cells. In this respect, the obtained results from Robertson et al. shows that tubular polymersomes are affected by an

internalisation kinetic much slower compared with spherical vesicles (Robertson et al., 2014).

1.8.1. PMPC-PDPA polymersome intracellular cargo release

PMPC-PDPA polymersomes are biocompatible synthetic vesicles that self-assemble at pH 7.4, formed by pH-sensitive polymer blocks that allows a controlled cargo release inside the cells upon acidification (Massignani et al., 2010b). The highly biocompatible block poly(2-(methacryloyloxy)ethyl phosphorylcholine) (PMPC) is based on phosphorylcholine. The pH-sensitive poly(2-(diisopropylamino)ethyl methacrylate) (PDPA) block (with a pK_a of ~ 5.5-6.5) controls the release in the endo-lysosomal compartment (Massignani et al., 2010b). For this reason, these polymeric vesicles are included in the nanocarriers category that exploit the chemical driven cargo release. Once cellularly internalised, the natural acidification, occurring in the endocytic pathway, rapidly overcomes the pKa of the DPA block copolymer, forcing the polymersomes to dissociate into the single polymer units. This consequently causes an increased osmotic pressure inside the early endosomes, which is compensated by the formation of a temporal membrane destabilisation that allows the cargo release (Massignani et al., 2010b). Rhodamine octadecyl ester loaded vesicles were used to validate this mechanism. LoPresti and colleagues exploited the polymersomes internalised cargo release using two different vesicular formulations. One formulation presented the DPA pH sensitive block, while the other formulation was deprived of it. The two copolymer formulations were thus *in vitro* tested with separate groups of Human Dermal Fibroblasts cells (HDF). Afterward, the cargo release mechanism was evaluated under confocal microscopy.

The reported results shows that the rhodamine loaded vesicles were able to release the cargo within the cytosol just in the case of pH sensitive polymersomes. On the other hand, in non pH sensitive vesicles, the delivered dye was found to be accumulate in limited areas across the fibroblasts cytosol (LoPresti et al., 2009).

These results strongly proved the biological selective functionality of PMPC-PDPA polymersomes as intracellular delivery system.

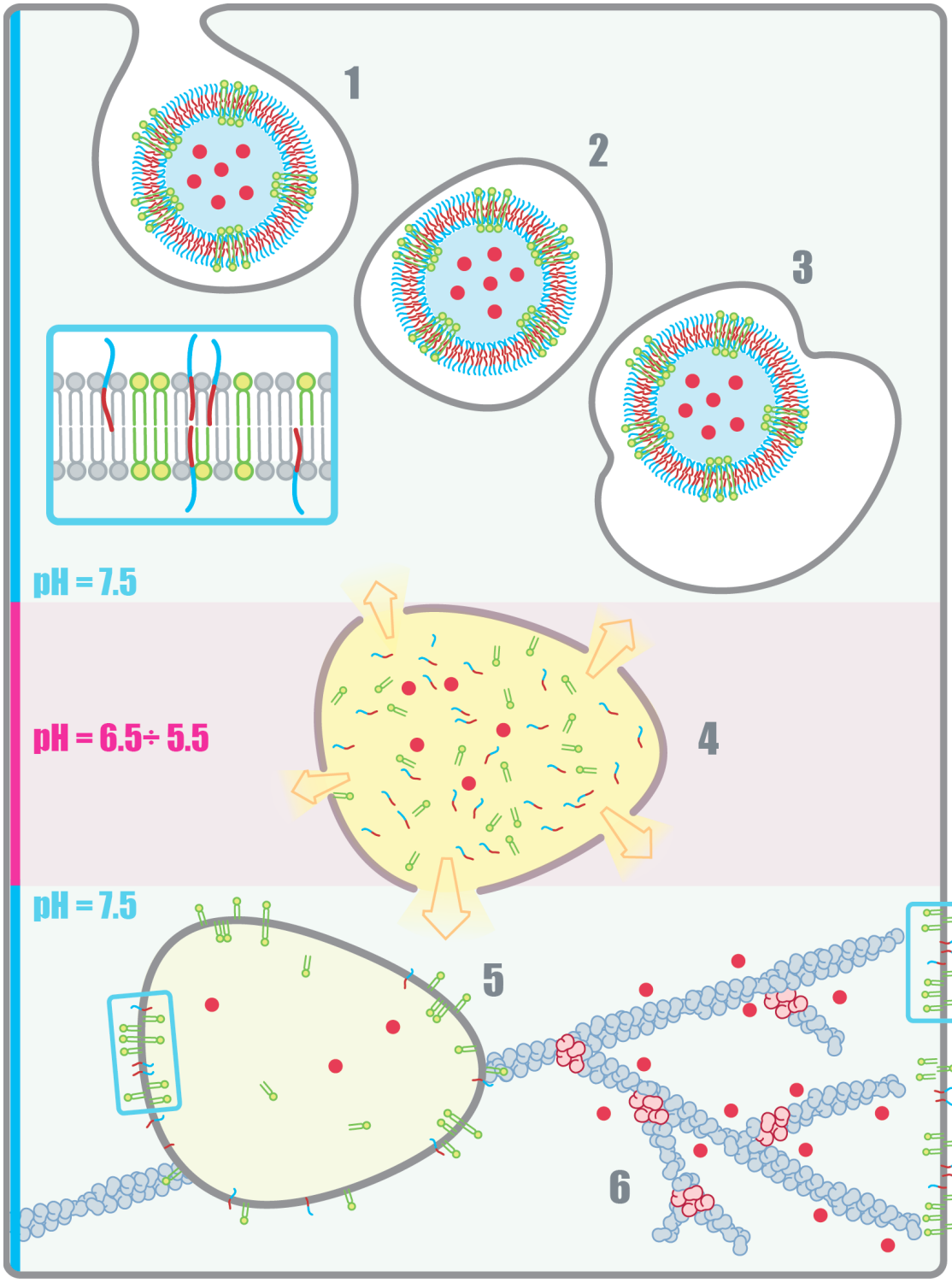

Figure 1.13. Illustration describing the consecutive steps that allows the cytosolic cargo delivery of PMPC-PDPA polymersome. (1) Endocytosis; (2) polymersomes accumulation into the initial trafficking vesicle; (3) sorting into the endosome organelle; (4) temporal membrane osmolysis of the acidic endo-lysosomal compartment; (5) cargo escape into the cytosol; (6) intracellular distribution of the delivered cargo.

1.9. TECHNOLOGIES APPLIED FOR THE DELIVERY OF PEPTIDES AND PROTEINS

In the last decades, the continuous progression of both biotechnology and nanotechnology has allowed important steps for the development of new biopharmaceutical entities. Since the discovery and productions of recombinant human insulin in the in the early '80s (Crea et al., 1978), biopharmaceutical drugs such as therapeutic proteins, anti-tumour enzymes (able to degrade amino acids essential for the tumour progression), anti-angiogenic peptides (angiogenesis inhibitors), antibodies and other biomolecules with therapeutic activity were developed. In 2012, the ~70% of the revenue generated from the first ten most important pharmaceutical industries in the world was obtained by selling biotechnology products (Tufts-CSDD-Impact-Report, 2013).

Compared with small chemical drugs, biotechnology drugs have the potential to be highly specific for their therapeutic target. Nevertheless, these active biomolecules are affected by important negative aspects correlated with their structural complexity. The lack of stability at physiological conditions, fast eliminations from the blood circulation (i.e. via RES) and poor permeability of biological barriers (i.e. skin, mucosa and cell membrane) affects the therapeutic action of peptides and proteins.

For this reason, the latter has to be associated with an appropriate drug delivery system able to overcome the mentioned obstacles. In this direction, over the last years, various delivery approaches were progressed in nanotechnology to optimise the therapeutic activity of biotechnology drugs. Below the principal ones are briefly described.

A. Injectable implants

Injectable implants of drugs are used to achieve a continuous drug release over time of the bioactive molecule within the treated patient. An important example of this category is represented by the Zoladex®, which is a formulation composed by poly(lactic-co-glycolic acid) (PLGA) and gonadotropin releasing hormone superagonist (GnRH agonist). This formulation is mostly used for the treatment of breast and prostate cancer (Kotake et al., 1999).

Other biocompatible polymers such as hyaluronic acid were studied for their applicability in depot formulations (Burdick and Prestwich, 2011). However,

because the application of these implants requires the use of invasive needles or incisions, the patient compliance represents a significative limitation on their use. Furthermore, the free-biomolecules released within the blood circulations are exposed to the RES activity, therefore subjected to renal clearance. Moreover, free peptides and proteins are characterised by poor permeability of biological barriers, such as the cell membrane, thus limiting their applicability to targets intracellular pathways.

B. Modification of peptides and proteins

In order to decrease the injections frequency and to increase the plasma half-life of therapeutic biomolecules (Meibohm, 2012), peptides and proteins can be chemically modified. Hydrophilic polymers such as polyethylene glycol (PEG), sialic acid, hydroxylethyl starch and hyaluronic acid are nowadays widely used for this purpose in combinations with peptides and proteins, and some of these formulations are currently clinically investigated (Constantinou et al., 2009; Mero et al., 2013; Pasut and Veronese, 2012). Furthermore, also the fusion of therapeutic biomolecules with albumin represent a promising way to increase the plasma half-life of a therapeutic modified biomolecule. Indeed, in 2014, the US Food and Drug Administration (FDA) have approved the albumin fusion peptide GLP1(7-36) for the treatment of type 2 diabetes (Bush et al., 2009).
Peptides and proteins can also be modified to achieve their specific intracellular delivery. To reach this scope, different technologies can be used, and these include the Presenting Transduction Domain sequence (PTDs) (Prochiantz, 2000) and chemical modifications with positively charged polyamines (Hervé et al., 2008; Kitazoe et al., 2005; Triguero et al., 1989). However, these modifications, which result with the creations of a new molecular entity, can generate disadvantages compared with the native compound, including reduced solubility and decreased therapeutic activity.

C. Cationic lipids or polymers formulations

Formulations based on the complexation between proteins and cationic lipids or polymers can be exploited to achieve proteins delivery, and their internalisation within the cells. An example of cationic lipid mixture evaluated for this purpose is the trifluoroacetylated lipopolyamine (TFA-DODAPL) / dioleoyl phosphatidylethanolamine (DOPE). Experimental evaluations show that the

complexation between proteins and the TFA-DODAPL / DOPE mixture allows the uptake of the latter in different cell models (Zelphati et al., 2001).
On the other hand, polyethyleneimine (PEI) represents an example of cationic polymer used for the complexation with proteins (Didenko et al., 2005). Although the proteins complexation with cationic polymers or lipids can facilitate their cellular internalisation, these approaches are however affected by downsides such as low plasma half-life (eliminations mediated via RES), inadequate cargo release and cellular toxicity.

D. Nanoparticles

In the last years, various nano-delivery systems were developed in nanotechnology to deliver peptides and proteins. These include viral vectors, liposomes and polymersomes. The first approach consists in the use of viral vectors as delivery systems that can be loaded with the desired protein. In this way, the viral structure can protect the cargo from the external physiological conditions, and release it intracellularly (Kondo et al., 2008). However, this approach is also characterised by negative aspects such as immunogenicity.
The second two delivery systems, previously discussed in Section 1.4.1, namely liposomes and polymersomes, enable proteins internalisation within their hydrophilic core. In this way the cargo is protected from the physiological conditions, thus increasing its plasma half-life. Both these vectors can also be characterised by pH sensitive properties that enable the intracellular release of the cargo, upon acidification at the endosomal level (Diego dos Santos Ferreira, 2013; LoPresti et al., 2009). Indeed, the possible intracellular delivery of biomolecules is still one of the most difficult target to be achieved. In this context, delivery systems such as pH sensitive liposomes and polymersomes represent promising technologies to introduce, and subsequently release, therapeutic biomolecules such as antibodies (Canton et al., 2013). Antibodies are able to target specific epitopes and, for this reason, they could represent a promising and powerful biomolecule to be exploited intracellularly as a potential therapeutic tool also in cancer therapy. The possibility to introduce these active proteins in a live cell could be used to precisely interfere with aberrant intracellular pathways, otherwise inaccessible for the free IgG (Ren et al., 2009). Furthermore, the promising pharmacological properties listed in Section 1.5, which belong to the polymersome nanocarrier, can elect it as an

optimal candidate for the development of new therapies based on intracellular protein delivery.

1.10. Ki-67 AS INTRACELLULAR TARGET IN ANTICANCER-THERAPY

As discussed, antibodies can be potentially used to interfere with mutated intracellular pathway, if combined with an appropriated delivery system.
In this context, mutated epitopes such as Rb, Bcl-2 and the enzyme telomerase, which are associated with uncontrolled cell cycle progression, could represent interesting targets for future anticancer therapies based on the intracellular delivery of IgG. Among the listed factors, another protein demonstrated to play a pivotal role in cell proliferation (Bullwinkel et al., 2006; Jakobsen and Sørensen, 2013) is Ki-67. Ki-67 is a nuclear protein, encoded by the gene *MKI67* on the chromosome 10 (10q26), which is present in two main different splice variants of 320 and 359 kDa (Schlüter et al., 1993). The expression of Ki-67 is strongly promoted during the phases G_1, S, and G_2 of the cell cycle (namely, the active states), while the protein, and its codifying mRNA, are both rapidly down-expressed when cells exit the active cell cycle (i.e., the G_0) (Bullwinkel et al., 2006; Gerdes et al., 1984; Gerdes et al., 1983). The cell transit, via mitosis, is promoted by the cyclin B / cdc2-dependet phospho- and Ki-67 dephosphorylation pathways (Endl and Gerdes, 2000b). The Ki-67 exclusive expression in specific phases of the cell cycle, combined with an overall short half-life, made this protein an ideal candidate for the development of specific antibodies useful for quantifying the cell proliferation, a crucial topic in cancer research (Endl and Gerdes, 2000a; Scholzen and Gerdes, 2000; Yerushalmi et al., 2010). It should be, in fact, mentioned that several studies highlighted Ki-67 as a strong prognostic biomarker for both breast and non-small cell lung cancer (Jakobsen and Sørensen, 2013; Pathmanathan and Balleine, 2013). This, in turn, has important implications for the further selection and improvement of follow-up protocols / treatments based on radiation, chemotherapy, and / or surgery. Despite these promising data, there are however still a high level of uncertainty, regarding both (*i*) the exact Ki-67 molecular function, and (*ii*) its definitive and reliable application for histopathological grating of different cancer types (Jakobsen and Sørensen, 2013; Pathmanathan and Balleine, 2013).

Concerning the first point, in fact, many efforts were mainly focused toward the exploration of Ki-67 as a specific structural nuclear element. Ki-67 was found to interact, for instance, with the fibrillarin-deficient region of the dense fibrillar components, the nucleoli (in the S phase), and the condensed chromosomes (through metaphase) and chromatin (during the anaphase) (Endl et al., 1997; Gerdes et al., 1984; Gerdes et al., 1983; Kill, 1996; Starborg et al., 1996). Furthermore, Ki-67 is associated also with the perichromosomal compartment assembly in human cells (Booth et al., 2014). However, there are not specific studies available on potential extra-nuclear Ki-67 pathways, in order to better understand its possible fate beyond the nucleus as well. With respect to the second point, an unanimously accepted agreement on the prognostic value of Ki-67 is still not available among the published works, mainly because of the different methods used for quantifying the Ki-67 labeling index (which estimates the mitotic activity of a cell population as a ratio between cells in S phase over the total cells) (Jakobsen and Sørensen, 2013). Taken together, all these evidences highlight the overall need to increase the current understanding on the molecular action and regulation of Ki-67, especially regarding its potential extra-nuclear pathways, which are almost unexplored.

In this framework, the possibility to uncover the intracellular fate and regulation of Ki-67 could be crucial to develop a new targeted approach in cancer therapy. Indeed, the results of this investigation can be exploited to develop an innovative anticancer therapy based on the polymersomes intracellular delivery of anti Ki-67 antibodies.

Project Aims

The aim of this project is to use pH sensitive polymeric vesicles, known as polymersomes, to achieve the intracellular delivery of antibodies for anticancer therapy. In this study, the polymersome system used is based on PMPC-PDPA block copolymer. Several studies already proved that the PMPC-PDPA polymersomes can be up taken and internalised by cells (Massignani et al., 2010a). Moreover, the pH sensitive properties that belong to the PDPA block allow the cargo escape from the endocytic pathway after cellular internalisation (LoPresti et al., 2009). Therefore, the antibodies encapsulation within polymersomes gave the opportunity to target sensitive intracellular sites, otherwise inaccessible for biological molecules such as immunoglobulins. In this work, the polymersomes stability in biological fluids (and, more precisely, the so called protein fouling process potentially occurring on their surface) was initially investigated. Furthermore, a technique named electroporation was explored to achieve a reproducible and reliable encapsulation of proteins within the nanocarrier. Finally I looked for important intracellular epitopes associated with cell proliferation, cell cycle regulation and the tumorgenesis in cancer cells. This biomolecular investigation highlighted new interesting differences between cancerous and non cancerous cells, regarding the expression and the subsequent degradation of the intracellular protein Ki-67, which is commonly used in diagnostic as a proliferation marker. This protein was furthermore evaluated as therapeutic target for the development of new selective anticancer treatments, by the intracellular delivery of polymersomes loaded with anti-Ki-67-antibody.

The principal objectives of the project are:

I. Polymersomes stability in biological fluids.
II. Antibodies encapsulation within polymersomes.
III. Intracellular delivery of antibodies.
IV. Identifications of new potential intracellular targets for anticancer applications.

Chapter 2

Results and Discussion

SURFACE INTERACTIONS BETWEEN POLYMERIC ASSEMBLIES AND PROTEINS

2.1. Preparation and characterisation of copolymer assemblies

The protein fouling process defines the interactions between proteins and synthetic surfaces. When this process occurs on the surface that belongs to nanocarriers, it promotes the formation of a protein "corona". Such a process, schematised in Figure 2.1, is critical in dictating the final fate of nanoparticles injected within biological fluids.

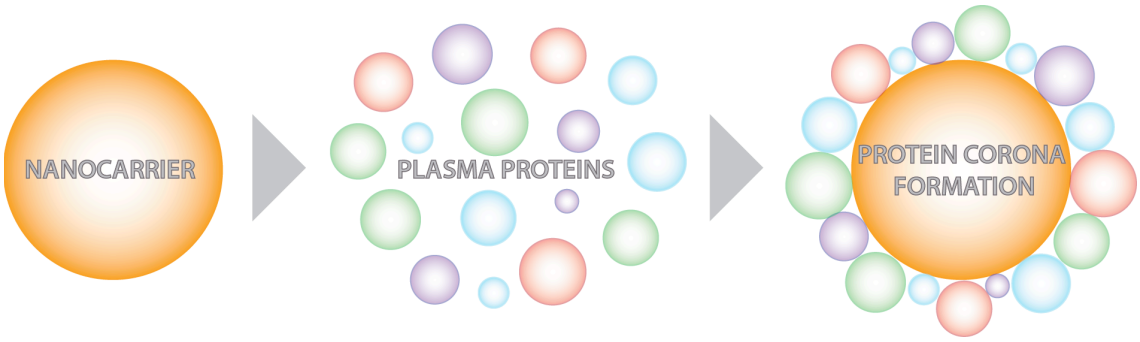

Figure 2.1. Schematic of protein corona formation on the surface of a nanocarrier injected within biological fluids.

These are aqueous fluids rich in proteins and other molecules with protein concentration up to 10% in volume. For example ~8% of blood plasma volume is constituted by proteins (Vogler, 2012). Such a crowded environment promotes the interactions between proteins and nanoparticles, thus controlling the protein fouling process becomes very difficult. Indeed, a nanocarrier covered by proteins has higher probability to be recognised by the immune

system and consequently be eliminated (Vonarbourg et al., 2006). Often the ability to avoid unspecific interaction with proteins is the key to achieve longer circulations times, targeting and consequently achieve efficient delivery.

In this research project, the proposed polymersome nanocarrier aims to be used for the encapsulation of therapeutic proteins and for its evaluations as nanocarrier that can be applied in anticancer therapy. Hence, it is critical to evaluate the possible interaction of polymersome with proteins since the adhesion of the latter on its external surface can result in overestimating the effective protein loading and can further affect its *in-vivo* pharmacokinetics. The protein corona formation on the surface of nanocarriers is affected by various properties including electrostatic interaction, hydrophobic effect and more specific interactions associated with defined chemical moieties such as hydroxyl groups which can interact with thioester groups (Pfeiffer et al., 2014; Tenzer et al., 2013). Protein fouling can be prevented by a combination of chemical and physical properties. From a chemical point of view, the ideal surface chemistry that characterise a nanocarrier should have a neutral nature that favours interaction with water molecules rather than other solutes. Polymers such as PEG (polyethylene glycol), PMPC (poly (2-methacryloyloxyethyl phosphorylcholine)), PVA (polyvinyl alcohol), PVP (polyvinylpyrrolidone), Dextran, and many others have the ability to strongly interact with water (Träubel, 1999). Such a preferential interaction hinders the protein adsorption since the latter have to first displace the water molecules to be able to bind to the polymer. However, when it comes to use this approach to coat either surfaces or nanoparticles, the chemical nature of the applied polymer is not sufficient to prevent the protein fouling. In fact, a surface coated with a dense polymer brush is required to form a steric hindrance. In presence of such surface coating, proteins will have first to deform the polymeric layer to access and interact with the underlying substrate. Thus, parameters such as molecular weight and grafting density are also critical to limit the protein fouling.

At the nanoscale, the interaction between protein and synthetic surfaces are strongly affected by the surface curvature. Several studies have reported considerable differences in protein adsorption between flat surfaces and nanoparticles in terms of kinetics and protein composition (Rahman, 2013). As the nanoparticle size approaches the size of proteins the protein / nanoparticle interaction decreases. Furthermore as the surface curvature increases, the

number of possible protein binding-arrangements decreases considerably (Lynch and Dawson, 2008). As schematised in Figure 2.2-A as the nanoparticle decreases in size, the effective polymer coating with adequate brush density becomes the critical factor. Two surfaces with different curvatures and with the same graft density will have very different brush density with the less curved being denser (Daoud and Cotton, 1982; Nagarajan and Ganesh, 1989). Typically as the curvature approaches zero the highly grafted polymer coating has conformations approaching the Alexander-De Gennes limit (i.e. with the single chains fully stretched). Such a condition gives the densest brush conformation and hence is the most effective in creating steric repulsion (de Gennes, 1980).

As summarised in Figure 2.2-B, for structures where the polymer that form the brush is also a structural unit that control the final geometry such as in micelles and vesicles, the brush density depends on the single copolymer packing density (i.e. the packing factor). Spherical micelles have the least dense configuration with packing factors, $p<1/3$, and vesicles have the densest configuration with packing factor approaching the unit (e.g. $p=1$) (Bates and Fredrickson, 1990; Fredrickson and Bates, 1996; Matsen and Bates, 1996a; Matsen and Bates, 1996b; Rahman, 2013).

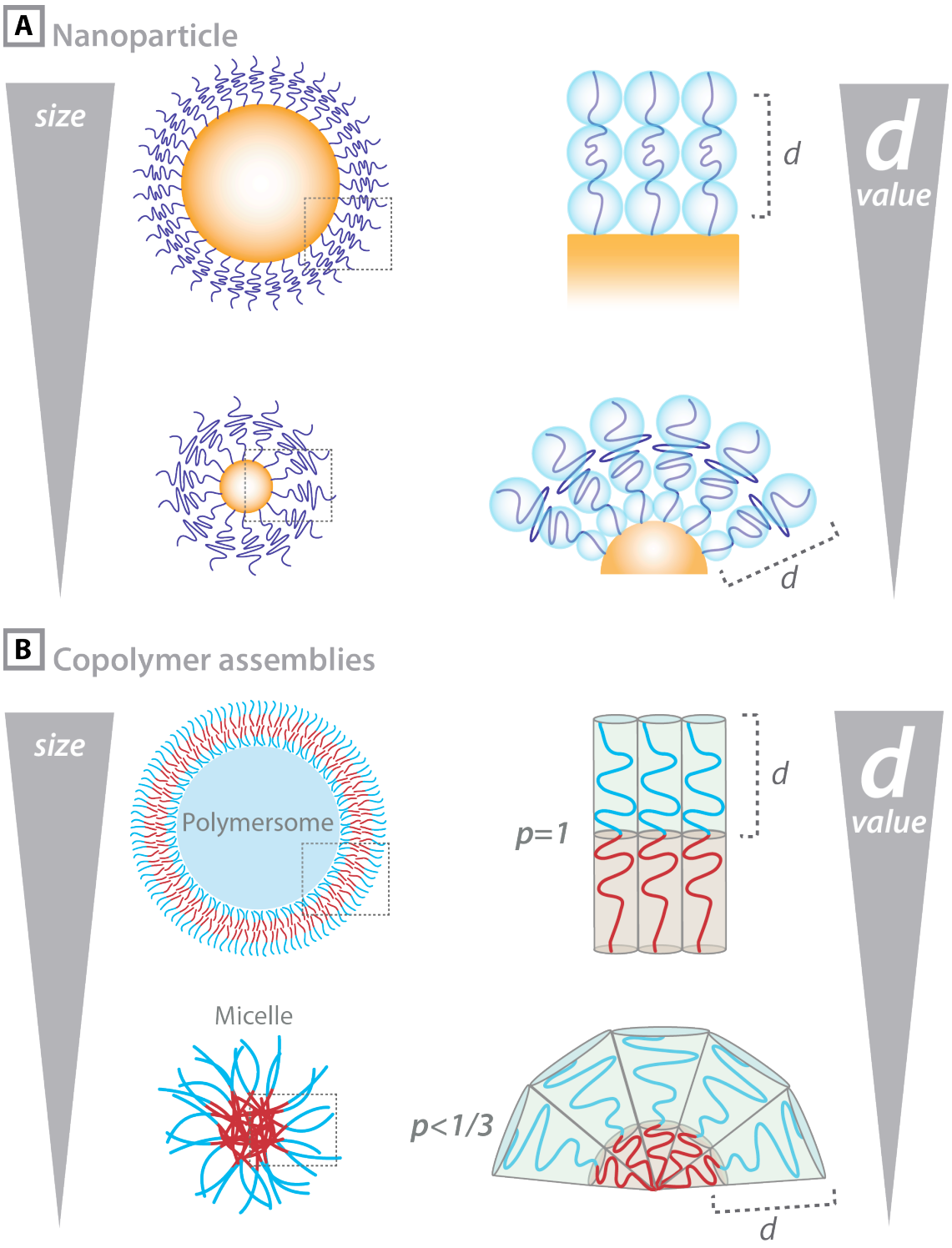

Figure 2.2. (A) Correlation between size and brush density (*d*) in polymer coated nanoparticle, where decreasing the particle size, decrease also the *d* value. (B) Schematic of copolymer assemblies and the factors that in this case contributes on the final brush density. Micelles are characterised by a smaller *p* (<1/3) and thus smaller size compared to polymersomes (*p*=1), consequently they presents also a lower *d* value.

In this thesis project this problem was studied using two well established polymers that are known to prevent protein fouling: the PEG and the PMPC. These are co-polymerised with hydrophobic poly(2-(diisopropylamino)ethyl methacrylate) (PDPA) in two different compositions to form polymersomes and micelles respectively. $PMPC_{25}$-$PDPA_{70}$ and PEG_{45}-$PDPA_{80}$ were used for the polymersomes formations. $PMPC_{30}$-$PDPA_{30}$ and PEG_{113}-$PDPA_{56}$ were used to obtain micelles. The relative protocols for the assemblies preparations are described in the materials and methods section (Section 7.1.2). Polymersomes and micelle dispersions were characterised by Dynamic Light Scattering (DLS) and Transmission Electron Microscopy (TEM) as shown in Figure 2.3.

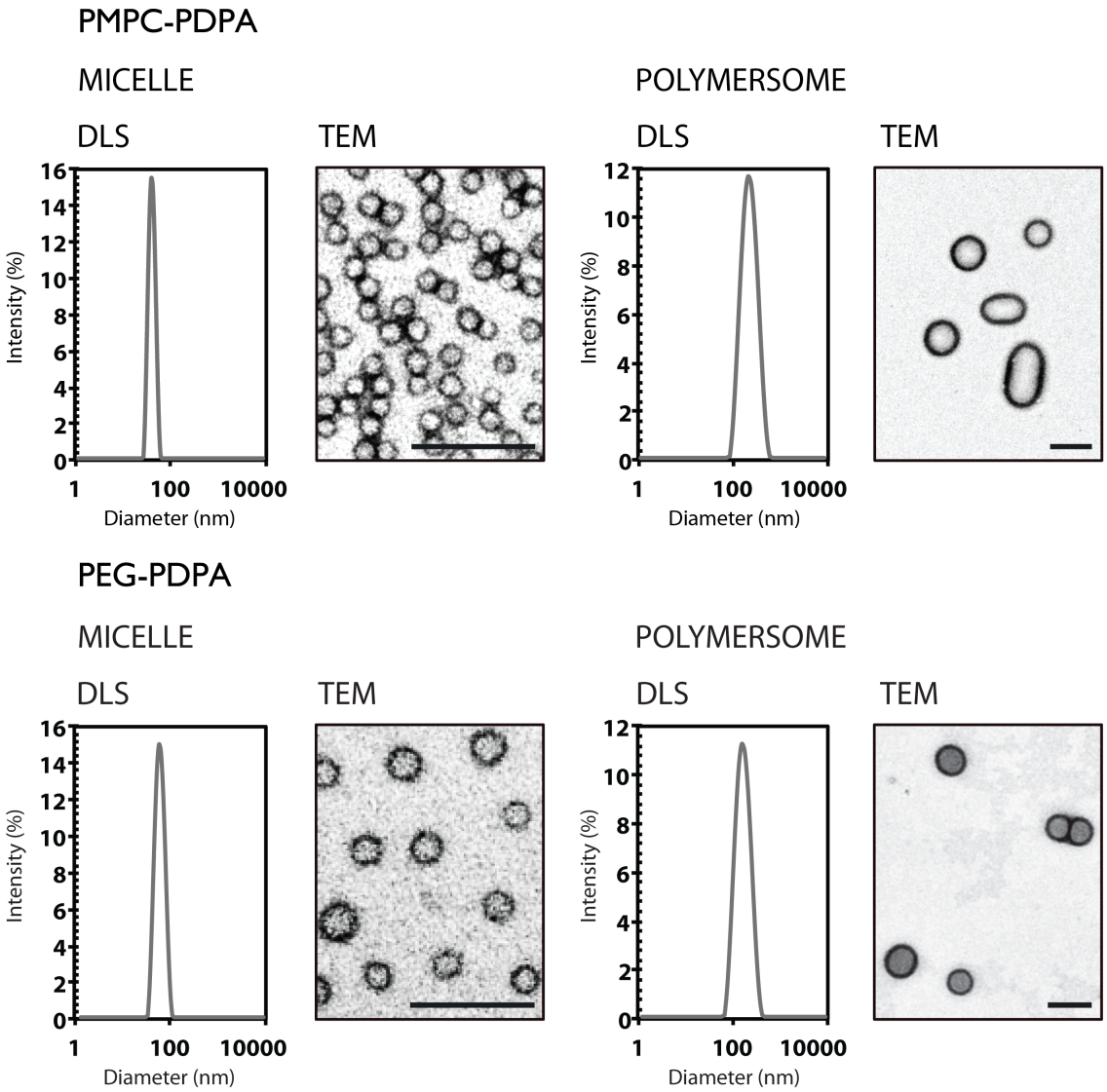

Figure 2.3. DLS and TEM analysis of micelle and polymersome assemblies derived from PMPC-PDPA and PEG-PDPA block copolymers. Scale bar: 150 nm.

The DLS and TEM analyses confirmed the evident difference between the average diameters of the two PMPC-PDPA and PEG-PDPA assemblies. The PMPC-PDPA polymersomes have an average diameter of approximately 150±10 nm, while the micelles have average diameter of 30±10 nm. The PEG-PDPA polymersomes and micelles have an average diameter of 145±5 and 40±15 nm respectively. Proteins such as the Bovine Serum Albumin (BSA), Immunoglobulin G (IgG), and lysozyme were chosen as a models. BSA and IgG are two abundant proteins found in the blood plasma and they are widely studied as models for opsonisation (Giacomelli et al., 2012). Lysozyme is one of the very few globular proteins to have positive net charges and it was used to evaluate the effect of electrostatic interactions. All these proteins were fluorescently labeled with Cy5 (Cyanine5) dye as described in the materials and methods section (Section 7.1.4).

2.2.2. Characterisation of protein fouling process

To evaluate the interaction between proteins and micelles and vesicles we used Size Exclusion Chromatography (SEC) to quantify the amount of protein bound and confirmed this binding using both TEM and Isothermal Titration Calorimetry (ITC).

SEC, initially developed by Moore and colleagues (Moore, 1964), is extensively used for the purification of macromolecules in solution and it can also be applied as analytic tool. The SEC principle is based on the use of a highly porous cross-linked resin that is settled in an appropriate column eluted with solvent (typically aqueous). Such a technique allows the separation of macromolecules and / or particles as a function of their size. The gravitationally driven elution through the resin of small particles requires longer time compared to larger ones. This is because small particles can access more volume than larger particles with consequent longer retention (Figure 2.4).

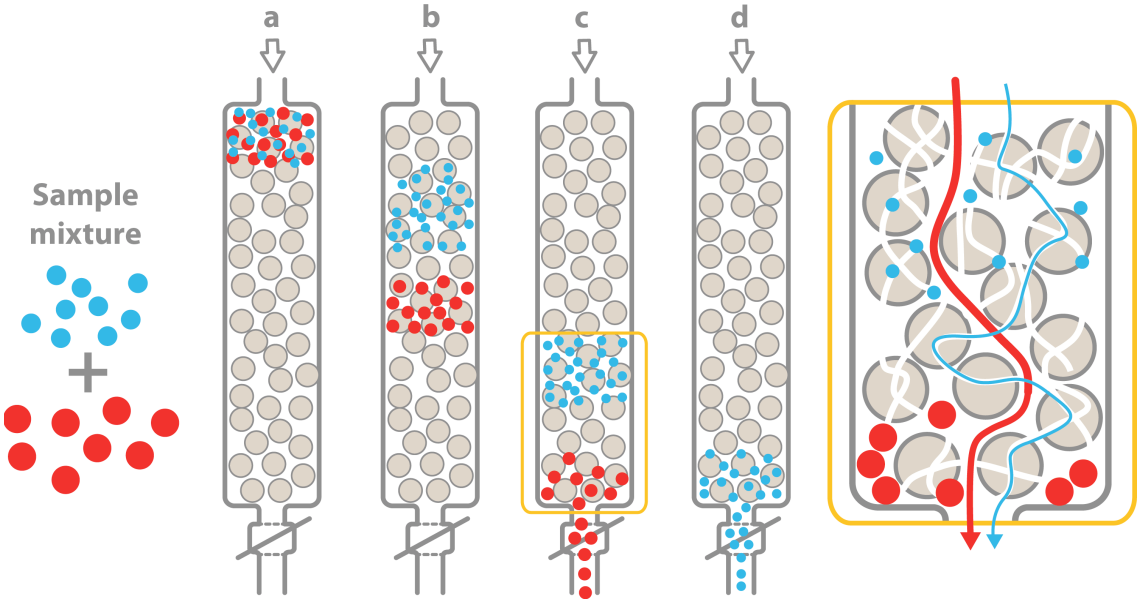

Figure 2.4. Size Exclusion Chromatography (SEC). This technique allows the purification of different macromolecules and / or particles depending on their size. Small macromolecules and / or particles have a longer retention volume compared to bigger particles, thus allowing their separation from the latter.

The concentration used for each experiment of the three tested fluorescently labeled protein; BSA, IgG and lysozyme, was set at 15 μM to avoid unwanted protein / protein interaction and yet enable enough sensitivity for their detection. 12 μM of PMPC-PDPA or PEG-PDPA were used for both, micelles and polymersomes which correspond to at least 100 proteins per particle (polymersome or micelle). Three different samples: free protein, polymersomes and micelles were also prepared at the described concentrations and evaluated separately as controls.

As shown in the chromatograms in Figure 2.5 A-B-C-D-E-F, the elution time resulting from the SEC analysis for micelles and vesicles (either PMPC-PDPA or PEG-PDPA) is respectively of ~35 and ~34 min. Instead, the protein peak is detected after ~78 min. The stationary phase used, (Sepharose 4B) was unable to separate particles larger than 40 nm, but with it was possible to separate effectively smaller sizes. Looking at the resulting spectra at both wavelengths (UV-Vis absorbance at 220 nm and fluorescence emission intensity at 669 nm) it is clear that polymersomes and micelles are detected in the fluorescent channel. Since the PMPC-PDPA or PEG-PDPA were not associated with any

inherent fluorescence is most likely that the signal detected by the spectrometer is derived from light scattering.

It is important to notice that no interactions were revealed for the mixture of protein (BSA, IgG and lysozyme) plus polymersomes. This result was confirmed in both PMPC-PDPA and PEG-PDPA polymersomes. In either cases, no differences in the proteins retentions time (~78 min) were found compared to the free proteins controls (~78 min).

On the other hand, the mixed samples between protein and micelle yields to a protein detected peak that appeared characterised by a different retention time (~38 min) and shape compared to the free protein control. The results reported in Figure 2.5 A-B-C-D-E-F, shows this effect in particular considering the fluorescence channel. It is important to notice, that the protein peak detected in mixed samples of protein plus micelle is characterised by a shape that follows the tailing trend that belongs to the micelles chromatogram measured at 220 nm. Taken together, these observations indicate that in a mixed micelles / proteins sample, part of the protein fraction is binding to the micelles. However, not relevant modifications on the micelles retention time are herein detected when these particles are mixed with proteins.

It is believed that this result is due to the small hydrodynamic volume that belongs to the proteins in comparison to the micelles. Thus, the interaction of the former with the micelles could be not sufficient to induce a relevant increment on the complex's size (micelle plus proteins) that can be detected using SEC.

To better explore this hypothesis, a DLS analysis was performed before and after micelle incubation with protein. However, the results of this analysis revealed no difference in terms of average diameter between the two samples (data not shown).

Nevertheless, experiments reported by Giacomelli and colleagues showed using both Small-Angle X-ray Scattering (SAXS) and Static light scattering (SLS) the correlation between minimal increase (~4 nm) on the micelle average diameter with the formation of a protein monolayer (Giacomelli et al., 2012).

It is further necessary to remark that the same results were obtained in presence of either PMPC-PDPA or PEG-PDPA structures.

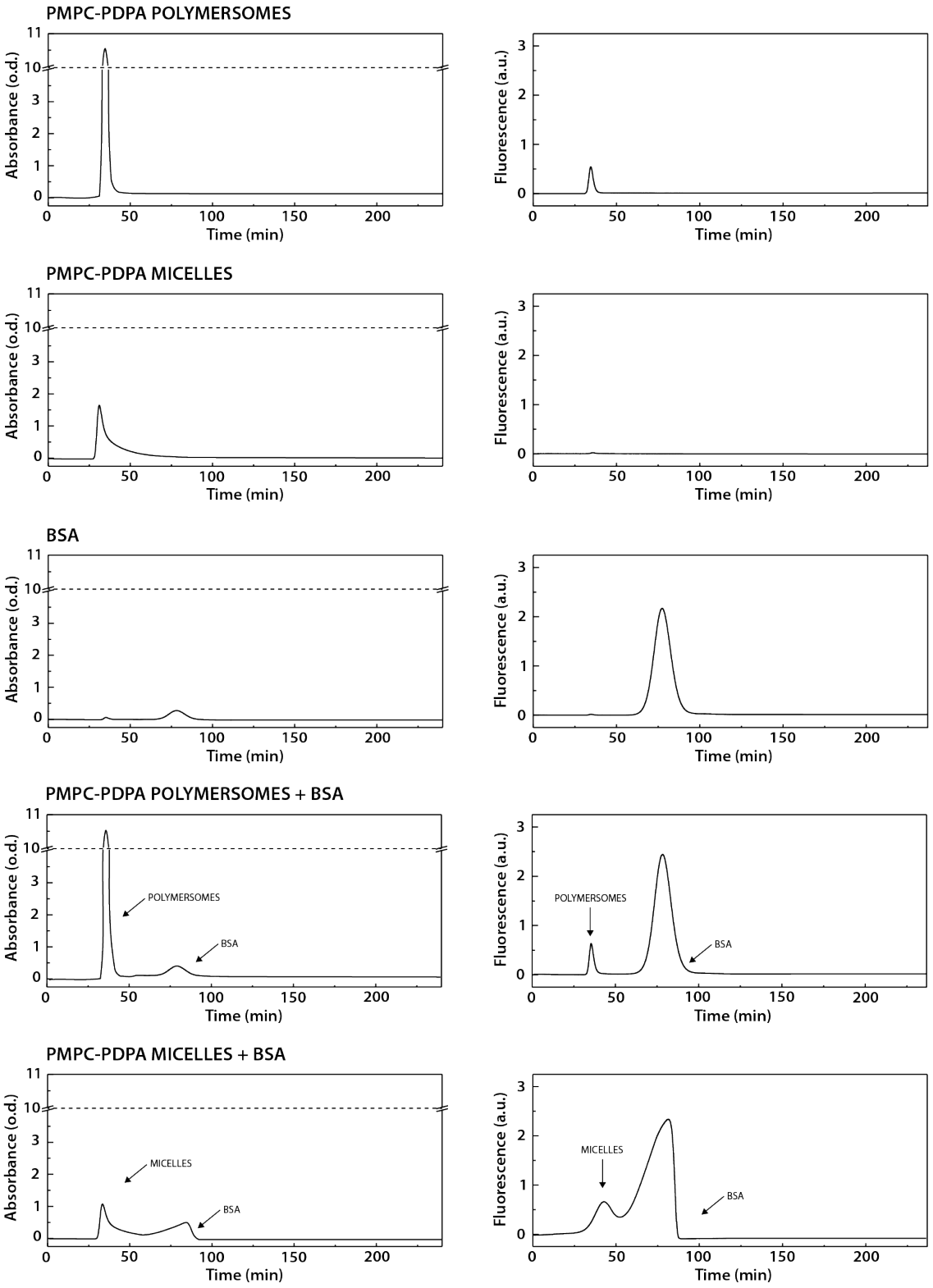

Figure 2.5-A. SEC analysis of PMPC-PDPA polymersomes and micelles mixed with BSA. The chromatograms were obtained measuring the UV-Vis absorbance at 220 nm (left side) and the fluorescence emission intensity at 669 nm (right side).

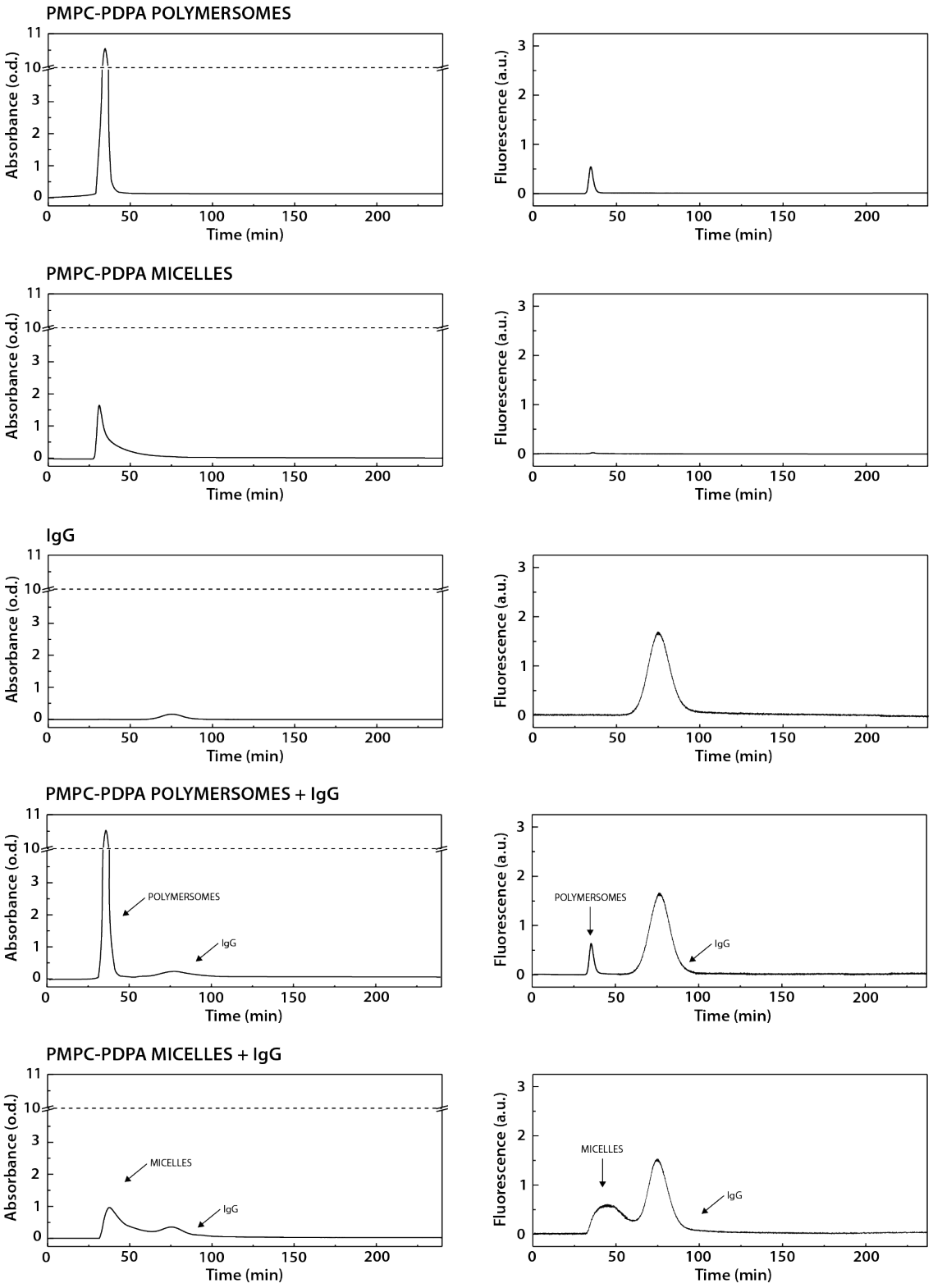

Figure 2.5-B. SEC analysis of PMPC-PDPA polymersomes and micelles mixed with IgG. The chromatograms were obtained measuring the UV-Vis absorbance at 220 nm (left side) and the fluorescence emission intensity at 669 nm (right side).

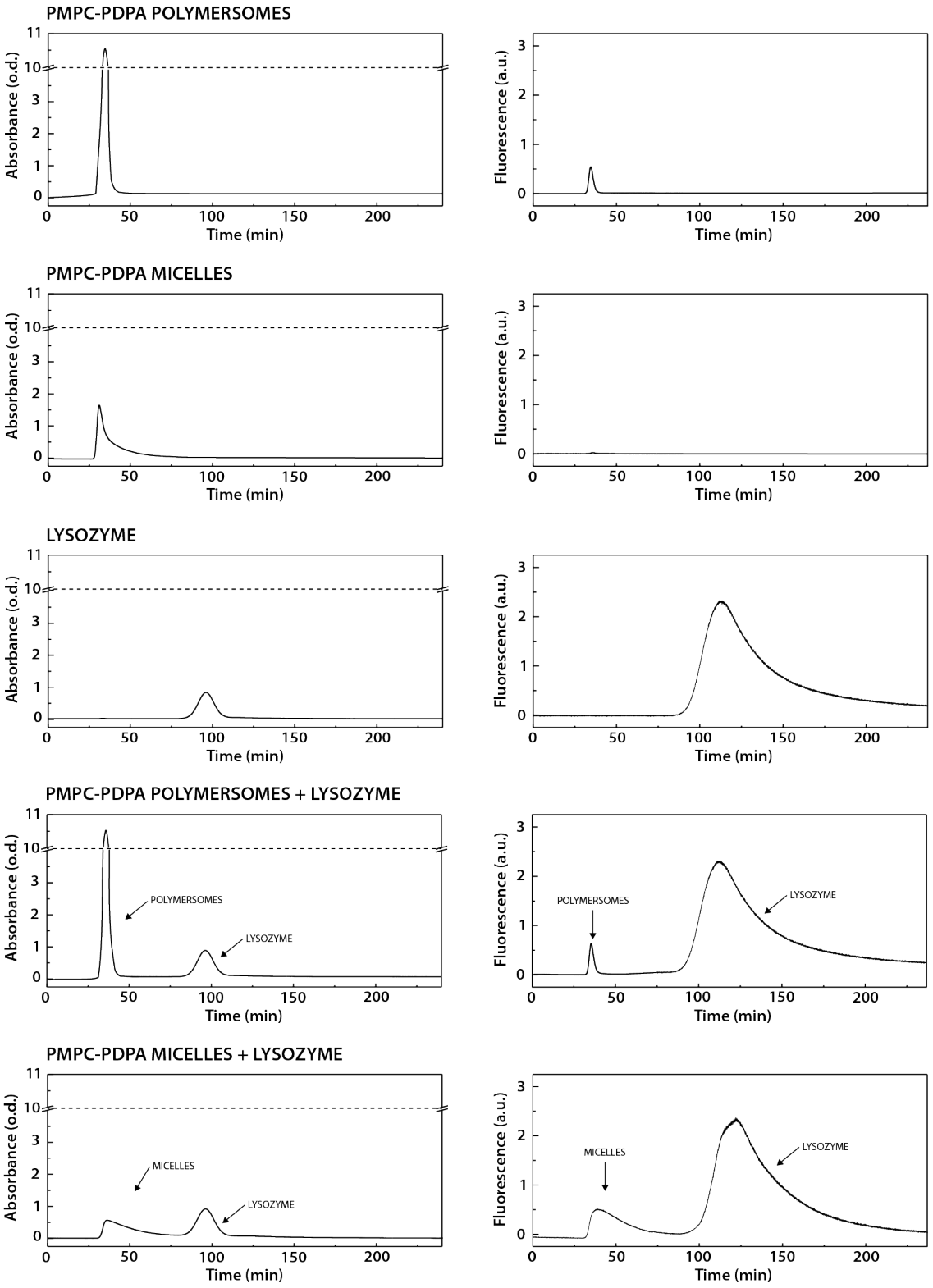

Figure 2.5-C. SEC analysis of PMPC-PDPA polymersomes and micelles mixed with lysozyme. The chromatograms were obtained measuring the UV-Vis absorbance at 220 nm (left side) and the fluorescence emission intensity at 669 nm (right side).

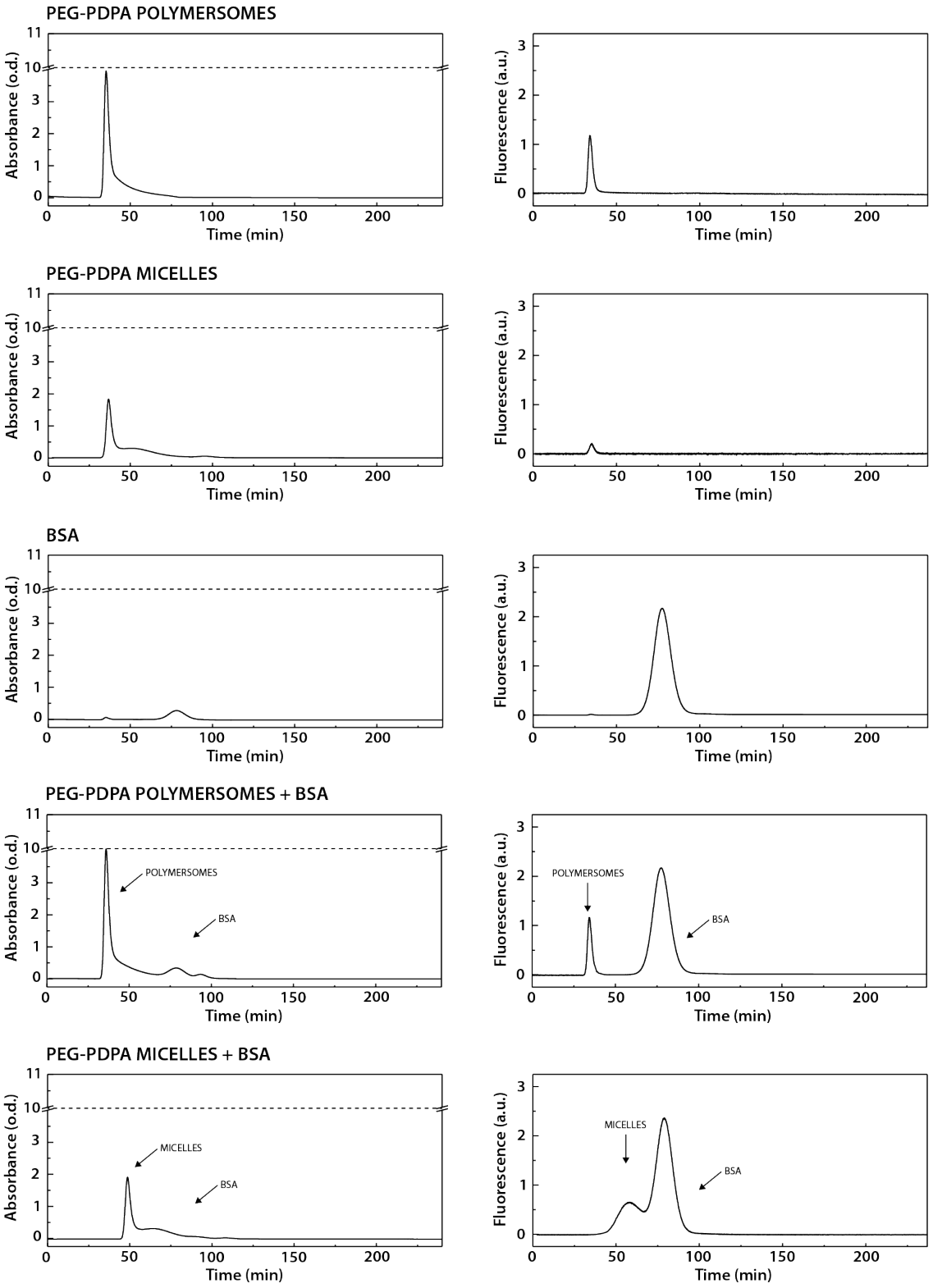

Figure 2.5-D. SEC analysis of PEG-PDPA polymersomes and micelles mixed with BSA. The chromatograms were obtained measuring the UV-Vis absorbance at 220 nm (left side) and the fluorescence emission intensity at 669 nm (right side).

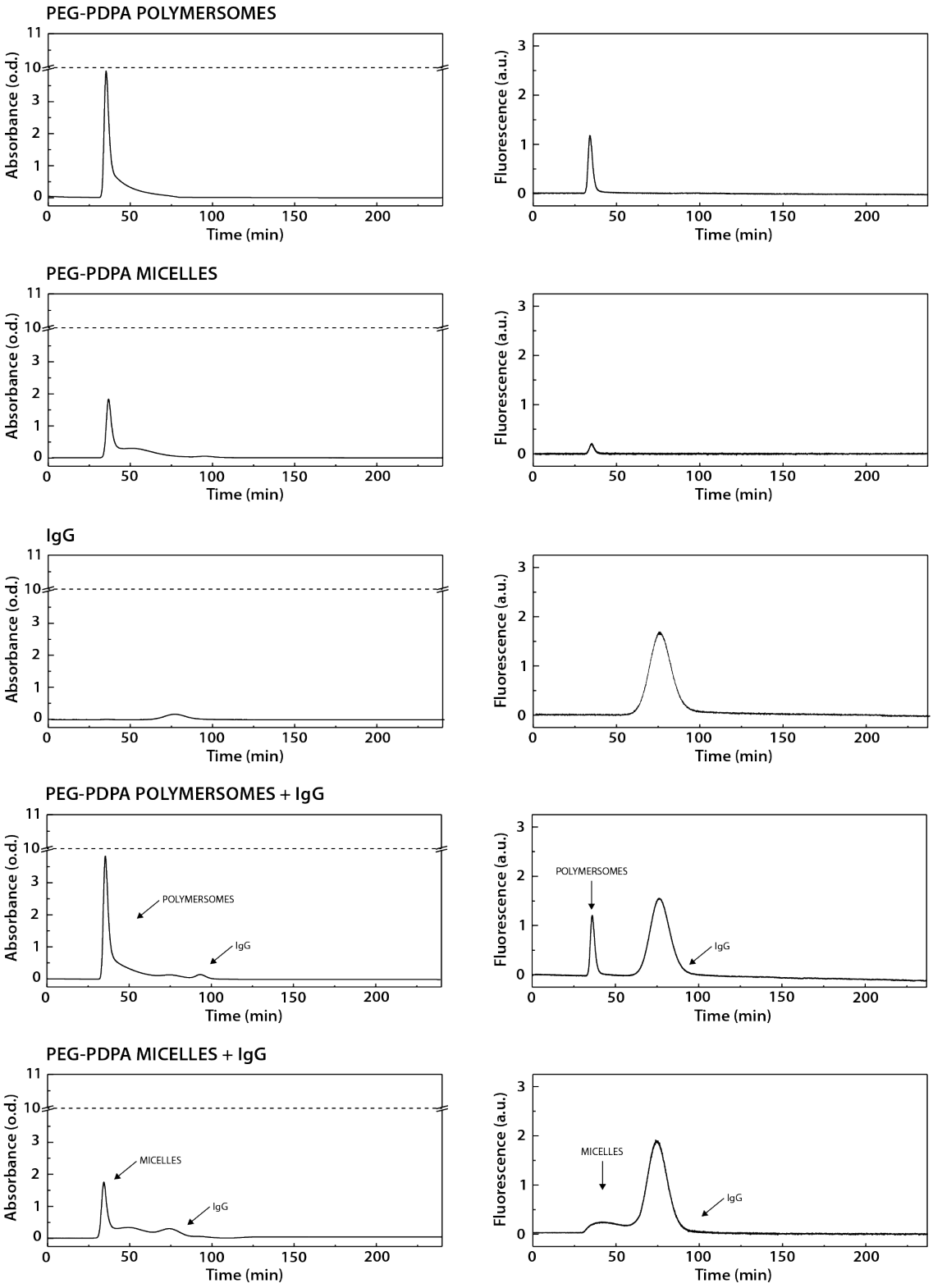

Figure 2.5-E. SEC analysis of PEG-PDPA polymersomes and micelles mixed with IgG. The chromatograms were obtained measuring the UV-Vis absorbance at 220 nm (left side) and the fluorescence emission intensity at 669 nm (right side).

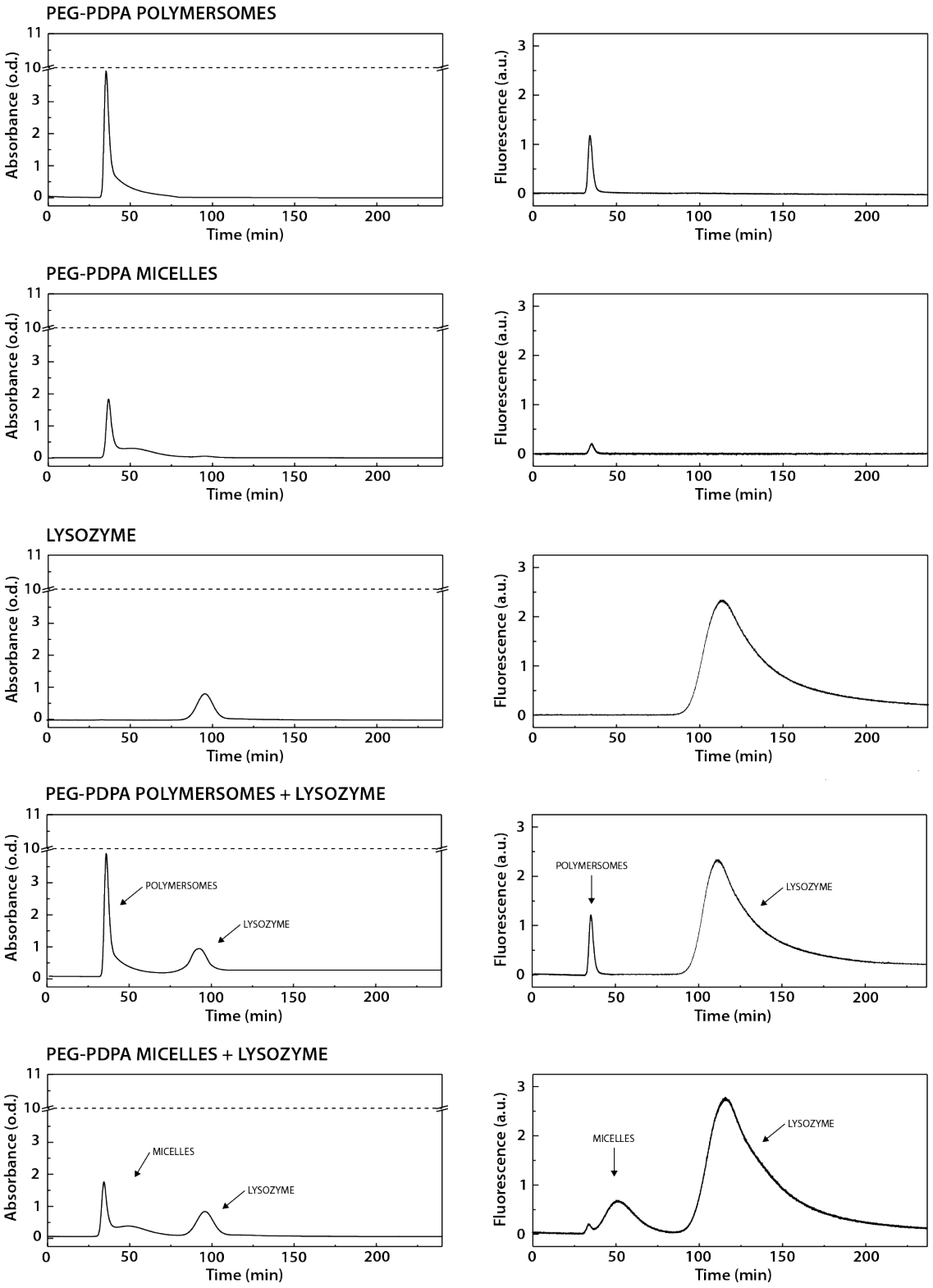

Figure 2.5-F. SEC analysis of PEG-PDPA polymersomes and micelles mixed with lysozyme. The chromatograms were obtained measuring the UV-Vis absorbance at 220 nm (left side) and the fluorescence emission intensity at 669 nm (right side).

To have a direct visualisation of the described micelles / proteins interactions a TEM analysis was also performed. For this purpose, the used model protein is a IgG labelled with 5 nm gold nanoparticle (AuNP-IgG). The presence of the electron dense gold nanoparticle allows the facile identification of the latter under the TEM. To perform this experiment, a final concentration of 1.5 μg/ml AuNP-IgG was placed in 300 μl of PMPC-PDPA micelles or polymersomes sample (10 mg/ml). Assuming a molecular mass of the gold nanoparticle of about 5 MDa (i.e. about 25,000 gold atoms per particles), these conditions corresponds to about 1 AuNP-IgG per micelle. Note that higher concentrations were inaccessible by the experimental set-up. The samples were incubated for about 10 min and purified by SEC. As shown in Figure 2.6, only the micelles show the presence of gold attached to their surfaces with configuration of about AuNP-IgG per micelle confirming the original calculation. On the contrary no gold was detected for the polymersomes sample confirming that polymersomes do not interact with the proteins.

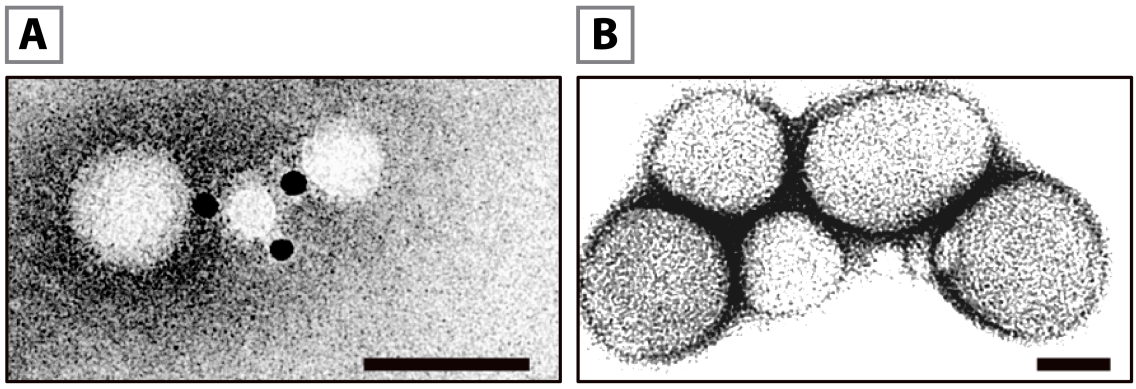

Figure 2.6. TEM characterisation of PMPC-PDPA (A) micelles and (B) polymersomes aimed to visualise their possible interaction with 5 nm AuNP-IgG. As it is possible to see in (A), AuNP-IgG bound the micelles after SEC purification, while this is not the case considering the polymersomes sample (B). Scale bar: 60 nm.

To establish the equilibrium between micelles and proteins, a thermodynamic characterisation of the system was performed by Isothermal titration calorimetry (ITC). This technique is usually applied to describe binding processes, for example between an enzyme and its substrate. The ITC device is generally constituted of two cells, containing separately in each one the

molecular species that has to be studied. One of the two cells, defined as the reference cell, is thermally controlled and capable to sense minimal temperature variations. Thus, for the thermodynamic interaction analysis between two different molecules, the temperature into the reference cell has to be continuously tracked during sequential injections of a species into the other. These injections are then repeated over time, until the investigated interactions analysis reach a point of saturation. Herein the ITC measurement was performed to disclose the energetics of the binding between IgG / BSA to polymersomes or micelles made by PMPC-PDPA or PEG-PDPA. 15.2 μM of analysed protein was initially introduced into the reference cell, and 47.6 μM of polymeric micelles or polymersomes (either PMPC-PDPA or PEG-PDPA) were in turn placed into a syringe (second cell) and injected 10 μl per time at regular intervals into the protein solution. The polymer molarity of the micellar and polymersomes sample, was calculated as a function of the single polymer chain. This would result as a more realistic situation, since the binding effect should be proportional to the surface area per micelle or polymersome rather than the total micelles or polymersomes number on the solution. The obtained ITC data are shown in Figure 2.7.

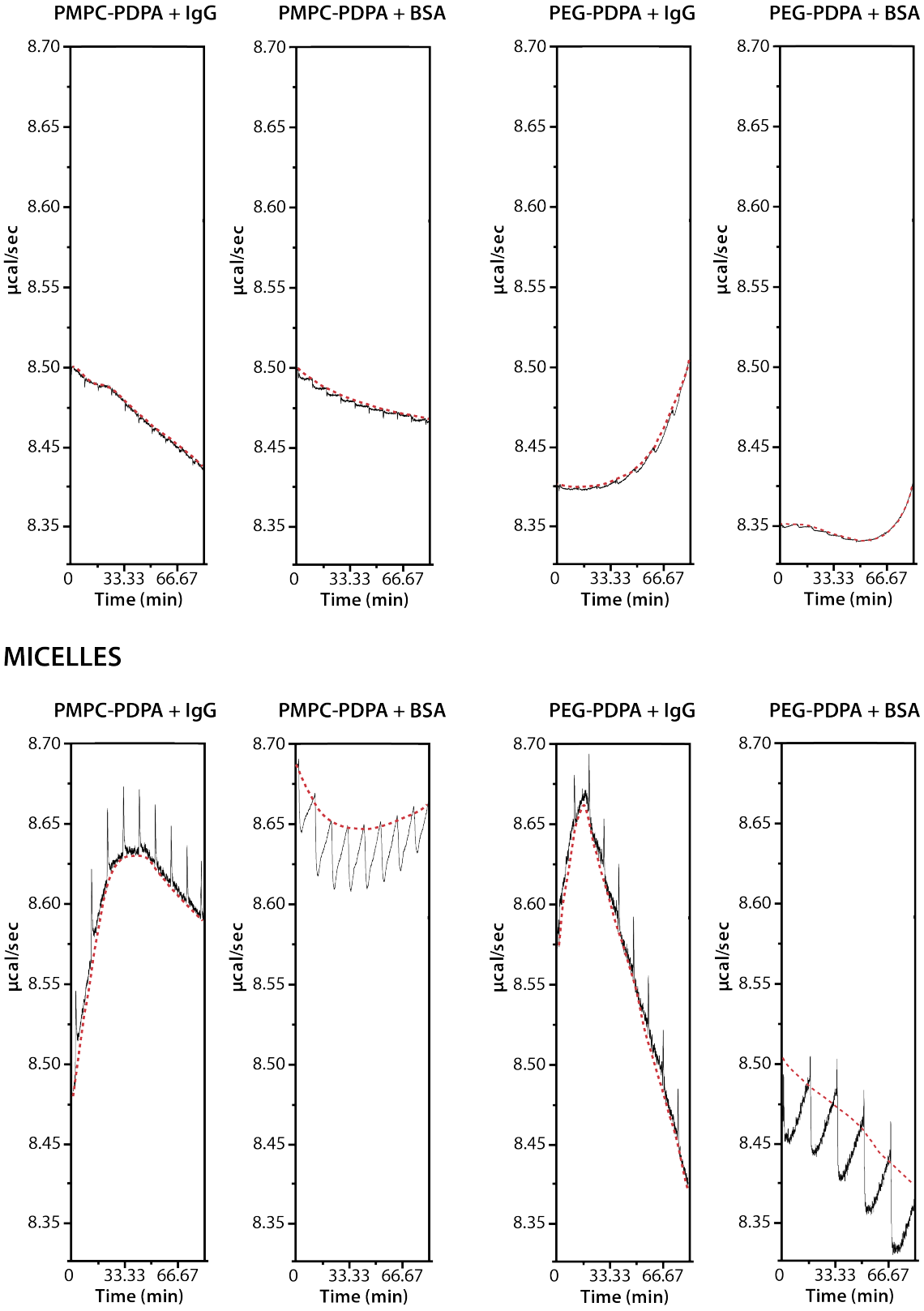

Figure 2.7. ITC analyses of PMPC-PDPA / PEG-PDPA micelles and polymersomes with two different proteins: IgG and BSA. The red line corresponds to the baseline of the measurement.

From the ITC data presented in Figure 2.7 it is evident that the polymersome samples do not show any detectable activity. No peaks were revealed analysing mixed samples of polymersomes plus proteins. On the other hand, the micelles ITC measurements displayed, depending on the experiment, positive or negative areas, indicating the detections of exothermic (negative areas) or endothermic (positive areas) contributions. It is important to observe that all the registered peaks (either positive or negative) have dissimilar area of integration, which indicates different occurring reactions, in terms of thermodynamic properties. This analysis result is quite difficult to be clearly interpreted and the actual measurements are quite noisy. In order to measure and assess the actual interaction between the micelle and the protein, one would have to repeat the experiment using an opposite configuration, i.e. adding small amount of proteins to a fixed amount of micelles. However, this experimental condition would not show the real case scenario. In fact, polymersomes or micelles exposed at normal physiological conditions would be diluted into fluids rich of proteins. While more ITC characterisation is underway, it is only possible to conclude here that the ITC measurements confirm that micelles interact with proteins while polymersomes do not show any detectable binding.

On the basis of these data, is confirmed that proteins interact strongly with micelles and do not interact with polymersomes.

Using the SEC analyses it is possible to parameterise the micelle / protein interaction as an apparent binding constant, K_a:

$$K_a \approx \frac{[P]_{bound}}{[P]_{free}}$$

Where $[P]_{bound}$ is the concentration of protein bound to the micelles, while $[P]_{free}$ is the concentration of the free protein. The $[P]_{bound}$ and $[P]_{free}$ values can be calculated by measuring the area under the peaks obtained in SEC chromatography evaluating the injected mixed sample (micelles / proteins) on the fluorescence channel. Since the most part of the analysed peaks resulted overlapping, the relative areas are integrated applying an exponentially broadened Gaussian (Attila, 1998) as reported in Figure 2.8.

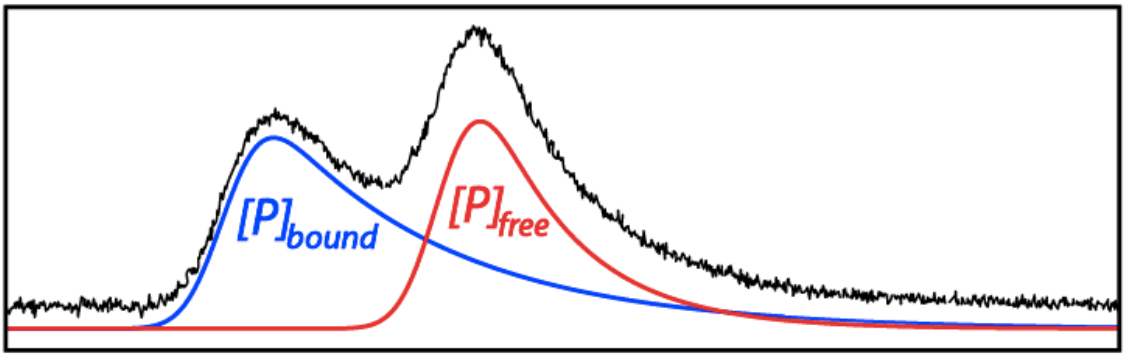

Figure 2.8. Areas of integration for the obtained SEC peaks. The integration was obtained measuring an exponentially broadened Gaussian.

It is important to emphasise that this analysis can only be performed for the micelles samples as the polymersomes samples show no sufficient bound protein and K_a equal to zero. The summarised K_a data calculated at the equilibrium between PMPC-PDPA / PEG-PDPA micelles and the tested proteins are shown in Figure 2.9.

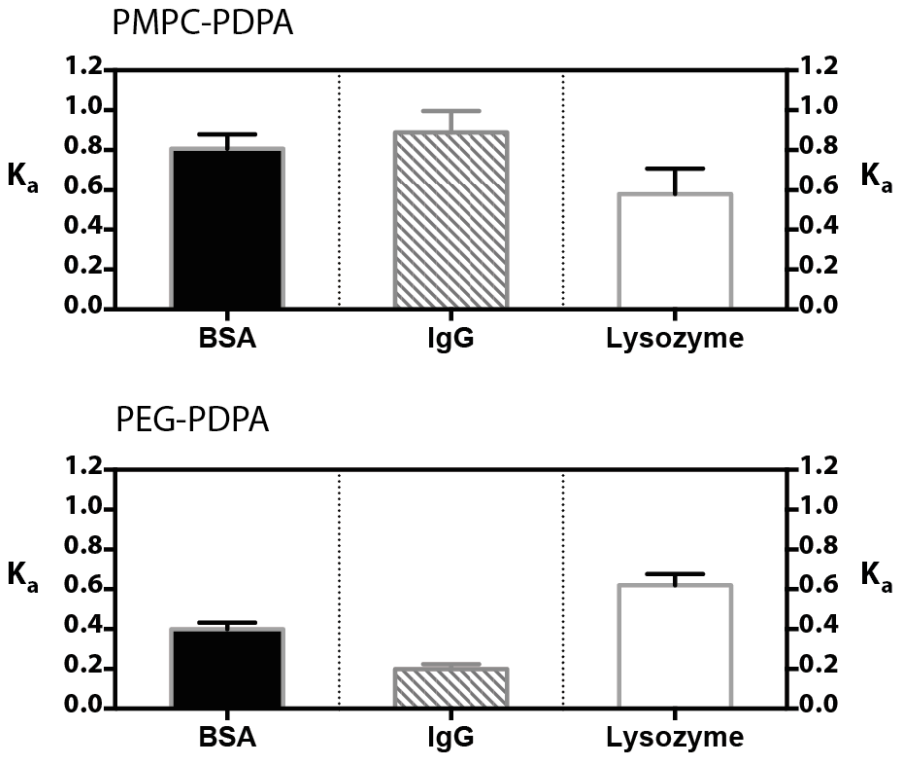

Figure 2.9. Affinity constant (K_a) extrapolated from the SEC analyses regarding the PMPC-PDPA / PEG-PDPA micellar binding with three different proteins namely BSA, IgG and lysozyme. (t-test, p-value * P ≤ 0.05; ** P ≤ 0.01; *** P ≤ 0.001; **** P ≤ 0.0001). The experimental error is expressed as standard deviation (N=3).

The PMPC-PDPA micelles show a similar grade of interaction within all the tested proteins. The resulting K_a values appears to be very similar, ranging from ~0.6 (lysozyme) to ~0.9 (IgG). The PEG-PDPA micelles instead show smaller K_a for the IgG and BSA (K_a = ~0.2; ~0.4) and similar values, compared to the PMPC-PDPA data, for the lysozyme with a resulting average K_a of ~0.7.

Figure 2.10 shows the different properties of the proteins evaluated in this study, using either values extracted from the Protein Data Bank (PDB) or from the literature. The table lists the hydrodynamic radius (R_H, nm), molecular mass (kDa), the protein net charge expressed as ζ-potential (mV) and the hydrophobic Solvent Accessible Surface Areas (SASAs) percentage calculated as reported from Fraternali and colleagues (Fraternali and Cavallo, 2002; Giacomelli et al., 2012).

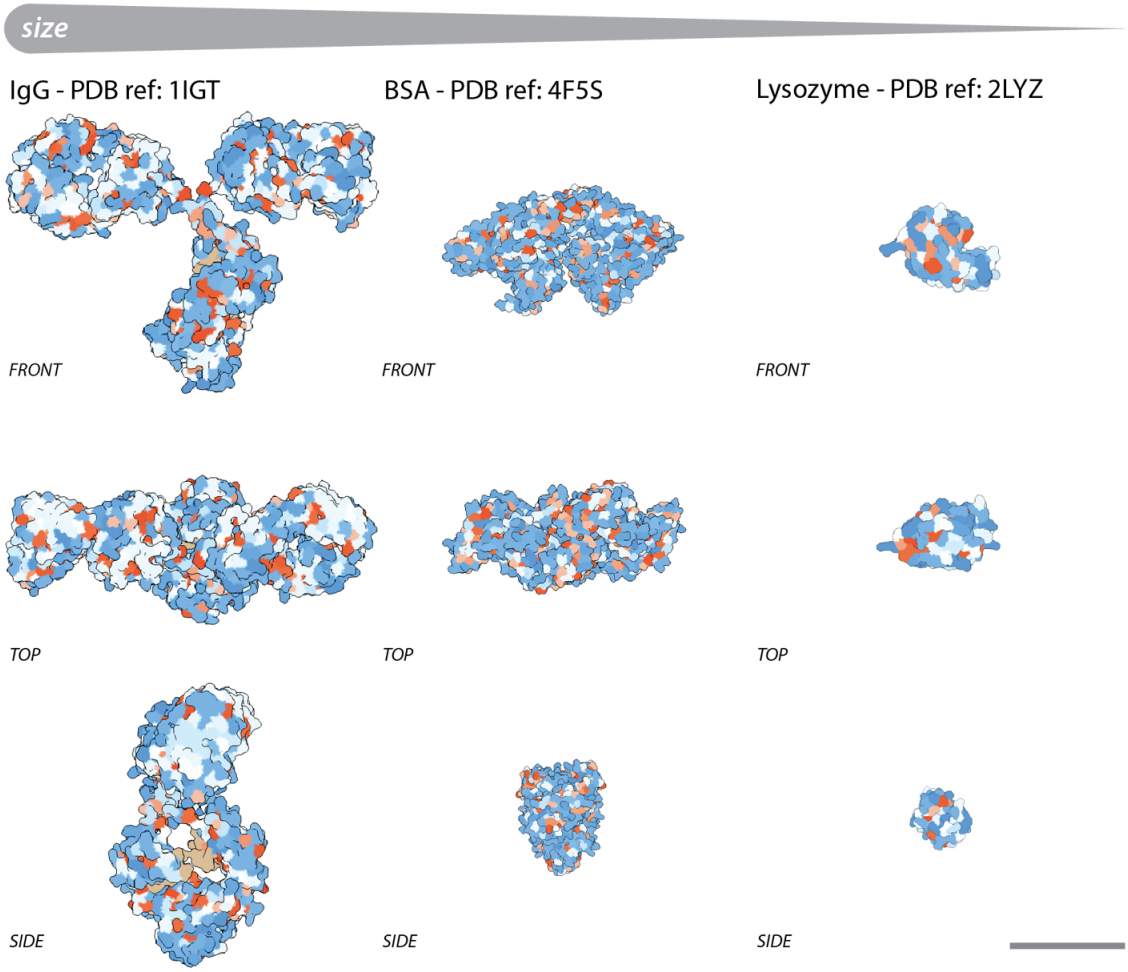

Protein	R_H (nm)	MW / kDa	ζ / mV	Hydrophobic SASAs %
IgG	*7*	*150*	*-13.9*	*56.6*
BSA	*4.2*	*66*	*-27.7*	*54.2*
Lysozyme	*2.1*	*14.4*	*+6*	*33.3*

Figure 2.10. Schematic showing the PDB references and physical / chemical properties such as hydrodynamic radius (R_H, nm), molecular mass (kDa), ζ-potential (mV) and hydrophobic Solvent Accessible Surface Areas (SASAs) percentage that belongs to the proteins evaluated in this study. Scale bar: 2 nm.

The three proteins evaluated in this study have different size, net charge and hydrophobicity and yet the data in Figure 2.9 show little differences on the binding effect revealed between the latter and PMPC micelles. Lysozyme shows in that case a slightly lower interaction with the micelles, however not statistically different from the other two models. On the other hand, the PEG micelles bind considerably less to IgG and BSA than the PMPC counterparts, but the binding to lysozyme is still equally detectable. The correlation with these data and the protein properties listed in Figure 2.10, would suggest that the electrostatic interaction between the residual positive charge of the PDPA (being 10% at pH 7.4 (Pearson et al., 2013) and the proteins are not involved since also the lysozyme (ζ-potential = +6) binds to the micelles. On the other hand, referring to the PMPC-PDPA micelles, a correlation between proteins hydrophobicity and obtained K_a values can be stipulated. Indeed, the greater the hydrophobicity of the protein, the greater the interaction with the micelle. Nevertheless, considering PEG-PDPA micelles, the described K_a trend is not maintained, and the lysozyme represent the protein more interacting. Clearly the data presented shows that PEG is superior to PMPC to protect the micelle from protein fouling. It is important to notice that PEG-PDPA micelles have a size of 40 nm compared to 30 nm for PMPC-PDPA micelles. This difference is due to the difference in the degrees of polymerisation of the hydrophilic block that characterise the two copolymers used. PMPC has a polymerisation degree of 30 while the PEG of 113. Previous studies based on PEG assemblies, show that increasing the degree of polymerisation of the hydrophilic block consequently increase the stealth properties of the nanocarrier reducing the protein adsorption (de Castro et al., 2014). This occurs because longer hydrophilic polymer chains can shield the hydrophobic core of the nanocarrier better than shorter chains and protect it from its interaction with the protein.

Furthermore, a recent study from Giacomelli and collaborators, highlighted the importance of the hydrophilic copolymer chains density (Giacomelli et al., 2012). They observed that micelles formed by PEG as hydrophilic block have a chain surface density per nm^2 equal to ~0.1, which is a considerably higher value compared to PMPC (as hydrophilic block) micelles which are characterised by a value of chain surface density equal to ~0.05. Giacomelli et al., showed that this parameter is a critical factor that strongly affects the interactions between the

hydrophobic micellar core and proteins. In fact, they established that the lower the hydrophilic chain surface density of the polymeric assemblies, the more exposed the hydrophobic micellar core is.

This increases the possibility for the proteins to penetrate the external hydrophilic shield. For this process to occur, the protein size represents a determining factor. Small proteins can penetrate external hydrophilic shield more easily compared to bigger one (Giacomelli et al., 2012).

These assumptions were confirmed from the obtained results where PMPC-PDPA micelles are equally interacting with all the tested proteins while PEG-PDPA micelles presents lower adsorption considering IgG and BSA compared with the higher absorption detected for the lysozyme. Thus, it is possible to rationalised the data for the PEG system as a function of the protein size, with lysozyme being considerably smaller than the IgG and BSA and therefore able to penetrate the polymer brush and interact to the hydrophobic core of the micelle.

However, the most striking observation is that the same copolymer stops protein interaction when assembled as polymersomes and fail to do so when assembled as micelles. As schematised in Figure 2.11, this of course suggests that the copolymer conformation has a fundamental role in this process and that the brush density correlated with the copolymer assemblies play a pivotal role.

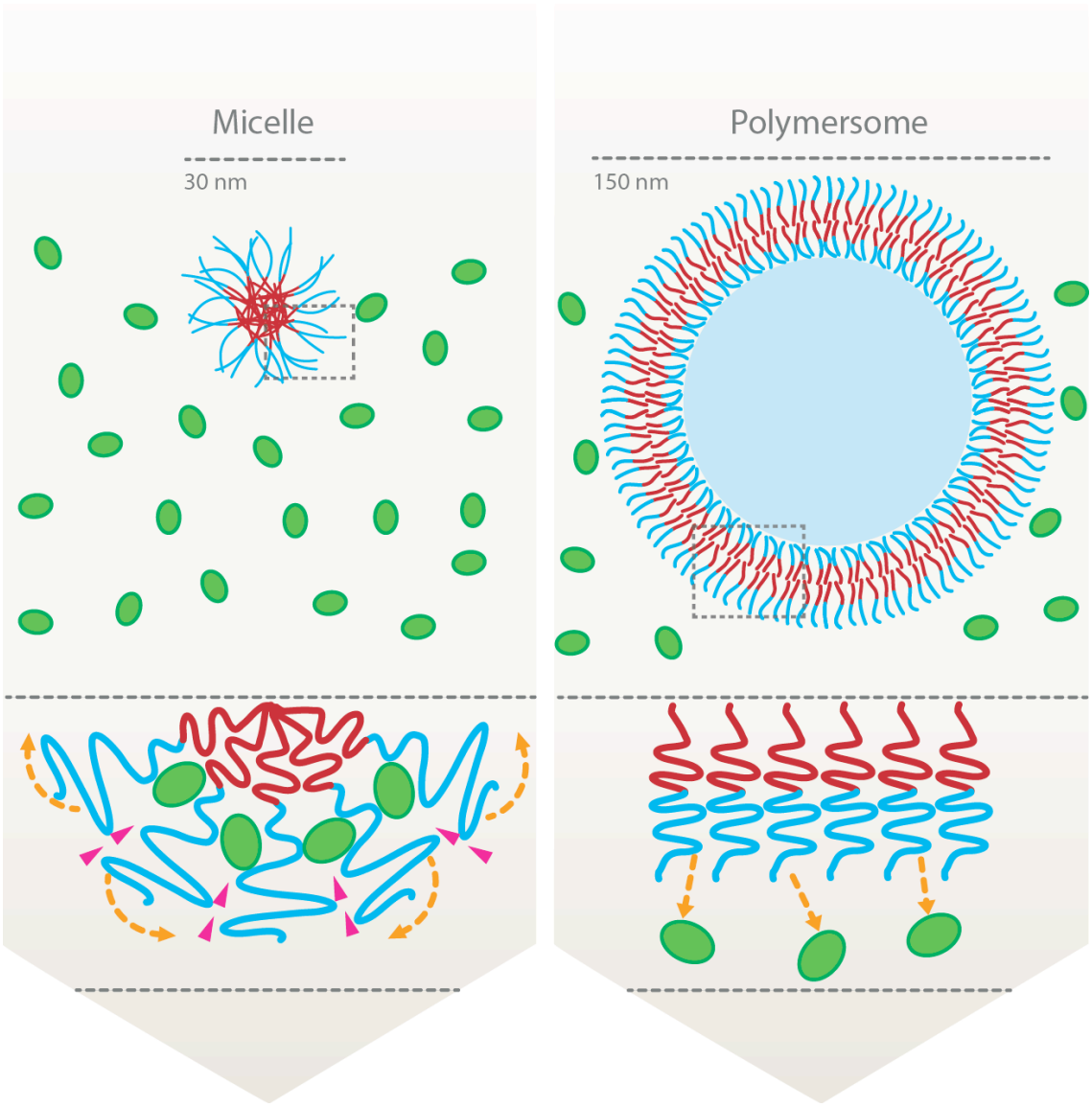

Figure 2.11. Illustration to explain the binding protein effect detected in presence of micelles. The different copolymer configuration is speculated to be the causing factor for the studied binding equilibrium. The lower brush density characterising the micellar conformation possibly allows the proteins penetrations of the external hydrophilic polymer brush, thus permitting their interactions with the hydrophobic core of the micelle. As experimentally confirmed, this is not occurring in presence of polymersomes, which are assemblies characterised by a higher brush density compared to micelles.

Chapter 3

Results and Discussion

ELECTROPORATION FOR PROTEIN ENCAPSULATION WITHIN POLYMERSOMES

3.1. Electroporation principles

The electroporation technique, also called electropermeabilisation, is a process widely applied in Molecular Biology. It is used with the aim of introducing into cells external molecules that are dissolved in an appropriate media. With this procedure it is possible to obtain the intracellular delivery of a vast range of different compounds, characterised by very different chemical and physical properties, including: proteins, DNA, and mRNA (Neumann et al., 1999). Electroporation consists of an externally applied electrical field that induces an increase in the electrical conductivity and, consequently, permeability of the cell plasma membrane (Ho and Mittal, 1996b; Neumann et al., 1982). Herein, electroporation was studied and developed as a consistent and reproducible way to introduce proteins into polymersomes.

Electroporation is based on an oscillatory electrical field occurring in an electrode chamber that produces ions displacement and the formation of charge poles across the subjected membrane. This, in turn, leads to an unbalanced concentration of fluid ions between the internal membrane enclosed environment and the external one. In such a way, the generated osmotic pressure induces the formation of pores and consequent diffusion of water soluble species across the membrane (Escoffre et al., 2009; Neumann et al., 1999).

The effectiveness of the electropermeabilisation technique is based on various parameters that range from the strength of the electrical field, the number of

pulses applied and the duration of a single pulse (Ho and Mittal, 1996a; Knutson and Yee, 1987). The electrical filed strength value results from the contributions of both the voltage used (V_a) and the distance between the electrodes. This parameter is responsible for the pore formations on the subject membrane. On the other hand, the number of pulses applied and their durations determine the size and number of the resulting pores. Studies performed using cell models, have shown that the temporal formation of pores at the cytoplasmic membrane level can be induced by adjusting both parameters (Escoffre et al., 2009; Neumann et al., 1999). Besides these parameters, other factors such as the type of membrane, the temperature of the system and ion concentrations can also influence the results of the electroporation process. Furthermore, the surface charge of the molecule that is to be permeated affects its internalisation process (Wang et al., 2012).

The polymersome membrane, as well as the lipid one, is held together by supramolecular forces and indeed is sensitive to electrical fields. Hence, as schematised in Figure 3.1, it was hypothesised that the application of an electrical field will cause the temporary formation of pores that will in turn be used to load proteins within the polymersomes. However from a physical point of view, Aranda-Espinoza and coworkers (Aranda-Espinoza et al., 2001) compared the electromechanical properties of a poly(ethylene oxide)-block-polybutadiene (PEO-PBD) polymersome membrane with a lipid one. They clearly demonstrated that the polymersome membrane can porate as a consequence of an electrical field, albeit with a voltage almost one order of magnitude larger than the required one for lipids. Precisely, they defined that the membrane breakdown potential value (V_c) is directly proportional to the membranes thickness (d). Thus, they calculated that a polymersome with a d value of 15 nm is characterised by a V_c = 9 V. Instead, liposome with a much smaller d value, equal to 3 nm, presents a V_c = 1 V (Aranda-Espinoza et al., 2001; Discher et al., 1999). Furthermore, the higher robustness that characterises a polymersome membrane compared to a lipid one is due to the entanglement effect that occurs between the hydrophobic polymer chains. For this reason, and in order to obtain the polymersome membrane poration and cargo encapsulation via electroporation, different parameters were herein explored. These parameters range from the number of repeated pulses to the ion concentration and the initial potential-cargo concentration in the sample

solution. Importantly, the structural integrity of both vesicles (morphology and size distributions) and encapsulated cargo (biological activity) was tested after the electroporation process. Furthermore, the encapsulation efficiency of complex bio-molecules such as Immunoglobulin G (IgG) achieved with electroporation was compared with other encapsulation methods such as pH switch and polymer-film rehydration.

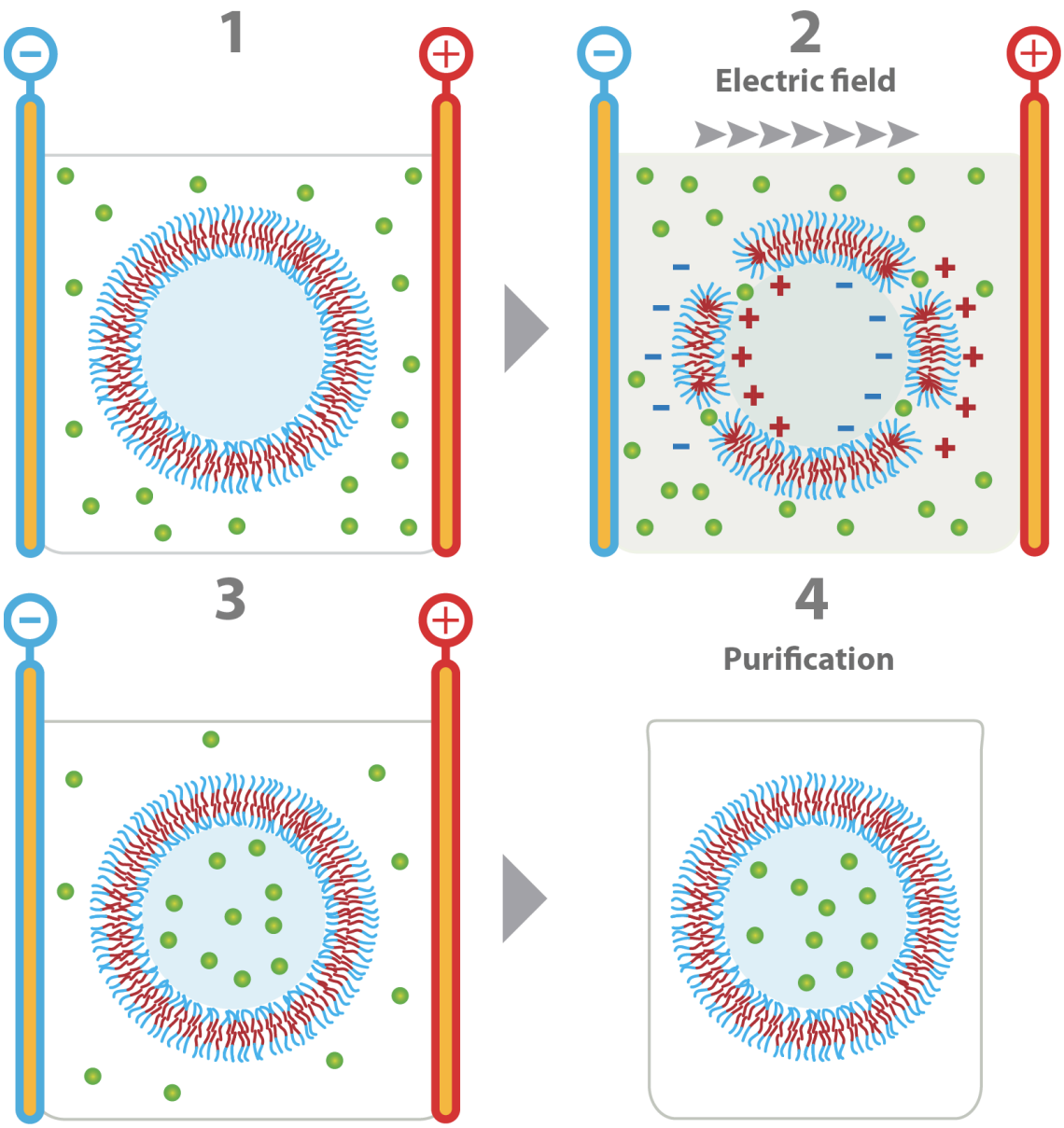

Figure 3.1. Schematic representation of the four steps required for the encapsulation of biomacromolecules within polymersomes, via electroporation. In the first step (1), polymersomes and the cargo are both loaded into the electroporation cuvette. Afterwards (2), the applied electric pulse leads the formation of transient pores on the polymersomes membrane, allowing the cargo encapsulation. The third step (3) represents the polymersomes membrane recovery, and the consequent intra-vesicular trapping of the loaded cargo. Finally, in the fourth step (4), the loaded polymersomes are purified from the non-encapsulated biomolecules.

3.2. Polymersome preparation and characterisation

First of all, it is important to note that in all the performed experiments, the PMPC-PDPA (Poly(2-methacryloyloxyethyl phosphorylcholine)-co-poly(2-(diisopropylamino)ethyl methacrylate) polymer concentration was kept constant at 10 mg/ml in phosphate-buffered saline 0.1 M (1X PBS). The polymersome samples were prepared with film rehydration method, which requires 8 weeks, under high shear rate stress (magnetic stirring at 200 rpm) (Robertson et al., 2014). The used electroporation protocol included a fixed voltage value (V_a) of 2500 V. This is in accordance with previous studies that reported that micrometer / nanometer vesicles require a considerably high voltage to be temporally affected by pore formation on their membrane (Schoenbach et al., 2001). Furthermore, 20 electrical pulses were applied. To confirm the vesicular formation and stability, before and after this high energy transfer, Dynamic Light Scattering (DLS) and Transmission Electron Microscopy (TEM) analyses were performed. These two techniques show respectively the average intensity of the particle diameter in solution (DLS) and a dehydrated representation of their morphology (TEM). As shown in Figure 3.2, no differences were observed in the polymersome sample before and after the electroporation process. Thus, TEM and DLS analyses confirmed that the size distribution and the structural particle integrity was maintained unaltered after electropermeabilisation. These results strongly corroborate the hypothesis of a transient pore formation on the polymersome membrane, which can be recovered after the electroporation process.

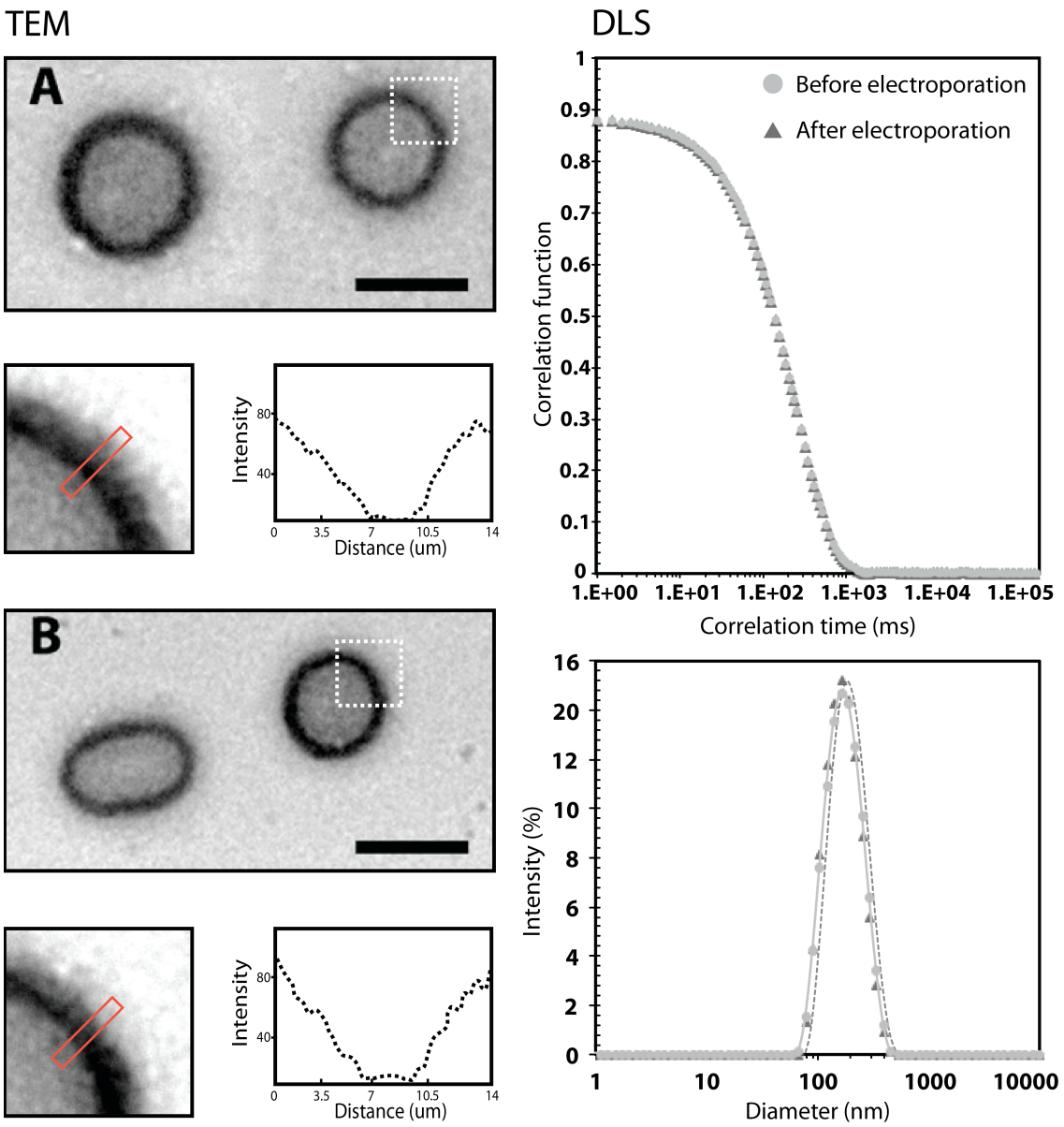

Figure 3.2. (Left) TEM analyses before (A) and after (B) electroporation, which includes the intensity against distance plot profile (the dark magnified region corresponds to the minimum revealed intensity). (Right) DLS analyses (correlation function and size distribution intensity graphs) of PMPC-PDPA polymersomes before (●) and after (▲) electroporation. Scale bar: 150 nm.

3.3. Antibody stability after electroporation process

Any potential damage caused by the electroporation process on the IgG stability and bioactivity was assessed by (*i*) Enzymatic Linked Immunosorbent Assay (ELISA) and (*ii*) immunohistochemistry. The first test used for this purpose was the ELISA assay (Engvall and Perlmann, 1971). This sensitive method is a quantitative sandwich immunoassay based technique. For normal biological applications, this colorimetric assay is utilised for the detection of a specific antigen solubilised in media. This test, in fact, involves the use of well plates that are pre-coated with a single-type of immobilised IgG antibody that is selectively able to bind the corresponding antigen (if it is present in the added liquid sample). After the first step of the ELISA protocol, that correspond to the antibody-antigen detection, to avoid any contamination from unbounded molecules, the latter are removed from the plate with consecutive washing steps. The subsequent step concerns the addition of a secondary enzyme-linked antibody, able in turn to detect if present, the previously immobilised antigen. After that, another washing step is necessary to exclude any unbound secondary IgG. The last part of the ELISA procedure is the reaction between the enzyme linked secondary IgG, with the appropriate substrate (see Figure 3.3). Importantly, the product derived from this colorimetric reaction can be quantified via spectroscopy and can be proportionally correlated to the amount of unknown antigen present in the sample.

For the validation purposes, the ELISA secondary enzyme-linked IgGs were initially subjected to the electroporation procedure. Subsequently to that, these IgGs were used in a standard ELISA assay. In such a way, it was possible to evaluate the IgGs ability to detect the presence of a previously absorbed antigen (bound to the primary antibodies) and thus to characterise their integrity after the electroporation process. These antibodies were compared to native untreated IgGs (negative control) and to degraded immunoglobulins (positive control obtained by placing the protein at 90°C for 15 min).

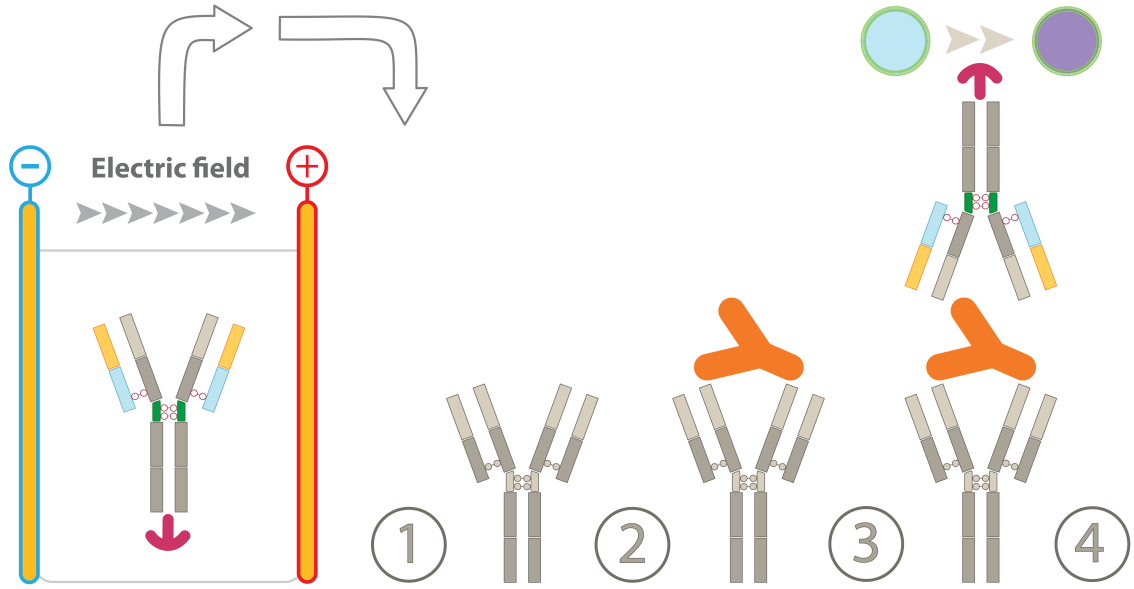

Figure 3.3. Schematic representation of the four steps applied on the customised ELISA assay, used to evaluate the antibody stability after electroporation. (1) In the first step of the protocol, the secondary IgG-linked enzyme is subjected to electroporation. (2) Subsequently, the pre-coated well plate, presenting the immobilised IgG, is exposed to the antigen solution. (3-4) In the last two steps of the protocol, antigen recognition of the electroporated IgG is evaluated through a colorimetric enzymatic reaction.

The second test performed to validate the antibody stability after electroporation was based on immunohistochemistry (Odell and Cook, 2013). This is a technique that involves the use of specific fluorescently labeled IgG able to recognise singular epitopes displaced on an appropriately permeabilised and fixed cell. The cellular permeabilisation and fixation steps are critical to allow penetration of the antibody into the targeted cell model; otherwise it is inaccessible to extracellular proteins such as free IgGs. After the fluorescently labelled-antibody epitope recognition, the targeting protein mechanism was assessed through confocal microscopy analysis. Also in this stability test, as in the ELISA, structural impairment of the antibody can affect the capability of the latter to bind the intracellular target. For the immunohistochemistry IgGs stability characterisation fluorescently labelled-antibodies were initially subjected to electroporation and their ability to target the corresponding epitope was compared (at equal concentrations) with a negative control (non-treated antibody) and a positive one (degraded antibody).

Figure 3.4 reports the results of both characterisations, namely ELISA and immunohistochemistry, regarding the IgGs stability after electroporation.

It is possible to notice in Figure 3.4-A, which shows the ELISA immunoglobulin stability data (using a detection kit against Interleukin 8 (IL-8)), there is not statistical difference when comparing the electroporated IgGs (enzyme conjugated IgG anti IL-8) with the native untreated control. Furthermore, no difference in the IgGs activity was observed after subjecting it to 5, 10 or 20 pulses. Indeed, after 20 electroporation pulses, more than 93% of the antibodies were capable of binding to the immobilized antigen, demonstrating the overall protein resilience to the process. On the other hand, the positive control antibody (obtained by placing the protein at 90°C for 15 min) indicated the expected protein degradation. Indeed, just 8% of the IgGs were still able to detect the corresponding antigen.

In the second stability test, an anti α-tubulin AlexaFluor®647 antibody was used as a model for the immunohistochemistry test after electroporation. Also in this case, the antibodies were subjected to 20 pulses during the encapsulation process simulation. After that, their ability to recognise the α-tubulin epitope in Human Dermal Fibroblast (HDF) was tested. The α-tubulin was exploited as a target model, since its tubular structure it is well established and easily recognisable in confocal microscopy analysis (Saxton et al., 1984). This facilitates the evaluations of the antibody structural stability. Also in this case, the results in Figure 3.4-B shown that the activity of the electroporated antibodies was similar to the control native protein. The control IgG and treated protein presented the same capability of interacting with the α-tubulin epitope, confirming that there was essentially no degradation after electroporation. On the other hand, the positive control antibody (obtained by placing the protein at 90°C for 15 min) as expected was unable to stain the α-tubulin.

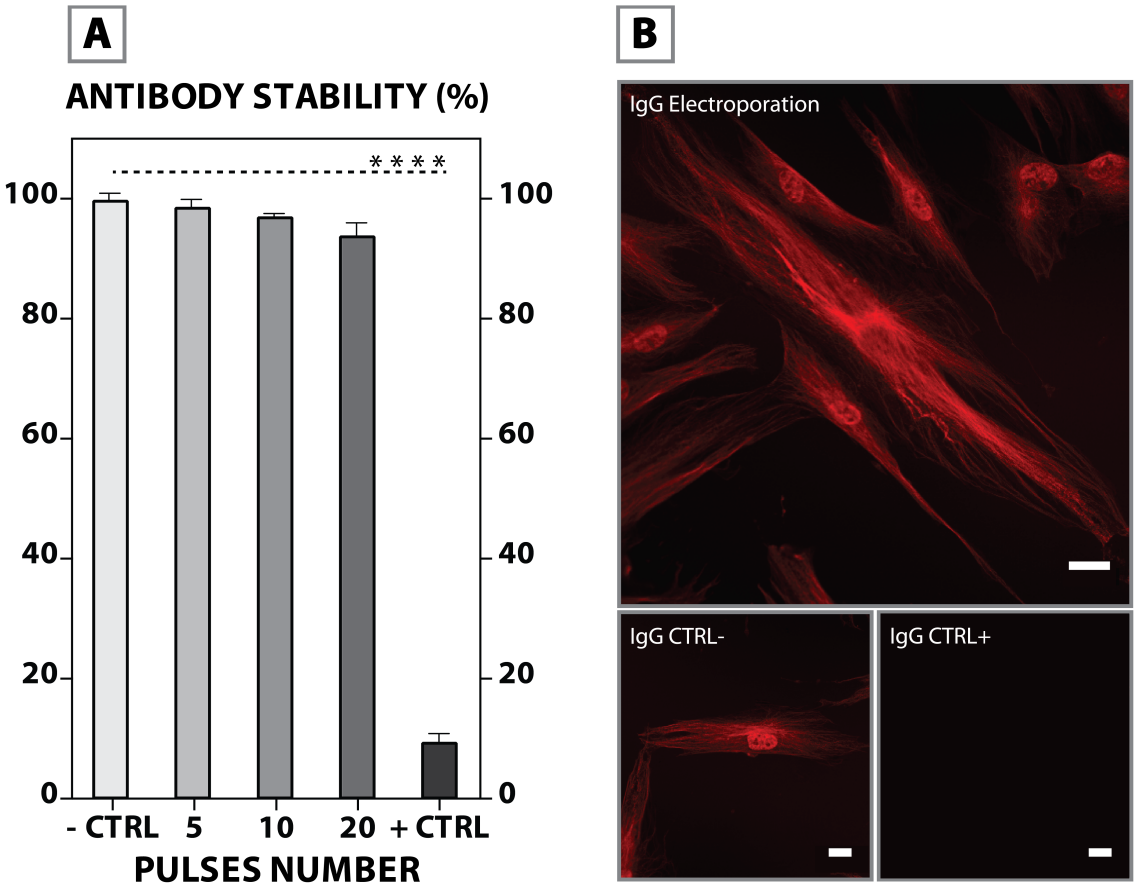

Figure 3.4. (A) ELISA assay results regarding the antibody stability evaluation after different electroporation pulses (t-test, p-value * P ≤ 0.05; ** P ≤ 0.01; *** P ≤ 0.001; **** P ≤ 0.0001). (B) Immunohistochemistry assay in HDFs to validate antibody stability after 20 electroporation pulses of anti α-tubulin AlexaFluor®647 antibody. In both experiments the IgG stability was compared to a negative control (untreated IgG, -CTRL) and a positive control (IgG placed at 90°C for 15 min, +CTRL). The experimental error is expressed as standard deviation (N=3). Scale bar: 20 μm.

3.4. Protein encapsulation within polymersome

Herein the evaluation of antibody (anti α-tubulin AlexaFluor®647 IgG) encapsulation within polymersomes was calculated using the encapsulation efficiency percentage (E) and loading efficiency (L). E is defined as the ratio between the final mass of encapsulated protein within polymersomes after purification and the initial mass of antibody and it is expressed as it follows:

$$E = \frac{n_p}{n_{p0}} x\ 100 \quad (1)$$

where n_{Po} is the initial moles of protein and n_P is the moles of protein after SEC purification (see materials and methods section). n_P is given by:

$$n_p = [P]_m \, x \, V_s \quad (2)$$

where $[P]_m$ is the molar concentration of protein measured by reversed phase high-pressure liquid chromatography (RP-HPLC) after purification (materials and methods Section 7.2.3) and V_s is the solution volume, while the initial moles of protein, n_{Po}, is calculated as follow:

$$n_{p0} = [P]_0 \; x \, V_s \quad (3)$$

where $[P]_o$ is the initial protein molar concentration. Combining equation 2 and 3 it is possible to re-write the encapsulation efficiency as follows:

$$E = \frac{[P]_m \, x \, V_s}{[P]_0 \; x \, V_s} \, x \, 100 \quad (4)$$

The loading efficiency, L, is the ratio between the measured number of proteins encapsulated per polymersome divided by the number of proteins that theoretically can be packed within the polymersome lumen. L can be expressed as it follows:

$$L = \frac{P_M}{P_T} \quad (5)$$

where P_M is the experimental number of proteins encapsulated with the polymersome and P_T is the theoretical number of proteins that can be encapsulated. P_M is given by:

$$P_M = [P]_m x \, V_s \, x \, N_A \quad (6)$$

where N_A is the Avogadro's number. The theoretical number of proteins, P_T, can be calculated as it follows:

$$P_T = [P]_0 \, x \, V_l \; x \, N_A \, x \, N_V \quad (7)$$

where, V_l is the polymersome lumen volume, and N_V is the total number of polymersomes in the sample. V_l can be calculated as it follows:

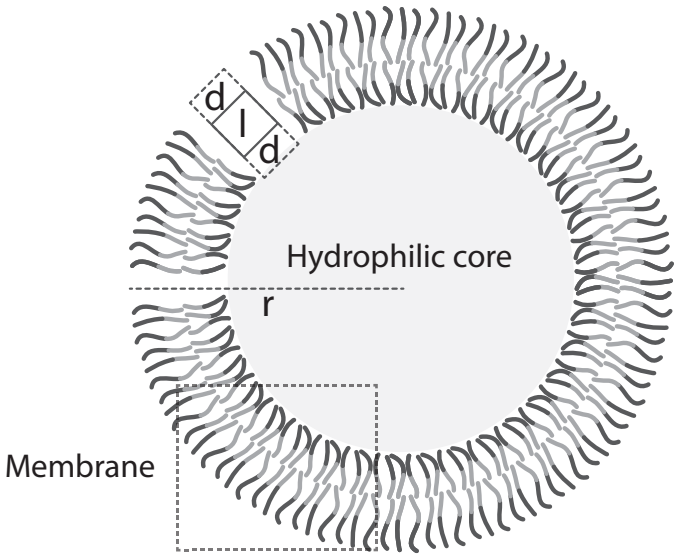

$$V_l = \frac{4}{3}\pi (r-2d-l)^3 \quad (8)$$

where r is the polymersome radius, d is the hydrophilic layer thickness and l is the hydrophobic membrane thickness, while N_V is calculated as:

$$N_V = [C] \times V_S \times N_A / N \quad (9)$$

where $[C]$ is the final copolymer concentration (measured by RP-HPLC), and N is the number of copolymer aggregates per polymersome and is given by:

$$N = \frac{V_M}{v_{PDPA}} \quad (10)$$

where V_M is the membrane volumes and is calculated as:

$$V_M = \frac{4}{3}\pi ((r-d)^3 - (r-d-l))^3 \quad (11)$$

while v_{PDPA} is the molecular volume of a single chain of PDPA and it is calculated as:

$$v_{PDPA} = \frac{M_{WPDPA}}{(\rho_{PDPA} \times N_A)} \quad (12)$$

where M_{WPDPA} is the PDPA molecular mass, and ϱ_{PDPA} is the PDPA bulk density. Combining equations 6-12 the loading efficiency can be re-written as a function of experimentally accessible parameters as:

$$L = \frac{[P]_m x\, N}{([P]_0 \times [C] \times V_I)} \quad (13)$$

Using such a formula, it is possible to determine if the encapsulation process is driven by simple diffusion between solution bulk and the polymersome lumen upon pore formation (i.e. statistical encapsulation, L=1), or if there is an external force that actively promotes / hinders protein diffusion within the polymersomes and overcomes the entropic barrier to concentrate / dilute them within the lumen. When L value is higher than the unity, an external applied force promotes the cargo encapsulation. Looking at the obtained L values summarised in Figure 3.5, it is clear that for all the tested conditions, electroporation promotes the protein encapsulation within polymersomes. Indeed, all the calculated L values appear to be much higher than the unity, ranging from 6 to 76.

IgG encapsulation was studied using different experimental conditions, including pulses number, initial amount of IgG and finally by increasing the solution ionic strength. It is important to remark that the polymersome concentration was kept constant for each experiment at 10 mg/ml in terms of PMPC-PDPA.

No significant effects were here detected on the protein and polymersome structure (see Section 3.2 and 3.3) when applying 20 pulses at 2500 V each, these experimental conditions were thus kept for the protein encapsulation studies. In this context, four different experiments were performed. In all of them, the protein and ion concentrations were kept constants at 5 μg/ml (IgG) and 0.1 M (1X PBS). On the other hand, the four samples were subjected to

different numbers of electroporation pulses: 5, 10, 15 or 20. As explained at the beginning of this chapter, the pulses number affects the size, the number, and the lifetime of the resulting membrane pores (Escoffre et al., 2009; Neumann et al., 1999). The second variable herein tested, that has the potential to affect protein encapsulation within polymersomes is the initial protein concentration present within the sample. An increase of this variable will consequently increase the statistical probability for the protein to be trapped within the polymersomes when the pores are formed. For this experiment, the PBS molarity and the number of electric pulses applied were kept constant at 0.1 M PBS and 5 (at 2500 V each). Instead, four different protein concentrations: 5, 10, 20 and 40 μg/ml were tested. The last parameter changed was the PBS molarity. Previous studies performed using cell models, already correlated the ion concentration in the sample solution, as a critical variable that has to be considered to obtain the maximal internalisation of extracellular compounds via electroporation (Ho and Mittal, 1996a; Knutson and Yee, 1987; Wolf et al., 1994). In this work, the protein encapsulation within polymersomes was evaluated using three different PBS molarities: 0.1, 0.2 and 0.5 M, keeping constant the initial amount of IgG (5 μg/ml) and the pulses number (5 pulses at 2500 V each). The experimental results expressed as L and E for all the mentioned variables, are summarised in Figure 3.5.

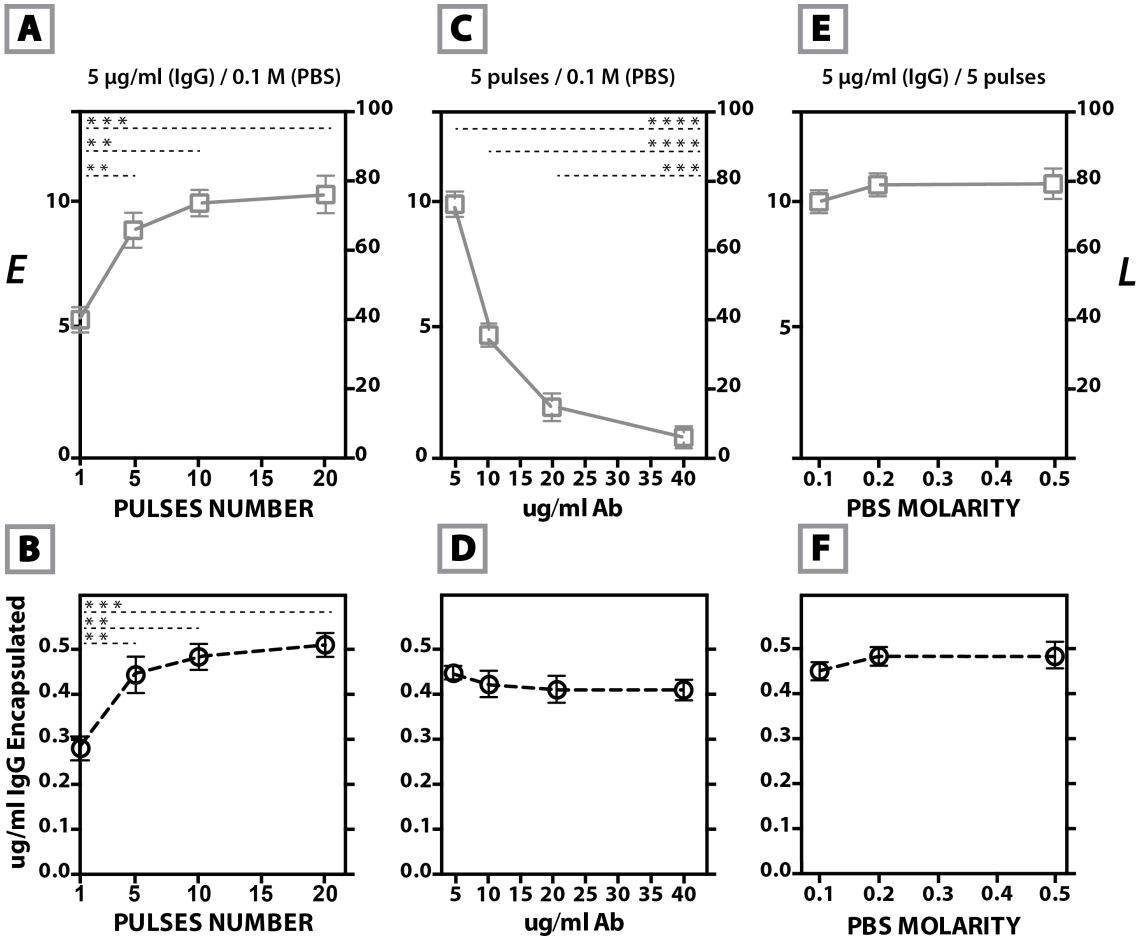

Figure 3.5. Encapsulation efficiency percentage (*E*), loading efficiency (*L*) (top graphs) and encapsulated amount of IgG (µg/ml, bottom graphs) within PMPC-PDPA polymersomes obtained by electroporation using different parameters. A-B, reports the results of samples subjected to different number of electroporation pulses: 5, 10, 15 and 20, keeping constant the protein and ion concentration at 5 µg/ml (IgG) and 0.1 M (PBS). C-D shows the data obtained from testing four different initial protein concentrations: 5, 10, 20 and 40 µg/ml. In C-D the PBS molarity and the number of electric pulses applied were kept constant at 0.1 M (1X PBS) and 5. Finally, E-F shows the data achieved by keeping constant the initial amount of IgG (5 µg/ml) and the number of pulses (5) and testing three different PBS molarities: 0.1, 0.2 and 0.5 M. In all the experiments, the applied voltage per single pulse was set at 2500 V (t-test, p-value * $P \leq 0.05$; ** $P \leq 0.01$; *** $P \leq 0.001$; **** $P \leq 0.0001$). The experimental error is expressed as standard deviation (N=3).

The first relevant outcome shown in Figure 3.5 is that the immunoglobulin G was successfully encapsulated within polymersomes via electroporation. Furthermore, analysing the results for all the different tested conditions, the maximum *L* value was obtained with 20 pulses, keeping constant the protein

and ion concentration at 5 μg/ml (IgG) and 0.1 M (1X PBS) (Figure 3.5 A-B). It is important to notice that subjecting the sample at increasing number of electroporation pulses (from 1 to 5), results in a statistically significant increased in internalisation of protein cargo within the polymersomes (t-test, $P \leq 0.05$). In fact, a single electroporation pulse leads to a loading efficiency of ~40, and this increases to ~70 as the number of electric pulses increases. No statistical significant difference between loading efficiency from 5 to 20 pulses was observed. The same trend was also observed by calculating the μg/ml of antibodies encapsulated per sample. More precisely, in such experiments the encapsulated amount of IgG was calculated, which ranged from 0.42 μg/ml (5 pulses) to 0.51 μg/ml (20 pulses). Whereas, after one pulse the protein concentration value calculated was 0.29 μg/mL These results agree with the theoretical principle behind the electroporation. As explained at the beginning of this chapter, the pulse number is the factor that determines the size and the number of pores resulting on the subjected membrane. The obtained data show that increasing the number of pulses increases the amount of protein internalised per vesicle. Therefore, these results indicated that 1 pulse is sufficient to induce the formation of pores with diameter superior of ~10 nm, as this is the average size of a single IgG molecule (Marquart et al., 1980; Wells et al., 1992).

The second variable herein tested was the initial amount of protein added to the polymersome dispersion (Figure 3.5 C-D). Despite the significant variations in *L*, with values ranging from 66 to 6 going from 5 μg/ml to 40 μg/ml of IgG initial concentration, the final amount of antibodies encapsulated using the four different initial IgG concentrations (5, 10, 20 and 40 μg/ml), was approximately always the same and corresponded to ~0.4 μg/mL. This result indicates that at the used experimental conditions (voltage value 2500 V, 5 pulses), all the tested IgG concentrations allowed the achievement of the maximum protein encapsulation within polymersomes. This result would suggest that *L* and *E* can be further improved by both increasing the polymersomes size and numbers and further experiments are ongoing to assess this.

Concerning the last analysed variable, the PBS molarity, it is evident that the obtained IgG encapsulation within polymersomes is not statistically affected by this factor within the protein concentrations measured herein (Figure 3.5 E-F). As previously explained, the cargo encapsulation via electroporation is mediated

by a sudden increase in osmotic pressure across the membrane. For this reason, it was expected a correlation between ion concentration on the sample solution and protein encapsulation.

Despite the obtained results, further experiments should be performed to confirm this possibly spanning across larger ionic strengths.

Similar conclusions can be drawn using the encapsulation efficiency to analyse the data. Indeed, for the tested conditions the obtained *E* values ranges from ~2 to ~12%. It is important to consider that the total polymersomes volume percent (ϕ_p) is estimated to be ~1% of the total sample volume (data derived from equation (5)). Thus, if the encapsulated proteins were loaded within polymersomes by simple diffusion (L=1) the resulting *E* should be around 1%. Because the obtained *L* value is considerably higher that 1 (>70), by applying electroporation the protein internalisation within polymersomes is forced, leading to an increase of *E* value (~10%) of one order of magnitude. One should expect to potentially reach 100% efficiencies by either increasing the polymersome numbers or by changing their size.

On these premises it is possible to speculate that protein encapsulation occurs via two possible mechanisms. On one hand, it is necessary to remark that highly charged proteins were used; the IgG has ζ-potential equal to -13.9 mV at neutral conditions and room temperature. This would suggest the possible implication of an electrophoretic push from the outside to the inside of the polymersomes. This hypothesis was partially verified in my original contribution using a different protein, the lysozyme (Wang et al., 2012). This enzyme is positively charge at neutral pH (ζ-potential = 3.2 mV at pH 7.3) while it is negatively charged in alkaline conditions (ζ-potential = -7.8 mV at pH 11). Interestingly, the different charges correspond to very different loading efficiencies with values close to the unity at neutral conditions and values of about 20 at pH 11. This would confirm the electrophoresis hypothesis, however, in the same work (Wang et al., 2012) also nucleic acids DNA and RNA were encapsulated with very different loading efficiency of 20 and 2 respectively. These molecules have similar net charges to the IgG and lysozyme at pH 11 and one should expect similar trend. Hence, it is hypothesised that there is further a possible entrapment effect, where the diffusion into the polymersomes is considerably more efficient that the diffusion out of the polymersomes. This would justify the

large differences observed between the very large DNA and the considerably smaller RNA. Furthermore, such a hypothesis would be in agreement with other works ongoing in the Battaglia research group, where it was demonstrated that encapsulated proteins within polymersomes have higher stability and unfolding kinetics which are considerably hindered compared to when they are free in solution (Cecchin et al., Nat. Commun., under review).

3.5. Electroporation encapsulation comparison with other techniques

To promote electroporation as the elective method to achieve protein encapsulation within polymersomes, it is necessary to compare it with other encapsulation methods such as solvent switch and polymer film rehydration. The results of this analysis, and in particular the obtained values of *L* and *E* for each technique, are shown in Figure 3.6. In all cases, the polymersome samples were prepared using the same initial amount of PMPC-PDPA (10 mg/ml) and IgG (5 μg/ml - anti α-tubulin AlexaFluor®647 IgG). Furthermore, for all the experiments the polymersomes were formed in 0.1 M 1X PBS, as described in the materials and methods section (Section 7.2.4).

Figure 3.6-A and B, show the TEM and DLS characterisations analyses for the polymersomes formed by the three different encapsulation methodologies (electroporation, solvent switch and polymer film rehydration). These data are critical to explain the final *L* and *E* values achieved for each method (see Figure 3.6-C). However, for such a comparison it is important to state that electroporation is a post-polymersome-formation protocol while the other two methods, namely solvent switch and polymer film rehydration, allows the protein encapsulation to occur during the polymersome formation (see Section 1.6.1). For this reason, these techniques are affected by a limited possibility to control and modulate the polymersome self assembly process. Therefore, the resulting protein encapsulation can be influenced from this lack of control. In fact, with these methods, it is critical to find a balance in the experimental conditions in order to obtain an adequate polymer self-assembly and to preserve the stability of the protein cargo.

Starting with the analysis of the TEM and DLS data obtained from the solvent switch encapsulation method (Figure 3.6-A and B), it is possible to notice the

simultaneous formation of both, vesicular (~200 nm) and micellar (~40 nm) structures. Furthermore, the *L* and *E* values resulting from this technique were respectively ~85 and ~12%. In this context it is thus necessary to remark that the experimental data shown in Section 2.2.2 regarding the established interactions subsisting between free proteins and micellar structures. These assessed interactions therefore could result in an overestimation of the calculated *L* and *E* values achieved via solvent switch method.

On the other hand, the physical characterisations (DLS and TEM) of polymersomes obtained via film rehydration shows the formation of larger structures with an average size of ~250 nm as opposed to about 150 nm for polymersomes used for the electroporation-based encapsulation. It is therefore necessary to mention that the different size, between the two samples, is certainly due to the minor shear time applied during the protein encapsulation via film rehydration (10 days for the film rehydration encapsulation technique compared 8 weeks for the preparation of the electroporation sample). This minor shear time was applied with the aim of preserving the protein stability overtime. Furthermore, the achieved data with regards to the protein *L* and *E* values were ~41 and ~23 % respectively. With this protocol it was possible to achieve a quite remarkable *E* value, which was double that of the one achieved via electroporation. However a previous study conducted using liposomes as a model, revealed that this techniques leads to a non homogeneous protein encapsulation (Luisi et al., 2010). This study carried out by Luisi and colleagues shows that the obtained liposome sample was characterised by two vesicular populations, one presenting the trapped cargo while another one characterised by empty vesicles. In this context, despite the promising data that were achieved with this approach, further investigations are necessary to reach a better understanding on the encapsulation mechanism that drives the protein internalisation via film rehydration using PMPC-PDPA block copolymers. Nevertheless, these data show that electroporation has the highest reproducibility and its post-polymersome-formation nature bodes well for future technological translation of polymersomes compared to the other techniques.

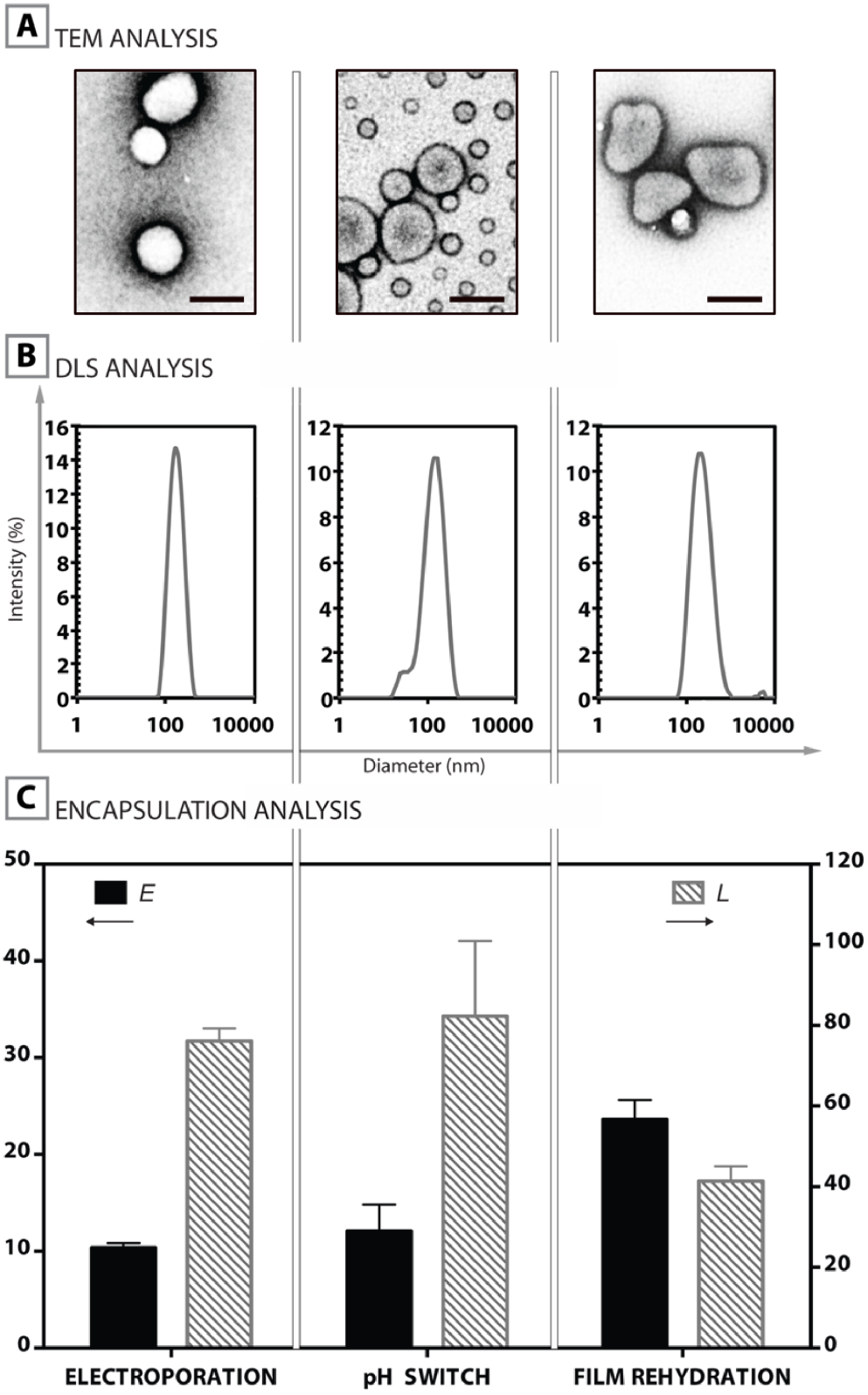

Figure 3.6. (A) TEM, (B) DLS and (C) Encapsulation efficiency percentage (*E*) / loading efficiency (*L*) analyses regarding the IgG encapsulation within PMPC-PDPA polymersomes obtained using three different methods namely electroporation, pH switch and film rehydration. The experimental error is expressed as standard deviation (N=3).

Chapter 4

Results and Discussion

POLYMERSOMES AS A FUNCTIONAL ANTIBODY DELIVERY SYSTEM IN LIVE CELLS

4.1. Polymersome treatment and cells viability

A first requisite for any delivery system in cells is to understand whether it can induce any adverse effects. Previous studies have already extensively assessed the biocompatibility of PMPC-PDPA (Poly(2-methacryloyloxyethyl phosphorylcholine)-co-poly(2-(diisopropylamino)ethyl methacrylate) polymersomes in several cells types and in vivo; so far no adverse effects are reported (Massignani et al., 2009). However, to biologically validate once more PMPC-PDPA polymersome as a biocompatible delivery system and to ensure that the batch used herein was not deteriorated, a cyto-compatibility study using an *in vitro* MTT assay was performed.

3-(4,5-Dimethyl-2-thiazolyl)-2,5-diphenyl-2H-tetrazolium bromide (MTT) is a molecule that can be reduced by two types of cellular enzyme, namely dehydrogenases and NAD(P)H-dependent oxidoreductases (Berridge et al., 2005). This enzymatic reaction is proportionally related to the metabolic activity of the cell, transforming the yellow coloured MTT substrate into the purple insoluble product formazan. This can be detected spectrophotometrically as it absorbs light with a peak at wavelength of 570 nm (van Meerloo et al., 2011). The MTT assays is an *in vitro* test widely used to verify the toxicity of drugs on cell models (Sadeghi Aliabadi et al., 2010). MTT assay was performed after 24 h incubation with polymersomes at concentrations of 0.5, 1 and 1.5 mg/ml. Cells were treated with an equal volume (compared to the added polymersomes sample) of 1X phosphate buffered saline (PBS 0.1 M) in media as a negative control.

Five different cells models were used in this validation; primary human dermal fibroblasts (HDF), a breast cancer cell line (MDA-MB-231), ovarian carcinoma cells (SKOV3), human skin melanoma cells (MEWO) and urinary bladder transitional carcinoma cells (RT112).

The obtained results are shown in Figure 4.1.

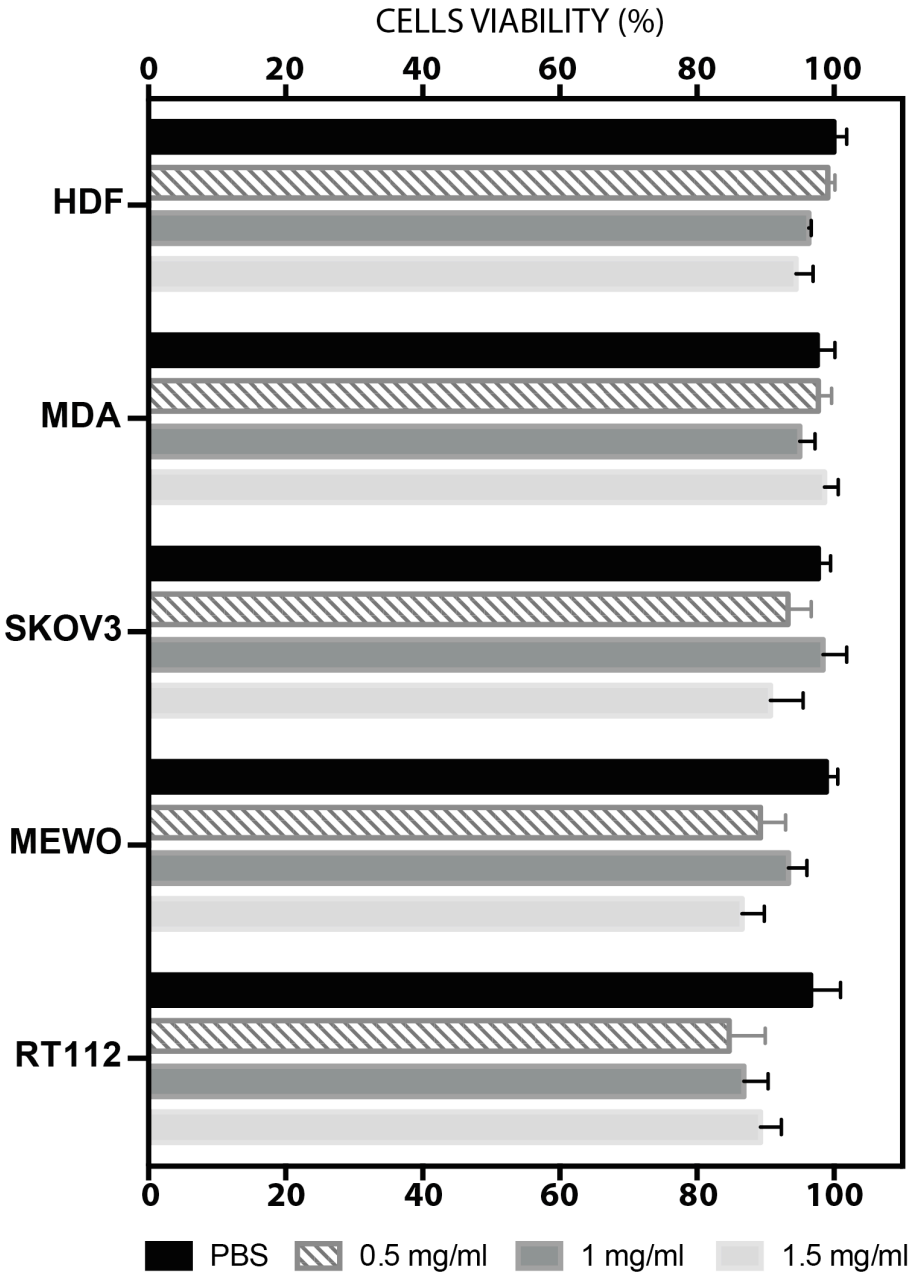

Figure 4.1. Cells viability (%) was tested by means of MTT assay performed in 5 different cell types: HDF, MDA-MB-231, SKOV3, MEWO and RT112. Three concentrations of PMPC-PDPA were evaluated (0.5, 1 and 1.5 mg/ml) and compared to the control cells incubated with 1X PBS (t-test, p-value * $P \leq 0.05$; ** $P \leq 0.01$; *** $P \leq 0.001$; **** $P \leq 0.0001$). The experimental error is expressed as standard deviation (N=3).

As shown in Figure 4.1, no significant decrease in the metabolic activity was observed in the four cell models used at any tested polymersome concentration. Beside the anomalous (yet not relevant) data from the RT112 cells at polymersomes concentration of 0.5 mg/ml no detrimental effect on the cells (t-test, p-value > 0.05) was observed.

4.2. Polymersome uptake and cargo delivery in live cell

The polymersomes ability to deliver cargoes into live cells was evaluated by encapsulating, AlexaFluor®546 labeled immunoglobulin G (IgG) antibodies, using the electroporation method described in Chapter 3. After the encapsulation and purification steps, the protein content within polymersomes was quantified by reversed phase high pressure liquid chromatography (RP-HPLC) (see Section 3.4 and 7.2.3). A concentration of 0.45 μg/ml was determined.

The cellular uptake of the polymersome formulations in HDFs was evaluated by confocal laser scanning microscopy analysis (CLSM). For this purpose, cells were seeded in a glass bottomed 96 well plate and grown for 24 h. Afterwards, the cell medium was replaced with fresh media containing antibody loaded polymersomes, at a concentration of 0.1 μg/ml IgG. Cellular uptake was subsequently visualised at 0, 1, 5, 18 and 24 h incubation. Control experiments were performed in which cells were treated for 24 h with 5 μg/ml of free antibody solution. All cells were treated with a cell nucleus staining probe (SYTO®9) 10 min before confocal analysis. The CLSM results in Figure 4.2, showed the increase of the IgG signal overtime. The fluorescence intensity is proportional to the elapsed cellular incubation time. No evident fluorescence was revealed in cells treated with free antibody. These data indicates the effectiveness of polymersomes to deliver proteins within live cells.

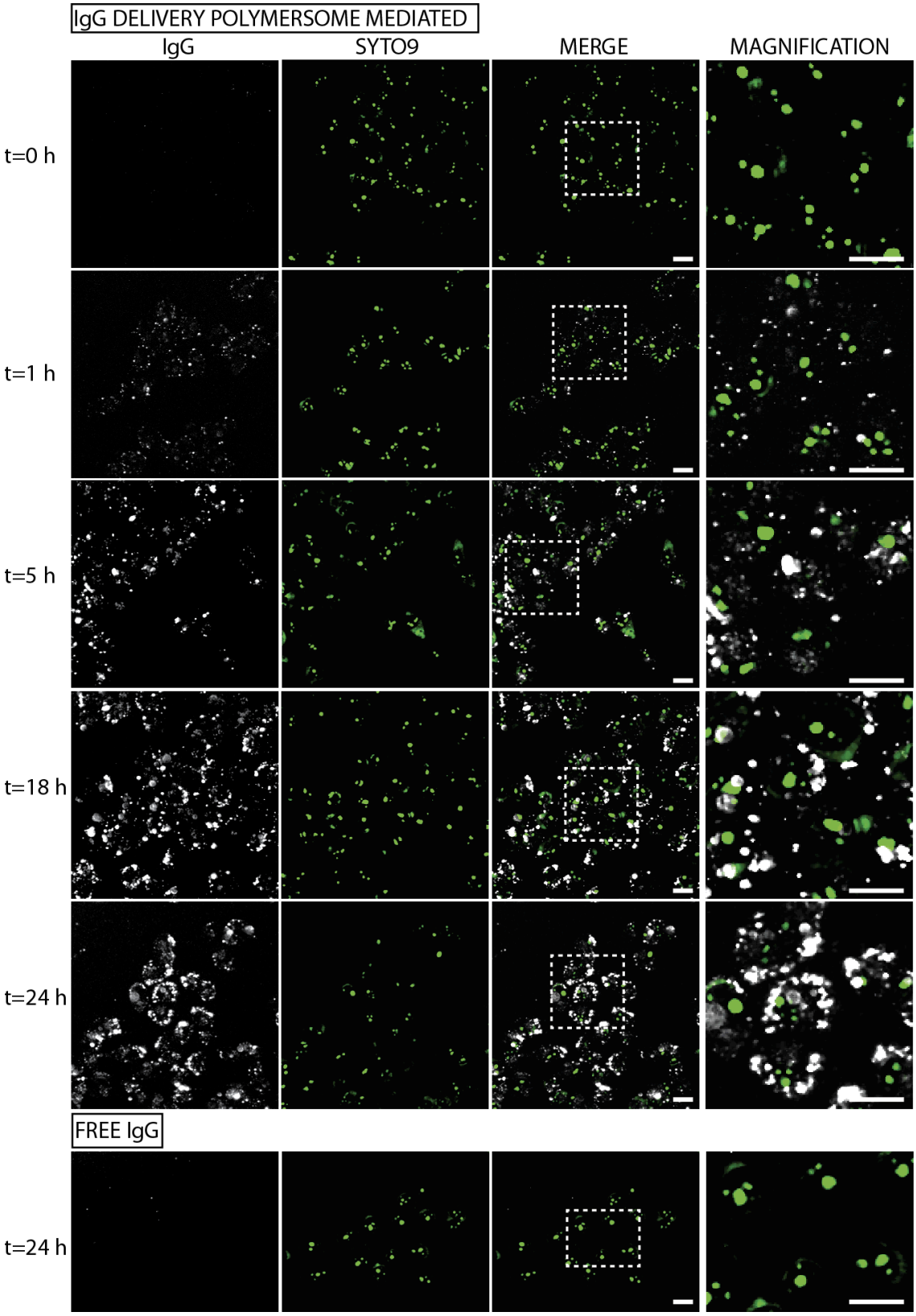

Figure 4.2. CLSM analysis of HDF cells, showing the cellular uptake of polymersomes loaded with 0.1 µg/ml AlexaFluor-546 labeled IgG. The efficiency of polymersomes as an intracellular delivery system was compared to a control experiment in which cells were treated for 24 h with 5 µg/ml of free antibody solution in medium. Scale bar: 25 μm.

The CLSM analysis was repeated in three additional independent experiments. The resulting mean fluorescent intensity values from one field of view were normalised with the fluorescence intensity obtained from cells treated with free antibody solution. The measured fluorescence intensity obtained after 24 h incubation time with IgG loaded polymersomes was taken as the upper limit of the analysis. In such a way, the measured average IgG emission intensities at 573 nm (calculated using ImageJ), corresponding to each time point were plotted on a graph reported in Figure 4.3-A. The image analysis was confirmed by RP-HPLC detection of lysed cells and the final data are also plotted in Figure 4.3-B.

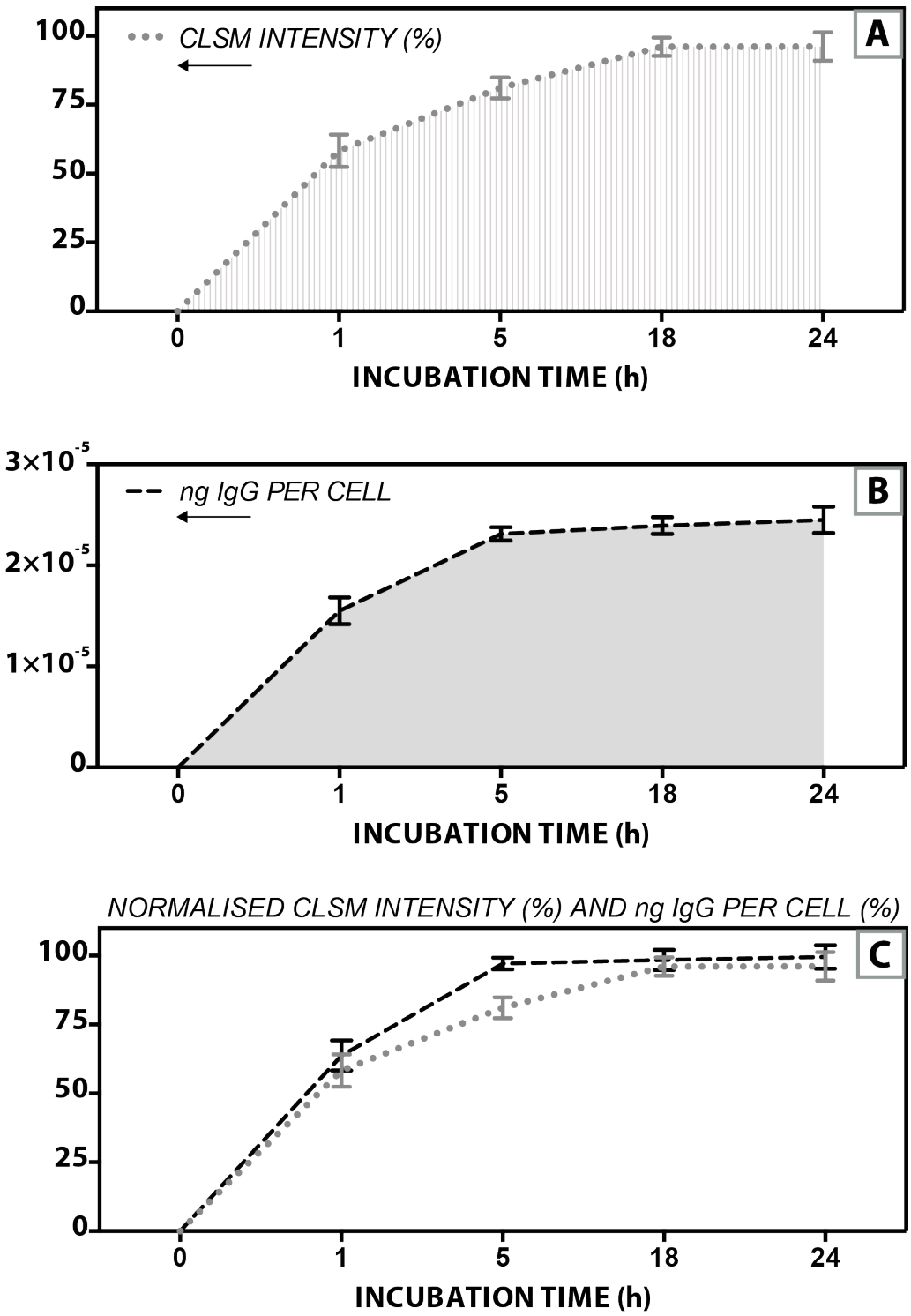

Figure 4.3. (A) CLSM and (B) RP-HPLC quantifications at different time points about the polymersome antibody (AlexaFluor-546 labeled IgG) delivery in HDF. In (C) the obtained results concerning the CLSM intensity (%) and the ng of IgG per cell are normalised (respectively to the maximum intensity or concentration value at 24 h) and compared. The experimental error is expressed as standard deviation (N=3).

As seen in Figure 4.3-C, both measurements are in close agreement, confirming the validity of the imaging method.

The data in Figure 4.3 show that after 1 h of polymersomes incubation, cells had internalised more than half the maximum, corresponding to ~12.5 x 10^{-5} ng of protein per cell. Several factors are implicated in the cellular uptake of polymersomes. Recent works produced in the Battaglia research group has singled out a specific scavenger receptor SR-B1 for the initial cellular recognition of the PMPC-PDPA polymersomes (Colley et al., 2014). It is also established that PMPC-PDPA polymersome uptake is strongly affected by particle size, shape and surface topologies (LoPresti et al., 2011; Massignani et al., 2009; Robertson et al., 2014).

It is important to note that polymersome uptake in HDFs reached a plateau at about 18 h, following which the amount of IgG detected inside the cells was constant.

To explain this result, two correlated hypothesis can be considered. The first one implicates the saturation of SR-B1 receptor on HDF.

The second is the degradation of the internalised IgG molecules involves the cytosolic IgG receptor, tripartite motif-containing 21 (TRIM21). TRIM21 is a cytosolic protein that recognizes the fragment crystallisable (Fc) domain of internalised IgG molecules (Mallery et al., 2010). It plays a crucial role in mediating the intracellular immune response that targets internalised viruses bound by IgG antibodies for proteasomal degradation.

It is possible to speculate a synergistic effect between SR-B1 saturation resulting in impaired uptake and TRIM21 activity promoting IgG degradation. The combination of the two effects could justify the observed plateau of uptake at 18 h.

4.3. Polymersome cytosolic cargo release

To further validate the intracellular-delivery of antibodies CLSM analysis was conducted in the presence of other fluid phase markers.

In Figure 4.4, this analysis was used to visualise the sub-cellular distribution of internalised antibodies (AlexaFluor®546 labeled unspecific rabbit IgG). HDFs were incubated overnight with antibody loaded polymersomes at a concentration of 0.1 μg/ml IgG in medium and subsequently treated with a

lysosomal marker (LysoTracker®) prior to visualisation. The data suggest that while some of the antibody signal colocalises with the lysosome, the majority is well distributed within the intracellular volume, indicating endosomal escape.

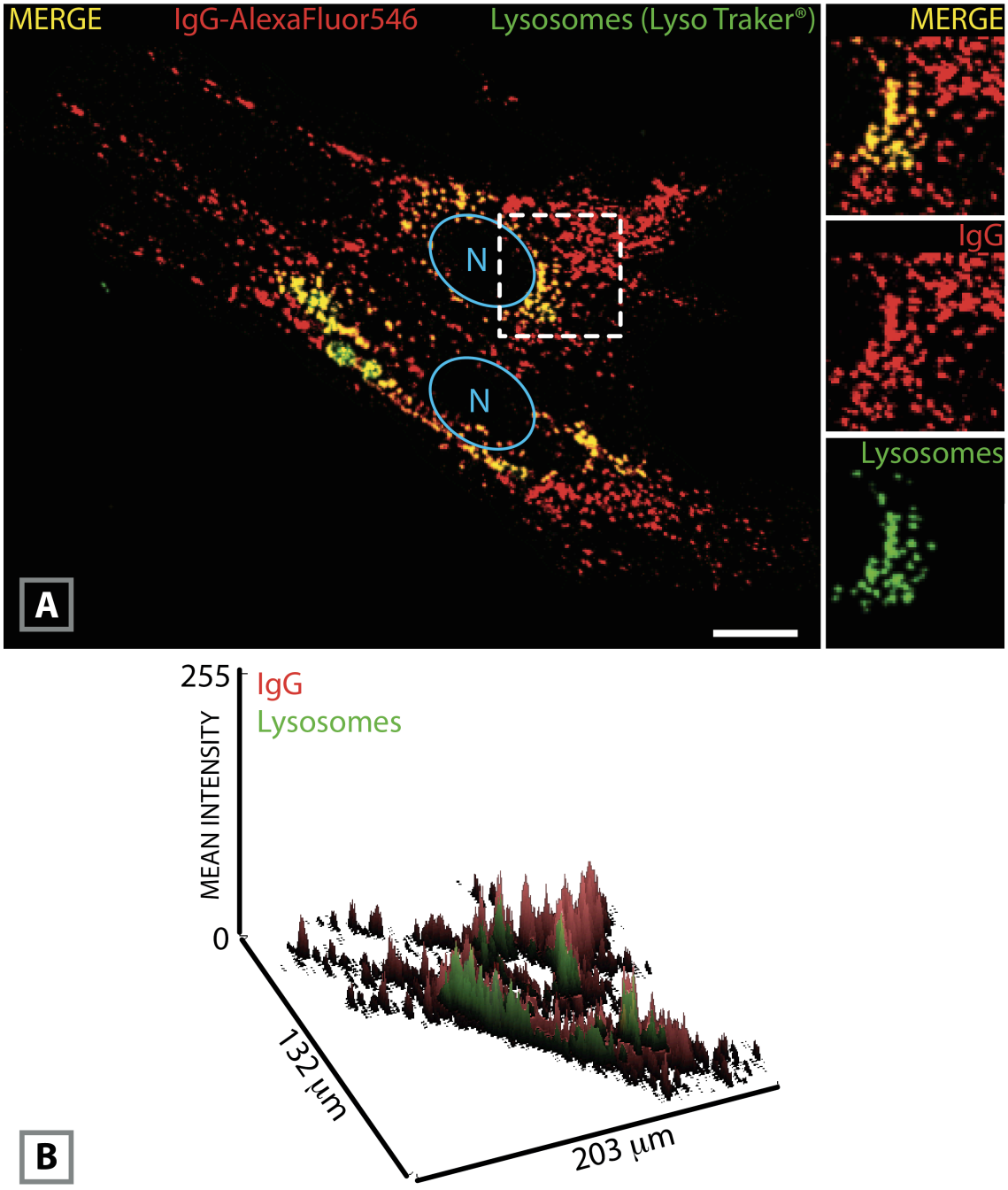

Figure 4.4. CLSM analysis (A) and z-stack micrograph (B) evaluating the sub-cellular distribution of polymersome delivered AlexaFluor-546 labeled IgG. Live HDFs were exposed overnight with the polymersomes formulations and subsequently treated with lysotracker to stain the endolysosomal compartment. Scale bar: 20 μm.

Previous studies by Battaglia and coworkers demonstrated that the pH-sensitive polymersomes disassemble within the early endosome (Massignani et al., 2009). The acidic pH that characterises endocytic organelles overcomes the pKa of PMPC-PDPA (6.4), subsequently driving polymersome disassembly. This, in turn, produces a considerable increase in the osmotic pressure within the endosome that eventually causes temporary endosomal membrane destabilisation and cytoplasmic release.

It is likely that this mechanism of endocytic release is affected by the size of the delivered cargo, and the number of polymersomes accumulated within a single endosomal compartment. Moreover, osmotic lysis is a temporary event resulting from excessive endosomal concentrations, thus it is likely that only a proportion of polymersome cargo will be released into the cytosol (Lomas et al., 2008; Massignani et al., 2010a; Massignani et al., 2009).

To further corroborate the obtained findings and assess the protein cargo escape from the endocytic pathway after polymersome mediated delivery, Transmission Electron Microscopy (TEM) using 15 nm gold labeled antibodies (AuNP-IgG) encapsulated within polymersomes were employed. HDFs were incubated overnight with antibody loaded polymersomes at a concentration of 0.1 μg/ml AuNP-IgG in medium. The metallic particles attached to the delivered IgG can be visualised by TEM and subsequently their sub-cellular localisations revealed. Control experiments were performed in which cells were treated with medium containing free AuNP-IgG.

Multiple images were acquired and the average amount of IgG escaped from the endocytic pathway quantified by image analysis (ImageJ).

The results of this analysis are summarised in Figure 4.5.

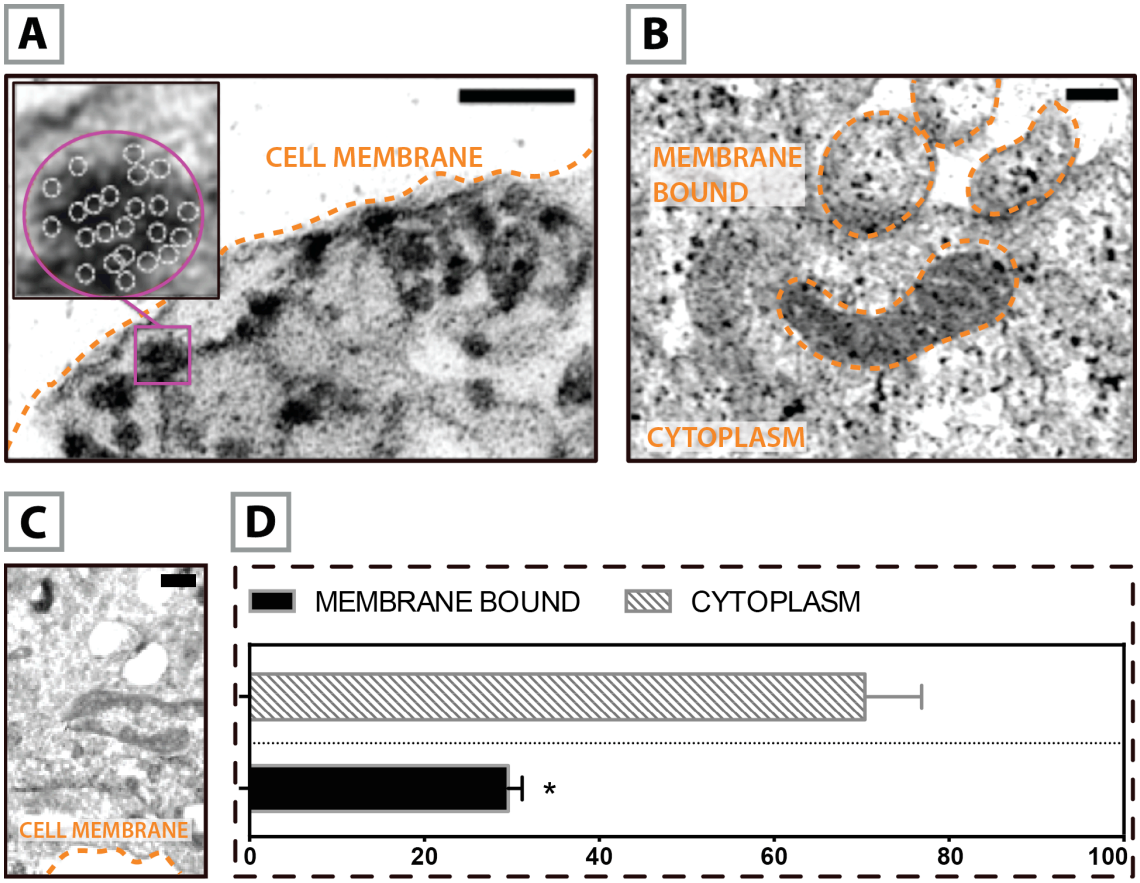

Figure 4.5. TEM analysis of HDF cells which were exposed for 24 h to polymersomes loaded with 15 nm gold labeled IgG. In (A) a cell section at the cell membrane edge is shown, while in (B) the antibody release into the cytosol, as well as antibodies still located within vesicular compartments can be seen. (C) Control experiment of cells treated with free antibody sample. (D) ImageJ quantification regarding the vesicular trapped and released antibody (t-test, p-value * $P \leq 0.05$; ** $P \leq 0.01$; *** $P \leq 0.001$; **** $P \leq 0.0001$). The experimental error is expressed as standard deviation (N=3). Scale bar: 200 nm.

TEM reveals that at the cell membrane, gold labelled IgG molecules are confined within spaces hundreds of nanometers in size. This would suggest the visualisation of the first step of polymersomes uptake, in which the protein is still encapsulated within the synthetic vesicles.

Midsections of the cell (Figure 4.5-B) show, dark dots located both within vesicular like spaces (likely endocytic organelles) as well as distributed throughout the cell cytosol. Quantification of antibodies located within cellular vesicles (see Figure 4.5-D), established that they correspond to ~30% of the total antibody per image, the remainder being found within the cytoplasmic space.

Taken together, these results bode well for intracellular targeting applications. However, when considering intracellular antibody delivery as a technique for live cell imaging, the presence of IgG within the endo-lysosomal compartments could prove problematic, since this may hinder the visualisation of other sub-cellular structures. Even though the majority of the proteins are delivered to the cytosol, those proteins remaining within the endo-lysosomal compartments are retained in compartments orders of magnitude smaller than cell cytosol. This translates to high endosomal antibody concentrations and stronger fluorescent signal than in the cytosol. Such a mismatch can be mitigated by co-delivering a membrane impermeable quencher that absorbs the fluorophores signal only when the two are localised into smaller compartment (i.e. at high concentration). Such absorption occurs by Förster resonance energy transfer (FRET) (Cheng, 2006). This was demonstrated by co-encapsulating Brilliant Violet 421™ labeled antibodies with the corresponding quenching molecule Trypan Blue. For this experiment, anti γ-Tubulin IgG (Brilliant Violet 421™ anti-Tubulin-gamma) was used as a model. The γ-Tubulin is a structural intracellular protein that functions to promote microtubule nucleation and branching. It is localised throughout the cytoplasm, though under particular conditions it accumulates within the nuclear region (Kollman et al., 2011; Raynaud Messina and Merdes, 2007).

Figure 4.6 shows the comparison between cells treated overnight with polymersomes loaded with only anti γ-Tubulin IgG antibodies (0.1 μg/ml IgG) (Figure 4.6-A), and polymersomes loaded with both antibody and Trypan Blue (Figure 4.6-B).

In the latter instance, a considerable reduction in signal originating from the endo-lysosomal organelles is apparent, suggesting that the Trypan Blue quenches the Brilliant Violet 421™ dye. Trypan Blue was subsequently used in all successive microscopy experiments.

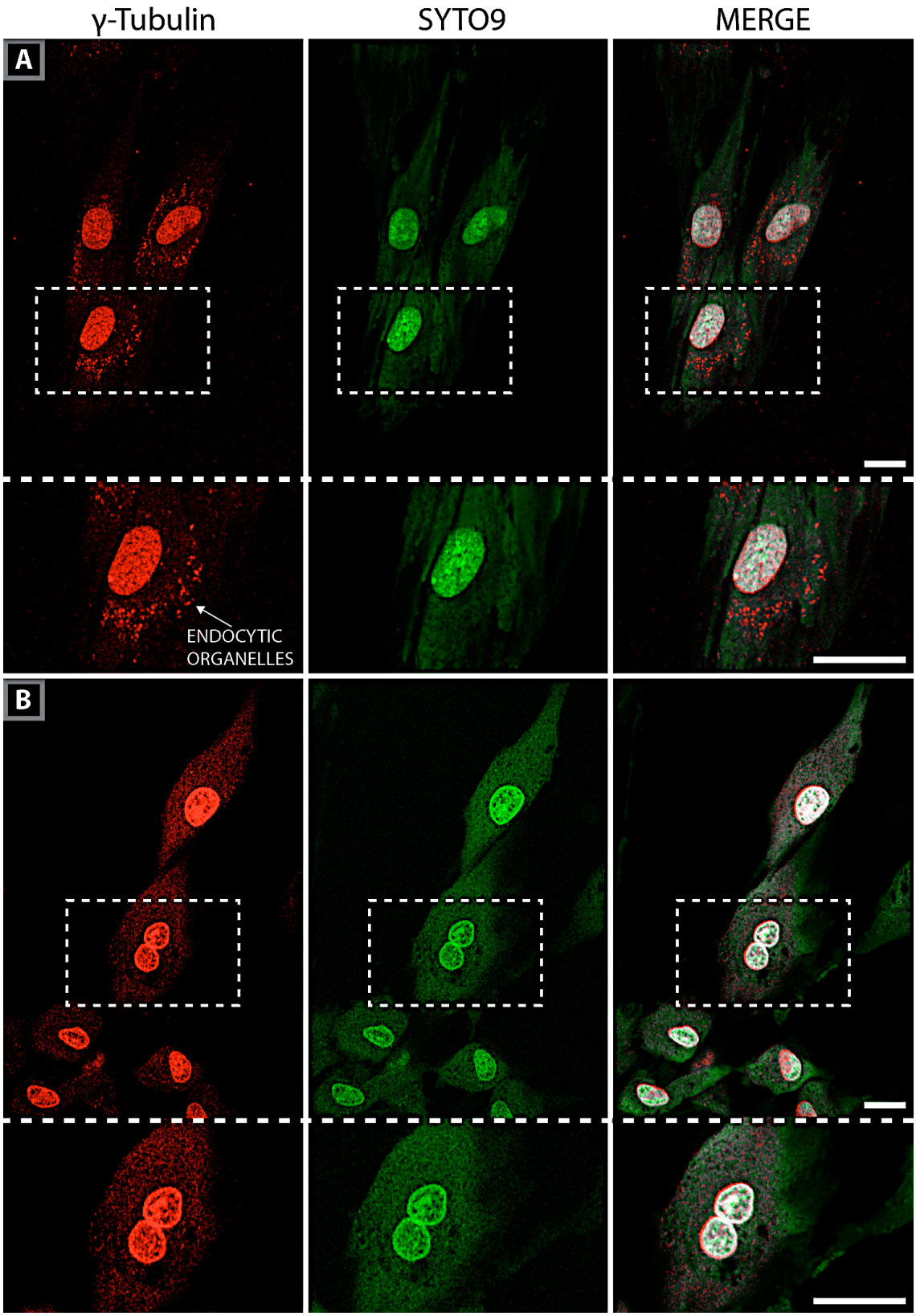

Figure 4.6. (A) CLSM analysis showing polymersome mediated live immunolabelling of γ-Tubulin (Brilliant Violet 421™anti-γ-Tubulin IgG) in live HDFs without the use of quencher (A) or with Trypan-Blue as a quencher (B). Cells were co-stained with green RNA / DNA probe SYTO®9. Scale bar: 50 μm.

4.4. Delivery of functional antibody for sub-cellular targeting in live cells

The ability to directly visualise intracellular proteins in live cells without genetic manipulation, could open many possibilities in the research of cell biology. Polymersomes mediated delivery of antibodies to the cell cytosol can be exploited to target structural proteins and study their activity without artefacts that can result from fixation techniques. This was demonstrated using polymersomes loaded with Brilliant Violet 421™ anti-γ-Tubulin IgG, which enabled real time visualisation of γ-Tubulin localisation during DNA damage caused by the nuclear stain SYTO®9. Though that γ-Tubulin is normally present on the cytoplasm, previous studies have reported that when DNA damage occurs, this protein is translocated to the cell nucleus, interacting with other cellular factors involved in DNA-repair mechanisms (Höög et al., 2011; Hořejší B1, 2012; Lesca et al., 2005; Zhang et al., 2007).

Figure 4.7, show HDF cells stained by SYTO®9 and γ-Tubulin either added to fixed cells (Figure 4.7-A) or delivered via polymersomes to live cells (Figure 4.7-B).

In live cells, SYTO®9 (green), has the dual function to highlight the cell RNA / DNA and to induce irreversible damages to DNA (Ferguson and Denny, 2007; Li et al., 2007a). In fixed cells, the anti γ-Tubulin is localised throughout the cell cytosol and concentrated along microtubule networks and centrosomes. SYTO®9, highlighted as expected the cell DNA and the nucleoli where the rRNA / DNA is accumulated.

Similar results were achieved in live cells imaged after 5 min incubation with high concentration of SYTO®9 (0.5 μM) and upon polymersomes mediated antibody delivery (HDFs were incubated overnight with antibody loaded polymersomes at a concentration of 0.1 μg/ml IgG in medium). Fluorescent signal from antibodies was found localised within the centrosomes, while the nuclear dye highlighted the cellular DNA and RNA. 30 min after SYTO®9 (0.5 μM) addition, the micrograph in Figure 4.7-C shows a different γ-Tubulin distribution, with a strong signal coming from the cell nuclei. It was hypothesised that this is an attempt by the cell to recover the DNA damage induced by SYTO®9. Indeed, previous studies have reported the translocation of γ-Tubulin into the nucleus with DNA repair mechanisms (Hořejší B1, 2012;

Lesca et al., 2005; Zhang et al., 2007). These results demonstrate once more the ability of PMPC-PDPA polymersomes to deliver antibodies in live cells and to use them to monitor internal dynamic.

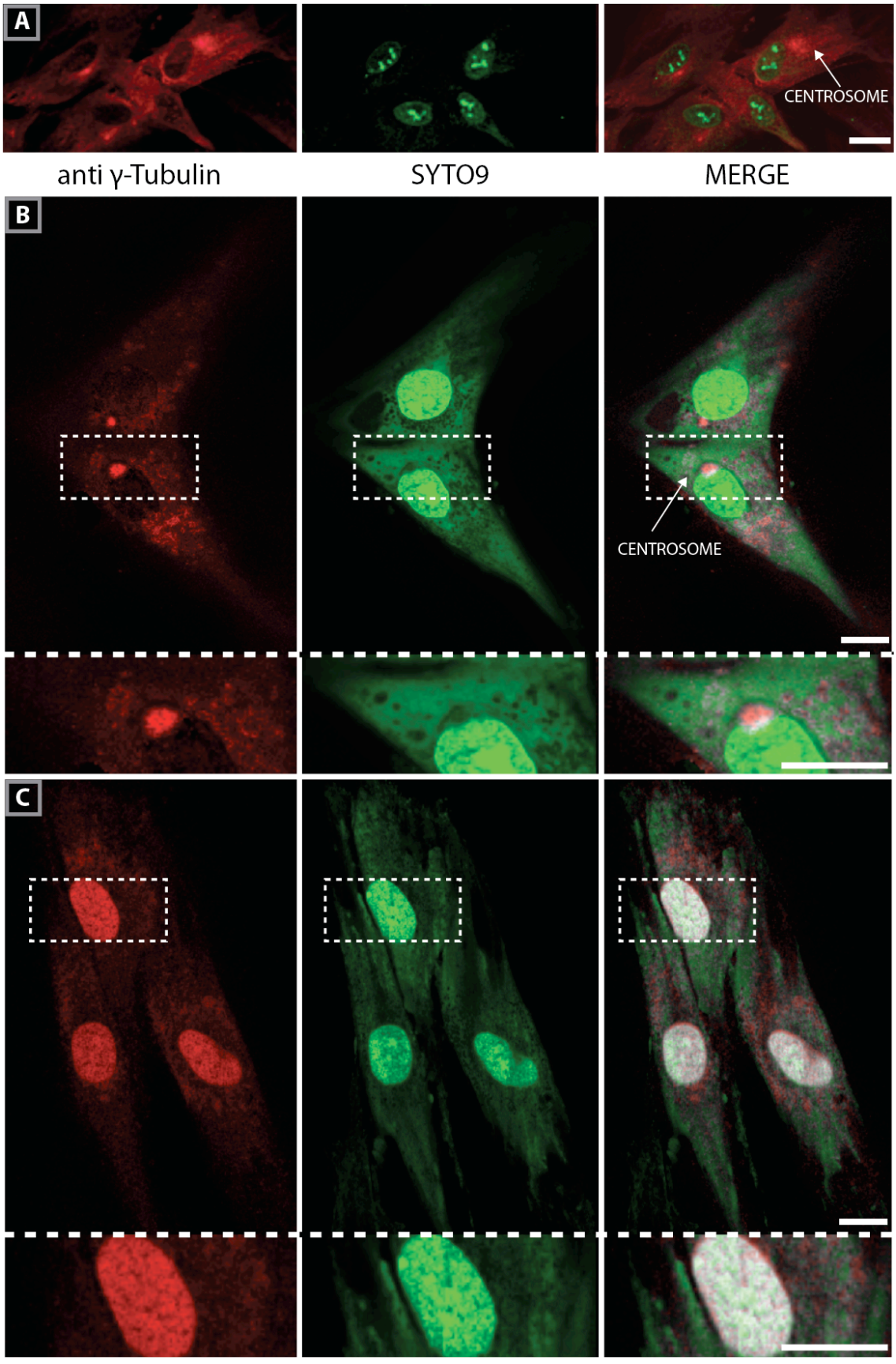

Figure 4.7. (A) γ-Tubulin (Brilliant Violet 421™anti-γ-Tubulin IgG) immunolabeling of fixed HDFs. (B) Polymersome mediated γ-Tubulin immunolabeling in live HDFs. (C) Polymersome mediated γ-Tubulin immunolabeling in live HDFs after SYTO®9 DNA damage. Scale bar: 30 μm.

The proposed mechanism of γ-Tubulin translocation after DNA damage induced by SYTO®9 is schematised in Figure 4.8.

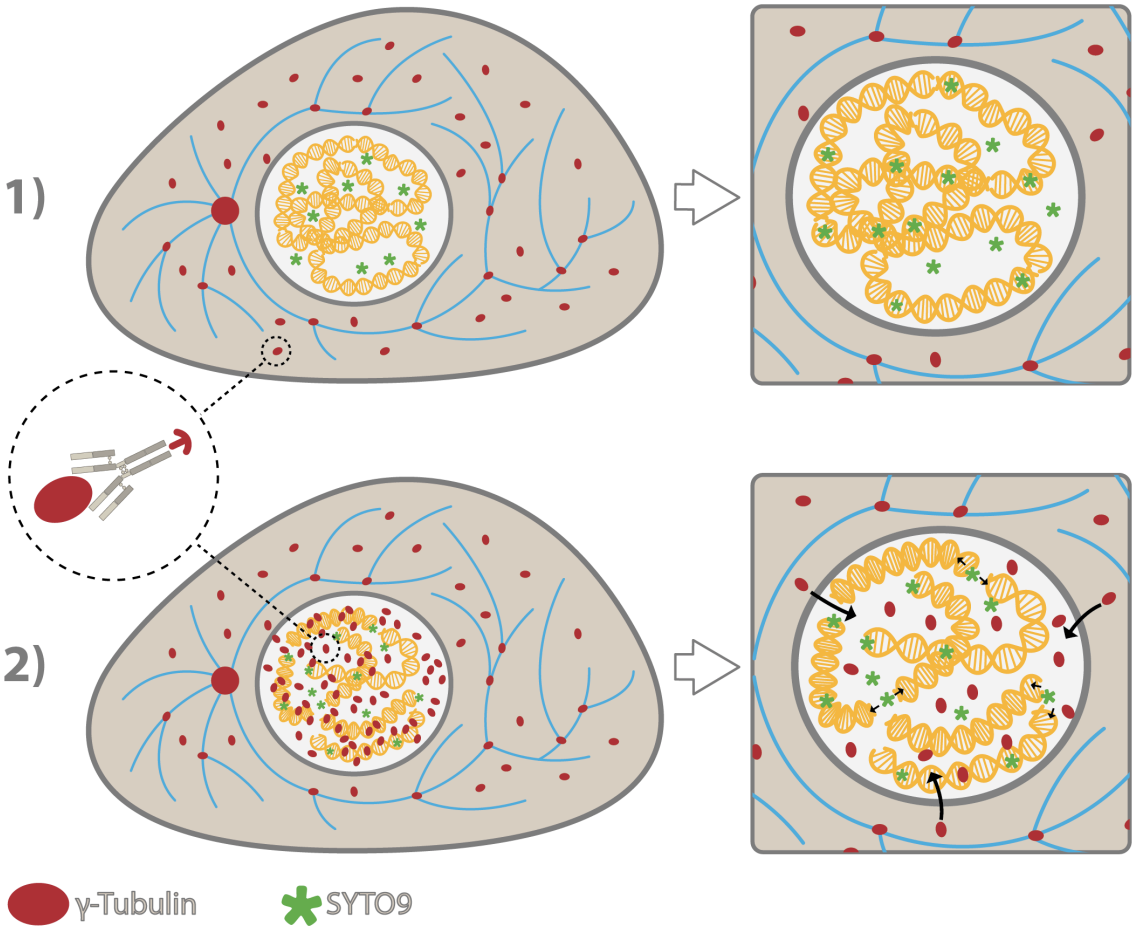

Figure 4.8. Schematic representation of γ-Tubulin intracellular distribution (revealed by the polymersomes delivery of functional Brilliant Violet 421™anti-γ-Tubulin) before (1) and after (2) SYTO®9 DNA damage which promote the γ-Tubulin translocation into the cell nucleus.

To further corroborate these findings, Figure 4.9 shows the CLSM analyses of polymersome delivery of the same IgG (overnight cellular incubation with anti γ-Tubulin antibody loaded polymersomes at a concentration of 0.1 μg/ml IgG in medium) in other cells including human embryonal carcinoma stem cells (NTera2), human adenocarcinoma cells (HeLa), human melanoma cell (A375), murine fibroblasts (NIH-3T3) and murine brain endothelial cells (bEnd3). The distribution of γ-Tubulin is quite different form cell model to cell model,

confirming the universality of polymersomes as protein delivery system in live cells.

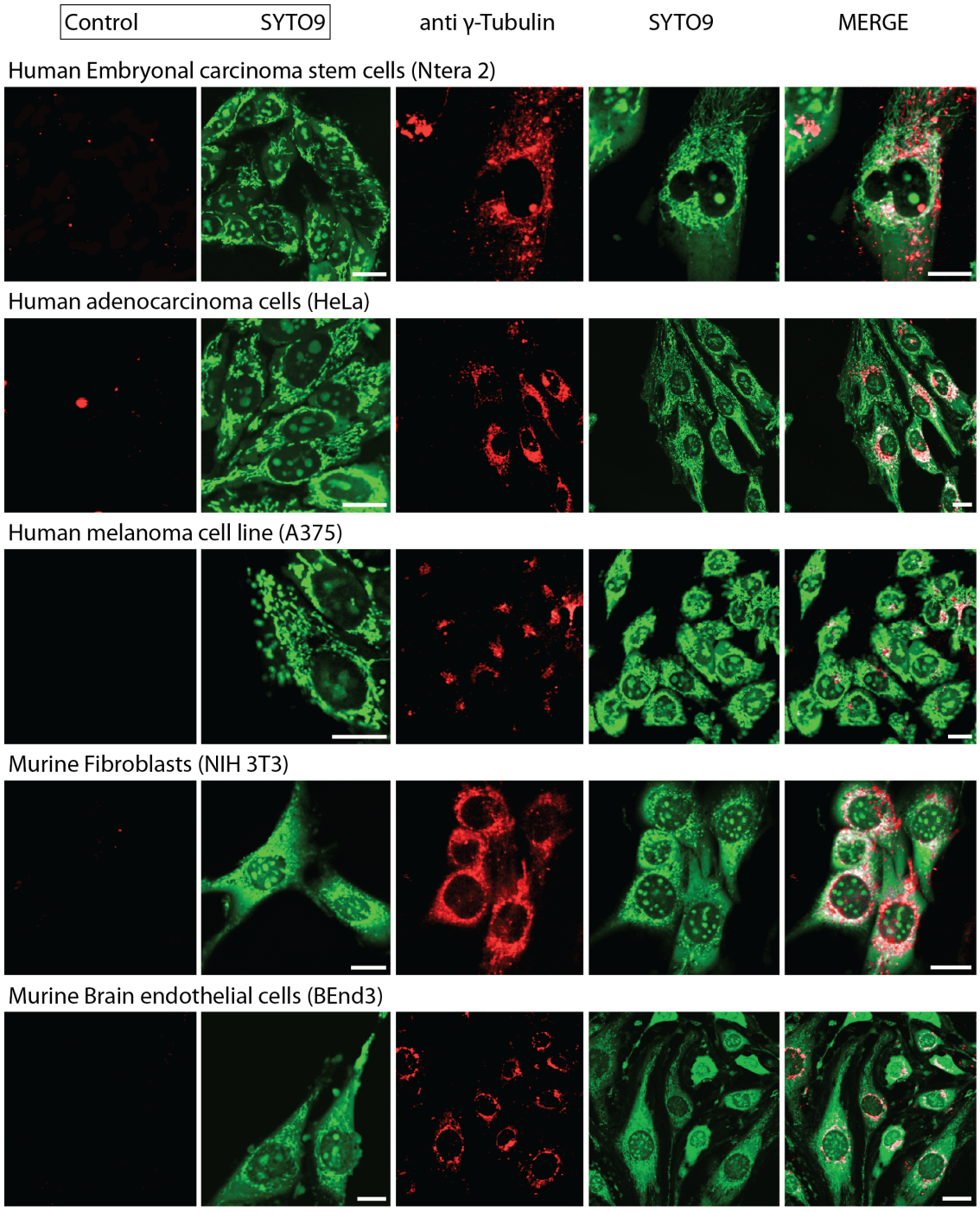

Figure 4.9. Immunolabeling of γ-Tubulin obtained exposing different cell models to polymersomes loaded with Brilliant Violet 421™ IgG-anti-γ-Tubulin. Cells were co-stained with green RNA / DNA probe SYTO®9. Scale bar: 20 μm.

Chapter 5

Results and Discussion

Ki-67 AS INTRACELLULAR TARGET IN ANTICANCER-THERAPY

5.1. Quantification of Ki-67 expression in different cell models

The first experimental approach aimed to quantify and localise the intracellular Ki-67 in non-cancerous and cancerous cells, as a function of their proliferative or quiescent phases. Confocal imaging investigations were carried out in fixed cells treated with SYTO®9 (green channel), to achieve the nucleolar staining, and Brilliant Violet™ 421 anti Ki-67 IgG antibodies (red channel), to quantify the Ki-67 protein. Different cell models were used for this purpose, including human dermal fibroblast (HDF) and human umbilical vein endothelial cells (HUVECs) (non-cancer cells), as well as on breast cancer cells (MDA-MB-231), human pharyngeal squamous carcinoma cells (FaDu), and human adenocarcinoma cells (HeLa) (cancer cells), upon incubating them in both normal and Fetal Bovine Serum (FBS) deprived media to control the proliferation status.

In particular, Figure 5.1 shows that, immediately after starvation (i.e., at time zero), HDF and HUVEC cells posses a high amount of Ki-67, which is located within the nucleus, as expected (top-left section of Figure 5.1).

The amount of protein becomes significant less after 18 h of starvation time, and it is completely undetected after 36 h of FBS deprivation, when cells enter the quiescent phase. On the other hand, confocal microscopy investigations on MDA-MB-231, HeLa, and FaDu cells demonstrated that Ki-67 is present even after 36 h of starvation time, and it is spread throughout the nucleus (top-right section of Figure 5.1). The graph in the bottom part of Figure 5.1, obtained with an *ad hoc* developed image software based on a MATLAB® platform, further

provides a quantification of Ki-67 in both non-cancerous and cancerous cells, as a function of starvation time. Also in this case, a strong decrease in the value of the fluorescence signal is evident for HDF and HUVEC cells, which shifts down of ~70% after 18 h, and becomes c.a. 80% and 98% less after 36 h for HUVEC and HDF, respectively. This condition is significantly different in cancer cells undergoing serum starvation, which does not lead to a down-expression of Ki-67. The quantification of the protein signal was, in fact, roughly the same between t=0 and t=18 h of FBS deprivation, and slightly decreases of ~25% after 36 h of starvation time. The obtained data show that non-cancerous cells are able to control the down-regulation of Ki-67 when forced in a quiescent phase of the cell cycle, while the same experimental conditions do not affect the regulation of Ki-67 in cancerous cells.

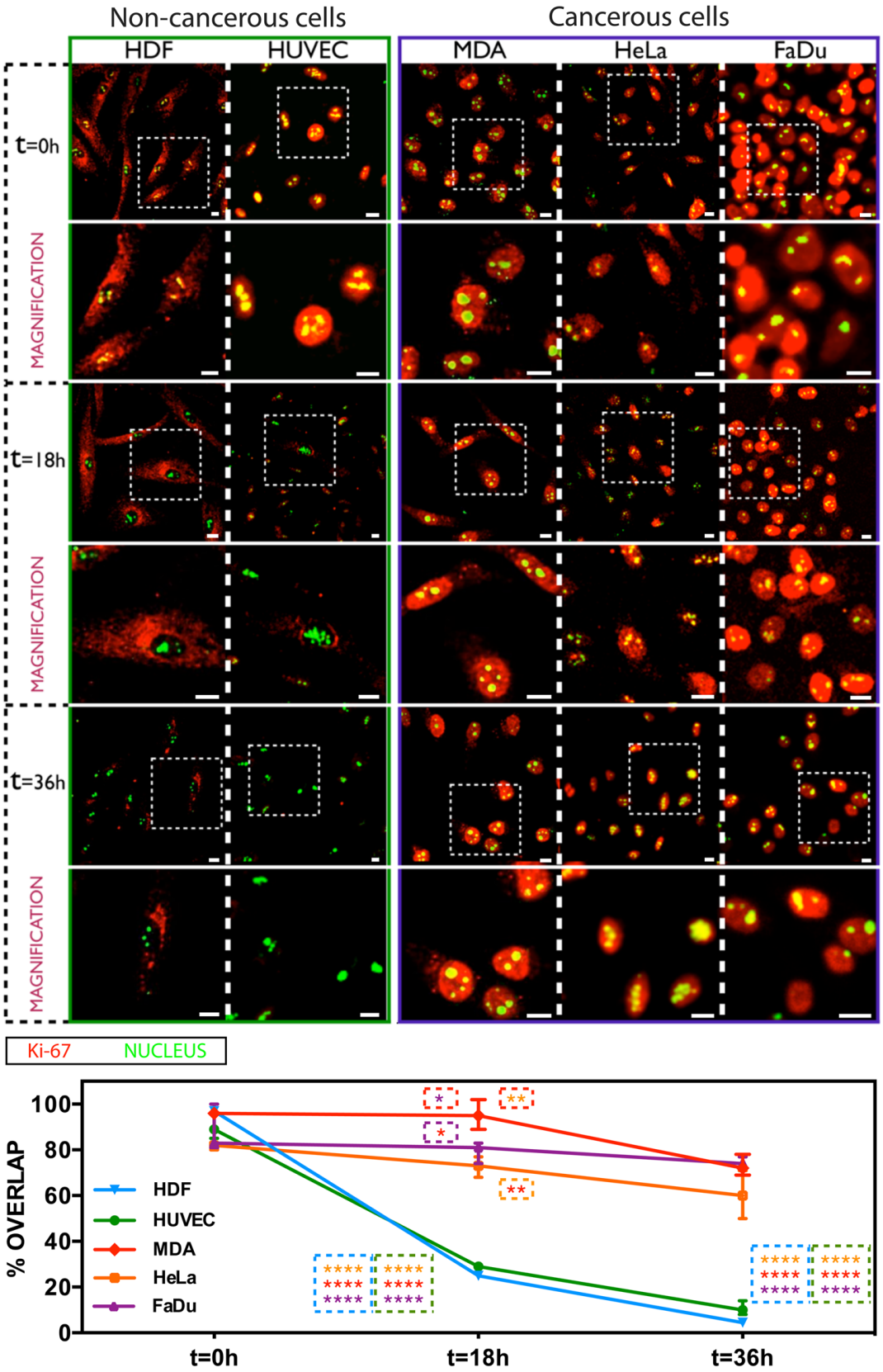

Figure 5.1. Confocal analyses of Ki-67 expression in HDF, HUVEC, MDA-MB-231, HeLa and FaDu cells (analysed overtime after serum deprivation), and the relative fluorescence signal quantification (average overlap value percent) (Two-way ANOVA, p-value * $P \leq 0.05$; ** $P \leq 0.01$; *** $P \leq 0.001$; **** $P \leq 0.0001$). The experimental error is expressed as standard deviation (N=3). Scale bar: 10 μm.

5.2. Ki-67 expression in function of the cell cycle

To further explore the cell cycle dynamics, and to better understand and quantify the Ki-67 expression in HDF and MDA-MB-231 cells during the cell cycle (considered, for the next experimental approaches, as representative non-cancer and cancer cells, respectively), a propidium iodide (PI) based fluorescence cytometry (FC) analysis was performed.

In particular, this characterisation confirmed that ~62% of HDF cells, incubated with a complete growth medium, are in the G_0/G_1 phase (namely, they are quiescent / synchronised), and ~38% are in the $S/G_2/M$ steps (i.e., in a proliferative status), as shown in Figure 5.2-A. Upon 36 h of serum starvation, ~98% of fibroblasts are quiescent, in the G_0/G_1, and only 2% of cells are in active $S/G_2/M$ phases (Figure 5.2-A). On the other hand, the same FC investigations on MDA-MB-231 cells revealed that a significant difference between normal cultured and starved cells is not evident. As depicted in the right side of Figure 5.2-B, in fact, ~54% of breast cancer cells incubated with complete medium were in the G_0/G_1 stage, and ~46% in the phases $S/G_2/M$. Similarly, after incubation with serum deficient growth medium, ~75% of MDA-MB-231 cells were in the G_0/G_1 and ~25% of cells were in the $S/G_2/M$ (Figure 5.2-B). This first evidence confirmed the inability of breast cancer cells to control the cell cycle check points (even after serum deprivation), and enabled to set the starvation condition for the next experimental approach, where the presence of Ki-67 was quantified (in both HDF and MDA-MB-231), as a function of the cell cycle phase. As shown in Figure 5.2-A, in fact, FC analyses of HDF cultured in normal medium displayed the presence of Ki-67 (the blue graph does not overlap with the control grey graph), while the protein is strongly down regulated during the cell stationary phase (G_0/G_1), induced by serum starvation. This is evident by the strong overlap between the blue and grey graph of Figure 5.2-A, and by the relative signal quantification. On the other hand, MDA-MB-231 displayed a different behaviour. The expression of Ki-67 in breast cancer cells is, hence, rather similar for cells growing in both complete and FBS-deprived medium (Figure 5.2-B), thus in strong agreement with the previous findings of Figure 5.1. Taken together these data indicate a different Ki-67 regulation pathway between HDF and MDA-MB-231 cells.

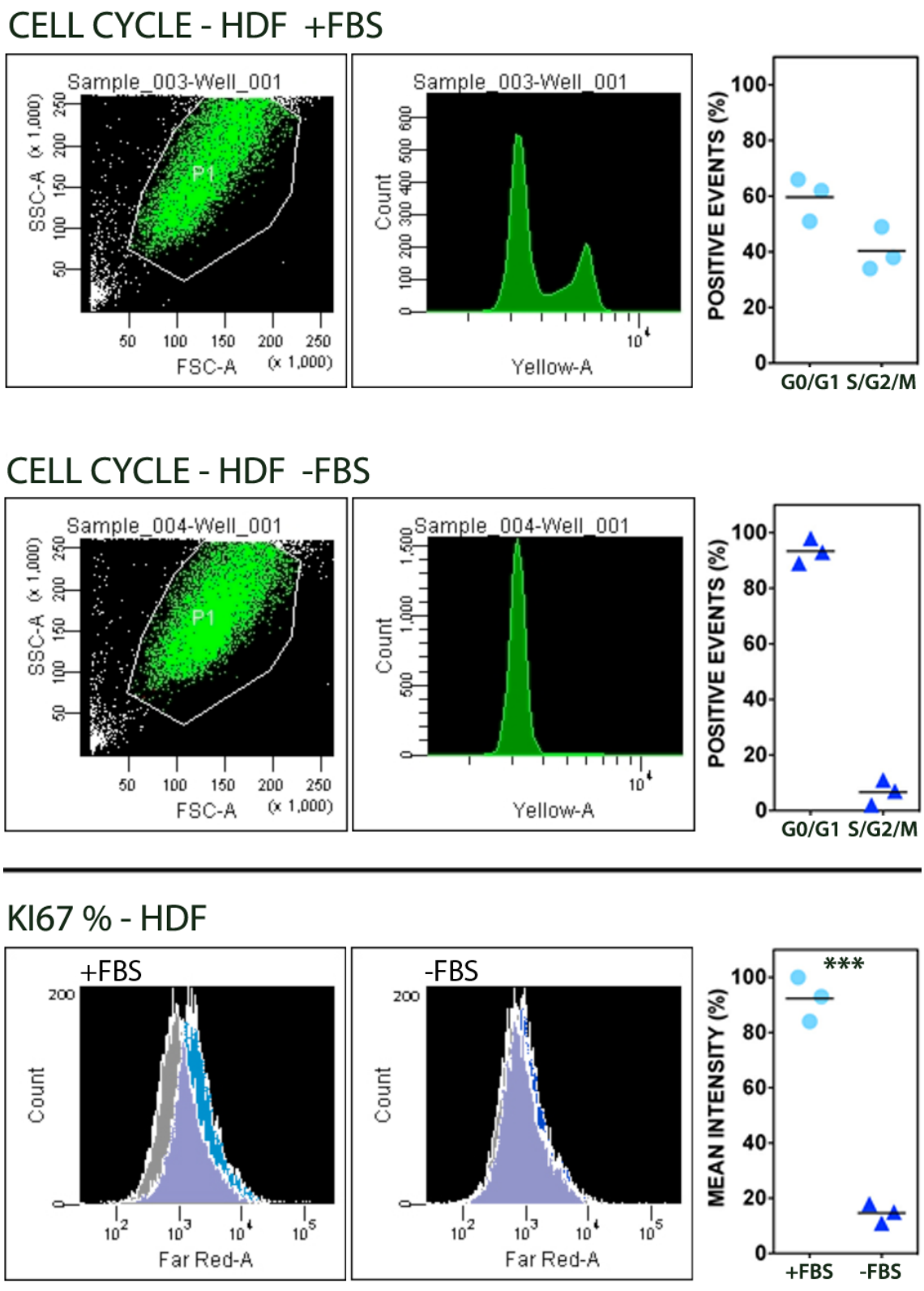

Figure 5.2-A. (Left) Flow cytometry analyses of the cell cycle in HDF before and after serum starvation. (Right) Flow cytometry quantification of Ki-67 expression in HDF cells as a function of the cell cycle stages (t-test, p-value * P ≤ 0.05; ** P ≤ 0.01; *** P ≤ 0.001; **** P ≤ 0.0001). The experimental error is expressed as standard deviation (N=3).

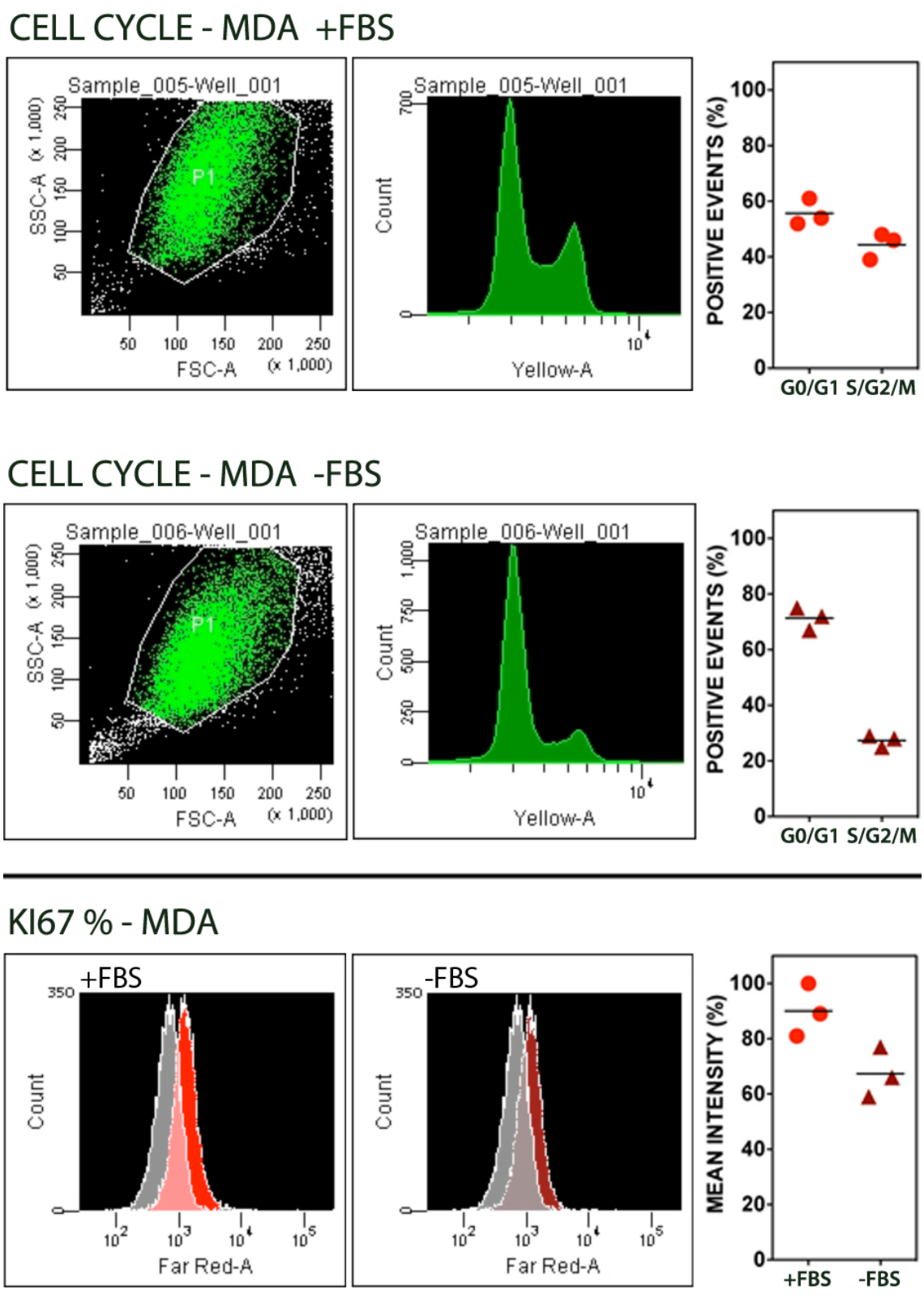

Figure 5.2-B. (Left) Flow cytometry analyses of the cell cycle in MDA-MB-231 before and after serum starvation. (Right) Flow cytometry quantification of Ki-67 expression in MDA-MB-231 cells as a function of the cell cycle stages (t-test, p-value * $P \leq 0.05$; ** $P \leq 0.01$; *** $P \leq 0.001$; **** $P \leq 0.0001$). The experimental error is expressed as standard deviation (N=3).

5.3. Ki-67 gene knock-down experiment

To further explore whether the regulation of Ki-67 expression is controlled at transcriptional level, a Ki-67 gene knock-down experiment was performed.
In particular, cells were transfected with a lentivirus, which codifies for short hairpin RNA (shRNA) involved in the transcriptional degradation of the α and β splice variants of Ki-67, respectively (Figure 5.3). The confocal analyses in Figure 5.3 show that HDF cells do not display the fluorescence signal from the reporter GFP gene immediately after viral infection (t=0 h), while it is evident the presence of Ki-67 as red spots. After 24 and 48 h, fibroblast cells are completely infected, as confirmed by the strong green signal, combined with the down-expression of Ki-67 (the red spots completely lack in this case). These outcomes are surprisingly different in MDA-MB-231 breast cancer cells. In this case, the viral infection with shRNA does not influence the down regulation of Ki-67, which is still present even after 24 and 48 h, as highlighted by the red signals. The graph in the bottom part of Figure 5.3, which provides a signal quantification, confirms the strong down-expression of Ki-67 in transfected HDF, together with the impossibility to repress the transcript expression in transfected MDA-MB-231 cells. In this latter case, the analysed signals are very close to those belonging to the control cells, which were infected with a not codifying (scrambled) sequence.

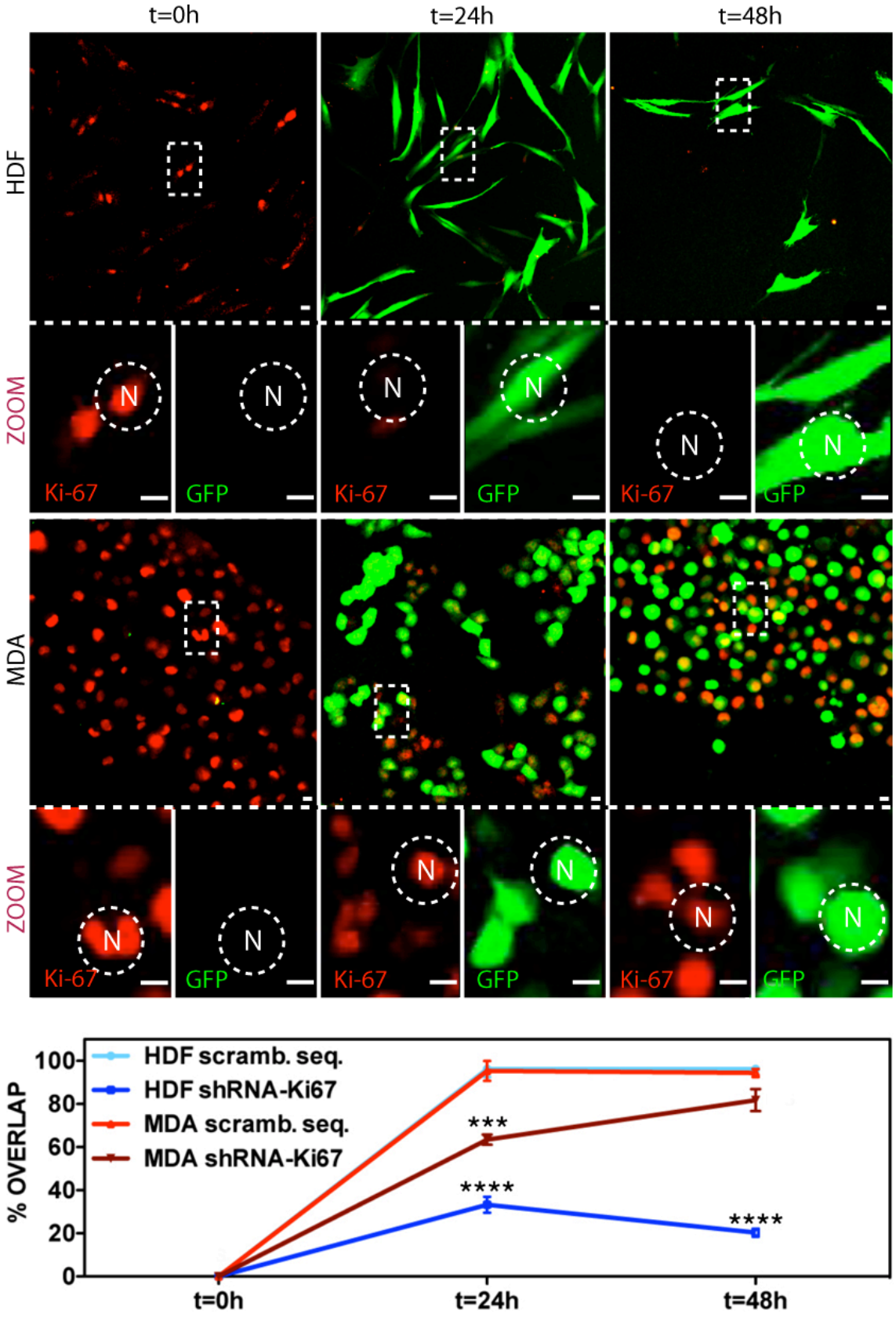

Figure 5.3. Confocal analyses of Ki-67 expression in HDF and MDA-MB-231 cells after shRNA knock-down. Bottom part: graph showing the Ki-67 protein quantification (Two-way ANOVA, p-value * $P \leq 0.05$; ** $P \leq 0.01$; *** $P \leq 0.001$; **** $P \leq 0.0001$). The experimental error is expressed as standard deviation (N=3). Scale bar: 10 μm.

In addition, Reverse Transcription Quantitative Polymerase Chain Reaction (RT-qPCR) analysis were carried out to precisely quantify the amount of mRNA codifying for the two α and β splice variants, upon shRNA assays (Figure 5.4).

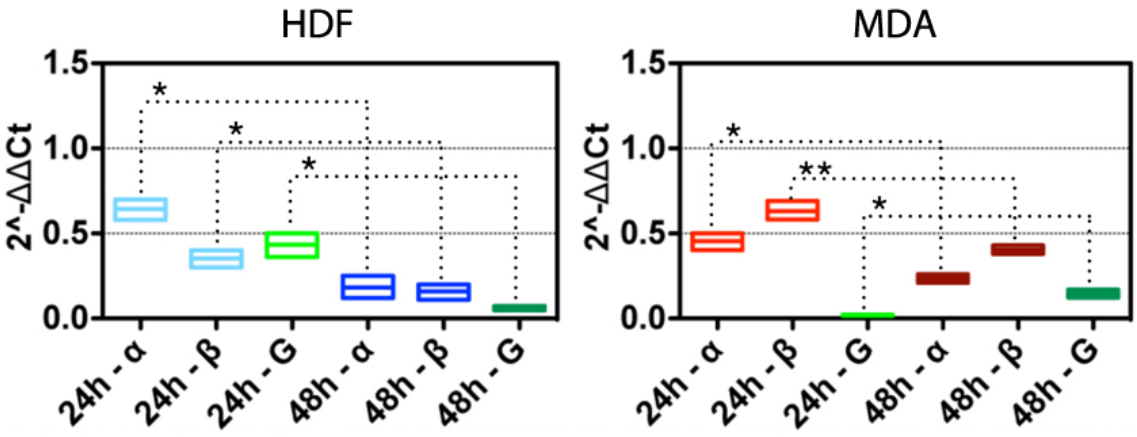

Figure 5.4. RT-qPCR quantification of the α and β splice variants of Ki-67, and GAPDH (G), after virus knock-down in HDF and MDA-MB-231 cells (t-test, p-value * P ≤ 0.05; ** P ≤ 0.01; *** P ≤ 0.001; **** P ≤ 0.0001). The experimental error is expressed as standard deviation (N=3).

As confirmed in Figure 5.4, the level of mRNA of HDF cells is significantly lower after 24 h of viral infection (the ΔΔCt was c.a. 0.7-0.8 for the β, and c.a. 0.3-0.4 for the α), and became even less after 48 h (the green graph represents the internal control). In addition, the amount of mRNA for the β splice variants was found to be overall higher than the α after 24 h, while these levels were rather similar after 48 h (Figure 5.4). On the other hand, the level of Ki-67 transcript in MDA-MB-231 cells was slightly higher than the HDF, upon both 24 and 48 h of viral infection (the ΔΔCt was about 0.5 for the β splice variant and 0.7 for the α after 24 h, and 0.3 for the β and 0.4 for the α after 48 h). Interestingly, there is also a significant difference in the expression levels of the two splice variants between HDF and MDA-MB-231 cells. In particular, while the α is more expressed in fibroblast, the β is much more present in breast cancer cells.

The ΔCt quantification in Figure 5.5 further corroborates the quality of the analyses. In fact, both HDF and MDA-MB-231 show that the internal control gene glyceraldehyde 3-phosphate dehydrogenase (GAPDH) is not affected during the overtime Ki-67 gene knockdown experiments.

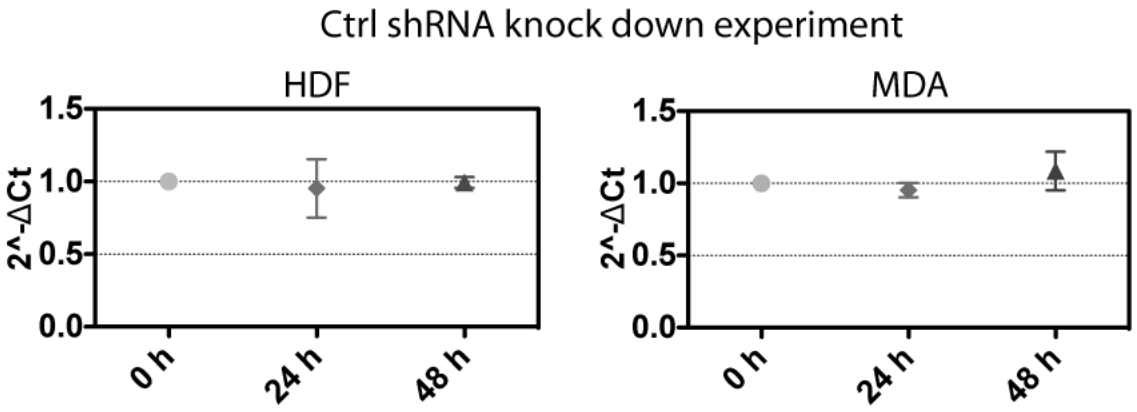

Figure 5.5. RT-qPCR ΔCt quantification of GAPDH internal control at different time points during Ki-67 gene knockdown experiments (t-test, p-value * P ≤ 0.05; ** P ≤ 0.01; *** P ≤ 0.001; **** P ≤ 0.0001). The experimental error is expressed as standard deviation (N=3).

The are two hypothesis that can be considered to explain the different expression levels of the α and β isoforms between HDF and MDA-MB-231 cells. The first one refers to the fact that the two isoforms may undergo very different degradation pathways in non-cancer and cancer cells. In the second hypothesis, each specific cell model could express different levels of the two variants. Furthermore, considering the data shown in Figure 5.4, another important outcome should be highlighted. Despite the Ki-67 transcript is degraded overtime by the action of the introduced shRNA, the protein is still present in MDA-MB-231 cells. This probably because Ki-67 is more stable herein or, alternatively, its post-translational degradation fails to occur in cancer cells.

5.4. Ki-67 expression in cancerous and non-cancerous cells before and after nutrients deprivation

To have a deeper insight into the molecular bases of Ki-67 expression (and of the relative splice variants) and to shed light on the different mechanisms of Ki-67 post-transcriptional and post-translational regulation, Western blot assays was carried out with the automated Simple Western™ (or Simon™). This automated Western blot technology is based on capillary-electrophoresis-SDS (Sodium Dodecyl Sulfate) (CE-SDS). The protein identification is performed upon incubation with a primary antibody, followed by an immunodetection based on a horseradish peroxidase (HRP), which is conjugated to the secondary

antibody, together with a chemiluminescent substrate for the binding detection. This automated Simple Western™ combines several advantages, including the possibility of quantification, together with the higher reproducibility of results over time and between different users (Boge et al., 2012; Rustandi et al., 2012).

This analysis was performed in both the cell models tested. In both cases, the Ki-67 protein expression was quantified before and after 36 h of FBS deprivation from the cell medium. As previously described in Figure 5.2-A and 5.2-B, this leads the ~98% and ~75% of HDF and MDA-MB-231 in a quiescent (G_0/G_1) state respectively.

As shown in Figure 5.6, the Western blot analysis confirms that Ki-67 is present within fibroblast cells grown in complete medium, although in this case the two different splice variants were not noticeable. This is evident in both the profile of expression, where the relative peak of the protein is present, and in the protein run lane in the inset (the dark spot above the profilometer analyses).

On the other hand, Ki-67 lacks in HDF undergoing 36 h of serum deprivation, as confirmed by the absence of both the relative intensity peak and the protein band in Figure 5.6. The chromatograms in the graph of Figure 5.6 further quantify that fibroblast forced to a quiescent state have c.a. 60% less amount of protein, compared to the same cells in the normal medium. However, this represents a rather underestimation since the software detects also the signal coming from the background region of the lane.

Concerning the MDA-MB-231 cells, the expression of Ki-67 is demonstrated to be constitutive / constant in the presence of FBS, as well as after 36 h of serum starvation. This is in fact evident in the Simple Western™ quantification profile of Figure 5.6, together with the relative protein band spot in the inset, which both confirm the significant presence of Ki-67 (the α and β splice variants were both detected in this case). The graph, in the right side of Figure 5.6, also assessed the similar amount of the protein either when the cells are pushed to a quiescent stated (-FBS) and were they are in normal conditions (+FBS).

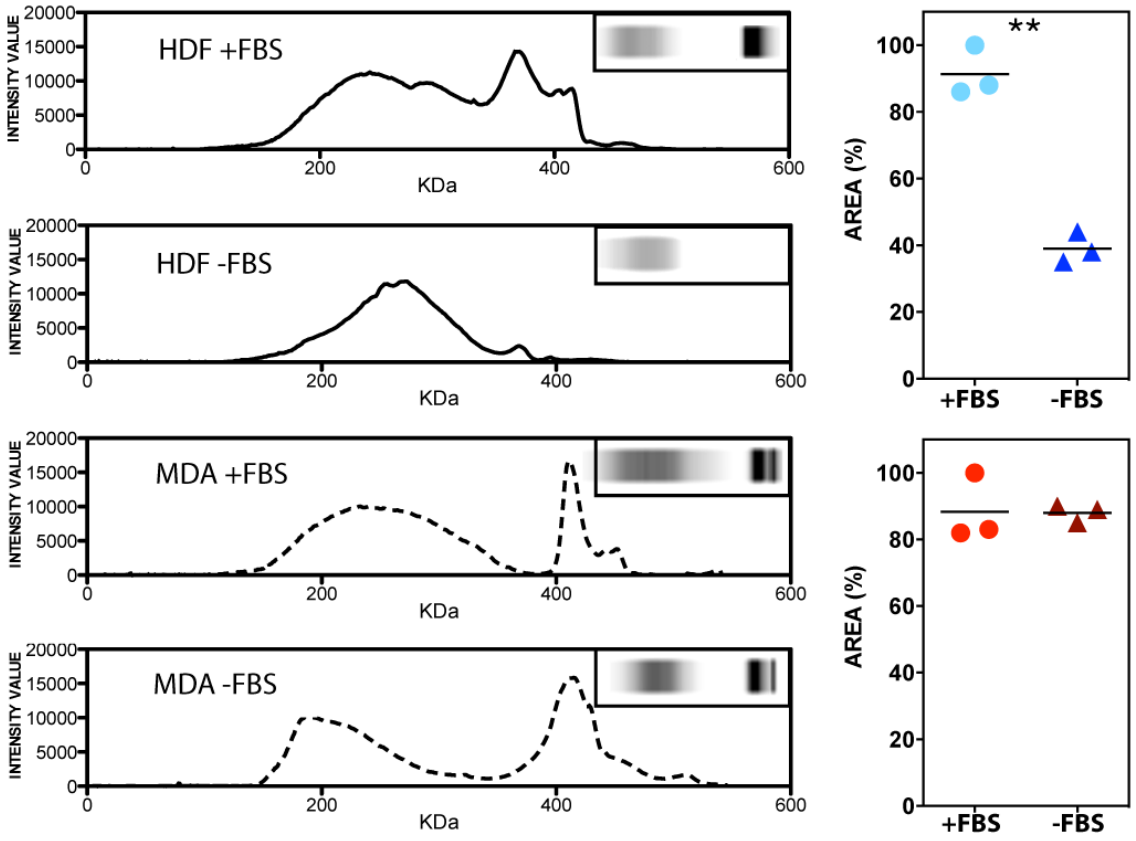

Figure 5.6. Simple Western™ quantification profile of Ki-67 in HDF and MDA-MB-231 breast cancer cells, growing in both media supplemented (+FBS) and lacking of FBS (-FBS) (t-test, p-value * $P \leq 0.05$; ** $P \leq 0.01$; *** $P \leq 0.001$; **** $P \leq 0.0001$). The experimental error is expressed as standard deviation (N=3).

To further validate the data obtained from the automated Simple Western™, the ERK 1/2 extracellular-signal-regulated kinases were quantified in the same cellular samples. ERK 1/2 are well conserved proteins that are implicated in essential functions for the cell maintenance and, for this reason, they were chosen as internal controls (Roskoski, 2012). As shown in Figure 5.7-A, ERK 1/2 resulted equally expressed for both models (HDF and MDA-MB-231) and in each cell culture conditions.

Moreover, to further corroborate the Simple Western™ analyses, a standard Western blot assay was also performed, confirming that the results are entirely comparable between the two methods (Figure 5.7-B).

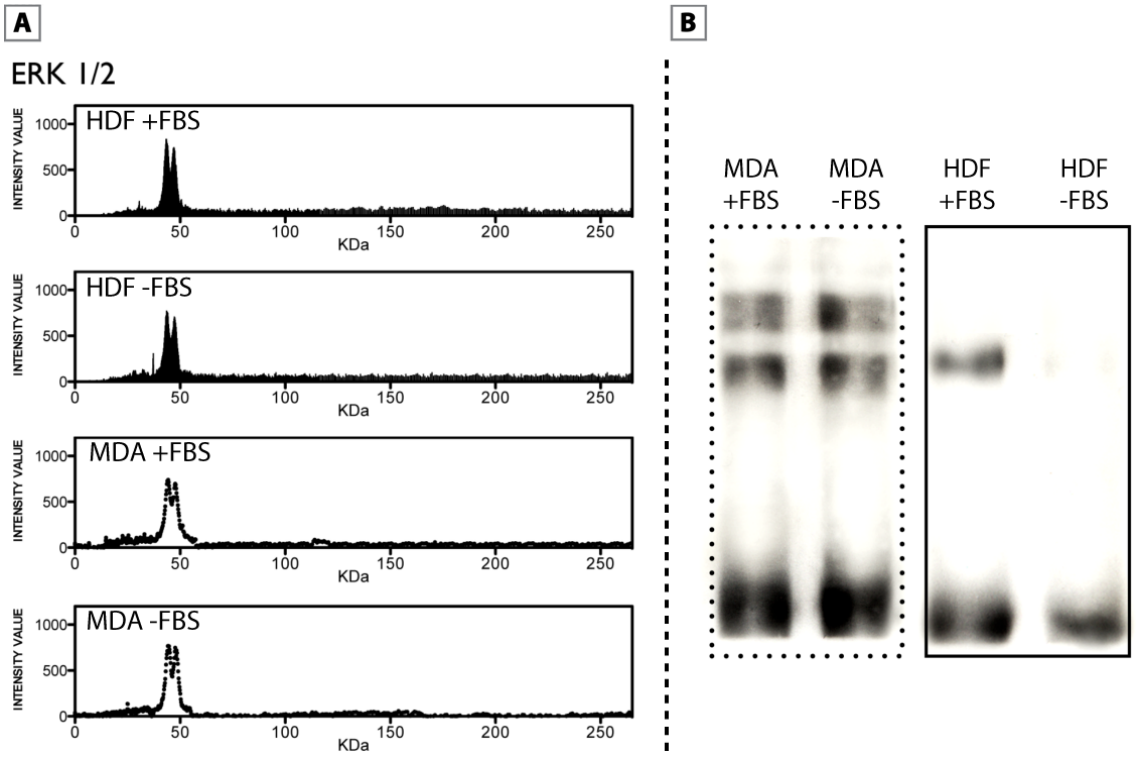

Figure 5.7. (A) Simple Western™ quantification profile of ERK 1/2 in HDF and MDA-MB-231 breast cancer cells, before and after FBS deprivation. (B) Standard Western blot analysis of Ki-67 in HDF and MDA-MB-231 breast cancer cells, before and after FBS deprivation.

5.5. Ki-67 α and β splice variant expression as a function of the nutrients deprivation

In addition to the presented data, it is herein further explored and discriminate the level of genetic expression of the two main Ki-67 splice variants (namely the α and β), in the two different cell models, as a function of the presence and absence of FBS. This approach may enable to better understand which subunit plays a key role in controlling the cell shifting in the different stages of the cell cycle. According to the obtained results, both subunits are present in HDF cells at time zero, as confirmed by the Reverse Transcription Polymerase Chain Reaction (RT-PCR) investigations in Figure 5.8.

After 18 h of serum starvation, the α subunit is still present, but the expression level is significant less comparing to time zero, while the β subunit is completely down regulated. Both the α and β splice variants are then completely unexpressed in HDF cells after 36 h of FBS absence.

On the other hand, RT-PCR analysis on MDA-MB-231 proved that the expression of transcript for both the α and β subunits of Ki-67 does not undergo significant modifications after 18 h (Figure 5.8). However, after 36 h of starvation, only the β subunit seems to be slightly down-expressed as compared to the α.

All these RT-PCR outcomes were further corroborated by means of quantitative PCR analysis (Figure 5.8). In particular, the ΔΔCt quantification displays that the mRNA level for the β splice variant of Ki-67 (with a value < 0.5) is less than the transcript of the α splice variant (value > 0.5), for HDF cells undergoing 18 h of incubation with growth medium lacking of serum.

Upon 36 h of starvation, the ΔΔCt value for both the α and β variants is significant low, confirming that control fibroblasts are able to regulate the down-expression of Ki-67 when they lie in the stationary phase of the cell cycle (G_0/G_1). This condition is significant different in the breast cancer cells, where the FBS deprivation does not lead to a down-regulation of Ki-67.

As shown in Figure 5.8, the MDA-MB-231 cells possess higher level of α and β variants with respect to the HDF ($0.4<\Delta\Delta Ct<0.7$ for the β, and $0.6<\Delta\Delta Ct<0.9$ for the α, respectively) after 18 h of FBS deprivation.

Upon longer starvation time (36 hours), the mRNA level for the β splice variant is significantly down-regulated, while the transcript for the α variant is almost unvaried. However, the most interesting data here is that both the RT-PCR and RT-qPCR confirm a different regulation of the two splice variants, as a function of nutrient starvation. In particular, the α variant seems to be mainly present in both fibroblast and breast cancer cells, suggesting that this splice variant may play a much more important role in regulating the cell cycle, with respect to the β. Alternatively, the α and β variants may undergo two distinct regulation pathways.

A further validation comes from the ΔCt quantification, an important parameter concerning the internal reference control gene GAPDH.

In Figure 5.8, the results of this validation are reported. It is clear that there is not a significant difference in the level of ΔCt signal in fibroblasts during starvation time. Similar data are evident for breast cancer cells.

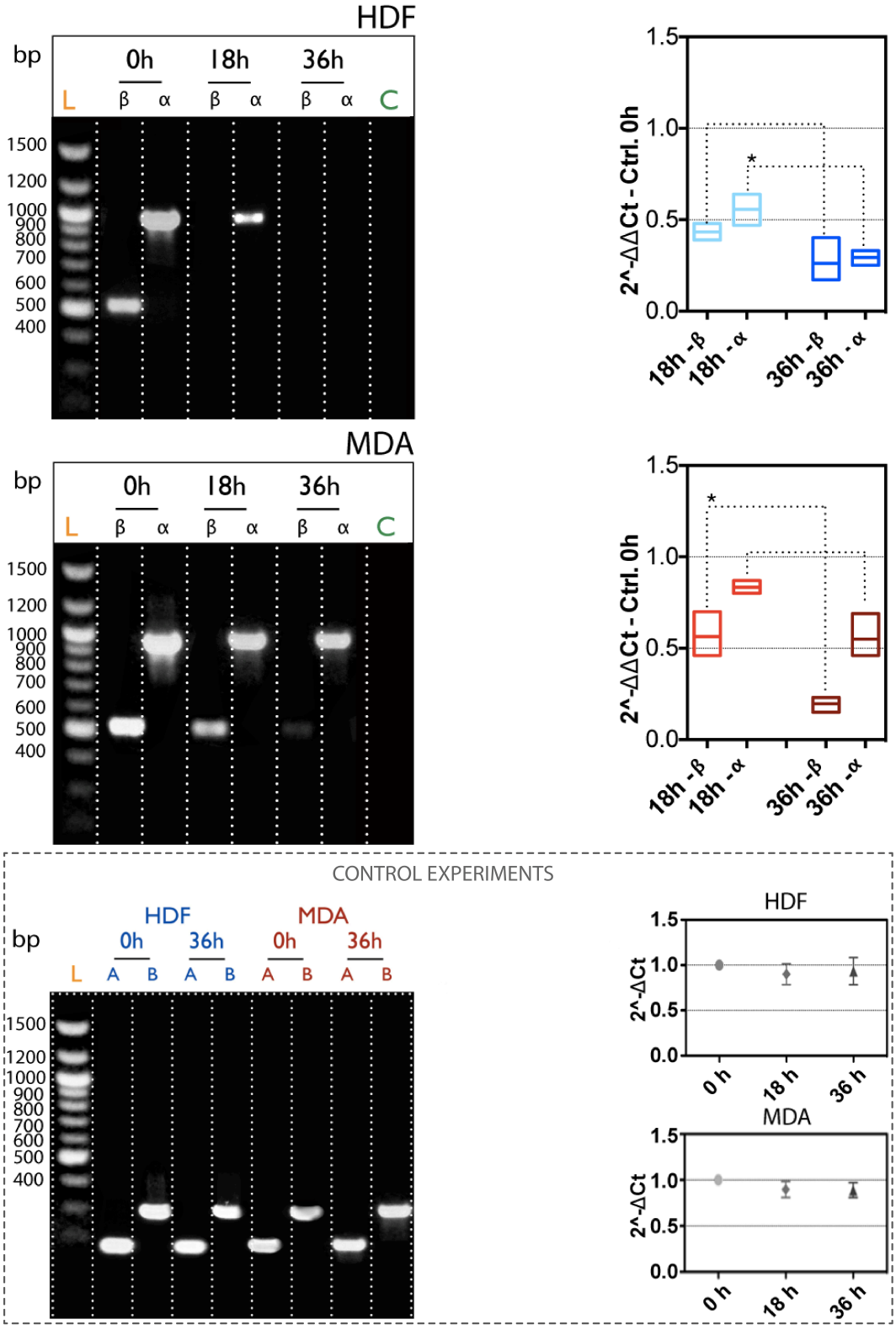

Figure 5.8. RT-PCR (left column), and RT-qPCR (right column) quantification of the α and β splice variants of Ki-67, as a function of nutrient starvation in HDF and MDA-MB-231 cells. Bottom figure: (left) RT-PCR analysis of β-actin (A) and GAPDH (B) as internal controls, before and after nutrient deprivation. (Right) RT-qPCR quantification of the internal control GAPDH after serum starvation (t-test, p-value * $P \leq 0.05$; ** $P \leq 0.01$; *** $P \leq 0.001$; **** $P \leq 0.0001$). The experimental error is expressed as standard deviation (N=3).

5.6. Nuclear-independent molecular mechanisms of Ki-67 regulation

With respect to the data shown in Figure 5.1, a set of confocal colocalisation experiments were performed to better investigate the extra-nuclear detection of Ki-67, and its possible interaction with cytoplasmic pathways.

In this respect, the first explored interaction was between Ki-67 and the proteasome, which is one of the most important cellular quality control mechanisms of proteins (Kish-Trier and Hill, 2013; Makino et al., 2013).

To do this, fibroblasts and breast cancer cells were co-stained with anti-proteasome 20s antibody (which specifically bind the subunit 20s of the proteasome complex), with Ki-67 antibody for targeting the protein of interest, and treated with a modified baculovirus expressing a fusion construct of a Golgi marker (to recognise the Golgi apparatus).

Then, confocal microscopy investigations enabled to explore the intracellular colocalisation and interactions between the proteasome complex, the Golgi apparatus, and Ki-67. As shown in Figure 5.9, HDF cells grown in complete medium display most of the proteasome system and the Ki-67 within the nucleus (in agreement with previous data). This is much more evident in the colocalisation confocal analyses, where it is clear that Ki-67 is mainly present in the nucleus and locally interacts with the nuclear proteasome (albeit the latter is also spread in the cytosol). A quantification of the colocalisation event is also provided by the graph in Figure 5.9, which confirms that fibroblasts growing in complete medium possess c.a. 50% less of Ki-67 interacting with proteasome at the cytosolic level, comparing to the nucleus (with a normalised fluorescence signal at 100%), where the interaction resulted to be stronger. At the same time, there is not a significant difference in the colocalisation signal between Ki-67 and the proteasome system both at the cell nucleus and the cytosol, for fibroblasts undergoing serum starvation. However, serum deprivation leads to an overall lower level of signal from Ki-67 in the nucleus.

On the other side, the confocal investigations in Figure 5.9 show that MDA-MB-231 cells display high levels of Ki-67 in the cytosol and nucleus (where it resulted more abundant), both for starved and non-starved cells. It is, in fact, evident that the protein is spread throughout the nucleus, and some spots are also present in the cytoplasm.

The quantification of the fluorescence signal, in the graph of Figure 5.9, further supports the evidence that the overlap value between the proteasome complex and Ki-67 is ~40% lower in the cytoplasm as compared to the overlap value of the nucleus, in both the conditions tested.

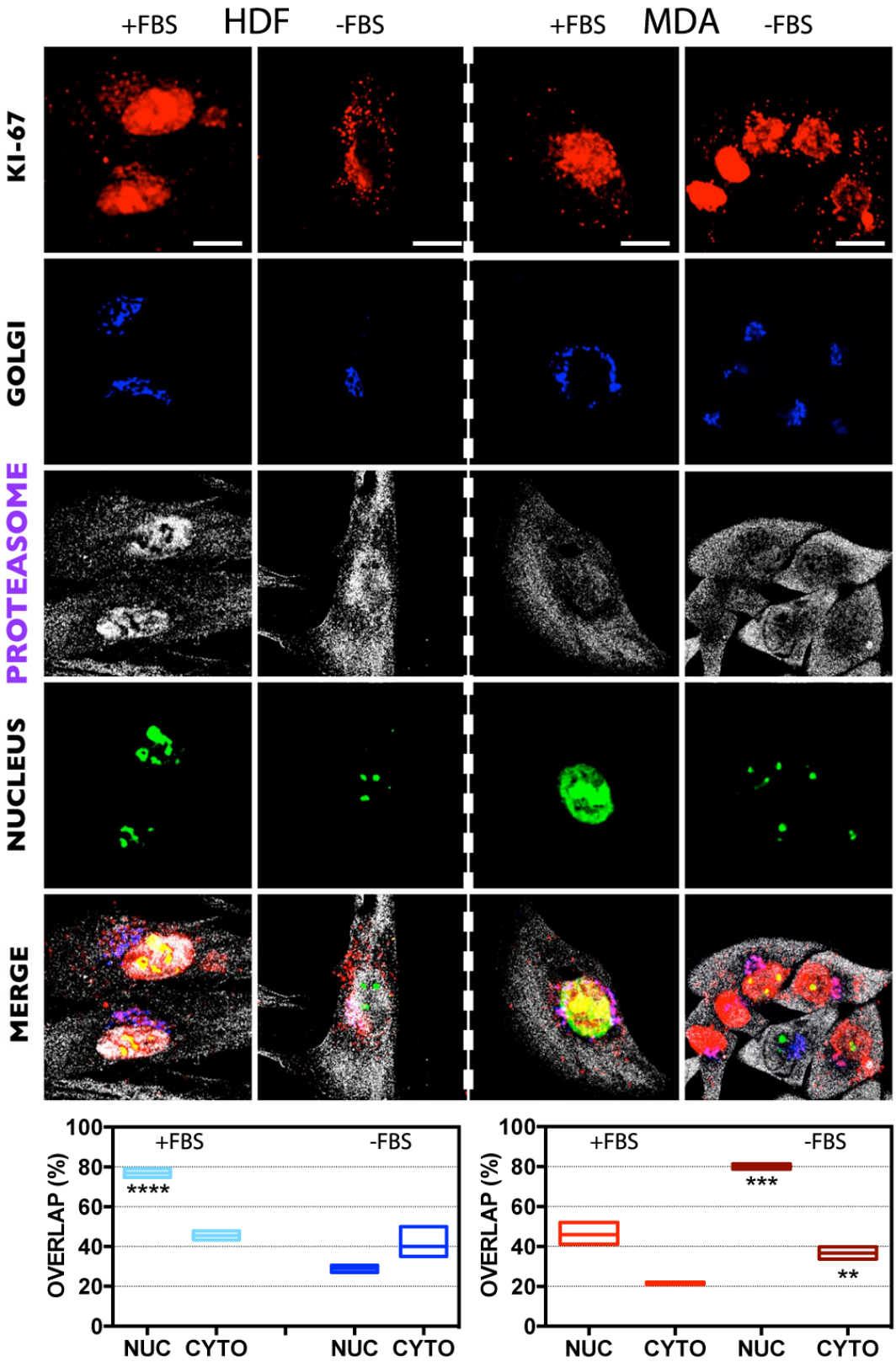

Figure 5.9. Confocal assays and quantification graphs (on the bottom of the picture) of the distribution and interaction between Ki-67 and the proteasome system, in both HDF (left column) and MDA-MB-231 cells (right column). The analyses were carried out with and without the presence of FBS (t-test, p-value * $P \leq 0.05$; ** $P \leq 0.01$; *** $P \leq 0.001$; **** $P \leq 0.0001$). The experimental error is expressed as standard deviation (N=3). Scale bar: 10 μm.

The next efforts were then focused on exploring the possible interaction between Ki-67 and the endoplasmic reticulum (ER) molecular chaperon Binging immunoglobulin protein (BiP). This chaperon is specifically located within the lumen of the ER, and it is responsible for binding the nascent polypeptides which are emerging in the lumen of the ER during co-translational translocation (Gething, 1999; Pimpl et al., 2006; Vashist and Ng, 2004; Zimmermann et al., 2011). BiP plays a pivotal quality control of protein folding: it hinders incomplete or unfolded proteins to reach their final sub-cellular compartments, by activating the ER-associated protein degradation (ERAD). The picture in Figure 5.10 shows the co-distribution of Ki-67 and BiP in active fibroblasts growing into a complete medium.

In this condition, Ki-67 is mainly present in the nucleus (as expected) and only a small portion of the protein seems to interact with the BiP, whose fluorescence signal is randomly spread throughout the cytosol. The overall weak interaction is also confirmed by the graph on the bottom of Figure 5.10, which confirms a low level of overlapping fluorescence signal between the nucleus and the cytosol in proliferating cells. Starved fibroblasts, however, demonstrated to possess a stronger interaction between the cytosolic Ki-67 and BiP that, in this case, is much more precisely localised in the ER / Golgi compartment, as depicted by Figure 5.10 and the relative quantification of fluorescence signal. On the other hand, a significant difference in the Ki-67 and BiP coupling in starved and non-starved breast cancer cells is less evident. Figure 5.10 shows, in fact, the weak interaction between the two proteins, as well as BiP seems to be randomly distributes in both the conditions tested, showing low accumulation at the Golgi compartment in FBS deprived cancer cells. It is worth also mentioning that, after 36 h of starvation time, all the extranuclear Ki-67 was founded to localise within the Golgi apparatus, where it may undergoes further modifications / regulations.

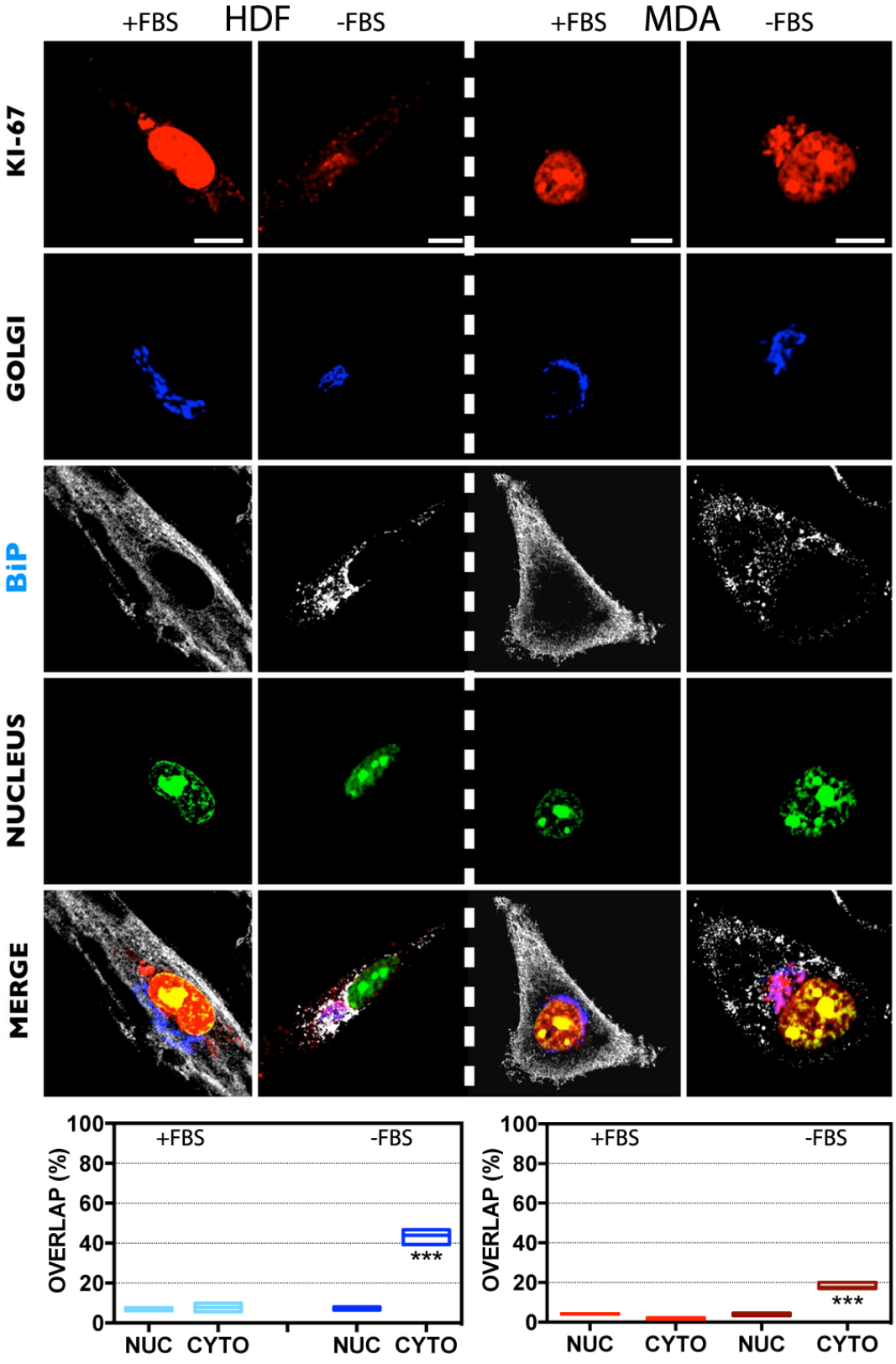

Figure 5.10. Confocal assays and quantification graphs (on the bottom of the picture) of the distribution and interaction between Ki-67 and the chaperone BiP, in both HDF (left column) and MDA-MB-231 cells (right column). The analysis were carried out with and without the presence of FBS (t-test, p-value * $P \leq 0.05$; ** $P \leq 0.01$; *** $P \leq 0.001$; **** $P \leq 0.0001$). The experimental error is expressed as standard deviation (N=3). Scale bar: 10 μm.

After uncovering the role of BiP in the control of Ki-67 degradation, the next investigations aimed to understand the possible interaction with the cytoplasmic coat protein complex II (COPII), mainly because of a preliminary observation of a fully Ki-67 loaded Golgi apparatus after a long starvation time of HDF cells (see Figure 5.1 and Figure 5.12). COPII is the main constituent of vesicles that bud from the endoplasmic reticulum and transport their cargo (namely, secretary proteins) to the Golgi system (Brandizzi and Barlowe, 2013; Derganc et al., 2013; Zanetti et al., 2012).

As depicted in Figure 5.11, there is a significant difference between the distribution of COPII in normal and synchronised fibroblasts, particularly at the cytoplasmic level. However, the overlap of fluorescence signal of Ki-67 and COPII suggests that a proximity between the two proteins is occurring in both the two growth conditions. Concerning MDA-MB-231 cell seeded with a complete media, the fluorescence signal of COPII vesicles displays a very well defined distribution pattern around the nucleus, together with a poor interaction with Ki-67. Upon serum starvation, COPII seems to be widely spread within the cytosol instead. In addition, the overlap signal with Ki-67 is higher as compared to non-starved cells, although this interaction resulted significant less with respect to the same one occurring in fibroblasts.

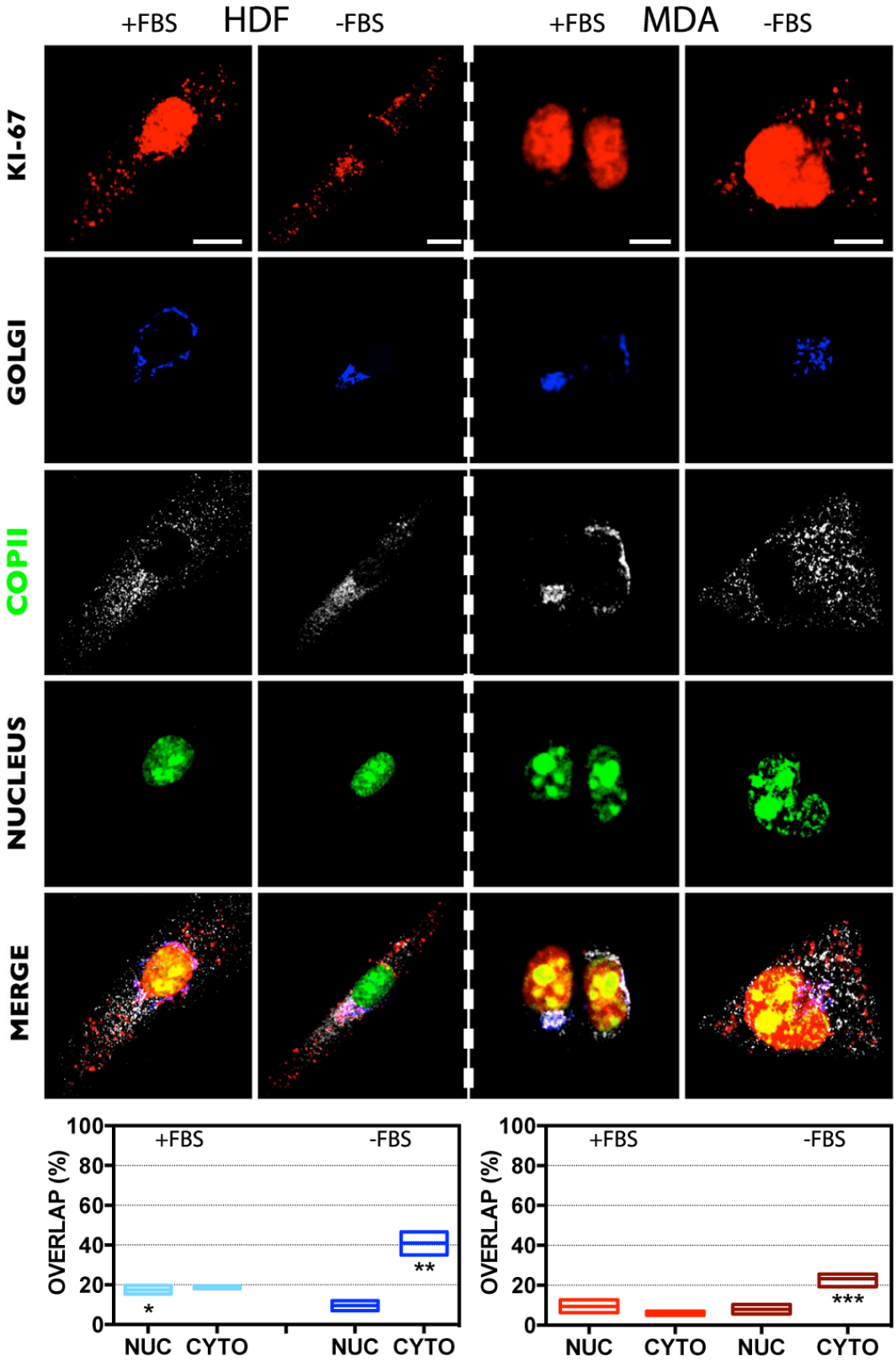

Figure 5.11. Confocal assays and quantification graphs (on the bottom of the picture) of the distribution and interaction between Ki-67 and the COPII, in both HDF (left column) and MDA-MB-231 cells (right column). The analyses were carried out with and without the presence of FBS (t-test, p-value * $P \leq 0.05$; ** $P \leq 0.01$; *** $P \leq 0.001$; **** $P \leq 0.0001$). The experimental error is expressed as standard deviation (N=3). Scale bar: 10 μm.

Finally, the possibility of Ki-67 translocation into the Golgi apparatus was investigated. Figure 5.12 (left hand side) shows that the protein is present in the Golgi system for starved, as well as in non-starved fibroblasts. However, the protein accumulation seems to be higher upon FBS deprivations, as confirmed by the quantification graph (bottom side of Figure 5.12). This condition is dissimilar in breast cancer cells. As displayed in Figure 5.12 and the relative quantification analysis (bottom side of Figure 5.12), in fact, both starved and non-starved MDA-MB-231 cells have a similar distribution of Ki-67 in the nucleus, as well as in the Golgi. In addition, two other possible cellular clearance / degradation mechanisms for Ki-67 were investigated: the lysosome and the autophagosome (see Figure 5.13). However, no interaction between the protein and these two degradation machineries was found.

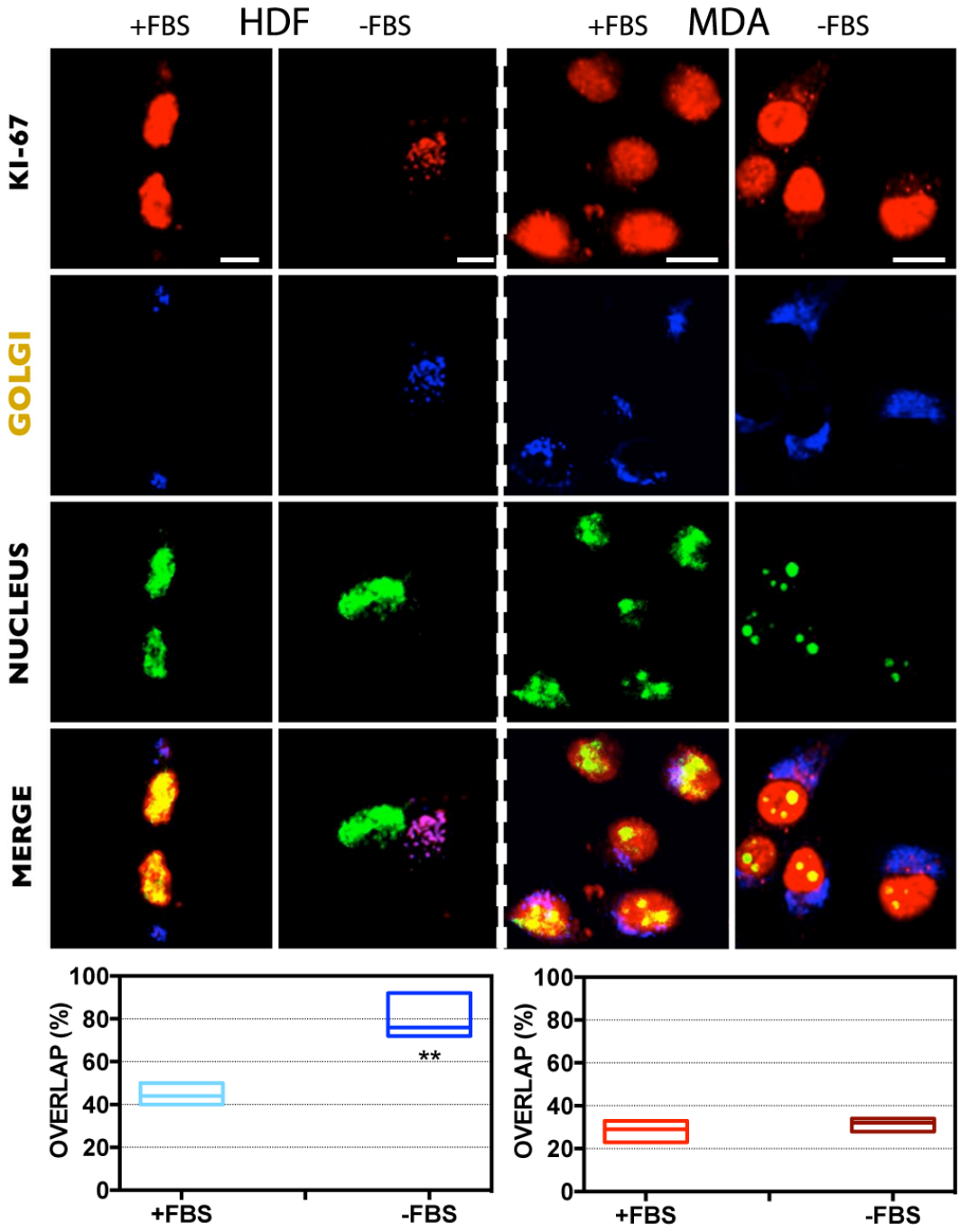

Figure 5.12. Confocal assays and quantification graphs (on the bottom of the picture) of the distribution and interaction between Ki-67 and Golgi apparatus, in both HDF (left column) and MDA-MB-231 cells (right column). The analyses were carried out with and without the presence of FBS (t-test, p-value * $P \leq 0.05$; ** $P \leq 0.01$; *** $P \leq 0.001$; **** $P \leq 0.0001$). The experimental error is expressed as standard deviation (N=3). Scale bar: 10 μm.

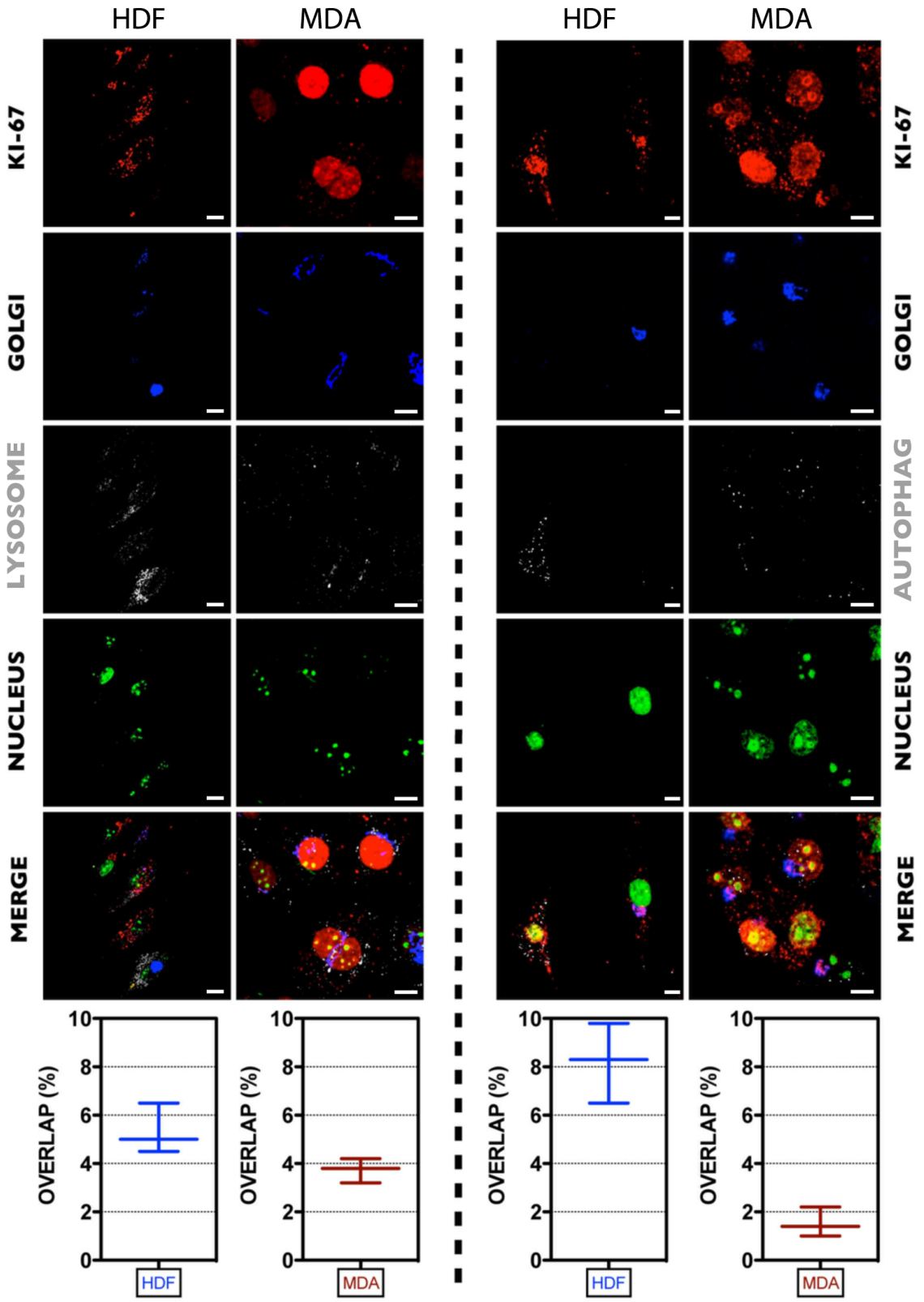

Figure 5.13. Confocal analyses of the interaction and cellular distribution of Ki-67 with LAMPI and LC3B, in HDF and MDA-MB-231 cells before and after serum starvation. Bottom part: graph showing the overlap signal between Ki-67 with LAMPI and LC3B, for HDF and MDA-MB-231 growing in both serum supplemented and deprived media (t-test, p-value * $P \leq 0.05$; ** $P \leq 0.01$; *** $P \leq 0.001$; **** $P \leq 0.0001$). The experimental error is expressed as standard deviation (N=3). Scale bar: 10 μm.

This imaging investigations confirm that Ki-67 is transported outside of the nucleus in proliferating HDF (i.e., during the $S/G_2/M$ phases of the cell cycle), where it interacts with the proteasome complex, which may, in turn, be responsible for the local degradation of the protein. At the same time, fibroblasts in the G_0/G_1 phase have a significant less amount of Ki-67 (the nucleus in this case completely lacks of the protein) that is mainly degraded by the nuclear proteasome. Despite fibroblasts, breast cancer cells seem to have a minor ability to translocate Ki-67 in the cytoplasm, or alternatively they overexpress it in the nucleus. In addition, the proteasome system is unlikely to regulate the degradation of the proteins in both the cytoplasm and the nucleus of cancer cells, resulting in an overall loss of control over the shifting through the different steps of the cell cycle.

Another important point is represented by the Ki-67 / BiP interactions. In this case, the translocation machinery of fibroblasts is able to effectively process the protein. In particular, HDF cells effectively control their ERAD, and this issue is also crucial for finely regulating the transit through the different steps of the cell cycle. This coupling with BiP should not be considered as trivial. Indeed, BiP is demonstrated to physically interact with Ire1α (inositol-requiring enzyme 1α), PERK (protein kinase RNA-like ER kinase), and ATF6 (activating transcription factor 6), which are the three signalling proteins important for the activation and regulation of the unfolded protein response (UPR) pathways (Bertolotti et al., 2000; Hetz et al., 2013; Kimata and Kohno, 2011; Onn and Ron, 2010). In particular, any ER-related stress leads to the activation of these sensor like proteins, which, then, transduce the signals to the cytosol and nucleus in order to restore protein-folding capacity through different and well-defined cellular adaptation pathways (usually, by activating transcription factors which induces the expression of genes involved in aminoacids metabolism, apoptosis, and authophagy) (Hetz et al., 2013). As a consequence, fibroblasts may “sense” misfolded Ki-67 through its coupling with BiP that, in turn, activate the UPR sensors Ire1α, PERK, and ATF6.

On the other side, breast cancer cells seem to fail to activate ERAD machinery, and extranuclear Ki-67 is not correctly degraded, with a consequent loss of control over the cell cycle check points.

Same considerations should be inferred for the ability to direct Ki-67 in the secretory pathways. The strong evidence of interaction between the protein and

COPII-coated vesicles further confirms that fibroblasts are able to correctly deliver the protein in the secretory pathways. Such a possibility is also confirmed by the considerable presence of Ki-67 at the Golgi level. These latter perspectives further support the idea that the transfer from an active to a quiescent phase (after a long starvation period) may be regulated by a dynamic degradation process of Ki-67, which is also related to the ability of non-cancerous cells to deliver the protein in the secretory pathway.

On the other hand, experimental evidences suggest that breast cancer cells fail to direct Ki-67 to the correct secretory pathway (the protein was found considerably less to be included in COPII-coated vesicles), which is crucial for controlling its degradation and / or regulation. In particular, serum deprivation does not lead to an increase of the protein in the Golgi complex, indicating that breast cancer cells may lose the control on Ki-67 turnover.

All these findings are summarised in the scheme in Figure 5.14, which finally shows a proposed molecular mechanisms involved in the extranuclear regulation of Ki-67.

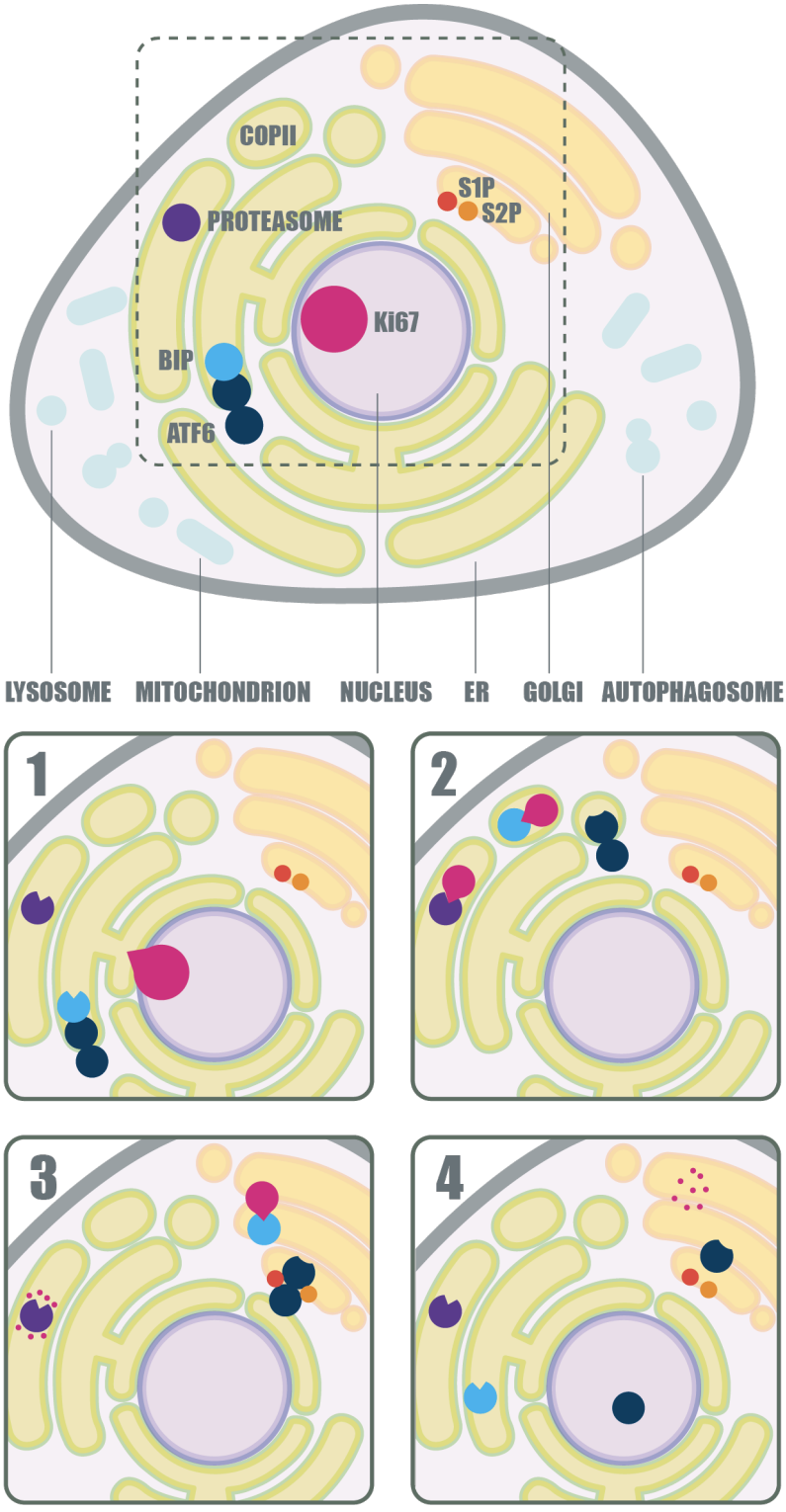

Figure 5.14. Scheme representing the proposed extranuclear molecular regulation and pathways of Ki-67. Upon the transferring of the cell in the G_0 of the cell cycle, Ki-67 is first translocated in the ER (1). This will activate the ERAD signal pathway, which lead BiP to bind the newly ER transferred Ki-67 (probably activating the UPR). Then, Ki-67 may interact with the proteasome system, and this complex buds from the ER into specific COPII coated vesicles (2), which transport their cargo to the Golgi apparatus (3) where Ki-67 may be further recycled and / or degraded (4).

5.7. Ki-67 as intracellular target for anticancer applications

In this chapter the biological investigation of Ki-67 in two cell models (HDF and MDA-MB-231) is presented. These data shed light on the still unexplored extranuclear translocation of this protein, as well as clarified its expression and intracellular localisation in cancerous and non-cancerous cells.

Indeed, while most of the Ki-67 is translocated outside the nucleus, and consequently down regulated in serum deprived HDF, this does not occur in MDA-MB-231.

Furthermore, by quantifying the Ki-67 two principal splice variants (namely, the α and β), it is demonstrated that the α variant is the mainly expressed.

Moreover, while the HDF did not present any sign of either α or β isoform after 36 h of starvation, the breast cancer cells MDA-MB-231 showed an evident expression of the α isoform (PCR analysis Figure 5.8).

These results suggest the implication of the α isoform in playing an important role in the regulation of the cell cycle, and thus in cancer progression. Aiming to validate the Ki-67 potential as intracellular target for anticancer applications, fluorescently labeled (Brilliant Violet™ 421) anti Ki-67 IgG antibodies were delivered intracellularly, by exploiting the PMPC-PDPA (Poly(2-methacryloyloxyethyl phosphorylcholine)-co-poly(2-(diisopropylamino)ethyl methacrylate) polymersome delivery system. MDA-MB-231 cells were used as a model system, and the ability of the introduced IgG to target Ki-67 was evaluated by means of confocal microscopy. The results of this investigation are reported in Figure 5.15.

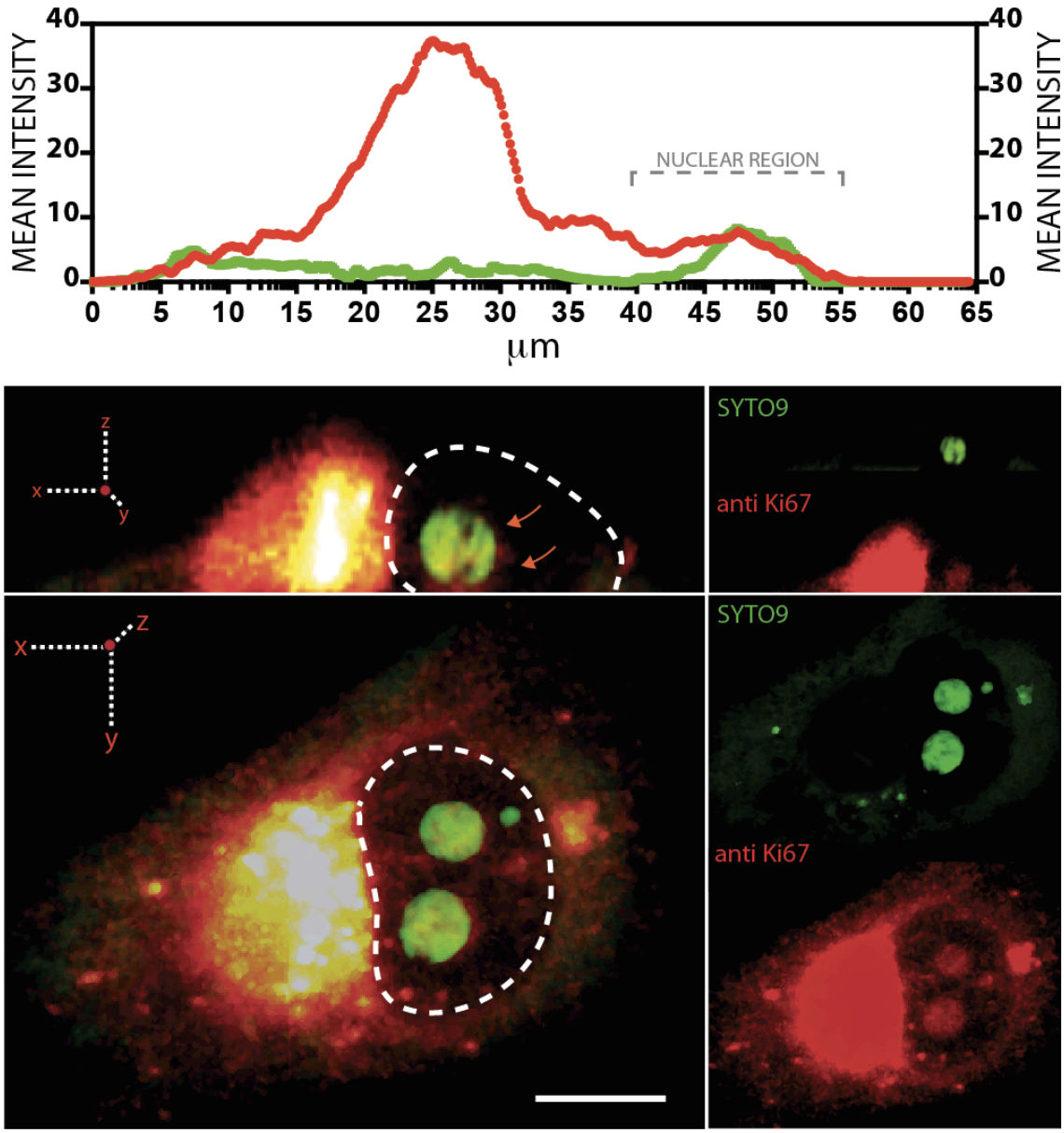

Figure 5.15. Z-stack versus mean intensity graphical reconstruction (Top figure) and imaging rendering (bottom figure) of the intracellular distribution of anti-Ki-67 antibody delivered (Brilliant Violet 421™anti-Ki-67 IgG) in live MDA-MB-231 cells with polymersomes. Cells were co-stained with green RNA / DNA probe SYTO®9. Scale bar: 10 μm.

As shown in Figure 5.15, the polymersomes delivered anti Ki-67 IgG (fluorescently labeled) are effectively up-taken and accumulated intracellularly. Evidently, the red signal revealed that most of the delivered proteins are accumulated within the cytoplasm. Nevertheless, the SYTO®9 nucleic acid staining (green channel) shows that part of the delivered IgG are penetrated within the cell nucleus, and are co-localised within the nucleolar region. These

results proved the targeting efficiency of the polymersomes delivered anti Ki-67 IgG.

After this preliminary validation, the next experimental step aimed to test in live cells the therapeutic potential of the delivered IgG, and more precisely their ability to interfere with the Ki-67 functionality. For this scope, antibody targeting the N-portion of Ki-67 that corresponds to the forkhead associated domain (FHA) were used. The FHA domain is a well conserved amino acid sequence that mediate the interactions with factors involved on the cell cycle progression, DNA repair and transcription (Byeon et al., 2005).

The FHA domain of Ki-67 allows the protein association with the kinesin-like protein Hklp2, and with the nucleolar protein interacting factor NIFK. The Ki-67 association with NIFK was described during the mitosis phase of the cell cycle, thus supporting the possible implication of these two proteins for the regulation of the latter (Sueishi et al., 2000; Takagi et al., 2001).

Moreover, the presented results showed that quiescent non-cancerous cells (upon serum starvation) express lower amount of Ki-67 comparing to cancerous cells (Figure 5.1). For this reason, it is expected that the intracellular delivery of anti Ki-67 antibodies should produce a considerable and selective effect in cancerous cells. To evaluate this therapeutic approach, HDF and MDA-MB-231 cells were used as a models. MTT assay was exploited to evaluate the cells viability, while a cell counting assay was performed to assess the cellular proliferation after the treatment. In both cases, cells were starved for 18 h and subsequently incubated 24 h with the respective formulations, and finally analysed. More precisely, different groups of cells were treated with antibody loaded polymersomes characterised by different concentrations of PMPC-PDPA (0.5 - 1 - 1.5 mg/ml) and IgG (0.05 - 0.1 - 0.15 μg/ml). The total amount of PMPC-PDPA and IgG per single formulations was quantified by RP-HPLC (see Section 7.2.3). Furthermore, two separated controls were used. One control group was characterised by cells treated with empty polymersomes using PMPC-PDPA concentrations of 0.5, 1 and 1.5 mg/ml. The other control group, was characterised by cells treated with an equal volume (compared to the added polymersomes sample) of 1X phosphate buffered saline (PBS 0.1 M) in media. All these analyses are summarised in Figure 5.16. The first relevant outcome is that HDF are not affected by the applied polymersomes formulations (i.e., empty, and antibody loaded polymersomes). This result was confirmed by both

MTT assay and cells counting. Different results were achieved by evaluating MDA-MB-231 cells.In particular, both cellular viability and the proliferative capacity of MDA-MB-231 cells decreased after the exposure to the polymersome formulations loaded with the antibody cargo. Indeed, cells treated with 0.5 and 0.1 μg/ml of IgG show a reduction on their viability of ~20 and ~25% comparing with cells exposed to the empty polymersomes. Furthermore, cells treated with 0.15 μg/ml of antibodies show a ~25% reductions on their proliferative activity. Taken together, these data indicate that antibodies targeting the FHA domain may inhibit the Ki-67 activity. Furthermore, only the cancerous cells resulted affected by the intracellular delivery of antibody with significant statistical validity, thus indicating the high specificity of the treatment. This result can be correlated with the higher expression of Ki-67 occurring in cancerous cells, compared to non-cancerous one. It was demonstrated that the former constitutively express this protein also when their proliferation is inhibited via serum starvation. Despite these promising results further investigations are however needed to better elucidate the Ki-67 pathway and the contributions of other key factors on it. It is also necessary to point out that most part of Ki-67 structural conformation is still unknown at the moment. This lack of knowledge strongly precludes, and makes difficult, the validations of others targeting sites on the Ki-67 structure (besides the FHA domain) that could be exploited for its inhibition.

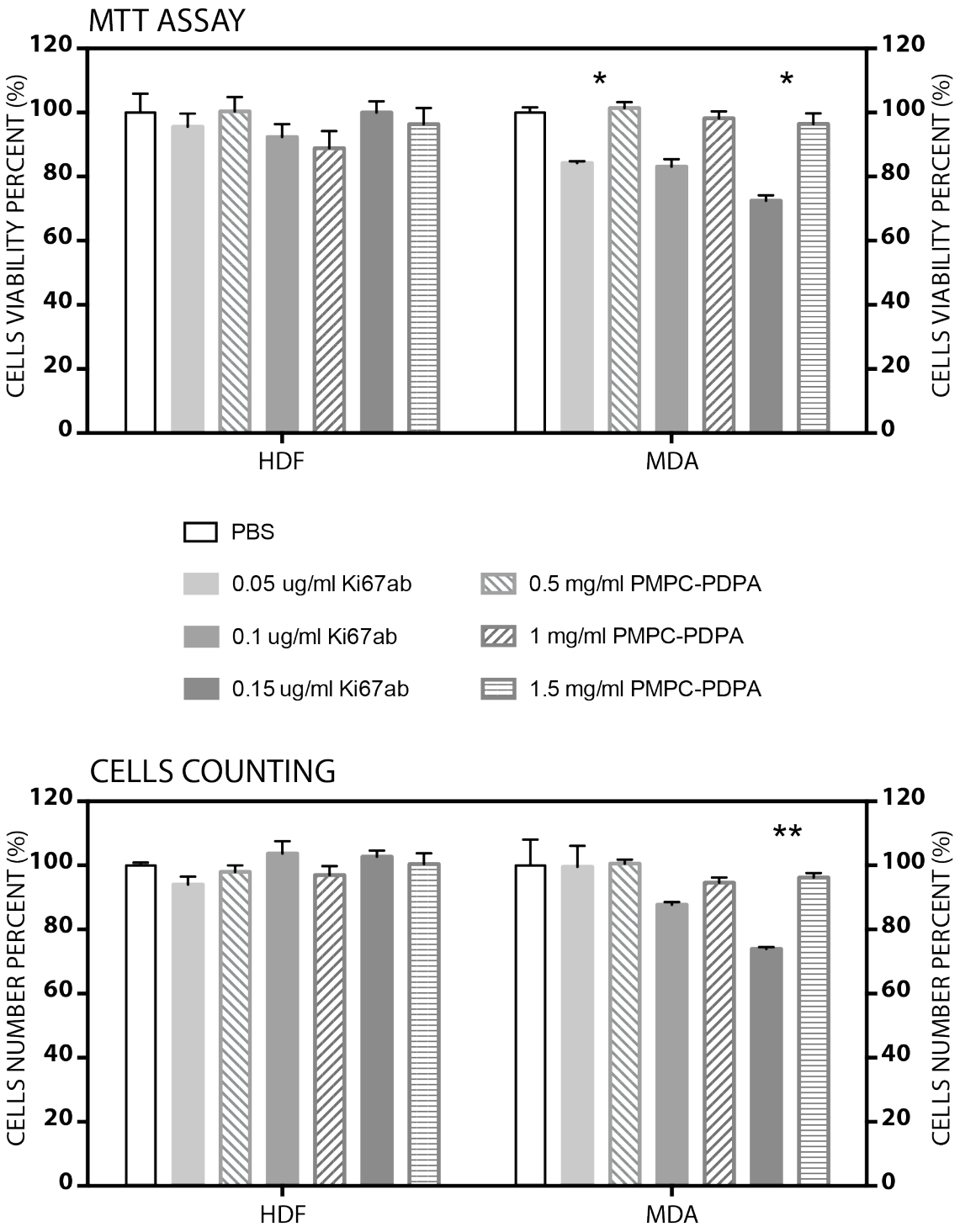

Figure 5.16. Cells viability (%) tested by means of MTT assay and cell counting assay, performed on HDF and MDA-MB-23 cells. Empty PMPC-PDPA polymersomes were compared to polymersome formulations (at the same overall amount of PMPC-PDPA, i.e. 0.5, 1 and 1.5 mg/ml) containing three different concentrations of anti-Ki-67 antibody (0.05 - 0.1 - 0.15 μg/ml; antibody targeting the N-portion of the protein). Furthermore, another control cells group was incubated with PBS (t-test, p-value * $P \leq 0.05$; ** $P \leq 0.01$; *** $P \leq 0.001$; **** $P \leq 0.0001$). The experimental error is expressed as standard deviation (N=3).

Chapter 6

General Conclusions and Future Directions

6.1. General conclusions

In this PhD project, it was exploited the use of pH sensitive polymersomes based on poly(2-methacryloyloxyethyl phosphorylcholine)-co-poly(2-(diisopropylamino)ethyl methacrylate (PMPC-PDPA) block copolymer, to achieve the intracellular delivery of antibodies for anticancer therapy.

As a first step, for the development of PMPC-PDPA polymersomes as efficient drug delivery system, the so called protein corona effect was initially studied.

This process was investigated using, as a model, three different proteins namely immunoglobulin G (IgG), Bovine Serum Albumin (BSA) and lysozyme and evaluating it on assemblies derived from two different block copolymers namely PMPC-PDPA and poly(ethylene glycol)-co-poly(2-(diisopropylamino) ethyl methacrylate (PEG-PDPA). The characterisation of the fouling process, which defines the interactions between proteins and synthetic surfaces was evaluated with both, polymersomes and micelles using techniques such as Size Exclusion Chromatography (SEC), Transmission Electron Microscopy (TEM) and Isothermal titration calorimetry (ITC) (see Figure 2.6, 2.7 and 2.9). The obtained results showed the binding effect occurring between proteins and micelles when the latter are mixed together in solution. On the other hand, the same effect was not detected in the presence of proteins and polymersomes. Aiming to describe the protein fouling, observed exclusively within the micelles, an important observation correlated with the polymer chains molecular organisation on the micellar structure has to be considered.

In fact, structural assemblies such as polymersomes and micelles made by copolymer with the same graft density differ by different brush density.
In copolymer assemblies, the latter parameter depends on two distinct factors which are *(i)* the curvature of the particle and *(ii)* the copolymer packing factor (*p*). Particles such as micelles that posses high surface curvature and low packing factor are also characterised by a low brush density (Bates and Fredrickson, 1990; Daoud and Cotton, 1982; Fredrickson and Bates, 1996; Matsen and Bates, 1996a; Matsen and Bates, 1996b; Nagarajan and Ganesh, 1989; Rahman, 2013). Furthermore, considering two distinct micellar assemblies differing by the hydrophilic block, another determining factor on the occurring of the protein fouling process is represented by the hydrophilic chain surface density per nm^2 (Giacomelli et al., 2012). The higher this value is, the more inaccessible is the hydrophobic micellar core. For this reason micelles characterised by the presence of PEG as hydrophilic block interact less with proteins compared with micelles presenting the PMPC block.
It is possible to assume that the structural difference between polymersomes and micelles is the key factor to explain the revealed protein fouling process. As a conclusion, it can be assumed that the micellar hydrophilic brush it is in some way not sufficient to prevent the proteins adsorption while the polymersomes higher brush density contributes the most to prevent this effect. Furthermore, the obtained data indicates that hydrophobic interactions and protein size are the driving factors on the observed proteins fouling process with micelles. In fact, the K_a values obtained regarding the tested protein models, resulted in all the cases correlated with their hydrophobicity and size. Indeed, the smallest tested proteins, the lysozyme, has proved capable more that BSA and IgG to penetrate the highly protective brush shield of well established anti-fouling polymers such as PEG.

After confirming that protein fouling does not occur in the presence of polymersomes, the next step was focused on the investigation of a new approach to achieve a reliable and reproducible protein encapsulation within these nanocarriers. For this purpose, the development of electroporation as a new encapsulation technique is reported herein. This method, commonly used in molecular biology to introduce biomolecules in live cells (Ho and Mittal, 1996b;

Neumann et al., 1982), it is explored here to achieve the encapsulation of proteins within polymersomes.

The overall data presented, indicates that the polymersome membrane is not permanently affected by the electropermeabilization energy applied. In fact, the nano-vector size and morphology remained unchanged after the process (Figure 3.2), thus indicating a transient polymersomes membrane destabilisation that is afterwards efficiently recovered. Moreover, the protein stability after electroporation, was evaluated with two different methods namely Enzymatic Linked Immunosorbent Assay (ELISA) and immunofluorescence. Both techniques proved a normal antibody functionality and integrity after the process (Figure 3.4).

With the aim of optimising the IgG cargo encapsulation using electroporation, different experimental parameters such as pulses number, initial amount of protein and ion concentration in the solution were evaluated. The loading efficiency (*L*) and encapsulation efficiency percentage (*E*) values showed a particularly consistent increment in correlation with the number of electrical pulses applied to the polymersomes sample. This was observed whilst keeping the protein and ion concentration constant at fixed values of 5 μg/ml and 0.1 M phosphate buffered saline (1X PBS) respectively. The maxima *L* (~76) and *E* (~12%) values were reached using 20 pulses (Figure 3.5). Furthermore, electroporation was compared with other encapsulation methods such as solvent switch and polymer film rehydration. The obtained experimental findings showed that the higher reproducibility in terms of *L* and *E* values was generated using the electroporation technique. Moreover, electroporation also shows the possibility to have better control over the final vesicle size homogeneity compared with the other encapsulation methodologies evaluated (Figure 3.6).

After establishing electroporation as a reliable approach to achieve the IgG encapsulation, functional antibodies were delivered into live cells using the same PMPC-PDPA polymersomes. Reversed phase high pressure liquid chromatography (RP-HPLC), confocal laser scanning microscopy analysis (CLSM), and TEM were all exploited to characterise the effectiveness of antibody delivery. It was demonstrated that PMPC-PDPA polymersomes allows the endo-lysosomal escape of the delivered cargo. It is likely that the

polymersome disassembly, mediated by the acidic pH present on those endocytic organelles, induces an increase in osmotic pressure that causes the temporary formation of pores in the endosome membrane, thus facilitating the polymersome cargo delivery into the cytosol.

The polymersome cargo release is experimentally well supported by the TEM analysis shown in Figure 4.5, where the distribution of gold labeled IgG in both vesicular spaces (likely endocytic organelles) and throughout the cell cytosol. These results also support the use of polymersomes for the intracellular delivery of probes applied in TEM imaging applications.

Fluorescently labeled antibodies, have shown an overall stability and targeting functionality after their introduction into the live intracellular milieu. In fact, in Figure 4.7 it is shown, through the use of fluorescently labeled anti γ-Tubulin IgG, sub-cellular targeting of this structural protein can be achieved and their intracellular dynamics in response to external stressors can be revealed.

In conclusion, PMPC-PDPA based polymersomes demonstrated their applicability for the delivery of complex biomolecules such as IgG, without causing relevant perturbations to the cellular viability.

Taken together, all these findings suggest that polymersomes can be used in combination with imaging techniques for the study of biological pathways in live experiments.

The assessed ability of polymersome as nanocarrier for the intracellular delivery of functional antibody makes them an important tool useful for targeting intracellular epitopes, associated with cancer cell development. In particular, interesting targets are represented by epitopes implicated with cell cycle regulation. For this reason, the intracellular pathway of the nuclear protein Ki-67, which is associated with cellular proliferation and cell cycle regulations, was investigated in this project (Scholzen and Gerdes, 2000).

In this work, it is demonstrated that Ki-67 undergoes completely different regulation / degradation pathways in non-cancerous and cancerous cells. This was specifically ascribed to the different expression of the two splice variants of the protein, combined with possible altered post-transcriptional and / or post-translational modification of Ki-67 occurring in cancer cells. In addition, it is demonstrated, for the first time, that the protein is translocated outside the

nucleus, and it is delivered to the endoplasmic reticulum (ER) first, and the Golgi apparatus later, where it can undergo further regulation steps.

As first general evidence, the obtained data clearly confirm that non-cancerous cells are able to control the down-regulation of Ki-67 during the G_0/G_1 phase of the cell cycle, while cancer cells over-express the protein during quiescence induced by nutrients starvation (Figure 5.1). In particular, as confirmed by fluorescence cytometry (FC) analysis, a different regulation pathway of Ki-67 between human dermal fibroblasts (HDF) (in which starvation leads cells to a quiescent stage, and to Ki-67 down-regulation) and breast cancer cells (MDA-MB-231) (where fetal bovine serum (FBS) deprivation does not affect the transfer through the cell cycle, neither the related down-expression of Ki-67) is likely to occur (Figure 5.2-A-B).

An important role seems to be played by the two different splice variants of the protein, namely the α and the β, for controlling the cellular proliferation (Figure 5.4 and 5.8). There is, in fact, a significant difference in the expression levels of the two isoforms between HDF and MDA-MB-231 cells. In particular, the α variant is much more expressed in breast cancer cells, compared with human dermal fibroblasts. This may be an indication that the two isoforms may undergo very different degradation pathways in non-cancer and cancer cells. Another possibility is that each specific cell may express different levels of the two variants. Hence, the possibility to control the transfer between the active and quiescent stage (a crucial aspect in cancer research) seems to be significantly related to the specific splice variant expressed by cells. Another consideration should be inferred. Although the transcript for Ki-67 undergoes a shRNA-related degradation process (Figure 5.4), the protein is anyway steadily present in MDA-MB-231 cells (Figure 5.3), probably because Ki-67 is more stable herein or, alternatively, its post-translational degradation fails to occur in cancer cells. Hence, these findings strongly support the hypothesis that the design of next generation of anticancer drugs, based on targeting the Ki-67 expression and / or regulation, should consider the possibility to selectively target the α variant.

However, the most interesting outcome regarding the Ki-67 study is the first demonstration about its translocation outside the nucleus. This represents a new and surprising topic. It was confirmed that cells entering to the G_0 phase of the cell cycle (i.e., during cell quiescence) promote a Ki-67 translocation outside

the nucleus, possibly into the ER (or, alternatively, cells may first transfer the protein in the ER in order to then enter the quiescent phase). This will result in the activation of the ER-associated protein degradation (ERAD) signal pathway, which leads the molecular chaperone binding immunoglobulin protein (BiP) to bind the newly ER transferred Ki-67 (Figure 5.10), eventually activating the unfolded protein response (UPR). In addition, it is demonstrated that Ki-67 interact with the proteasome system (resulting in the degradation of the protein) (Figure 5.9), and this complex buds from the ER into specific cytoplasmic coat protein complex II (COPII) coated vesicles (Figure 5.11), which are responsible to transport their cargo to the Golgi apparatus (Figure 5.12). Herein, Ki-67 may be further recycled and / or degraded. While these data suggested that the extranuclear molecular pathways of Ki-67 are well controlled in fibroblasts (control non-cancerous cell model), breast cancer cells may lose the ability to regulate the different checkpoints of Ki-67 translocation and regulation. Hence, the fine balance between expressed and degraded Ki-67 results hindered, and cancer cells are not able to control the transfer between the quiescent (i.e., the G_0 phase of the cell cycle) and the proliferating state (namely, the $S/G_2/M$ steps) of the cell cycle.

At the end, it is shown the possibility to target the Ki-67 factor via the polymersomes-mediated intracellular delivery of anti Ki-67 N-Terminus antibodies (Figure 5.15). These antibodies target the Ki-67 forkhead associated (FHA) domain present on the N-terminus amino acid sequence of the protein. The FHA domain is strongly correlated with others factors such as kinesin-like protein Hklp2 and nucleolar protein interacting factor NIFK. The interaction between Ki-67 FHA, Hklp2 and NIFK is further described during the cellular division and thus postulated as promoting elements for the cell cycle progression (Sueishi et al., 2000; Takagi et al., 2001). The MTT assay and the quantification of the cellular proliferation, carried out using non-cancerous (HDF) and cancerous cells (MDA-MB-231) models, showed the biological effectiveness of the applied approach. The cancerous cells resulted affected on their metabolic and proliferative activity when treated with a polymersomes formulation containing the antibody cargo. On the other hand, similar results were not achieved with non-cancerous cells, thus indicating a selective action of the treatment (Figure 5.16). Despite these promising results, further investigations are needed to have a better picture concerning the Ki-67 role in

the cell cycle regulation. Indeed, a better understanding of the Ki-67 pathway could have the real potential to open new avenues in targeted anticancer therapies.

6.2. Future directions

In this project, it is shown the possibility to use polymersomes as a nanocarrier for the intracellular delivery of functional antibodies targeting epitopes associated with cancer cell development.

An important limitation affecting polymersomes as delivery system is represented by the effective and reproducible encapsulation of hydrophilic biomolecules, such as IgG, within their lumen.

To achieve this scope, the electroporation technique was employed. Despite the promising results obtained in terms of loading efficiency (L) and encapsulation efficiency percentage (E), the use of electroporation as encapsulation method can still be improved. For instance, parameters such as total polymersomes volume (ϕ_p), polymersomes size, as well as the ions strength of the sample solution are all variables that have the potential to affect the final cargo encapsulation.

Besides that, the comparison between electroporation technique with other encapsulations methods has demonstrated film rehydration as reliable approach for the IgG encapsulation within polymersomes. The promising encapsulation data obtained via film rehydration need however more insights, in order to better understand the mechanism driving in such a way the protein loading within polymersomes.

Concerning the intracellular delivery of IgG, it is important to remark that more studies are necessary to explain the observed plateau over time. Different hypotheses can be considered to explain this result, including the saturation of the scavenger receptor SR-B1, and the implication of the tripartite motif-containing 21 (TRIM21). Therefore, future experimental efforts should focus on the clarification of the intracellular fate of the delivered IgG.

In conclusion, I demonstrated that Ki-67 can be a potential target to block the proliferation of cancerous cells. However, because the complete pathway of this protein is still not well characterised, more experimental data are necessary to

disclose the role of Ki-67 for the regulation of the cell cycle. More characterisations are also needed to better understand the structural conformation of Ki-67, which is still mostly unknown.

The study of both the intracellular pathway of Ki-67 and its structural conformation could finally provide new important details on the possible strategies to target this protein. This is very much important to stop uncontrolled proliferation of cancerous cells.

Chapter 7

Materials and Methods

7.1. SURFACE INTERACTIONS BETWEEN POLYMERIC ASSEMBLIES AND PROTEINS

7.1.1 Block copolymers synthesis

The poly(2-(methacryloyloxy)ethyl phosphorylcholine)-poly(2-(diisopropylamino)ethyl methacrylate) ($PMPC_{25}$-$PDPA_{70}$ / $PMPC_{30}$-$PDPA_{30}$) and poly(ethylene glycol)-poly(2-(diisopropylamino)ethyl methacrylate) (PEG_{113}-$PDPA_{56}$ / PEG_{45}-$PDPA_{80}$) were synthesised by Prof. S. Armes' group, Chemistry Department, University of Sheffield as previously reported (Du et al., 2005).

The molecular structure of both block copolymers is shown in Figure 7.1.

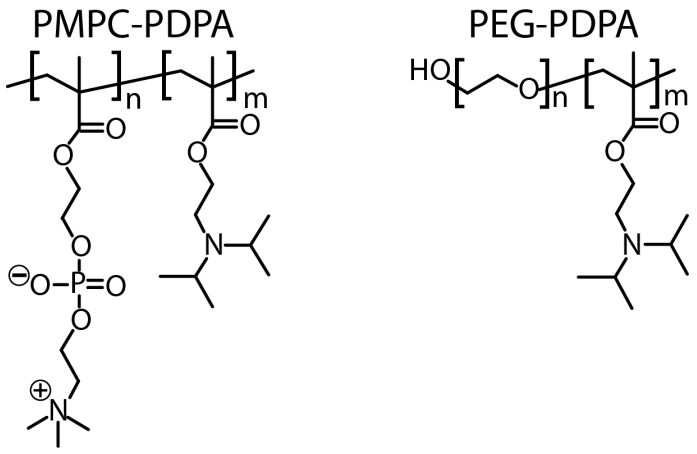

Figure 7.1. Molecular structure of the block copolymers used in this project.

7.1.2. Polymersome and micelle preparation

Polymersome and micelle were prepared using two different techniques: (A) film hydration and (B) pH switch. In both methods, initially 10 mg of diblock copolymer were solubilised in a glass vial containing 9 ml of chloroform ($CHCl_3$) : methanol (CH_3OH) in 2:1 ratio (Sigma-Aldrich, UK). The dissolved copolymer was placed in a vacuum desiccator until the complete evaporation of the solvent and deposition of a thin layer of polymer to the vial wall. The polymer film was subjected either to film hydration or pH switch protocol. Thus, polymersomes were obtained applying the film hydration method on copolymers such as $PMPC_{25}$-$PDPA_{70}$ and PEG_{45}-$PDPA_{80}$. The film hydration method was also used for the assembly of micelles derived from the $PMPC_{30}$-$PDPA_{30}$. Instead, the pH switch method was applied for the formation of PEG_{113}-$PDPA_{56}$ micelles as reported from Pearson and colleagues (Pearson et al., 2013).

A. Film hydration

For the film hydration protocol, the vial containing the copolymer film was rehydrated by adding 2 ml of 1X phosphate buffered saline (PBS 0.1 M) at pH 7.4. The buffered solution was stirred (magnetic stirring at 200 rpm) for 8 weeks to allow polymersomes self-assembling.
Micelles were obtained by film hydration reducing the stirring time from 8 weeks to 12 h.

B. pH switch

For the pH switch assembling protocol, the copolymer film was dissolved in pH 2 1X PBS at the final concentration of 10 mg/ml. The pH of the solution was increased to pH 7.4 with 1 M NaOH, added a flow rate of 15 µl/min using an automated syringe pump. The process was performed under constant stirring at 70 °C, as previously reported (Pearson et al., 2013).
Samples were purified using Size Exclusion Chromatography (SEC). For this propose, a 1 x 15 cm column was packed with Sepharose 4B (resin-bead sizes ranging from 45 to 165 µm; GE Healthcare, UK) and 500 µl of sample were loaded to the head of the column and the eluted through it using 1X PBS.

7.1.3. Polymersome and micelle characterisation

Polymersome and micelle physical characterisation was performed by Dynamic Light Scattering (DLS) and Transmission Electron Microscopy (TEM).
The DLS analysis was achieved using the Malvern Zetasizer Nano set at 20 °C. Samples were diluted to 0.15 mg/ml in 1X PBS pH 7.4. 800 µl of diluted sample was then placed into a polystyrene cuvette (Malvern, DTS0012) and analysed. TEM analyses were performed using a FEI Tecnica Spirit microscope with maximal working voltage of 120 KV and equipped with Gatan1K MS600CW CCD camera. The copper grids used for the samples analysis were initially coated with a carbon layer (thickness: ~20 nm) using a carbon coater. Subsequently, the prepared grids were submerged in the copolymer assemblies sample (micelles or polymersomes) and afterwords stained using a phosphotungstic acid (PTA) solution (0.75% w/w) as described in previous works (Pearson et al., 2013; Wang et al., 2012). The PTA staining was herein applied since it enables the detections of the ester bonds presents in the PMPC-PDPA molecular structure.

7.1.4. Protein labelling

To study the surface-surface interactions between polymeric structures and proteins, Bovine Serum Albumin (BSA) (Sigma-Aldrich, UK), lysozyme (Sigma-Aldrich, UK) and immunoglobulin G (IgG) (I5006; Sigma-Aldrich, UK) were opportunely labelled with a fluorescent dye.
The labelling protocol consisted of four steps:

1. In the first step the proteins were solubilised in pH ~8.3 sodium bicarbonate buffered solution at a final concentration of 5 mg/ml.

2. In the second step, 0.25 mg of Cy5 (Cyanine5) NHS ester dye (λ_{ex}= 649 nm, and λ_{em}= 669 nm; Lumiprobe) previously dissolved in 20 µl of dimethyl sulfoxide (DMSO) (Sigma-Aldrich, UK), were added to the protein solutions and incubated at room temperature for 2 h in stirring conditions. This step was necessary to allow the protein-dye conjugations between the succinimidyl ester group present on the dye chemical structure and primary amines presents on the proteins.

3. After this step, the labelled proteins were purified from the unbounded dye via SEC using a Sephadex G-25 (Sigma-Aldrich, UK).

4. Finally, the absorbance at 280 nm of the purified product was measured. The absorbance of free dye was subtracted from the total absorbance and protein concentration was determined against a standard curve.

7.1.5. Protein zeta potential calculation

The protein zeta potential was measured using a Malvern Zetasizer Nano. Samples were diluted in 1 ml of distilled water and the measurement was performed at 20 °C.

7.1.6. Size exclusion chromatography for the evaluation of surface-surface interaction

The SEC analysis was used to evaluate the surface-surface interplay between polymeric structures and proteins.
The protocol involved the use of a 1.5 x 30 cm column packed with Sepharose 4B (Sigma-Aldrich, UK), directly connected to a high pressure liquid chromatography (HPLC) instrument (Dionex, Ultimate 3000).
100 µl of mixed samples containing proteins plus polymersomes or proteins plus micelles were injected into the column and eluted through it using 1X PBS with constant flow of 260 µl/min.
Two different chromatograms were registered. One, detecting the copolymer UV-Vis absorbance at 220 nm and the other one exciting the sample at 649 nm and detecting the labelled protein fluorescent emission at 669 nm.
The areas corresponding to the detected packs were calculated with a MATLAB® based script.

7.1.7. TEM visualisation of the subsisting interaction between micelle / polymersome and protein

TEM was used to visualise the interaction between polymeric micelle / polymersome and proteins after SEC purification. Both polymeric samples:

$PMPC_{25}$-$PDPA_{70}$ polymersomes and $PMPC_{30}$-$PDPA_{30}$ micelles were prepared by film hydration as described in Section 7.1.2.

Two separated samples containing respectively 300 µl of 10 mg/ml of PMPC-PDPA micelles or polymersomes and ~1.5 µg/ml 5 nm AuNP-IgG (gold labelled immunoglobulin G) (Sigma-Aldrich, UK) were placed in a 2 ml plastic vial (Eppendorf, UK) and kept in moderate agitation for about 10 min. Subsequently, the samples were passed through the SEC applying the same protocol as explained in Section 7.1.6 and the eluted fraction corresponding either to the polymersomes or to the micelles (depending on the injected sample) was collected and analysed by TEM.

The TEM AuNP-IgG visualisation was performed using a FEI Tecnica Spirit microscope with maximal working voltage of 120 KV and equipped with Gatan1K MS600CW CCD camera using the same protocol described in Section 7.1.3.

7.1.8. Isothermal titration calorimetry (ITC)

A MicroCal VP-ITC instrument was used for the isothermal titration calorimetry analysis. 10 µl of 1X PBS solution, containing 47.6 µM of micelles or polymersomes, was injected at regular interval of 10 min into the reference cell containing 15.2 µM of protein solution. The reference cell power was set at 10 µcal/s.

7.1.9. Statistical analysis

The statistical comparison between two group of data resulting from the K_a calculation was performed using a t-test setting the significance level with $p<0.05$. The experimental error is expressed as standard deviation (N=3).

7.2. ELECTROPORATION FOR PROTEIN ENCAPSULATION WITHIN POLYMERSOMES

7.2.1. Polymersome preparation and characterisation

The PMPC-PDPA polymersomes preparation for the subsequent protein encapsulation via electroporation was achieved by film hydration as described in Section 7.1.2. Samples were purified by SEC and characterised by DLS and TEM as previously described (Section 7.1.2-B and 7.1.3).

7.2.2. Antibody stability after electroporation process

Antibody stability after electroporation was assessed by (A) Enzymatic Linked Immunosorbent Assay (ELISA) and (B) immunohistochemistry.

A. ELISA assay

This assay was performed following the product protocol, using the anti Interleukin 8 (IL-8) IgG as a model. Briefly, 50 µl of provided anti IL-8 IgG enzyme conjugated antibodies, were diluted in 500 µl of 1X PBS and placed into a 2 mm width gap electroporation cuvette (Eppendorf, UK). This antibody solution was subjected to electroporation using an Electroporator 2510 (Eppendorf, UK) instrument and applying 5, 10 or 20 pulses depending on the experiment, and applying 2500 V each pulse. Every pulse was spaced with a time gap of 30 sec. Untreated antibodies were used as negative control, while the positive control antibodies (degraded proteins) were obtained placing them at 90 °C for 15 min.

After the samples preparation, the ELISA assay (R&D Systems Inc., USA) was performed and the first step of it included the addition and the incubation for 2 h at room temperature of 100 µl of standard antigen into an anti IL-8 pre-coated 96 well plated.

At this point, three consecutive washing steps with 1X PBS were thus necessary to remove all the unbounded antigen. Afterward, the prepared antibodies samples (electroporation treated IgG, positive and negative control IgG) were added into separated wells of the plate and incubated for 2 h at room temperature. After this step, the reacting wells were opportunely washed again

and subsequently the enzyme substrate solution was added. After 30 min of incubation protecting the samples from the light, the reaction was stopped and the absorbance was measured at 450 nm using a micro-plate reader (ELx800 BioTek, USA). The protein stability was thus evaluated normalising the measured absorbance resulting for the treated samples with the value obtained for the untreated antibodies control (100% absorbance value).

B. Immunohistochemistry

The second validation method used was based on confocal laser scanning microscopy analysis performed in fixed Human Dermal Fibroblast (HDF - American Type Culture Collection (ATCC®, USA)). In this case, anti α-tubulin antibody (Abcam, UK) conjugated with AlexaFluor®647 dye (λ_{ex}=649 nm, λ_{em}=669 nm - Life Technologies™), was used as a model and subjected to electroporation using the same protocol as before. Furthermore, also for this validation, positive and negative control samples were prepared as described before for the ELISA assay (Section 7.2.2-A).

HDF cells were seeded in glass bottom dishes (35 mm diameter-IBIDI®) at a density of 8 x 10^3 cells per well and grown for 24 h in complete Dulbecco's Modified Eagle Medium (DMEM) added with 10% (v/v) fetal calf serum, 2 mM L-glutamine, 100 mg/ml streptomycin and 100 IU/ml penicillin. Cells were incubated at 37 °C/5% CO_2. Cells were periodically sub-cultured using Trypsin-Ethylenediaminetetraacetic acid (EDTA) solution 0.25% for the detachment process and centrifuged at 2000 rpm for 5 min for the pellet collection.

The antibodies structural stability was investigated under confocal microscope (Leica TCS SP8), and the cellular samples were prepared applying immunofluorescence protocol: fixation with formaldehyde 3.7% for 10 min, permeation with 0.1% Triton X-100 in 1X PBS for 10 min, blocking of unspecific sites with BSA 2% for 2 h and overnight incubation at 4 °C with the antibody sample. The microscope laser intensities and detector gains were kept constant between all images.

7.2.3. RP-HPLC characterisation of polymer and protein concentration

Reversed-phase high pressure liquid chromatography (RP-HPLC) is a technique that allows the separation of different molecules that are initially adsorbed within a solid material (Aguilar, 2004; Jacob Bongers, 1997). The components of the analyte mixture pass over a stationary-phase of particles bearing pores large enough for them to enter. The analyte interactions within the adsorbent surface remove them from the flowing mobile-phase stream. As the ratio between different solvents (organic and non) in the mobile phase change, it reaches a critical value for each analyte, which desorbs it from the stationary-phase surface and allows it to elute from the column in the flowing mobile phase. Since this elution depends on the physical and chemical properties in each species, each analyte elutes from the column at a characteristic time, and the resulting peak detected can be used to confirm its identity and quantify the latter (Aguilar, 2004; Jacob Bongers, 1997).

The RP-HPLC technique was herein applied for the quantification of both IgG and PMPC-PDPA and thus to subsequently calculate the resulting encapsulation efficiency.

An anti-tubulin IgG conjugated with AlexaFluor® 647 dye (λ_{ex}= 650 nm, and λ_{em}= 669 nm) (ab6161; Abcam®, UK) was used as a model. The calibration curves were obtained using an RP-HPLC (Dionex, Ultimate 3000) with a C18 analytic column (Phenomenex® Jupiter C18, 300A, 150 x 4.60 mm, 5 micron) and using a constant flow ratio of 1 ml/min. The eluents used were milliQ H2O added of 0.05 % V/V trifluoroacetic acid (TFA) (eluent A) and CH_3OH with 0.05 % TFA (eluent B). The gradient profile used is shown in Figure 7.2.

Time (min)	B phase (%)
0	20
6	40
16	45
19	50
20	50
23	70
24	100
25	100
27	20
30	20

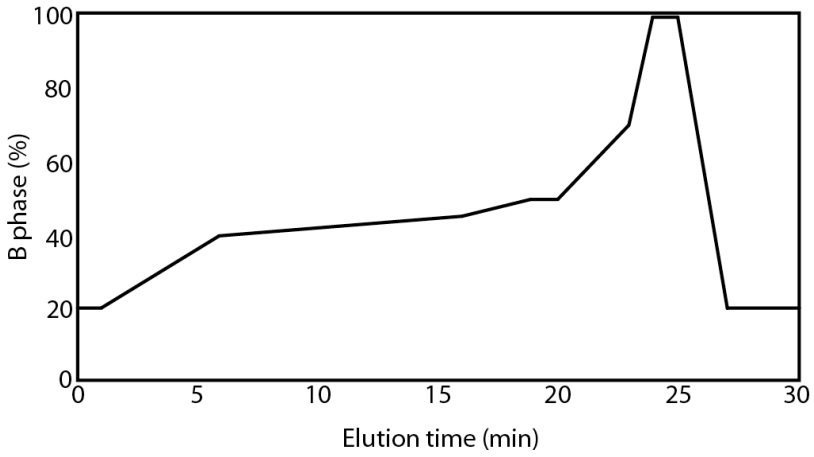

Figure 7.2. Gradient used for the RP-HPLC characterisation of PMPC-PDPA and IgG.

The samples containing the specific amounts of antibody and copolymer were prepared by dilution in 1X PBS at pH 5.5. The polymer UV-Vis absorbance was detected at 220 nm, while the antibodies fluorescence intensity was acquired at 669 nm. Standard curves for PMPC-PDPA and IgG are shown in Figure 7.3.

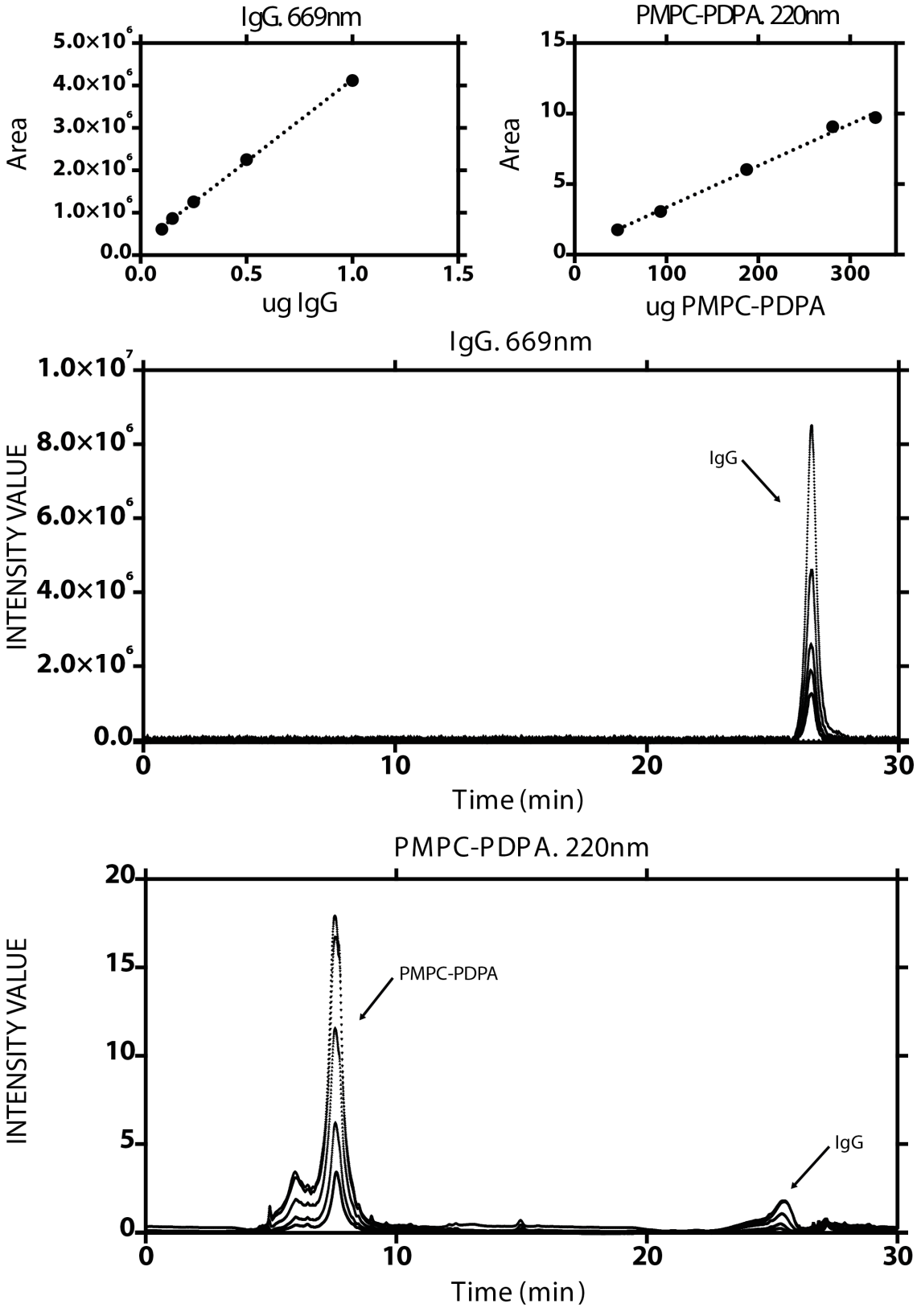

Figure 7.3. Standard curves of IgG and PMPC-PDPA obtained by RP-HPLC characterisation. The detections of the fluorescently labelled AlexaFluor® 647 anti-tubulin IgG was performed measuring its fluorescent emission at 669 nm, while the block copolymer PMPC-PDPA UV-Vis absorbance was detected at 220 nm.

As presented in Figure 7.3, the IgG signal is detectable in both fluorescence (because of the bounded dye) and UV-Vis channel. The UV-Vis detections is attributable to the i.e. tryptophan residues, that have absorbance between 280 and 200 nm (Stoscheck, 1990). As a control experiment, it was also tested whether the fluorescent signal attributed to the IgG can be affected by the contamination of free dyes. The data showed in Figure 7.4 demonstrated that the dye has a different elution time when it's not bound to the protein and it's not detectable in the UV-vis channel at 220 nm.

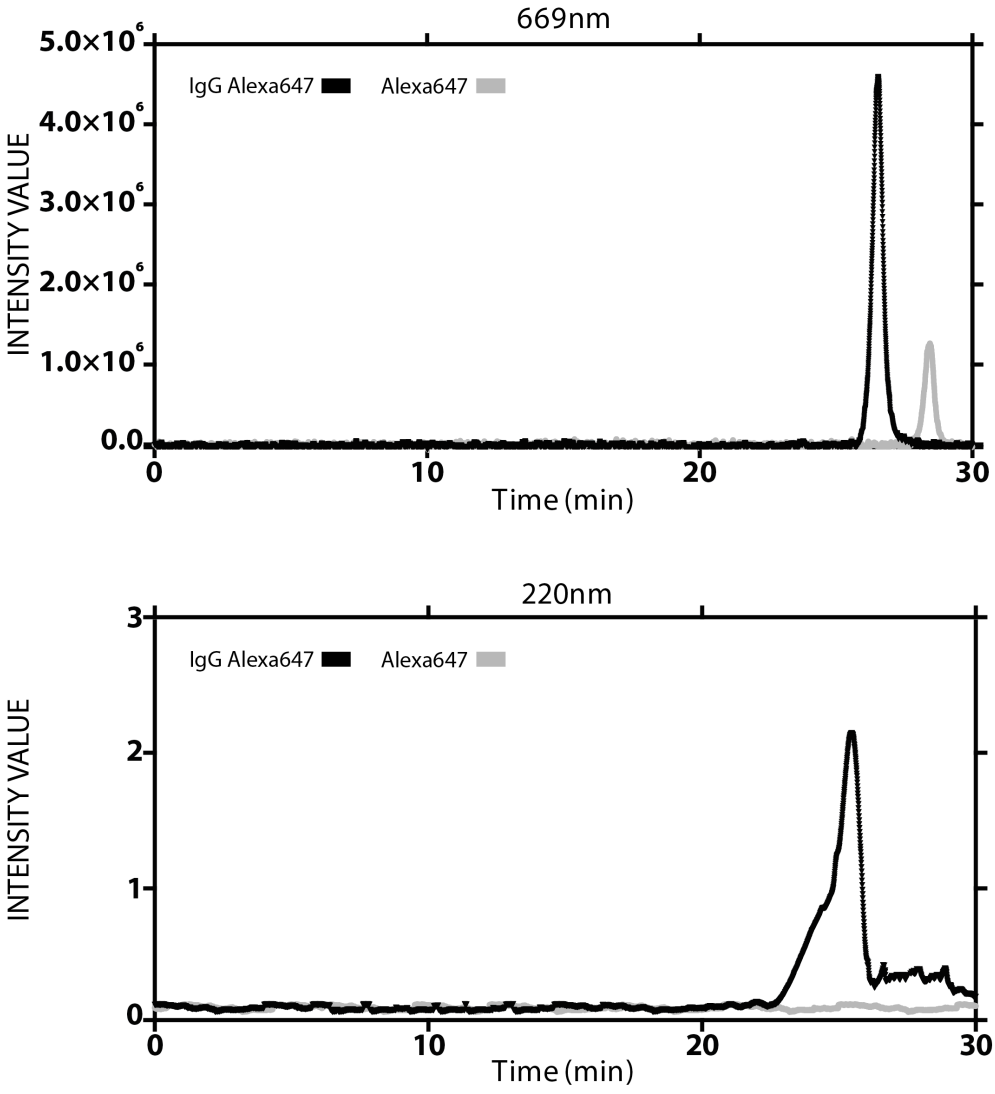

Figure 7.4. RP-HPLC analysis aimed to exclude the presence of free dye on the AlexaFluor® 647 (λ_{ex}= 650 nm, and λ_{em}= 669 nm) labelled IgG sample. The free dye or labelled protein detections was performed evaluating its fluorescent emission at 669 nm, while the protein UV-Vis absorbance was detected at 220 nm.

As shown in the chromatograms in Figure 7.4, the fluorescently labelled antibodies were detected at a retention time of approximately 27 min in UV-Vis (220 nm) and fluorescence emission channel (669 nm), whilst the free-dye was revealed at ~29 min and only on the fluorescent emission channel (669 nm). Since the peak at ~29 min was not revealed on the previous protein standard curve RP-HPLC analysis (see Section 7.2.3), the data shown in Figure 7.4 exclude any possible over-estimations on the detected amount of protein given by the presence of free-dye thus validating the quantification method.

7.2.4. Protein encapsulation within polymersome

Encapsulation efficiency of antibodies was compared across a range of different techniques such as electroporation, inclusion during pH switch and film rehydration. For this comparison, anti α-tubulin IgG (ab7291; Abcam®, UK) labeled with AlexaFluor®647 dye (Life Technologies™, USA) was used as a model.

A. Electroporation

Empty polymersomes were prepared by film hydration as previously described (Section 7.2.1). The antibody encapsulation by electroporation was tested using different conditions such as different final protein concentrations (5, 10, 20 and 40 μg/ml), different PBS molarity (0.1, 0.2 and 0.5 M) and different number of electroporation pulses (5, 10, 15 and 20). After mixing proteins and polymersomes at the desired conditions depending on the experiment, 400 μl of the mixture was loaded into a 2 mm width gap electroporation cuvette (Eppendorf, UK) and electroporated using an Electroporator 2510 (Eppendorf, UK) instrument, applying a voltage of 2500 V each pulse. 400 μl of sample was purified from the free protein by SEC using a 1 x 15 cm column packed with Sepharose 4B in 1X PBS. Purified samples were characterised by DLS and TEM (Section 7.1.3) and the collected total amount of polymer and protein was calculated via RP-HPLC as described in Section 7.2.3.

B. pH switch

The protein encapsulation exploiting the pH switch method was done following a modified version of the protocol described in Section 7.1.2-B. The acidified 1X PBS solution of copolymer was added of NaOH 1 M at room temperature. The antibody solution (final IgG concentration on the sample = 5 μg/ml) was added at pH=6. This step was necessary to avoid any protein structural damage possibly occurring exposing the latter at acidic conditions or high temperature. Samples were purified by SEC and the protein and polymer concentrations were calculated via RP-HPLC analysis (Section 7.2.3). Purified samples were characterised by DLS and TEM as previously showed (Section 7.1.3).

C. Film hydration

The general film hydration protocol is described in Section 7.1.2. In this case, to achieve the protein encapsulation within polymersomes, the antibody was diluted in 2 ml of 1X PBS (final IgG concentration on the sample = 5 μg/ml) and this solution was added to the thin film of copolymer. Samples were purified by SEC and characterised by DLS and TEM as previously described (Section 7.1.2-B and 7.1.3).

7.2.5. Statistical analysis

The statistical comparison between two group of data resulting from the ELISA assay and from the encapsulation experiments was performed using a t-test, setting the significance level with $p<0.05$. The experimental error is expressed as standard deviation (N=3).

7.3. POLYMERSOME AS FUNCTIONAL ANTIBODY DELIVERY SYSTEM IN LIVE CELLS

7.3.1. Cell culture

Primary human dermal fibroblasts (HDF), breast cancer cells (MDA-MB-231), ovarian carcinoma cells (SKOV3), human skin melanoma cells (MEWO) and urinary bladder transitional carcinoma cells (RT112) were purchased from the ATCC®. HDF cells were cultured and maintained in DMEM (Sigma-Aldrich, UK). MDA-MB-231 and RT112 cells were cultured and maintained in Roswell Park Memorial Institute (RPMI) 1640 medium (Sigma-Aldrich, UK). SKOV3 cells were cultured and maintained in McCoy's 5a Medium Modified (Sigma-Aldrich, UK) and MEWO cells instead were cultured in Eagle's Minimum Essential Medium (MEM) (Sigma-Aldrich, UK). All the cell culture mediums were supplemented with 10 (v/v) fetal calf serum, 2 mM L-glutamine, 100 mg/ml streptomycin and 100 IU/ml penicillin (Sigma-Aldrich, UK). Cells were incubated at 37 °C/5% CO_2.
Cells were routinely sub-cultured using Trypsin-EDTA (Sigma-Aldrich, UK) solution 0.25% for the detachment process and centrifuged at 2000 rpm for 5 min for the pellet collection.

7.3.2. MTT-assay

Cell viability after exposure to polymersomes was quantified by MTT assay. HDF, MDA-MB-231, SKOV3, MEWO and RT112 cells were seeded in a 24-well plate at a density of 3 x 10^4 cells per well and grown for 48 h in complete medium. Cells were divide in four groups and treated for 24 h with fresh medium containing 10% volume of 1X PBS as a negative control and the three different polymersomes concentrations: 0.5 mg/ml, 1 mg/ml and 1.5 mg/ml. Cells were washed three times with 1X PBS and then incubated in MTT solution (Sigma-Aldrich, UK) (0.5 mg ml-1 MTT in 1X PBS, 1 ml per well) for 1 h at 37 °C/5% CO_2. Intracellular metabolic activity reduces MTT to a purple water insoluble formazan salt. Subsequently, the solution was aspirated and the insoluble formazan product was solubilised by adding acidified isopropanol (0.001 N of HCl in isopropanol - 0.5 ml per well) (Sigma-Aldrich, UK) and

incubating the samples for 5 min. The absorbance of the purple formazan salt was measured using a plate reader spectrophotometer with optical density at 570 nm (ELx800 BioTek, USA).

7.3.3. Polymersome cargo delivery: microscopy quantification

For the confocal laser scanning microscopy (CLSM) quantitative analysis a glass bottom 96 well plate (BD Bioscience, USA) was seeded with HDFs at a density of 1.5 x 10^3 cells per well and grown for 24 h in standard medium DMEM. Cells were treated with fresh medium containing polymersomes encapsulated rabbit IgG (I5006; Sigma-Aldrich, UK) labelled with AlexaFluor®546 λ_{ex}=550 nm, and λ_{em}=573 nm (Life Technologies™, USA) (1 mg/ml PMPC-PDPA and 0.1 μg/ml IgG as a final concentration in medium).

The polymersomes preparation was performed as described in Section 7.1.2-A by film hydration, and the antibody cargo was encapsulated by electroporation (Section 7.2.4-A).

Briefly, 5 μg/ml of IgG were added to 400 μl of a solution containing 10 mg/ml of PMPC-PDPA polymersomes and the obtained sample was subjected at electroporation (5 pulses, 2500 V each pulse).

After the encapsulation step, both samples were purified by SEC and the relative copolymer and IgG concentrations were characterised by means of RP-HPLC as described in Section 7.2.3. All the materials applied were kept in sterile conditions.

Furthermore, a control group of cells was set up treating it with 5 μg/ml of free antibody diluted in sterile medium. Cells were thus incubated for different time points (0, 1, 5, 18 and 24 h) at 37 °C/5% CO_2 and afterwards they were washed three times with 1X PBS and incubated for 8 min with a H_2O solution containing the nucleic acid staining SYTO®9 (λ_{ex}= 485 nm, and λ_{em}=498 nm - Molecular probes®). Cells were then washed again three times with 1X PBS and added of DMEM imaging medium (Life Technologies™, USA).

The CLSM analysis was performed using a Leica TCS SP8 confocal laser microscope and the average IgG emission intensities calculation was achieved with ImageJ (U.S. National Institutes of Health, Bethesda, MD, USA).

The microscope laser intensities and detector gains were kept constant between all images.

7.3.4. Polymersome cargo delivery: RP-HPLC quantification

HDFs were seeded in 6 well plates (5 x 10^4 cells per well) and incubated in DMEM medium for 24 h as previously described (Section 7.3.3). After this first step, cells were treated with encapsulated antibody as described in Section 7.3.3. At the desired time point (0, 1, 5, 18 and 24 h) cells were washed three times with 1X PBS and placed at -20 °C overnight to induce the cellular lysis. 250 µl of 1X PBS at pH 5.5 were used to recover the cell aggregates, the antibody and to solubilise the copolymer. The solution was collected in a 2 ml plastic vial (Eppendorf, UK) and centrifuged at 20000 rpm for 10 min to eliminate cell aggregates. 100 µl of the resulting supernatant were analysed in RP-HPLC using the same protocol explained in Section 7.2.3, adjusting the fluorescence channel detection considering the IgG bonded dye. The mathematical equation to calculate the amount of protein per cell is reported below:

$$\text{ng IgG x cell} = \text{Total ng IgG} / N$$

$$N = N_0 \times e^{Kt}$$

N = Cells number

N_0 = Cells initial number

K = log2/cells replication time

t = Cells incubation time

7.3.5. Polymersome cargo release: CLSM analysis

Polymersomes endolysosomal escape and cargo release in HDF cells was analysed by CLSM. HDFs were seeded in glass bottom dishes (35 mm diameter-IBIDI®, UK) at a density of 8 x 10^3 cells per well and grown for 24 h in complete DMEM medium. Cells were treated with fresh medium containing polymersomes encapsulated rabbit IgG (I5006; Sigma-Aldrich, UK) labelled with AlexaFluor®546 λ_{ex}=550 nm, and λ_{em}=573 nm (Life Technologies™, USA) (1 mg/ml PMPC-PDPA and 0.1 µg/ml IgG as a final concentration in medium). The polymersomes preparation was performed as described in Section 7.1.2-A by film hydration, and the antibody cargo was encapsulated by electroporation (Section 7.3.3), keeping all the materials applied in sterile conditions.

Cells were thus incubated overnight at 37 °C/5% CO_2 and afterwards they were washed three times with 1X PBS and incubated for 15 min at 37°C / 5% CO_2 this

time with fresh DMEM medium containing 50 nM of LysoTracker® probe (λ_{ex}=490 nm, and λ_{em}=511 nm). Cells were then washed again three times with 1X PBS and added of DMEM imaging medium (Life Technologies™, USA).
CLSM analyses were performed with a Leica TCS SP8 confocal laser microscope and the images were analysed with ImageJ.

7.3.6. Polymersome cargo release: TEM analysis

HDFs were used as a cellular model also in this analysis and they were cultured and maintained as previously described (Section 7.3.1). The polymersomes sterile sample containing 15 nm AuNP-IgG (ab27236; Abcam, UK) was encapsulated in polymersomes as previously described in Section 7.3.3. The cells were treated with fresh medium containing 1 mg/ml of PMPC-PDPA polymersomes loaded with 0.1 μg/ml of AuNP-IgG and incubated overnight in medium at 37 °C/5% CO_2. Control cells were treated with fresh medium containing 0.1 μg/ml of free AuNP-IgG and incubated overnight using the same conditions applied for cells treated with the polymersomes antibodies loaded sample. Subsequently, the cells were washed three times with 1X PBS and fixed in epoxy resin to be sectioned with a microtome (Tian, 2014). The slides were analysed by TEM (FEI Tecnai 120 kV, FEI Co., USA). Images were analysed with ImageJ. This experiment was performed thanks to the help of Dr Tian Xhiaohe.

7.3.7. Polymersome cargo release: CLSM analysis optimisation

To study the possibility to reduce the signal originating from the endo-lysosomal organelles thus improving the confocal microscopy analysis regarding the specific antibodies-antigen intracellular recognition (mediated by the delivered of fluorescently labelled IgG), two groups of HDFs were treated with two different polymersome formulations and the respective results were compared.
Polymersome were loaded with Brilliant Violet 421™ anti-γ-Tubulin IgG (λ_{ex}=407 nm, and λ_{em}=421 nm - 529201; BioLegend®, USA) and the quencher molecule Trypan blue (Sigma-Aldrich, UK). Instead, the other polymersomes formulation contained only the fluorescent antibodies without the quencher.

Both formulations were prepared following the protocol described in Section 7.1.2-A, and the encapsulation of both quencher and antibodies was performed as explained in Section 7.2.4-A.

Briefly, to produce the first formulation (polymersome loaded with IgG and quencher molecule), 10 µl of Trypan blue 0.4% were added into 400 µl of a solution containing 10 mg/ml of PMPC-PDPA polymersomes and 5 µg/ml of Brilliant Violet 421™ IgG and subjected at electroporation (5 pulses, 2500 V each pulse). Instead, to obtain the second formulation (polymersome loaded with only IgG), 5 µg/ml of Brilliant Violet 421™ IgG were added to 400 µl of a solution containing 10 mg/ml of PMPC-PDPA polymersomes and the obtained sample was subjected also in this case at electroporation as a before (5 pulses, 2500 V each pulse).

After the encapsulation step, both samples were purified by SEC and the relative copolymer and IgG concentrations were characterised by means of RP-HPLC as described in Section 7.2.3. All the materials applied were kept in sterile conditions.

HDF cells were seeded in glass bottom dishes (35 mm diameter-IBIDI®, UK) at a density of 8 x 10^3 cells per well and grown for 24 h in complete DMEM medium. Afterwards, the two groups of cells were treated separately with fresh medium with one of the two polymersomes formulations (in both cases containing 1 mg/ml PMPC-PDPA, ~0.1 µg/ml of Brilliant Violet 421™ IgG) and incubated with it overnight at 37 °C/5% CO_2. Cells were washed three times with 1X PBS and incubated for 15 min with a H_2O solution containing the nucleic acid staining SYTO®9 (λ_{ex}= 485 nm, and λ_{em}=498 - Molecular probes®). At this stage, cells were added of DMEM imaging medium and analysed by confocal microscopy (Leica TCS SP8).

7.3.8. Delivery of functional antibody for sub-cellular targeting

The γ-Tubulin sub-cellular targeting was performed at the same conditions as described in Section 7.3.7. Two groups of cells were seeded in glass bottom dishes (35 mm diameter-IBIDI®, UK) at a density of 8 x 10^3 cells per well and grown for 24 h in complete DMEM medium. Subsequently, the cells were treated with a polymersome formulation (1 mg/ml PMPC-PDPA) loaded with fluorescently labelled anti-γ-Tubulin IgG (0.1 µg/ml of Brilliant Violet 421™

IgG; λ_{ex}=407 nm, and λ_{em}=421 nm) and Trypan Blue, thus incubated overnight at 37 °C/5% CO_2. Subsequently, each group of cells was washed three times with 1X PBS and incubated for 5 or 30 min with a H_2O solution containing the nucleic acid staining SYTO®9 (λ_{ex}= 485 nm, and λ_{em}=498). Afterward, they were placed in DMEM imaging medium and analysed under confocal microscopy (Leica TCS SP8).

7.3.9. Intracellular delivery of anti γ-Tubulin IgG in different cell models

The experiment described in Section 7.3.8 was repeated at identical conditions with other cell models. The only difference was that in this case all the cells were all exposed at 5 min with a H_2O solution containing the nucleic acid staining SYTO®9 (λ_{ex}= 485 nm, and λ_{em}=498). Indeed, human adenocarcinoma cells (HeLa), murine fibroblasts (NIH-3T3) and murine brain endothelial cells (bEnd3) were purchased from the ATCC® and cultured in DMEM (Sigma-Aldrich, UK). Human embryonal carcinoma stem cells (NTera2) were provided from Prof. Peter Andrews (University of Sheffield, UK) and they were also cultured DMEM (Sigma-Aldrich, UK). Human melanoma cell (A375) instead were provided by Prof. Sheila MacNeil (University of Sheffield, UK) and cultured in MEM (Sigma-Aldrich, UK). All the used cell culture mediums were supplemented with: 10 (v/v) fetal calf serum, 2 mM L-glutamine, 100 mg/ml streptomycin and 100 IU/ml penicillin (Sigma-Aldrich, UK) and the cells were grown at 37 °C/95% air/5% CO_2. All the cell models were routinely sub-cultured using Trypsin-EDTA (Sigma-Aldrich, UK) solution 0.25% for the detachment process and centrifuged at 2000 rpm for 5 min for the pellet collection.

7.3.10. Statistical analysis

The statistical comparison between two group of data resulting from the MTT assay and from the TEM analysis was performed using a t-test, setting the significance level with $p<0.05$. The experimental error is expressed as standard deviation (N=3).

7.4. Ki-67 AS INTRACELLULAR TARGET IN ANTICANCER-THERAPY

7.4.1. Cell culture

HDF, MDA-MB-231, HeLa, and oral carcinoma (FaDu) cells were purchased from ATCC®. HDF, HeLa, and FaDu cells were cultured and maintained using DMEM (Sigma-Aldrich, UK) containing: 10 (v/v) fetal calf serum, 2 mM L-glutamine, 100 mg/ml streptomycin and 100 IU/ml penicillin (Sigma-Aldrich, UK). Cells were cultured at 37 °C/95% air/5% CO_2. Human umbilical vein endothelial cells (HUVECs) were purchased from Life Technologies™ and cultured using Medium 200 with Low Serum Growth Supplement (LSGS) (Life Technologies™, USA) and maintained as described for the previous cells. MDA-MB-231 cells were cultured in RPMI 1640 medium (Lonza, UK), containing: 10 (v/v) fetal calf serum, 2 mM L-glutamine, 100 mg/ml streptomycin and 100 IU/ ml penicillin (Sigma-Aldrich, UK). Cells were periodically sub-cultured using Trypsin-EDTA solution 0.25% (Sigma-Aldrich, UK) for the detachment process and centrifuged at 2000 rpm for 5 min for the pellet collection.
The cellular synchronisation was obtained by incubating the cells with serum-deprived medium, at different time points (18, 24, 36 and 48 h), depending on the experimental conditions.

7.4.2. Quantification of Ki-67 expression in different cell models

For the quantification of Ki-67 expression HDF, HUVEC, MDA-MB-231, HeLa and FaDu cells were initially seeded in glass bottom dishes (35 mm diameter-IBIDI®) at a density of 8 x 10^3 cells per well, grown for 24 h in complete medium. Afterward the cells were subjected to three washing steps with 1X PBS and finally analysed by confocal microscopy (Leica TCS SP8). A CLSM analysis was applied to visualise the protein expression. The cellular samples were prepared with immunofluorescence protocol: fixation with formaldehyde 3.7% for 10 min, permeation with 0.1% Triton X-100 in 1X PBS for 10 min and blocking of unspecific sites with BSA 2% for 2 h and overnight incubation at 4 °C with the antibody sample.
Ki-67 protein was directly investigated through a mouse IgG anti-Ki-67

(ab15580; Abcam®, UK), conjugated with Brilliant Violet 421™ dye (BioLegend® - λ_{ex}=405 nm, and λ_{em}=421 nm). Cell nucleus were stained with SYTO®9 (Life Technologies™ - λ_{ex}=490 nm and a λ_{em}=525 nm). The microscope laser intensities and detector gains were kept constant between all images. The average Ki-67 overlap value intensity with SYTO®9 was calculated with a specifically developed MATLAB® script.

7.4.3. Ki-67 expression as a function of the cell cycle

Fluorescence cytometry (FC) analysis was used to quantify the Ki-67 expression in relation to the cell cycle stage using a BD FACSArray instrument. HDF and MDA-MB-231 cells were cultured and maintained as previously described and growth in T75 flasks. The cell cycle analysis was performed as previously reported (Pozarowski and Darzynkiewicz, 2004). Briefly, the cells were detached from the T75 flasks using Trypsin-EDTA solution 0.25% (Sigma-Aldrich, UK) and centrifuged at 2000 rpm for 5 min for the pellet collection. Subsequently, the cells were fixed and permeabilised in 70% ethanol for 2 h at 4 °C. The cellular DNA staining was obtained exposing the fixed cells to a propidium iodide (PI) solution (0.1% (v/v) Triton X-100, 10 μg/mL PI (Molecular Probes, Inc.), and 100 μg/mL DNase-free RNase A in 1X PBS). The Ki-67 detection was instead achieved treating the cells for 2 h with a blocking solution containing 2% BSA in 1X PBS and subsequently incubating them overnight at 4 °C with the anti-Ki67 antibody sample (ab15580; Abcam®, UK), conjugated with Alexa Fluor® 647 dye (BioLegend, USA - λ_{ex}=635 nm, and a λ_{em}=670 nm).

The PI staining used in this study, allows the deconvolution analysis of the cellular DNA content histogram (see Figure 7.5). This in turn lead to reveal the cellular distributions across the three major phases of the cell cycle (G_1, S and G_2/M). Furthermore, these phases were correlated with the Ki-67 expression.

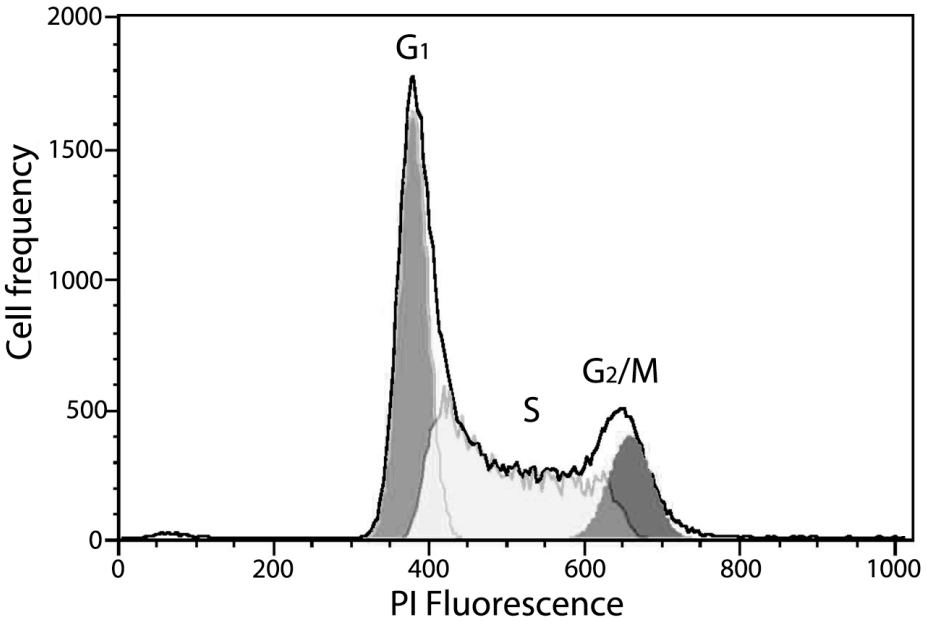

Figure 7.5. Cellular DNA content histogram, obtained by nucleic acid staining with PI. This analysis reveals the cellular distributions across the cell cycle phases: G_1, S and G_2/M.

7.4.4. Ki-67 gene knock-down experiment

The genes knockdown analysis was performed using the Thermo Scientific™ GIPZ lentiviral™ system, following the company protocol.

Briefly, HDF and MDA-MB-231 cells were treated with shRNA loaded viruses, and cultured in serum-free medium respectively with 12 x 10^6 Transducing units per ml (TU/ml) and 3.6 x 10^6 TU/ml for 6 h. Subsequently, the medium was substituted with fresh one and the cells were incubated for 0 h, 24 h and 48 h at 37 °C/95% air/5% CO_2. The effectiveness of the shRNA gene translation was evaluated under confocal microscopy (Leica TCS SP8) detecting the expression of the TurboGFP reporter gene (λ_{ex}=490 nm, and a λ_{em}=525 nm) which is also present on the pGIPZ lentiviral vector.

Afterward, the mRNA gene target expression was quantify with (A) CLSM analysis and in (B) RT-qPCR.

As negative control, a non-silencing virus, expressing the scrambled sequence TCTCGCTTGGGCGAGAGTAAG was used; Ki-67 gene was targeted with the following shRNA antisense sequence: TCCTTAGGAGTCTGTAGCT (cloneId: V3LHS_387958).

Finally, the antisense sequence CCTCATTTCCTGGTATGACAA was used to

silence the positive control GAPDH.

A. CLMS analysis

The CLMS analysis was performed in a glass bottom 96 well plate (BD Bioscience, USA) and both HDF and MDA-MB-231 cells were seeded with a density of 1.5 x 10^3 cells per well and grown for 24 h. After the treatment with Thermo Scientific™ GIPZ lentiviral™, the Ki-67 was quantified as described in Section 7.4.2 while the TurboGFP reporter gene was detected at λ_{ex}=490 nm, and a λ_{em}=525 nm. The microscope laser intensities and detector gains were kept constant between all images.

B. Real time-quantitative polymerase chain reaction (RT-qPCR)

HDF and MDA-MB-231 cells were cultured in a 6 well plates with a density of 5 x 10^4 cells per well and incubated in appropriate medium for 24 h as previously described (see Section 7.4.1). Subsequent to that, the cells were incubate with the Thermo Scientific™ GIPZ lentiviral™ treatment following the company protocol.

Following lentivirus treatment, cells were washed three times in 1X PBS and lysed with radio-immunoprecipitation assay (RIPA) buffer (20 mmol/L Tris, pH 7.5, 150 mmol/L NaCl, 1% Nonidet P-40, 0.5% sodium deoxycholate, 1 mmol/L EDTA, 0.1% SDS) (Sigma-Aldrich, UK), containing complete mini protease inhibitors (Roche, UK) used according company protocol.

Total RNA was collected using RNeasy Mini Kit (Qiagen, UK). RNA concentration was measured with NanoDrop8000 spectrophotometer. Complementary DNA (cDNA) was synthesized from every 1 μg of total mRNA in 20 μl volume per tube with QuantiTect Rev. Transcription Kit (Qiagen, UK). GAPDH was used as a reference gene, and the two Ki67 isoforms (α and β) were analysed using the following list of primers:

RT-qPCR			
Primer	**Sequence (5'⟶3')**	**Prod. length**	**NCBI RefSeq**
GAPDH forward	ACAGTCAGCCGCATCTTCTT	94 bp	NM_002046
GAPDH reverse	ACGACCAAATCCGTTGACTC		
Ki67 α forward	TGTTGGTCTCGCGTAAGTCAA	120 bp	NM_002417.4
Ki67 α reverse	CAGACTCCACGTCTCTTCCC		
Ki67 β forward	AGCACGTCGTGTCTCAAGAT	60 bp	NM_001145966.1
Ki67 β reverse	GGTATTCCCTCACTCTCATCAGG		

Table 7.1. List of primers used in RT-qPCR characterisation.

Quantitative analysis was performed with QuantiTect SYBR Green RT-qPCR Kit (Qiagen, UK). The amplification process was done in 20 μL/tube, using the following steps: 95°C for 5 min to make active the DNA Polymerase, followed by 40 cycles of 95°C (10 sec) for denaturation, and 60°C (30 sec) for combined annealing and extension for all primers. Melting curve was also acquired, to analyse the sample quality, from 55°C to 99°C, by increasing of 1°C/min. Data were analysed via ΔΔCt value. $2^{-\Delta\Delta Ct}$ was calculated as follows: $\Delta Ct = Ct_{Ki67} - Ct_{GAPDH}$; ΔΔCt=ΔCt (treated) - ΔCt (control).

7.4.5. Ki-67 expression in cancerous and non-cancerous cells before and after nutrients deprivation: western blot analysis

For the western blot analysis the cells were cultured in T75 flasks and they were lysed and prepared as describe for the RT-qPCR samples preparation. The total protein initial concentration was calculated using the bicinchoninic acid assay (BCA) (Smith et al., 1985) (Thermo Fisher Scientific, USA) and thus normalised for all the cellular samples. All the samples were denatured for 5 min at 95°C prior the western size-based assay or the standard western blot assay.

A. Western size-based assay

The western blot analysis for the KI-67 protein quantifications was performed with an automated western size-based assay (ProteinSimple-Simon™, USA),

following the company standard protocol and using 20 μg of protein per sample. The specific antibody applied against Ki-67 was purchased from Abcam® (ab15580), while the ERK 1/2 positive control antibody was provided by the Simon™ analysis kit (Boge et al., 2012; Rustandi et al., 2012).

B. Standard western blot assay

NuPAGE4-12% TrisGels (Life Technologies™) was used to achieve the protein fractions separation. Each sample (20 μg of protein in a volume of 40 μl) was loaded into the gel well and their alignment on the gel front was achieved applying a voltage of 100 V for 15 min. Subsequently, the protein fractions separation was obtained with a voltage of 180 V per 150 min.

After this step, the gel trapped proteins were transferred thanks to the iBlot instrument (Life Technologies™) to a nitrocellulose membrane. The transfer was performed applying a voltage of 100 V per 60 min.

Subsequently, the membrane was blocked with 1 h incubation at room temperature with 5% (w/v) milk powder in Tris-buffer with 0.5% (v/v) Tween 20 (blocking solution). The membrane was stained for Ki-67 by overnight incubation at 4°C with anti-Ki-67 antibodies diluted in blocking solution (ab 15580; 1:500; Abcam®, UK). The membrane was then washed three times with 1X PBS and incubated with horse-radish peroxidase (HRP) secondary antibodies, also diluted in blocking solution (1:10000; Cell Signaling Technologies, UK). Finally, the membrane was treated for 5 min with the enhanced chemiluminescence kit (Thermo Fisher Scientific, USA). The photographic development of the obtained results was performed in a dark room exposing a photographic film to the obtained membrane for 1 min. Afterwards, the photographic film was immersed for 5 sec in a developing solution and fixed by placing it for 30 sec in a fixing solution.

7.4.6. Ki-67 α and β splice variant expression as a function of the nutrients deprivation

HDF and MDA-MB-231 cells were cultured in a 6 well plates with a density of 5 x 10^4 cells per well and incubated in appropriate medium for 24 h as previously described (see Section 7.4.1). Afterwards, the cells were subjected at serum deprived medium at different time point and the cDNA was subsequently

obtained as described in Section 7.4.4-B.

A. Reverse transcription polymerase chain reaction (RT-PCR), and PCR assays

For the RT-PCR, the samples were run in a standard agarose gel (1%).
GAPDH was used as a reference gene, and the two Ki67 isoforms (α and β) were analysed using the list of primers shown in Table 7.2.

RT-PCR			
Primer	**Sequence (5'⟶3')**	**Prod. length**	**NCBI RefSeq**
GAPDH forward	CAGCCTCAAGATCATCAGCA	135 bp	NM_002046.5 NM_001256799.2 NM_001289745.1 NM_001289745.1
GAPDH reverse	GTCTTCTGGGTGGCAGTGAT		
Ki67 α forward	GAAAGCTCAAGATTCCAAGGC	1000 bp	NM_002417.4
Ki67 α reverse	GCCCAATTTCTCAGGCTTGC		
Ki67 β forward	TATCAAAAGGAGCGGGGTCG	494 bp	NM_001145966.1
Ki67 β reverse	TTGGGGCTTCTCCCCTTTTG		

Table 7.2. List of primers used RT-PCR characterisation.

B. Real time-quantitative polymerase chain reaction (RT-qPCR)

This analysis was performed with identical protocol and materials as described in paragraph 7.4.4-B.

7.4.7. Nuclear-independent molecular mechanisms of Ki-67 regulation

Intracellular proteins distribution and interactions were analysed by CLSM. Cells were seeded at a density of 8 x 10^3 cells per well and allowed to grown for 24 h in complete medium before analysis.
The protein-protein interactions were investigated under confocal microscope (Leica TCS SP8), and the cellular samples were obtained with

immunofluorescence protocol: fixation with formaldehyde 3.7% for 10 min, permeation with 0.1% Triton X-100 in 1X PBS for 10 min, block with BSA 2% for 2 h.

Ki67 protein was directly investigated through a mouse IgG anti-Ki-67, conjugated with Brilliant Violet 421™ dye (350505; BioLegend® - λ_{ex}=405 nm, and λ_{em}=421 nm). The Golgi compartment staining was achieved by treating cells with a modified baculovirus expressing a fusion construct of a Golgi marker and a red fluorescent protein (CellLight® Golgi-RFP - C10593; Life Technologies™ - λ_{ex}=540 nm, and a λ_{em}=625 nm). All the other confocal characterisations were carried out using specific unlabelled primary rabbit IgG incubating the cellular sample for 2 h with the latter. Proteins were then enlighten by secondary DyLight™ 649 donkey anti-rabbit IgG (406406; BioLegend® - λ_{ex}=655, nm and a λ_{em}=670 nm) which was incubated within the sample overnight. The proteasome detections was achieved with a specific IgG recognising the 20s proteins subunit (ab3325; Abcam®, UK). The COPII-vesicles detections was performed using an IgG recognising the Sec31A subunit (HPA005457; Sigma-Aldrich®). The BiP investigation was obtained through an antibody recognising the specific N-term aa sequence of the protein (G9043; Sigma-Aldrich®). Finally, the nucleic acid staining was obtained with the molecular probe SYTO®9 (Life Technologies™ - λ_{ex}=490 nm and a λ_{em}=525 nm).

7.4.8. Ki-67 as intracellular target for anticancer applications

A. CLSM analysis

This analysis was performed using MDA-MB-231 cells as model. The cells were treated with a polymersome formulation loaded with a mouse anti-Ki-67 IgG conjugated with Brilliant Violet 421™ dye (350505; BioLegend® - λ_{ex}=405 nm, and λ_{em}=421 nm) (1 mg/ml PMPC-PDPA and 0.1 μg/ml IgG as a final concentration in medium). The protocol applied for this experiment is the same protocol as described in Section 7.3.8. The image analysis was performed with ImageJ software.

B. MTT assay

The MTT assay was herein performed as explained in Section 7.3.2. After 18 h of serum starvation, the HDF and MDA-MB-231 cells were treated with different concentrations of empty polymersomes or polymersomes loaded with anti Ki-67 IgG (39799; ActiveMotif®, UK) (0.5, 1 and 1.5 mg/ml PMPC-PDPA, 0.05 - 0.1 - 0.15 μg/ml IgG). Furthermore, a control group of cells treated with 10% 1X PBS in media was tested. The MTT analysis was performed 24 h after the treatment.

C. Cells counting assay

For this analysis, HDF and MDA-MB-231 cells were cultured and treated following the same protocol and materials as described for the MTT assay in Section 7.4.8-B. The cell counting was performed using the BIO-RAD TC20™ Automated Counter.

7.4.9. Statistical analysis

The statistical comparison between two group of data obtained in experiments such as FC characterisation, Simple Western™ quantification, RT-qPCRs, confocal colocalisation experiments and MTT assay was performed using a t-test. The statistical comparison between more than two groups of data obtained in experiments such as the confocal quantitative analysis and the gene knock-down experiment was performed using a two-way ANOVA test. For both statistical comparisons (t-test and two-way ANOVA), the significance level was set-up with $p<0.05$. The experimental error is expressed as standard deviation (N=3).

References

Adams, J. M., and Cory, S. (2007). The Bcl-2 apoptotic switch in cancer development and therapy. Oncogene *26*, 1324-1337.

Aguilar, M.-I. (2004). Reversed-Phase High-Performance Liquid Chromatography. In HPLC of Peptides and Proteins, M.-I. Aguilar, ed. (Springer New York), pp. 9-22.

Ahmed, F., Pakunlu, R. I., Brannan, A., Bates, F., Minko, T., and Discher, D. E. (2006). Biodegradable polymersomes loaded with both paclitaxel and doxorubicin permeate and shrink tumors, inducing apoptosis in proportion to accumulated drug. Journal of Controlled Release *116*, 150-158.

Akinc, A., and Battaglia, G. (2013). Exploiting endocytosis for nanomedicines. Cold Spring Harbor Perspectives in Biology *5*.

Alderton, G. K., and Bordon, Y. (2012). Tumour immunotherapy - leukocytes take up the fight. Nature Reviews Immunology *12*, 237-237.

Alexander, A., Dwivedi, S., Ajazuddin, T., Giri, S., Saraf, S., Saraf, D., and Tripathi (2012). Approaches for breaking the barriers of drug permeation through transdermal drug delivery. Journal of Controlled Release *164*, 26-40.

Allen, T. M., and Cullis, P. R. (2013). Liposomal drug delivery systems: From concept to clinical applications. Advanced drug delivery reviews *65*, 36-48.

Aranda-Espinoza, H., Bermudez, H., Bates, F. S., and Discher, D. E. (2001). Electromechanical limits of polymersomes. Physical Review Letters *87*, 208301.

Attila, F. (1998). Data analysis and signal processing in chromatography. In data handling in science and technology. Elsevier, pp. 1-414.

Balmain, A., Barrett, J. C., Moses, H., and Renan, M. J. (1993). How many mutations are required for tumorigenesis? Implications from human cancer data. Molecular Carcinogenesis *7*, 139-146.

Barenholz, Y. (2001). Liposome application: problems and prospects. Current Opinion in Colloid & Interface Science *6*, 66-77.

Bates, F. S., and Fredrickson, G. H. (1990). Block copolymer thermodynamics: theory and experiment. Annual Review of Physical Chemistry *41*, 525-557.

Battaglia, G., and Ryan, A. J. (2006). Pathways of polymeric vesicle formation. The Journal of Physical Chemistry B *110*, 10272-10279.

Battaglia, G., Ryan, A. J., and Tomas, S. (2006). Polymeric vesicle permeability: a facile chemical assay. Langmuir *22*, 4910-4913.

Ben-Haim, N., Broz, P., Marsch, S., Meier, W., and Hunziker, P. (2008). Cell-specific integration of artificial organelles based on functionalized polymer vesicles. Nano Letters *8*, 1368-1373.

Bermudez, H., Brannan, A. K., Hammer, D. A., Bates, F. S., and Discher, D. E. (2002). Molecular weight dependence of polymersome membrane structure, elasticity, and stability. Macromolecules *35*, 8203-8208.

Berridge, M., Herst, P., and Tan, A. (2005). Tetrazolium dyes as tools in cell biology: new insights into their cellular reduction. Biotechnology Annual Review *11*, 127-152.

Bertolotti, A., Zhang, Y., Hendershot, L. M., Harding, H. P., and Ron, D. (2000). Dynamic interaction of BiP and ER stress transducers in the unfolded-protein response. Nature Cell Biology *2*, 326-332.

Bhowmick, N. A., Neilson, E. G., and Moses, H. L. (2004). Stromal fibroblasts in cancer initiation and progression. Nature *432*, 332-337.

Blanco, E., Hsiao, A., Mann, A. P., Landry, M. G., Meric-Bernstam, F., and Ferrari, M. (2011). Nanomedicine in cancer therapy: innovative trends and prospects. Cancer Science *102*, 1247-1252.

Blasco, E., Barrio, J. d., Sanchez-Somolinos, C., Pinol, M., and Oriol, L. (2013). Light induced molecular release from vesicles based on amphiphilic linear-dendritic block copolymers. Polymer Chemistry *4*, 2246-2254.

Blasco, M. A. (2005). Telomeres and human disease: ageing, cancer and beyond. Nature Reviews Genetics *6*, 611-622.

Boge, A., Ramirez, F., Nguyen, U., Kazakova, I., Dermody, J., Yang, T., and Gavin, R. (2012). An automated reinvention of the western blot - A Simple Western Analysis of the AKT pathway signaling cascade. Faseb Journal *26*.

Booth, D. G., Takagi, M., Sanchez-Pulido, L., Petfalski, E., Vargiu, G., Samejima, K., Imamoto, N., Ponting, C. P., Tollervey, D., Earnshaw, W. C., *et al.* (2014). Ki-67 is a PP1-interacting protein that organises the mitotic chromosome periphery. eLife *3*.

Bories-Azeau, X., Armes, S. P., and van den Haak, H. J. W. (2004). Facile synthesis of zwitterionic diblock copolymers without protecting group chemistry. Macromolecules *37*, 2348-2352.

Both, G. (2009). Recent progress in gene-directed enzyme prodrug therapy: an emerging cancer treatment. Current opinion in molecular therapeutics *11*, 421-432.

Brandizzi, F., and Barlowe, C. (2013). Organization of the ER-Golgi interface for membrane traffic control. Nature Reviews Molecular Cell Biology *14*, 382-392.

Brown, L., McArthur, S. L., Wright, P. C., Lewis, A., and Battaglia, G. (2010). Polymersome production on a microfluidic platform using pH sensitive block copolymers. Lab on a Chip *10*, 1922-1928.

Bullwinkel, J., Baron-Lühr, B., Lüdemann, A., Wohlenberg, C., Gerdes, J., and Scholzen, T. (2006). Ki-67 protein is associated with ribosomal RNA transcription in quiescent and proliferating cells. Journal of Cellular Physiology *206*, 624-635.

Burdick, J. A., and Prestwich, G. D. (2011). Hyaluronic acid hydrogels for biomedical applications. Advanced Materials *23*, H41-H56.

Burkhart, D. L., and Sage, J. (2008). Cellular mechanisms of tumour suppression by the retinoblastoma gene. Nature Reviews Cancer *8*, 671-682.

Bush, M. A., Matthews, J. E., De Boever, E. H., Dobbins, R. L., Hodge, R. J., Walker, S. E., Holland, M. C., Gutierrez, M., and Stewart, M. W. (2009). Safety, tolerability, pharmacodynamics and pharmacokinetics of albiglutide, a long-acting glucagon-like peptide-1 mimetic, in healthy subjects. Diabetes, obesity and metabolism *11*, 498-505.

Byeon, I.-J., Li, H., Song, H., Gronenborn, A., and Tsai, M.-D. (2005). Sequential phosphorylation and multisite interactions characterize specific target recognition by the FHA domain of Ki67. Nature structural & molecular biology *12*, 987-993.

Cabane, E., Malinova, V., and Meier, W. (2010). Synthesis of photocleavable amphiphilic block copolymers: toward the design of photosensitive nanocarriers. Macromolecular Chemistry and Physics *211*, 1847-1856.

Calleja, P., Huarte, J., Agüeros, M., Ruiz-Gatón, L., Espuelas, S., and Irache, J. (2012). Molecular buckets: cyclodextrins for oral cancer therapy. Therapeutic delivery *3*, 43-57.

CancerResearchUK (2014). UK cancer incidence 2011 and mortality 2011 summary. Counts, January 2014.

Canton, I., and Battaglia, G. (2012). Endocytosis at the nanoscale. Chemical Society Reviews *41*, 2718-2739.

Canton, I., Massignani, M., Patikarnmonthon, N., Chierico, L., Robertson, J., Renshaw, S. A., Warren, N. J., Madsen, J. P., Armes, S. P., Lewis, A. L.,

and Battaglia, G. (2013). Fully synthetic polymer vesicles for intracellular delivery of antibodies in live cells. FASEB J *27*, 98-108.

Cavallaro, U., and Christofori, G. (2004). Cell adhesion and signalling by cadherins and Ig-CAMs in cancer. Nature Reviews Cancer *4*, 118-132.

Cavallaro, U., and Dejana, E. (2011). Adhesion molecule signalling: not always a sticky business. Nature Reviews Molecular Cell Biology *12*, 189-197.

Cerritelli, S., Velluto, D., and Hubbell, J. A. (2007). PEG-SS-PPS: reduction-sensitive disulfide block copolymer vesicles for intracellular drug delivery. Biomacromolecules *8*, 1966-1972.

Chen, H.-T., Neerman, M. F., Parrish, A. R., and Simanek, E. E. (2004). Cytotoxicity, hemolysis, and acute in vivo toxicity of dendrimers based on melamine, candidate vehicles for drug delivery. Journal of the American Chemical Society *126*, 10044-10048.

Chen, X., Ding, X., Zheng, Z., and Peng, Y. (2006). Thermosensitive cross-linked polymer vesicles for controlled release system. New Journal of Chemistry *30*, 577-582.

Cheng, N., Chytil, A., Shyr, Y., Joly, A., and Moses, H. L. (2008). Transforming growth factor-β signaling–deficient fibroblasts enhance hepatocyte growth factor signaling in mammary carcinoma cells to promote scattering and invasion. Molecular Cancer Research *6*, 1521-1533.

Cheng, P.-C. (2006). The contrast formation in optical microscopy. In handbook of biological confocal microscopy, J.B. Pawley, ed. (Springer US), pp. 162-206.

Chierico, L., Joseph, A. S., Lewis, A. L., and Battaglia, G. (2014). Live cell imaging of membrane / cytoskeleton interactions and membrane topology. Scientific Reports *4*.

Chithrani, B. D., Ghazani, A. A., and Chan, W. C. W. (2006). Determining the size and shape dependence of gold nanoparticle uptake into mammalian cells. Nano Letters *6*, 662-668.

Colley, H. E., Hearnden, V., Avila-Olias, M., Cecchin, D., Canton, I., Madsen, J., MacNeil, S., Warren, N., Hu, K., McKeating, J. A., *et al.* (2014). Polymersome-mediated delivery of combination anticancer therapy to head and neck cancer cells: 2D and 3D in vitro evaluation. Molecular Pharmaceutics *11*, 1176-1188.

Constantinou, A., Epenetos, A. A., Hreczuk Hirst, D., Jain, S., Wright, M., Chester, K. A., and Deonarain, M. P. (2009). Site-specific polysialylation of an antitumor single-chain Fv fragment. Bioconjugate Chemistry *20*, 924-931.

Cox, B. D., Natarajan, M., Stettner, M. R., and Gladson, C. L. (2006). New concepts regarding focal adhesion kinase promotion of cell migration and proliferation. Journal of Cellular Biochemistry *99*, 35-52.

Crea, R., Kraszewski, A., Hirose, T., and Itakura, K. (1978). Chemical synthesis of genes for human insulin. Proceedings of the national academy of sciences *75*, 5765-5769.

Daoud, M., and Cotton, J. P. (1982). Star shaped polymers : a model for the conformation and its concentration dependence. Journal of Physics France *43*, 531-538.

De Castro, C. E., Mattei, B., Riske, K. A., Jager, E. e., Jager, A., Stepańek, P., and Giacomelli, F. C. (2014). Understanding the structural parameters of biocompatible nanoparticles dictating protein fouling. Langmuir *30*, 9770-9779.

De Gennes, P. G. (1980). Conformations of polymers attached to an interface. Macromolecules *13*, 1069-1075.

Derganc, J., Antonny, B., and opi, A. (2013). Membrane bending: the power of protein imbalance. Trends in biochemical sciences *38*, 576-584.

DeVita, V. T., and Chu, E. (2008). A history of cancer chemotherapy. Cancer Research *68*, 8643-8653.

Didenko, V. V., Ngo, H., and Baskin, D. S. (2005). Polyethyleneimine as a transmembrane carrier of fluorescently labeled proteins and antibodies. Analytical biochemistry *344*, 168-173.

Diego dos Santos Ferreira, S. C. d. A. L., Marina Santiago Franco & Mônica Cristina Oliveira (2013). pH-sensitive liposomes for drug delivery in cancer treatment. Therapeutic delivery *4*, 1099-1123.

Discher, B. M., Won, Y.-Y., Ege, D. S., Lee, J. C.-M., Bates, F. S., Discher, D. E., and Hammer, D. A. (1999). Polymersomes: tough vesicles made from diblock copolymers. Science *284*, 1143-1146.

Discher, D. E., and Eisenberg, A. (2002). Polymer vesicles. Science *297*, 967-973.

Discher, D. E., Ortiz, V., Srinivas, G., Klein, M. L., Kim, Y., Christian, D., Cai, S., Photos, P., and Ahmed, F. (2007). Emerging applications of polymersomes in delivery: From molecular dynamics to shrinkage of tumors. Progress in Polymer Science *32*, 838-857.

Donaldson, J. (2008). Arfs and membrane lipids: sensing, generating and responding to membrane curvature. Biochemical journal *414*, e1-e2.

Du, J., and Armes, S. P. (2005). pH-Responsive vesicles based on a hydrolytically self-cross-linkable copolymer. Journal of the American Chemical Society *127*, 12800-12801.

Du, J., Tang, Y., Lewis, A. L., and Armes, S. P. (2005). pH-Sensitive vesicles based on a biocompatible zwitterionic diblock copolymer. Journal of the American Chemical Society *127*, 17982-17983.

Dumontet, C., and Jordan, M. A. (2010). Microtubule-binding agents: a dynamic field of cancer therapeutics. Nature Reviews Drug Discovery *9*, 790-803.

Duncan, R. (2003). The dawning era of polymer therapeutics. Nature Reviews Drug Discovery *2*, 347-360.

Endl, E., and Gerdes, J. (2000a). The Ki-67 Protein: fascinating forms and an unknown function. Experimental Cell Research *257*, 231-237.

Endl, E., and Gerdes, J. (2000b). Posttranslational modifications of the KI-67 protein coincide with two major checkpoints during mitosis. Journal of Cellular Physiology *182*, 371-380.

Endl, E., Steinbach, P., Knüchel, R., and Hofstädter, F. (1997). Analysis of cell cycle-related Ki-67 and p120 expression by flow cytometric BrdUrd-Hoechst/7AAD and immunolabeling technique. Cytometry *29*, 233-241.

Engvall, E., and Perlmann, P. (1971). Enzyme-linked immunosorbent assay (Elisa) quantitative assay of immunoglobulin-G. Immunochemistry *8*, 871-&.

Ensign, L., Cone, R., and Hanes, J. (2012). Oral drug delivery with polymeric nanoparticles: the gastrointestinal mucus barriers. Advanced drug delivery reviews *64*, 557-570.

Escoffre, J.-M., Portet, T., Wasungu, L., Teissié, J., Dean, D., and Rols, M.-P. (2009). What is (still not) known of the mechanism by which electroporation mediates gene transfer and expression in cells and tissues. Molecular biotechnology *41*, 286-295.

Ferguson, L., and Denny, W. (2007). Genotoxicity of non-covalent interactions: DNA intercalators. Mutation research - Fundamental and Molecular Mechanisms of Mutagenesis *623*, 14-23.

Feron, O. (2009). Pyruvate into lactate and back: from the Warburg effect to symbiotic energy fuel exchange in cancer cells. Radiotherapy and oncology *92*, 329-333.

Ferrara, N. (2009). Vascular endothelial growth factor. Arteriosclerosis, thrombosis, and vascular biology *29*, 789-791.

Flannagan, R. S., Jaumouillé, V., and Grinstein, S. (2012). The cell biology of phagocytosis. Annual Review of Pathology: Mechanisms of Disease *7*, 61-98.

Fraternali, F., and Cavallo, L. (2002). Parameter optimized surfaces (POPS): analysis of key interactions and conformational changes in the ribosome. Nucleic Acids Research *30*, 2950-2960.

Fredrickson, G. H., and Bates, F. S. (1996). Dynamics of block copolymers: theory and experiment. Annual Review of Materials Science *26*, 501-550.

Gaitzsch, J., Appelhans, D., Wang, L., Battaglia, G., and Voit, B. (2012a). Synthetic bio-nanoreactor: mechanical and chemical control of polymersome membrane permeability. Angewandte Chemie International Edition *51*, 4448-4451.

Gaitzsch, J., Canton, I., Appelhans, D., Battaglia, G., and Voit, B. (2012b). Cellular interactions with photo-cross-linked and pH-sensitive polymersomes: biocompatibility and uptake studies. Biomacromolecules *13*, 4188-4195.

Gentile, F., Ferrari, M., and Decuzzi, P. (2008). The transport of nanoparticles in blood vessels: the effect of vessel permeability and blood rheology. Annals of biomedical engineering *36*, 254-261.

Gerdes, J., Lemke, H., Baisch, H., Wacker, H. H., Schwab, U., and Stein, H. (1984). Cell cycle analysis of a cell proliferation-associated human nuclear antigen defined by the monoclonal antibody Ki-67. The Journal of Immunology *133*, 1710-1715.

Gerdes, J., Schwab, U., Lemke, H., and Stein, H. (1983). Production of a mouse monoclonal antibody reactive with a human nuclear antigen associated with cell proliferation. International Journal of Cancer *31*, 13-20.

Gething, M.-J. (1999). Role and regulation of the ER chaperone BiP. Seminars in Cell & Developmental Biology *10*, 465-472.

Giacinti, C., and Giordano, A. (2006). RB and cell cycle progression. Oncogene *25*, 5220-5227.

Giacomelli, F. C., Stepanek, P., Schmidt, V., Jager, E., Jager, A., and Giacomelli, C. (2012). Light scattering evidence of selective protein fouling on biocompatible block copolymer micelles. Nanoscale *4*, 4504-4514.

Glebov, O., Bright, N., and Nichols, B. (2006). Flotillin-1 defines a clathrin-independent endocytic pathway in mammalian cells. Nature Cell Biology *8*, 46-54.

Gong, J., Chen, M., Zheng, Y., Wang, S., and Wang, Y. (2012). Polymeric micelles drug delivery system in oncology. Journal of Controlled Release *159*, 312-323.

Goodman, L. S., Wintrobe, M. M., Dameshek, W., Goodman, M. J., Gilman, A., and Mc, L. M. (1946). Nitrogen mustard therapy use of methyl-Bis(Beta-Chloroethyl)amine Hydrochloride and Tris(Beta-Chloroethyl)amine hydrochloride for Hodgkin's disease, lymphosarcoma, leukemia and

certain allied and miscellaneous disorders. Journal of the American Medical Association *132*, 126-132.

Grem, J. L., and Keith, B. (2005). Mechanisms of action of cancer chemotherapeutic agents: antimetabolites. In The Cancer Handbook, (John Wiley & Sons, Ltd).

Grivennikov, S., Greten, F., and Karin, M. (2010). Immunity, inflammation, and cancer. Cell *140*, 883-899.

Hall, P. A., and Watt, F. M. (1989). Stem cells: the generation and maintenance of cellular diversity. Development *106*, 619-633.

Hanahan, D., and Folkman, J. (1996). Patterns and emerging mechanisms of the angiogenic switch during tumorigenesis. Cell *86*, 353-364.

Hanahan, D., and Weinberg, R. A. (2011). Hallmarks of cancer: the next generation. Cell *144*, 646-674.

Hervé, F., Ghinea, N., and Scherrmann, J.-M. (2008). CNS delivery via adsorptive transcytosis. The AAPS journal *10*, 455-472.

Hetz, C., Chevet, E., and Harding, H. P. (2013). Targeting the unfolded protein response in disease. Nature Reviews Drug Discovery *12*, 703-719.

Heyman, B. (1996). Complement and Fc-receptors in regulation of the antibody response. Immunology Letters *54*, 195-199.

Hickman, E. S., Moroni, M. C., and Helin, K. (2002). The role of p53 and pRB in apoptosis and cancer. Current Opinion in Genetics & Development *12*, 60-66.

Ho, S. Y., and Mittal, G. S. (1996a). Electroporation of cell membranes: a review. Critical Reviews in Biotechnology *16*, 349-362.

Holohan, C., Van Schaeybroeck, S., Longley, D. B., and Johnston, P. G. (2013). Cancer drug resistance: an evolving paradigm. Nature Reviews Cancer *13*, 714-726.

Höög, G., Zarrizi, R., von Stedingk, K., Jonsson, K., and Alvarado Kristensson, M. (2011). Nuclear localization of γ-tubulin affects E2F transcriptional activity and S-phase progression. The FASEB journal *25*, 3815-3827.

Hořejší B1, V. S., Sládková V, Dráberová E, Sulimenko V, Sulimenko T, Vosecká V, Philimonenko A, Hozák P, Katsetos CD, Dráber P (2012). Nuclear γ-tubulin associates with nucleoli and interacts with tumor suppressor protein C53. Journal of cellular physiology *227*, 367-382.

Hume, D. (2006). The mononuclear phagocyte system. Current opinion in immunology *18*, 49-53.

Jacob Bongers, S. B., George M. Hilliard, and Jacek Mozdzanowski (1997). Assignment of disulfide pairings in an IgG1 monoclonal antibody: comparison of a new Trypsin/Glu-C approach versus fragmentation with pepsin. Journal of Biomolecular Techniques.

Jain, S., Hirst, D. G., and O'Sullivan, J. M. (2012). Gold nanoparticles as novel agents for cancer therapy. The British Journal of Radiology *85*, 101-113.

Jakobsen, J. N., and Sørensen, J. B. (2013). Clinical impact of ki-67 labeling index in non-small cell lung cancer. Lung Cancer *79*, 1-7.

Jaskiewicz, K., Larsen, A., Lieberwirth, I., Koynov, K., Meier, W., Fytas, G., Kroeger, A., and Landfester, K. (2012a). Probing bioinspired transport of nanoparticles into polymersomes. Angewandte Chemie International Edition *51*, 4613-4617.

Jaskiewicz, K., Larsen, A., Schaeffel, D., Koynov, K., Lieberwirth, I., Fytas, G., Landfester, K., and Kroeger, A. (2012b). Incorporation of nanoparticles into polymersomes: size and concentration effects. ACS Nano *6*, 7254-7262.

Kazerounian, S., Yee, K. O., and Lawler, J. (2008). Thrombospondins in cancer. Cellular and Molecular Life Sciences *65*, 700-712.

Kennedy, K., and Dewhirst, M. (2010). Tumor metabolism of lactate: the influence and therapeutic potential for MCT and CD147 regulation. Future oncology *6*, 127-148.

Khan, M. (2008). Role of cytokines. In Immunopharmacology. (Springer US), pp. 33-59.

Kill, I. R. (1996). Localisation of the Ki-67 antigen within the nucleolus. Evidence for a fibrillarin-deficient region of the dense fibrillar component. Journal of Cell Science *109*, 1253-1263.

Kim, K. T., Cornelissen, J. J. L. M., Nolte, R. J. M., and van Hest, J. C. M. (2009). A polymersome nanoreactor with controllable permeability induced by stimuli-responsive block copolymers. Advanced Materials *21*, 2787-2791.

Kimata, Y., and Kohno, K. (2011). Endoplasmic reticulum stress-sensing mechanisms in yeast and mammalian cells. Current Opinion in Cell Biology *23*, 135-142.

Kish-Trier, E., and Hill, C. P. (2013). Structural biology of the proteasome. Annual Review of Biophysics *42*, 29-49.

Kitazoe, M., Murata, H., Futami, J., Maeda, T., Sakaguchi, M., Miyazaki, M., Kosaka, M., Tada, H., Seno, M., Huh, N.-h.*, et al.* (2005). Protein transduction assisted by polyethylenimine-cationized carrier proteins. Journal of Biochemistry *137*, 693-701.

Klein, I. K., Predescu, D. N., Sharma, T., Knezevic, I., Malik, A. B., and Predescu, S. (2009). Intersectin-2L regulates caveolae endocytosis secondary to Cdc42-mediated actin polymerization. The Journal of Biological Chemistry.

Knutson, J. C., and Yee, D. (1987). Electroporation: parameters affecting transfer of DNA into mammalian cells. Analytical biochemistry *164*, 44-52.

Kollman, J., Merdes, A., Mourey, L., and Agard, D. (2011). Microtubule nucleation by γ-tubulin complexes. Nature reviews Molecular cell biology *12*, 709-721.

Kondo, Y., Fushikida, K., Fujieda, T., Sakai, K., Miyata, K., Kato, F., and Kato, M. (2008). Efficient delivery of antibody into living cells using a novel HVJ envelope vector system.Journal of Immunological Methods *332*, 10-17.

Kope*f*çek, J. ô. (2013). Polymer–drug conjugates: Origins, progress to date and future directions. Advanced drug delivery reviews *65*, 49-59.

Kotake, T., Usami, M., Akaza, H., Koiso, K., Homtna, Y., Kawabe, K., Aso, Y., Orikasa, S., Shimazaki, J., Isaka, S., *et al.* (1999). Goserelin acetate with or without antiandrogen or estrogen in the treatment of patients with advanced prostate cancer: a multicenter, randomized, controlled trial in japan. Japanese Journal of Clinical Oncology *29*, 562-570.

Kyomoto, M., Moro, T., Yamane, S., Hashimoto, M., Takatori, Y., and Ishihara, K. (2014). Effect of UV-irradiation intensity on graft polymerization of 2-methacryloyloxyethyl phosphorylcholine on orthopedic bearing substrate. Journal of biomedical materials research Part A *102*, 3012-3023.

Lasic, D. D. (1997). Recent developments in medical applications of liposomes: sterically stabilized liposomes in cancer therapy and gene delivery in vivo. Journal of Controlled Release *48*, 203-222.

Lee, J. S., and Feijen, J. (2012). Biodegradable polymersomes as carriers and release systems for paclitaxel using Oregon Green 488 labeled paclitaxel as a model compound. Journal of Controlled Release *158*, 312-318.

Lee, K., Chung, H., Im, S., Park, Y., Kim, C., Kim, S.-B., Rha, S., Lee, M., and Ro, J. (2008). Multicenter phase II trial of Genexol-PM, a Cremophor-free, polymeric micelle formulation of paclitaxel, in patients with metastatic breast cancer. Breast cancer research and treatment *108*, 241-250.

Lesca, C., Germanier, M., Raynaud Messina, B., Pichereaux, C., Etievant, C., Emond, S. p., Burlet Schiltz, O., Monsarrat, B., Wright, M., and Defais, M. (2005). DNA damage induce gamma-tubulin-RAD51 nuclear complexes in mammalian cells. Oncogene *24*, 5165-5172.

Lewis, A. L. (2000). Phosphorylcholine-based polymers and their use in the prevention of biofouling. Colloids and Surfaces B: Biointerfaces *18*, 261-275.

Li, H.-H., Aubrecht, J., and Fornace, A. (2007a). Toxicogenomics: overview and potential applications for the study of non-covalent DNA interacting chemicals. Mutation research - Fundamental and Molecular Mechanisms of Mutagenesis *623*, 98-108.

Li, S., Byrne, B., Welsh, J., and Palmer, A. F. (2007b). Self-assembled poly (butadiene)-b-poly(ethylene oxide) polymersomes as paclitaxel carriers. Biotechnology Progress *23*, 278-285.

Lichtor, T., and Glick, R. (2012). Immunogene therapy. Advances in Experimental Medicine and Biology *746*, 151-165.

Lim, J., and Gleeson, P. (2011). Macropinocytosis: an endocytic pathway for internalising large gulps. Immunology and cell biology *89*, 836-843.

Lomas, H., Canton, I., MacNeil, S., Du, J., Armes, S. P., Ryan, A. J., Lewis, A. L., and Battaglia, G. (2007). Biomimetic pH Sensitive polymersomes for efficient DNA encapsulation and delivery. Advanced Materials *19*, 4238-4243.

Lomas, H., Massignani, M., Abdullah, K., Canton, I., Lo Presti, C., MacNeil, S., Du, J., Blanazs, A., Madsen, J., Armes, S.*, et al.* (2008). Non-cytotoxic polymer vesicles for rapid and efficient intracellular delivery. Faraday discussions *139*, 143-159.

LoPresti, C., Lomas, H., Massignani, M., Smart, T., and Battaglia, G. (2009). Polymersomes: nature inspired nanometer sized compartments. Journal of Materials Chemistry *19*, 3576-3590.

LoPresti, C., Massignani, M., Fernyhough, C., Blanazs, A., Ryan, A. J., Madsen, J., Warren, N. J., Armes, S. P., Lewis, A. L., Chirasatitsin, S.*, et al.* (2011). Controlling polymersome surface topology at the nanoscale by membrane confined polymer/polymer phase separation. ACS Nano *5*, 1775-1784.

Lowy, D. R., and Willumsen, B. M. (1993). Function and regulation of RAS. Annual Review of Biochemistry *62*, 851-891.

Luisi, P. L., Allegretti, M., Pereira de Souza, T., Steiniger, F., Fahr, A., and Stano, P. (2010). Spontaneous protein crowding in liposomes: a new vista for the origin of cellular metabolism. ChemBioChem *11*, 1989-1992.

Lundmark, R., Doherty, G., Howes, M., Cortese, K., Vallis, Y., Parton, R., and McMahon, H. (2008). The GTPase-activating protein GRAF1 regulates the CLIC/GEEC endocytic pathway. Current Biology *18*, 1802-1808.

Lundqvist, M., Stigler, J., Elia, G., Lynch, I., Cedervall, T., and Dawson, K. A. (2008). Nanoparticle size and surface properties determine the protein

corona with possible implications for biological impacts. Proceedings of the National Academy of Sciences *105*, 14265-14270.

Luo, L., and Eisenberg, A. (2001). Thermodynamic stabilization mechanism of block copolymer vesicles. Journal of the American Chemical Society *123*, 1012-1013.

Lynch, I., and Dawson, K. A. (2008). Protein-nanoparticle interactions. Nano Today *3*, 40-47.

Lynch, I., Salvati, A., and Dawson, K. (2009). Protein-nanoparticle interactions: What does the cell see? Nature nanotechnology *4*, 546-547.

Ma, Y., Tang, Y., Billingham, N. C., Armes, S. P., Lewis, A. L., Lloyd, A. W., and Salvage, J. P. (2003). Well-defined biocompatible block copolymers via atom transfer radical polymerization of 2-methacryloyloxyethyl phosphorylcholine in protic media. Macromolecules *36*, 3475-3484.

Mac Gabhann, F., and Popel, A. (2008). Systems biology of vascular endothelial growth factors. Microcirculation *15*, 715-738.

Madsen, J., Armes, S. P., Bertal, K., MacNeil, S., and Lewis, A. L. (2009). Preparation and aqueous solution properties of thermoresponsive biocompatible AB diblock copolymers. Biomacromolecules *10*, 1875-1887.

Madsen, J., Armes, S. P., and Lewis, A. L. (2006). Preparation and aqueous solution properties of new thermoresponsive biocompatible ABA triblock copolymer gelators. Macromolecules *39*, 7455-7457.

Maeda, H., Bharate, G. Y., and Daruwalla, J. (2009). Polymeric drugs for efficient tumor-targeted drug delivery based on EPR-effect. European Journal of Pharmaceutics and Biopharmaceutics *71*, 409-419.

Maeda, H., Wu, J., Sawa, T., Matsumura, Y., and Hori, K. (2000). Tumor vascular permeability and the EPR effect in macromolecular therapeutics: a review. Journal of Controlled Release *65*, 271-284.

Makino, D. L., Halbach, F., and Conti, E. (2013). The RNA exosome and proteasome: common principles of degradation control. Nature Reviews Molecular Cell Biology Biol *14*, 654-660.

Mallery, D. L., McEwan, W. A., Bidgood, S. R., Towers, G. J., Johnson, C. M., and James, L. C. (2010). Antibodies mediate intracellular immunity through tripartite motif-containing 21 (TRIM21). Proceedings of the National Academy of Sciences *107*, 19985-19990.

Marguet, M., Edembe, L., and Lecommandoux, S. (2012). Polymersomes in polymersomes: multiple loading and permeability control. Angewandte Chemie International Edition *51*, 1173-1176.

Markman, J., Rekechenetskiy, A., Holler, E., and Ljubimova, J. (2013). Nanomedicine therapeutic approaches to overcome cancer drug resistance. Advanced drug delivery reviews *65*, 1866-1879.

Marquart, M., Deisenhofer, J., Huber, R., and Palm, W. (1980). Crystallographic refinement and atomic models of the intact immunoglobulin molecule Kol and its antigen-binding fragment at 3.0 Å and 1.9 Å resolution. Journal of Molecular Biology *141*, 369-391.

Massignani, M., Canton, I., Sun, T., Hearnden, V., MacNeil, S., Blanazs, A., Armes, S. P., Lewis, A., and Battaglia, G. (2010a). Enhanced fluorescence imaging of live cells by effective cytosolic delivery of probes. Plos One *5*.

Massignani, M., Lomas, H., and Battaglia, G. (2010b). Polymersomes: a synthetic biological approach to encapsulation and delivery. Advances in Polymer Science *229*, 115-154.

Massignani, M., LoPresti, C., Blanazs, A., Madsen, J., Armes, S. P., Lewis, A. L., and Battaglia, G. (2009). Controlling cellular uptake by surface chemistry, size, and surface topology at the nanoscale. Small *5*, 2424-2432.

Matsen, M. W., and Bates, F. S. (1996a). Origins of complex self-assembly in block copolymers. Macromolecules *29*, 7641-7644.

Matsen, M. W., and Bates, F. S. (1996b). Unifying weak- and strong-segregation block copolymer theories. Macromolecules *29*, 1091-1098.

Matsumura, Y., and Maeda, H. (1986). A New Concept for macromolecular therapeutics in cancer chemotherapy: mechanism of tumoritropic accumulation of proteins and the antitumor agent smancs. Cancer Research *46*, 6387-6392.

McCormick, F. (2001). Cancer gene therapy: fringe or cutting edge? Nature Reviews Cancer *1*, 130-141.

McMahon, H. T., and Boucrot, E. (2011). Molecular mechanism and physiological functions of clathrin-mediated endocytosis. Nature Reviews Molecular Cell Biology *12*, 517-533.

McNeil, P. L. (1984). Mechanisms of nutritive endocytosis. III. A freeze-fracture study of phagocytosis by digestive cells of chlorohydra. Tissue and Cell *16*, 519-533.

Meibohm, B. (2012). Pharmacokinetics and half-life of protein therapeutics. In Therapeutic Proteins, (Wiley-VCH Verlag GmbH & Co. KGaA), pp. 23-38.

Meng, F., Engbers, G. H. M., and Feijen, J. (2005). Biodegradable polymersomes as a basis for artificial cells: encapsulation, release and targeting. Journal of Controlled Release *101*, 187-198.

Mero, A., Pasqualin, M., Campisi, M., Renier, D., and Pasut, G. (2013). Conjugation of hyaluronan to proteins. Carbohydrate polymers *92*, 2163-2170.

Minotti, G., Menna, P., Salvatorelli, E., Cairo, G., and Gianni, L. (2004). Anthracyclines: molecular advances and pharmacologic developments in antitumor activity and cardiotoxicity. Pharmacological Reviews *56*, 185-229.

Moghimi, S. M., Hunter, A. C., and Murray, J. C. (2001). Long-circulating and target-specific nanoparticles: theory to practice. Pharmacological Reviews *53*, 283-318.

Monopoli, M., Walczyk, D., Campbell, A., Elia, G., Lynch, I., Bombelli, F., and Dawson, K. (2011). Physical-chemical aspects of protein corona: relevance to in vitro and in vivo biological impacts of nanoparticles. Journal of the American Chemical Society *133*, 2525-2534.

Moore, J. C. (1964). Gel permeation chromatography. I. A new method for molecular weight distribution of high polymers. Journal of Polymer Science Part A: General Papers *2*, 835-843.

Morgan, D. O. (1995). Principles of CDK regulation. Nature *374*, 131-134.

Mougiakakos, D., Choudhury, A., Lladser, A., Kiessling, R., and Johansson, C. C. (2010). Regulatory T cells in cancer. Advances in Cancer Research *107*, 57-117.

Nagarajan, R. (2002). Molecular packing parameter and surfactant self-assembly: the neglected role of the surfactant tail. Langmuir *18*, 31-38.

Nagarajan, R., and Ganesh, K. (1989). Block copolymer self-assembly in selective solvents: spherical micelles with segregated cores. The Journal of Chemical Physics *90*, 5843-5856.

Nagy, J., Chang, S.-H., Shih, S.-C., Dvorak, A., and Dvorak, H. (2010). Heterogeneity of the tumor vasculature. Seminars in thrombosis and hemostasis *36*, 321-331.

Nagy, J., and Dvorak, H. (2012). Heterogeneity of the tumor vasculature: the need for new tumor blood vessel type-specific targets. Clinical & experimental metastasis *29*, 657-662.

Nakai, T., Kanamori, T., Sando, S., and Aoyama, Y. (2003). Remarkably size-regulated cell invasion by artificial viruses. saccharide-dependent self-aggregation of glycoviruses and its consequences in glycoviral gene delivery. Journal of the American Chemical Society *125*, 8465-8475.

Napoli, A., Valentini, M., Tirelli, N., Muller, M., and Hubbell, J. A. (2004). Oxidation-responsive polymeric vesicles. Nature Materials *3*, 183-189.

Nelson, A. L., and Reichert, J. M. (2009). Development trends for therapeutic antibody fragments. Nature Biotechnology *27*, 331-337.

Neumann, E., Kakorin, S., and Tœnsing, K. (1999). Fundamentals of electroporative delivery of drugs and genes. Bioelectrochemistry and Bioenergetics *48*, 3-16.

Neumann, E., Schaeferridder, M., Wang, Y., and Hofschneider, P. H. (1982). Gene-transfer into mouse lyoma cells by electroporation in high electric-fields. Embo J *1*, 841-845.

NHS-UK (2013). Side effects of chemotherapy.

NHS-UK (2014). Cancer survival rates 'threatened by rising cost' NHS UK website.

North, B., Lehmann, A., and Dunbrack Jr, R. L. (2011). A new clustering of antibody CDR loop conformations. Journal of Molecular Biology *406*, 228-256.

Odell, I. D., and Cook, D. (2013). Immunofluorescence techniques. Journal of Investigative Dermatology *133*, e4.

Olson, M. F., and Marais, R. (2000). Ras protein signalling. Seminars in Immunology *12*, 63-73.

Onaca, O., Enea, R., Hughes, D. W., and Meier, W. (2009). Stimuli-responsive polymersomes as nanocarriers for drug and gene delivery. Macromolecular Bioscience *9*, 129-139.

Onaca, O., Sarkar, P., Roccatano, D., Friedrich, T., Hauer, B., Grzelakowski, M., Güven, A., Fioroni, M., and Schwaneberg, U. (2008). Functionalized nanocompartments (synthosomes) with a reduction-triggered release system. Angewandte Chemie International Edition *47*, 7029-7031.

Onn, A., and Ron, D. (2010). Modeling the endoplasmic reticulum unfolded protein response. Nature Structural & Molecular Biology *17*, 924-925.

Owens, D., and Peppas, N. (2006). Opsonization, biodistribution, and pharmacokinetics of polymeric nanoparticles. International journal of pharmaceutics *307*, 93-102.

Pappenheimer, J. R., Renkin, E. M., and Borrero, L. M. (1951). Filtration, diffusion and molecular sieving through peripheral capillary membranes; a contribution to the pore theory of capillary permeability. American journal of physiology *167*, 13-46.

Pardee, A. B. (1974). A restriction point for control of normal animal cell proliferation. Proceedings of the National Academy of Sciences *71*, 1286-1290.

Pardridge, W. M. (2012). Drug transport across the blood-brain barrier. Journal of Cerebral Blood Flow & Metabolism *32*, 1959-1972.

Pasquali, S., and Mocellin, S. (2010). The anticancer face of interferon alpha (IFN-Alpha): from biology to clinical results, with a focus on melanoma. Current Medicinal Chemistry *17*, 3327-3336.

Pasut, G., and Veronese, F. (2012). State of the art in PEGylation: the great versatility achieved after forty years of research. Journal of Controlled Release *161*, 461-472.

Pathmanathan, N., and Balleine, R. L. (2013). Ki67 and proliferation in breast cancer. Journal of Clinical Pathology *66*, 512-516.

Pearse, B. M. (1976). Clathrin: a unique protein associated with intracellular transfer of membrane by coated vesicles. Proceedings of the National Academy of Sciences *73*, 1255-1259.

Pearson, R. T., Warren, N. J., Lewis, A. L., Armes, S. P., and Battaglia, G. (2013). Effect of pH and Temperature on PMPC, PDPA Copolymer Self-Assembly. Macromolecules *46*, 1400-1407.

Pegram, M., Konecny, G., and Slamon, D. (2000a). The molecular and cellular biology of HER2/neu gene amplification/overexpression and the clinical development of herceptin (Trastuzumab) therapy for breast cancer. In advances in breast cancer management, W. Gradishar, and W. Wood, eds. (Springer US), pp. 57-75.

Pegram, M. D., Konecny, G., and Slamon, D. J. (2000b). The molecular and cellular biology of HER2/neu gene amplification/overexpression and the clinical development of herceptin (trastuzumab) therapy for breast cancer. Cancer Treatment and Research *103*, 57-75.

Pfeiffer, C., Rehbock, C., Hühn, D., Carrillo-Carrion, C., de Aberasturi, D. J., Merk, V., Barcikowski, S., and Parak, W. J. (2014). Interaction of colloidal nanoparticles with their local environment: the (ionic) nanoenvironment around nanoparticles is different from bulk and determines the physico-chemical properties of the nanoparticles. Journal of The Royal Society Interface *11*.

Photos, P. J., Bacakova, L., Discher, B., Bates, F. S., and Discher, D. E. (2003). Polymer vesicles in vivo: correlations with PEG molecular weight. Journal of Controlled Release *90*, 323-334.

Pimpl, P., Taylor, J. P., Snowden, C., Hillmer, S., Robinson, D. G., and Denecke, J. (2006). Golgi-mediated vacuolar sorting of the endoplasmic reticulum chaperone BiP may play an active role in quality control within the secretory pathway. The Plant Cell Online *18*, 198-211.

Platt, V. M., and Szoka, F. C. (2008). Anticancer therapeutics: targeting macromolecules and nanocarriers to hyaluronan or CD44, a hyaluronan receptor. Molecular Pharmaceutics *5*, 474-486.

Plosker, G. (2011). Sipuleucel-T. Drugs *71*, 101-108.

Potten, C. S., and Loeffler, M. (1990). Stem cells: attributes, cycles, spirals, pitfalls and uncertainties. Lessons for and from the crypt. Development *110*, 1001-1020.

Pozarowski, P., and Darzynkiewicz, Z. (2004). Analysis of cell cycle by flow cytometry. Checkpoint Controls and Cancer. Springer, ed. (Humana Press), pp. 301-311.

PrabhuDas, M., Bowdish, D., Drickamer, K., Febbraio, M., Herz, J., Kobzik, L., Krieger, M., Loike, J., Means, T. K., Moestrup, S. K., *et al.* (2014). Standardizing scavenger receptor nomenclature. The Journal of Immunology *192*, 1997-2006.

Prochiantz, A. (2000). Messenger proteins: homeoproteins, TAT and others. Current opinion in cell biology *12*, 400-406.

Putnam, F. W., Liu, Y. S., and Low, T. L. (1979). Primary structure of a human IgA1 immunoglobulin. IV. Streptococcal IgA1 protease, digestion, Fab and Fc fragments, and the complete amino acid sequence of the alpha 1 heavy chain. The Journal of Biological Chemistry *254*, 2865-2874.

Qian, B.-Z., and Pollard, J. (2010). Macrophage diversity enhances tumor progression and metastasis. Cell *141*, 39-51.

Qin, S., Geng, Y., Discher, D. E., and Yang, S. (2006). Temperature-controlled assembly and release from polymer vesicles of poly(ethylene oxide)-block- poly(N-isopropylacrylamide). Advanced Materials *18*, 2905-2909.

Rahman, M., Laurent, S., Tawil, N., Yahia, L., Mahmoudi, M. (2013). Protein-nanoparticle interactions. Springer *15*.

Rameez, S., Alosta, H., and Palmer, A. F. (2008). Biocompatible and biodegradable polymersome encapsulated hemoglobin: a potential oxygen carrier. Bioconjugate Chemistry *19*, 1025-1032.

Raynaud Messina, B., and Merdes, A. (2007). Gamma-tubulin complexes and microtubule organization. Current opinion in cell biology *19*, 24-30.

Reed, A. L., Califano, J., Cairns, P., Westra, W. H., Jones, R. M., Koch, W., Ahrendt, S., Eby, Y., Sewell, D., Nawroz, H., *et al.* (1996). High frequency of p16 (CDKN2/MTS-1/INK4A) inactivation in head and neck squamous cell carcinoma. Cancer Research *56*, 3630-3633.

Ren, H., Chu, Z., and Mao, L. (2009). Antibodies targeting hepatoma-derived growth factor as a novel strategy in treating lung cancer. Molecular cancer therapeutics *8*, 1106-1112.

Riento, K., Frick, M., Schafer, I., and Nichols, B. (2009). Endocytosis of flotillin-1 and flotillin-2 is regulated by Fyn kinase. Journal of Cell Science *122*, 912-918.

Robertson, A., Smythe, E., and Ayscough, K. (2009). Functions of actin in endocytosis. Cellular and Molecular Life Sciences *66*, 2049-2065.

Robertson, J. D., Yealland, G., Avila-Olias, M., Chierico, L., Bandmann, O., Renshaw, S. A., and Battaglia, G. (2014). pH-sensitive tubular polymersomes: formation and applications in cellular delivery. ACS Nano.

Roger, E., Lagarce, F., Garcion, E., and Benoit, J.-P. (2010). Biopharmaceutical parameters to consider in order to alter the fate of nanocarriers after oral delivery. Nanomedicine *5*, 287-306.

Roskoski, R. (2012). ERK1/2 MAP kinases: structure, function, and regulation. Pharmacological research *66*, 105-143.

Rothberg, K. G., Heuser, J. E., Donzell, W. C., Ying, Y. S., Glenney, J. R., and Anderson, R. G. (1992). Caveolin, a protein component of caveolae membrane coats. Cell *68*, 673-682.

Rowinsky, E. (2003). The vinca alkaloids. Holland-Frei Cancer Medicine 6th edition.

Ruge, C., Kirch, J., and Lehr, C.-M. (2013). Pulmonary drug delivery: from generating aerosols to overcoming biological barriers-therapeutic possibilities and technological challenges. The Lancet Respiratory Medicine *1*, 402-413.

Ruoslahti, E., Bhatia, S. N., and Sailor, M. J. (2010). Targeting of drugs and nanoparticles to tumors. The Journal of Cell Biology *188*, 759-768.

Rustandi, R. R., Loughney, J. W., Hamm, M., Hamm, C., Lancaster, C., Mach, A., and Ha, S. (2012). Qualitative and quantitative evaluation of Simon™, a new CE-based automated Western blot system as applied to vaccine development. ELECTROPHORESIS *33*, 2790-2797.

Sadeghi Aliabadi, H., Minaiyan, M., and Dabestan, A. (2010). Cytotoxic evaluation of doxorubicin in combination with simvastatin against human cancer cells. Research in Pharmaceutical Sciences *5*, 127-133.

Sandal, T. (2002). Molecular aspects of the mammalian cell cycle and cancer. The Oncologist *7*, 73-81.

Saxton, W. M., Stemple, D. L., Leslie, R. J., Salmon, E. D., Zavortink, M., and McIntosh, J. R. (1984). Tubulin dynamics in cultured mammalian cells. The Journal of Cell Biology *99*, 2175-2186.

Schlüter, C., Duchrow, M., Wohlenberg, C., Becker, M. H., Key, G., Flad, H. D., and Gerdes, J. (1993). The cell proliferation-associated antigen of antibody Ki-67: a very large, ubiquitous nuclear protein with numerous repeated elements, representing a new kind of cell cycle-maintaining proteins. The Journal of Cell Biology *123*, 513-522.

Schmid, S. L. (1997). Clathrin-coated vesicle formation and protein sorting: an integrated process. Annual Review of Biochemistry *66*, 511-548.

Schoenbach, K. H., Beebe, S. J., and Buescher, E. S. (2001). Intracellular effect of ultrashort electrical pulses. Bioelectromagnetics *22*, 440-448.

Scholzen, T., and Gerdes, J. (2000). The Ki-67 protein: From the known and the unknown. Journal of Cellular Physiology *182*, 311-322.

Shannahan, J. H., Lai, X., Ke, P. C., Podila, R., Brown, J. M., and Witzmann, F. A. (2013). Silver nanoparticle protein corona composition in cell culture media. Plos One *8*, e74001.

Shay, J. W., and Wright, W. E. (2011). Role of telomeres and telomerase in cancer. Seminars in Cancer Biology *21*, 349-353.

Sherr, C. J. (1996). Cancer cell cycles. Science *274*, 1672-1677.

Sherr, C. J. (2000). The Pezcoller lecture: cancer cell cycles revisited. Cancer Research *60*, 3689-3695.

Sherr, C. J. (2004). Principles of tumor suppression. Cell *116*, 235-246.

Sherr, C. J., and Roberts, J. M. (1999). CDK inhibitors: positive and negative regulators of G1-phase progression. Genes & Development *13*, 1501-1512.

Sidhu, S. S., and Fellouse, F. A. (2006). Synthetic therapeutic antibodies. Nature Chemical Biology *2*, 682-688.

Siegel, R., Naishadham, D., and Jemal, A. (2013). Cancer statistics, 2013. CA: A Cancer Journal for Clinicians *63*, 11-30.

Smart, T., Lomas, H., Massignani, M., Flores-Merino, M. V., Perez, L. R., and Battaglia, G. (2008). Block copolymer nanostructures. Nano Today *3*, 38-46.

Smith, P. K., Krohn, R. I., Hermanson, G. T., Mallia, A. K., Gartner, F. H., Provenzano, M. D., Fujimoto, E. K., Goeke, N. M., Olson, B. J., and Klenk, D. C. (1985). Measurement of protein using bicinchoninic acid. Analytical biochemistry *150*, 76-85.

Soenen, S. J., Rivera-Gil, P., Montenegro, J.-M. a., Parak, W. J., De Smedt, S. C., and Braeckmans, K. (2011). Cellular toxicity of inorganic nanoparticles: Common aspects and guidelines for improved nanotoxicity evaluation. Nano Today *6*, 446-465.

Solomon, M. J., and Kaldis, P. (1998). Regulation of CDKs by phosphorylation. In Cell Cycle Control, M. Pagano, ed. (Springer Berlin Heidelberg), pp. 79-109.

Starborg, M., Gell, K., Brundell, E., and Hoog, C. (1996). The murine Ki-67 cell proliferation antigen accumulates in the nucleolar and heterochromatic

regions of interphase cells and at the periphery of the mitotic chromosomes in a process essential for cell cycle progression. Journal of Cell Science *109*, 143-153.

Storm, G., Belliot, S. O., Daemen, T., and Lasic, D. D. (1995). Surface modification of nanoparticles to oppose uptake by the mononuclear phagocyte system. Advanced drug delivery reviews *17*, 31-48.

Stoscheck, C. M. (1990). Quantitation of protein. Methods Enzymol *182*, 50-68.

Strebhardt, K., and Ullrich, A. (2008). Paul Ehrlich's magic bullet concept: 100 years of progress. Nature Reviews Cancer *8*, 473-480.

Sueishi, M., Takagi, M., and Yoneda, Y. (2000). The Forkhead-associated Domain of Ki-67 antigen Interacts with the novel kinesin-like protein Hklp2. The Journal of Biological Chemistry *275*, 28888-28892.

Sutherland, R., and Musgrove, E. (2004). Cyclins and breast cancer. Journal of Mammary Gland Biology and Neoplasia *9*, 95-104.

Takagi, M., Sueishi, M., Saiwaki, T., Kametaka, A., and Yoneda, Y. (2001). A novel nucleolar protein, NIFK, interacts with the forkhead associated domain of Ki-67 antigen in mitosis. The Journal of Biological Chemistry *276*, 25386-25391.

Talve, L., Sauroja, I., Collan, Y., Punnonen, K., and Ekfors, T. (1997). Loss of expression of the p16INK4/CDKN2 gene in cutaneous malignant melanoma correlates with tumor cell proliferation and invasive stage. International Journal of Cancer *74*, 255-259.

Tazawa, H., Kagawa, S., and Fujiwara, T. (2013). Advances in adenovirus-mediated p53 cancer gene therapy. Expert opinion on biological therapy *13*, 1569-1583.

Teng, M. W. L., Swann, J., Koebel, C., Schreiber, R., and Smyth, M. (2008). Immune-mediated dormancy: an equilibrium with cancer. Journal of leukocyte biology *84*, 988-993.

Tenzer, S., Docter, D., Kuharev, J., Musyanovych, A., Fetz, V., Hecht, R., Schlenk, F., Fischer, D., Kiouptsi, K., Reinhardt, C.*, et al.* (2013). Rapid formation of plasma protein corona critically affects nanoparticle pathophysiology. Nat Nano *8*, 772-781.

Tetsu, O., and McCormick, F. (1999). Beta-catenin regulates expression of cyclin D1 in colon carcinoma cells. Nature *398*, 422-426.

Thiele, J., Abate, A. R., Shum, H. C., Bachtler, S., Förster, S., and Weitz, D. A. (2010). Fabrication of polymersomes using double-emulsion templates in glass-coated stamped microfluidic devices. Small *6*, 1723-1727.

Tian, X. (2014). CNS, Blood-brain barrier,transcytosis, functionalised-polymersomes, microscopy. PhD thesis, University of Sheffield.

Timerbaev, A. R., Hartinger, C. G., Aleksenko, S. S., and Keppler, B. K. (2006). Interactions of antitumor metallodrugs with serum proteins: advances in characterization using modern analytical methodology. Chemical Reviews *106*, 2224-2248.

Träubel, H. (1999). Hydrophilic Polymers. In New Materials Permeable to Water Vapor, (Springer Berlin Heidelberg), pp. 133-152.

Triguero, D., Buciak, J. B., Yang, J., and Pardridge, W. M. (1989). Blood-brain barrier transport of cationized immunoglobulin G: enhanced delivery compared to native protein. Proceedings of the National Academy of Sciences *86*, 4761-4765.

Trivedi, R., and Kompella, U. B. (2010). Nanomicellar formulations for sustained drug delivery: strategies and underlying principles. Nanomedicine *5*, 485-505.

Tufts-CSDD-Impact-Report (2013). Biotech products in big pharma clinical pipelines have grown dramatically. *15*, 1–4.

van Dongen, S. F. M., Nallani, M., Cornelissen, J. J. L. M., Nolte, R. J. M., and van Hest, J. C. M. (2009). A three-enzyme cascade reaction through positional assembly of enzymes in a polymersome nanoreactor. Chemistry – A European Journal *15*, 1107-1114.

van Meerloo, J., Kaspers, G. J. L., and Cloos, J. (2011). Cell sensitivity assays: the MTT assay. Methods in Molecular Biology *731*, 237-245.

Vander Heiden, M., Cantley, L., and Thompson, C. (2009). Understanding the Warburg effect: the metabolic requirements of cell proliferation. Science *324*, 1029-1033.

Vashist, S., and Ng, D. T. W. (2004). Misfolded proteins are sorted by a sequential checkpoint mechanism of ER quality control. The Journal of Cell Biology *165*, 41-52.

Vogler, E. (2012). Protein adsorption in three dimensions. Biomaterials *33*, 1201-1237.

Vonarbourg, A., Passirani, C., Saulnier, P., and Benoit, J.-P. (2006). Parameters influencing the stealthiness of colloidal drug delivery systems. Biomaterials *27*, 4356-4373.

Wang, L., Chierico, L., Little, D., Patikarnmonthon, N., Yang, Z., Azzouz, M., Madsen, J., Armes, S. P., and Battaglia, G. (2012). Encapsulation of biomacromolecules within polymersomes by electroporation. Angewandte Chemie International Edition *51*, 11122-11125.

Wang, S.-C., and Hung, M.-C. (2001). HER2 overexpression and cancer targeting. Seminars in Oncology *28, Supplement 16*, 115-124.

Wang, X., Liu, G., Hu, J., Zhang, G., and Liu, S. (2014). Concurrent block copolymer polymersome stabilization and bilayer permeabilization by stimuli-regulated “traceless” crosslinking. Angewandte Chemie International Edition *53*, 3138-3142.

Weinhouse, S. W., Otto Burk, Dean Schade, Arthur L. (1956). On respiratory impairment in cancer cells. Science *124*, 267-272.

Wells, T. N. C., Stedman, M., and Leatherbarrow, R. J. (1992). Imaging of proteins by scanning tunnelling microscopy. Ultramicroscopy *42,Äì44, Part 2*, 1200-1203.

Werner, M. E., Cummings, N. D., Sethi, M., Wang, E. C., Sukumar, R., Moore, D. T., and Wang, A. Z. (2013). Preclinical evaluation of Genexol-PM, a nanoparticle formulation of paclitaxel, as a novel radiosensitizer for the treatment of non-small cell lung cancer. International Journal of Radiation Oncology*Biology*Physics *86*, 463-468.

Williams, G., and Stoeber, K. (2007). Cell cycle markers in clinical oncology. Current opinion in cell biology *19*, 672-679.

Wolf, H., Rols, M. P., Boldt, E., Neumann, E., and Teissié, J. (1994). Control by pulse parameters of electric field-mediated gene transfer in mammalian cells. Biophysical Journal *66*, 524-531.

Won, Y.-Y., Davis, H. T., and Bates, F. S. (2003). Molecular exchange in PEO-PB micelles in water. Macromolecules *36*, 953-955.

Yan, Q., Wang, J., Yin, Y., and Yuan, J. (2013). Breathing polymersomes: CO2-tuning membrane permeability for size-selective release, separation, and reaction. Angewandte Chemie International Edition *52*, 5070-5073.

Yang, L., Pang, Y., and Moses, H. (2010). TGF-beta and immune cells: an important regulatory axis in the tumor microenvironment and progression. Trends in immunology *31*, 220-227.

Yassin, M. A., Appelhans, D., Mendes, R. G., Rümmeli, M. H., and Voit, B. (2012). pH-dependent release of doxorubicin from fast photo-cross-linkable polymersomes based on benzophenone units. Chemistry – A European Journal *18*, 12227-12231.

Yerushalmi, R., Woods, R., Ravdin, P. M., Hayes, M. M., and Gelmon, K. A. (2010). Ki67 in breast cancer: prognostic and predictive potential. The Lancet Oncology *11*, 174-183.

Yu, Q., Geng, Y., and Sicinski, P. (2001). Specific protection against breast cancers by cyclin D1 ablation. Nature *411*, 1017-1021.

Yu, S., Azzam, T., Rouiller, I., and Eisenberg, A. (2009). "Breathing" vesicles. Journal of the American Chemical Society *131*, 10557-10566.

Yuan, J.-J., Schmid, A., Armes, S. P., and Lewis, A. L. (2006). Facile synthesis of highly biocompatible poly(2-(methacryloyloxy)ethyl phosphorylcholine)-coated gold nanoparticles in aqueous aolution. Langmuir *22*, 11022-11027.

Zanetti, G., Pahuja, K. B., Studer, S., Shim, S., and Schekman, R. (2012). COPII and the regulation of protein sorting in mammals. Nature Cell Biology *14*, 20-28.

Zelphati, O., Wang, Y., Kitada, S., Reed, J. C., Felgner, P. L., and Corbeil, J. (2001). Intracellular delivery of proteins with a new lipid-mediated delivery system. The Journal of Biological Chemistry *276*, 35103-35110.

Zhang, L., and Eisenberg, A. (1995). Multiple morphologies of "crew-cut" aggregates of polystyrene-b-poly(acrylic acid) block copolymers. Science *268*, 1728-1731.

Zhang, S., Hemmerich, P., and Grosse, F. (2007). Centrosomal localization of DNA damage checkpoint proteins. Journal of Cellular Biochemistry *101*, 451-465.

Zimmermann, R., Eyrisch, S., Ahmad, M., and Helms, V. (2011). Protein translocation across the ER membrane. Biochimica et Biophysica Acta (BBA) - Biomembranes *1808*, 912-924.